DIFFUSION CONTROLLED GROWTH AND DISSOLUTION OF GAS BUBBLES

A Thesis presented

by

JORGE RIBEIRO FRADE

for the degree of

Doctor of Philosophy

of the

University of Sheffield

Department of Ceramics, Glasses and Polymers,
Faculty of Materials,
The University of Sheffield

July 1983

ORIGINAL COPY TIGHTLY BOUND

ACKNOWLEDGEMENTS

I am indebted to Dr M. Cable for his keen interest, constructive criticisms, helpful suggestions and encouragement during the course of this work.

Many thanks are due to Mrs M. Hodgins for typing this thesis.

Permission for a leave of absence from the Departmento de Engenharia Cerâmica e do Vidro, University of Aveiro, Portugal and financial support from the same University are gratefully acknowledged.

Thanks are also due to Calouste Gulbenkian Foundation for generous financial support.

The author acknowledges the help of Mrs M.H.V. Fernandes and Professor Baptista of the University of Aveiro in taking care of his personal interests in Portugal.

SUMMARY

The material transfer between an isolated stationary bubble and the surrounding liquid has been formulated mathematically and methods were developed to solve the relevant differential equations. Solutions were made dimensionless to generalize their application.

Exact solutions have long been available to describe growth of one-component spheres from zero size. These solutions were used to show that the corresponding finite difference solutions for growth from finite size are accurate. Exact solutions were also derived for diffusion controlled growth from zero size of one-component spheres with concentration dependent diffusivity and for growth of multi-component bubbles. This type of solution was also used to demonstrate the accuracy of the finite difference solutions of corresponding problems for growth from finite size. These finite difference methods were also used for dissolving bubbles where analytical solutions are not possible.

Several approximate solutions are discussed and quasi steady-state solutions were obtained for growth or dissolution with concentration dependent diffusivity and inclusion of surface tension. For small solubilities and concentrations, (low solubility parameters), the correct diffusion controlled solutions always converge to the corresponding quasi steady-state.

A large number of solutions was obtained to cover the significant ranges of values of the relevant parameters for gases in glass melts. These solutions include the study of limiting regimes for very low and very large solubility parameters as well as the intermediate range.

Solutions for multicomponent stationary bubbles were used to discuss some experimental observations of bubbles in glass melts.

The effect of surface kinetics on growth or dissolution of spheres was investigated and solved to illustrate the transition between control by diffusion and control by surface kinetics.

An extensive study of the effect of surface tension was carried out. The roles of viscosity and inertia were considered and are usually negligible.

List of Symbols

i) Main variables

a radius of the sphere. (a_o denotes the initial value.)

C molar concentration of solute.

C_a value of C at the interface.

C_{P_i} equilibrium concentration of species i at pressure P.

C_s molar concentration of the sphere. (C_s^o denotes a uniform and time invariant value.)

C_∞ value of C in the bulk liquid medium.

C^* concentration of solute in equilibrium with the content of the sphere.

D diffusivity. (D_a denotes the diffusivity at the interface.).

g_i mole fraction of species i in a multicomponent bubble.

$g_{i,eq}$ equilibrium value of g_i.

J_i molar flux of species i into the sphere.

K' kinetic constant (Chapter VIII).

N_i number of moles of species i in the sphere.

P pressure. (P_∞ denotes the pressure in the bulk medium.)

P_g pressure inside a gas bubble.

r radial distance from the centre of the bubble.

t time

u velocity of the liquid.

v partial molar volume of solute.

y_i volume fraction of species i in solution.

θ angle measured from the point of incidence of liquid flowing around a moving bubble.

μ viscosity of the fluid.

ν kinematic viscosity = μ/ρ.

ρ fluid density.

σ surface tension.

ii) Dimensionless variables

$A = g\, a_o^3/(D\nu)$ (Chapter I).

$\hat{D}$ dimensionless diffusivity = D/D_a.

$\hat{D}_{eq}$ equivalent dimensionless diffusivity.

$\hat{D}_{av}$ average dimensionless diffusivity.

e dimensionless radial distance = r/a_o.

$f = C^*/(C_\infty - C^*)$ (Chapter VIII).

f_i ratio of diffusivities = D_i/D_1.

F dimensionless concentration = $(C - C_\infty)/[C_s^o(1 - \nu C_a)]$.

except in Chapter VII where $F = (C - C_a)/[C_s^o(1 - \nu C_a)]$.

F_a solubility parameter = $(C_a - C_\infty)/[C_s^o(1 - \nu C_a)]$.

$F_{o_i} = C_{\infty_i}/C_s^o$.

$F_s = C^*/C_s^o$ (Chapter VIII).

$G_i = N_i/(a_o^3\, C_s^o)$.

$h = \rho\, D^2/(a_o^2\, P_\infty)$.

$K = K'\, a_o\, D^{-1}\, (C_s^o)^{n-1}$ (n denotes n-order surface kinetics)

$P^* = P_g/P_\infty$ Chapter IX).

$q = C^*/(C_\infty - C^*)$ (Chapter IX).

R dimensionless radius = a/a_o.

$s = r/(2\sqrt{Dt}) = e/\sqrt{Z}$

$S = \sigma/(a_o\, P_\infty)$

$x = r/a$

Z dimensionless time = tD/a_o^2 ($Z = t\, D_a/a_o^2$ in Chapter VII).

Z_d or dimensionless time required for complete dissolution

Z_o (Z_o is a reference value).

Z_g or Z_2 — dimensionless time required to double the size of a sphere (Z_2 is a reference value).

$\alpha_i = C_{P_i}/C_s^{\circ}$

β — growth constant ($R = 2\beta\sqrt{Z}$)

$\varepsilon = 1 - v C_s^{\circ}$

η — dimensionless viscosity $= \mu D/(a_o^2 P_\infty)$

ϕ — solubility parameter $= (C_\infty - C_a)/[(1 - v C_a)C_s^{\circ}]$.

$\phi_i = F_{o_i} - \alpha_i g_{i,eq}$ (Chapter VI).

iii) Subscripts

i — denotes species i

a — denotes the value at the interface

∞ — denotes the value at infinite distance from the centre.

CONTENTS

CHAPTER I

1.1 Introduction

Refining refers to the elimination of bubbles from glass melts. Glass melts are very viscous even at the highest temperatures used so that small bubbles rise to the surface only very slowly.

Glasses are usually melted from mixtures of raw materials which give off very large volumes of gas during their initial reactions as carbonates, sulphates and nitrates decompose in effect to oxides

$$Na_2CO_3 + xSiO_2 \longrightarrow Na_2O.xSiO_2 + CO_2\uparrow \ .$$

Most of this gas escapes before the materials such as silica are completely dissolved but removing the residual bubbles (refining) can often take much longer than dissolving the materials. In some cases reaching a sufficiently good standard of refining determines the total melting time, or the maximum output from a continuous furnace.

Experience has shown that relatively small additions of certain compounds (refining agents) to the batch can considerably accelerate the disappearance of these bubbles. It is also clear that bubbles disappear faster than could be accounted for only by rise to the surface.

The most obvious ways in which removal of bubbles could be assisted would be either

1) diffusion of gas into them, making them grow and rise to the surface faster,

or 2) diffusion of gas out of them into the melt so that they dissolve and rise to the surface becomes unnecessary.

Other experiments have shown that the composition of gas found in these bubbles changes with time during melting, especially when refining agents are used.

Understanding of these phenomena is very limited so that commercial practice and experimental studies have until now been largely empirical. Growth or dissolution of bubbles must be largely determined by the solubilities and diffusivities of gases in the glass melt as well as the actual dissolved concentrations.

Whatever other factors may be involved in refining, improved understanding of the nucleation, growth, and dissolution of multicomponent gas bubbles must help to understand this complex process.

The basic understanding of refining requires precise mathematical formulation of the chemical and physical mechanisms. Their interpretation requires experimental data which are scarce and not always reliable. Mathematical analysis may help to select the significant parameters and contribute to minimize the amount of experimental data required to improve the refining process.

During the earliest stages of melting the system undergoes complex reactions which make the identification of equilibria very difficult and lead to highly inhomogeneous media. Some electrochemical reactions involving metallic objects and corrosion of refractories are occasional sources of problems due to their effects on equilibria and their ability to provide sites for heterogeneous bubble nucleation. The atmosphere can also influence the refining behaviour.

Chemical agents are used to improve the refining of glasses. Adding sulphate may assist melting and refining but the process is more difficult to control than without sulphate. It is necessary to control the amount of

sulphate added and the amount of reducing agents, as well as fining conditions and the atmosphere above the melt. Change of these conditions may cause foaming and reboil. Excess reduction may cause colouration of glass. Other disadvantages of using sulphates are the corrosion of refractories and atmospheric pollution.

Arsenic and antimony are also efficient refining agents but are poisonous and require careful handling.

Which additives are used and the optimum amounts are dependent on the batch constituents, glass composition and melting conditions. Improvement of refining relies mostly on experimental and empirical basis.

Arsenic and antimony are considered to be responsible for changes of bubble composition from mostly CO_2 to O_2, and sulphur compounds, especially sulphates, may cause a change from CO_2 to SO_2 and O_2. Nitrogen often seems to become a major constituent of bubbles late in refining but there is no apparent relation between nitrate additions and N_2 in those bubbles.

Chemical equilibria involving the common refining agents, especially arsenic, antimony, and sulphur compounds change dramatically at temperatures somewhat lower than typical melting conditions. These thermodynamic characteristics may explain the ability of refining agents to promote growth or the dissolution of bubbles during slow cooling of glass melts.

So far even the apparently trivial analysis of the behaviour of spherical bubbles is poor. This will be the scope of the present work. It is impossible to present a clear fitting of the most significant experimental results because the data are scarce and not entirely reliable. Instead we concentrated our attention on the mathematical simulation of the main mechanisms covering both growth and dissolution and a wide variety of significant parameters.

Freely rising bubbles are in practice far more important than stationary ones. However, growth or dissolution of freely-rising bubbles are considerably

more complex than the equivalent behaviour of stationary bubbles. A short account of some approximate mathematical analysis is here discussed as well as a criterion to analyse their applicability to experimental conditions.

1.2 Quantification of refining

Lyle (1945) measured the time required to produce bubble-free melts after adding some batch to glass which had been previously melted and refined. More commonly the changes of the number N of bubbles per unit volume of glass have been used to represent the refining behaviour (Bastick, 1955; Cable, 1958a).

The refining of batch-free melts was found to follow nearly linear relations between log N and time t in laboratory scale (bastick, 1955; Cable, 1958a) and in commercial scale pots (Dubrul, 1955; Cable and co-authors, 1968). The same dependence has been found with a variety of different refining agents, namely, arsenic (Bastick, 1955; Cable, 1958b, 1960b), antimony (Cable and Naqvi, 1975), sulphate (Bhuiyan and Cable, 1965) and halides (Higham and Cable, 1973). All these systems suggest the reduction in the apparent initial value N_0 (obtained by extrapolation of N to zero time), and the change of the slope of the relation log N versus t. A linear relation between log N and log t may describe better some experimental results (Cable and co-authors, 1968, 1975). Even more common is the decrease in the absolute numerical value of the slope of the relation log N versus t at low N.

Nemec (1977a) proposed the decomposition of the time required to produce bubble-free glass samples into two terms: the time required to produce batch-free melts and the time required to remove the residual bubbles by a combination of growth and rise to the surface.

The size distribution of bubbles during refining has been investigated by a few authors (Cable, 1958a). Linear relations between log N and t apply

to narrow ranges of bubble sizes. Size distributions vary with time and refining agents (Cable and Naqvi, 1975) and with the composition of the glass (Haroon, 1967).

Linear relations between the percentage of oxygen in bubbles and log t were found by Cable and co-authors (1968, 1969).

Scatter of experimental measurements is often severe so that large numbers of experiments are required to increase the degree of certainty.

1.3 Refining agents

1.3.1 Arsenic and antimony

Arsenic and antimony are usually efficient refining agents for lead glasses and soda-lime-silica glasses. In the beginning of the XXth century it was still believed that these effects were due to volatilization of arsenic or antimony. Experimental evidence has shown that volatilization rarely is severe (Allen and Zies, 1918).

Gehlhoff et al. (1930) reported results which suggested that as little as 0.02% As_2O_3 promoted the best refining behaviour of soda-lime-silica glasses. Later information showed that about 0.25-0.5% As_2O_3 are frequently the best additions (Cable, 1960b, Cable et al., 1969). These authors confirmed that too large additions can be harmful and that refining with arsenic can be assisted by sodium nitrate and some oxidizing agents (sodium peroxide). Nitrate alone can be deleterious (Potts, 1941) and has no significant effect on bubble composition during refining. Arsenic can also interact with sulphate (Zschimmer et al., 1926; Bhuiyan and Cable, 1965).

Melts with arsenic may require shorter times to become batch-free, than melts without refining additions (Cable, 1961b). Changes of bubble composition from CO_2 to O_2 are also assisted by arsenic (Cable et al., 1969). Arsenic

may even cause an increase of average bubble size and changes of size distributions of bubbles.

The effects of antimony are frequently qualitatively similar to those of arsenic. Zschimmer and Ernuyi (1932) noticed a progressive improvement of refining by increasing the antimony additions, with an optimum at about 0.5% Sb_2O_3. Cable and Naqvi (1975) confirmed optimum additions around 0.6% Sb_2O_3. These authors also found that antimony can shorten the batch-free time, and decrease the concentration of bubbles at that stage, and alkali nitrates improve the effects of antimony.

However, it is clear that arsenic and antimony may have different effects (Bastick, 1955; Reth and Van Velzen, 1973). Antimony is usually more efficient at relatively low melting temperatures and arsenic may perform better at relatively higher temperatures (above about 1400°C). Oxygen rich bubbles can also appear earlier in glasses containing antimony than in glasses with arsenic (Appen and Polyakova, 1938).

The thermodynamics of arsenic and antimony in glasses (Baak, 1959; Baak and Hornyak 1966; Kühl et al., 1938; Cameron, 1965) must influence the refining behaviour. The equilibrium is commonly written

$$\tfrac{1}{2}O_2 + M^{3+}_{(m)} \rightleftharpoons M^{5+}_{(m)} + O^{2-}_{(m)} \qquad (1.1)$$

where (m) denotes the glass melt and M the polyvalent element (As or Sb). The ratio Sb^{3+}/Sb^{5+} in glasses is usually greater than As^{3+}/As^{5+}. If the temperature is sufficiently high the equilibrium is shifted towards the left (large As^{3+} or Sb^{3+} fractions). This change occurs at relatively higher temperatures (above 1500°C) in the case of arsenic than in the case of antimony (Kühl et al., 1938). It is also known that As^{3+}/As^{5+} increases in

reducing conditions (Baak, 1959) and decreases by adding nitrate to the batch, (Cable et al., 1969) and with increasing basicity of the melt (Paul and Lahira, 1963). From equation (1.1) one should expect the ratio As^{3+}/As^{5+} to increase with increasing basicity, which demonstrates that equation (1.1) is wrong about the effect of glass composition.

1.3.2 Sulphate

The improvement of refining by adding sulphate to the glass batch is well known and is widely used in industry. Gehlhoff and co-authors (1930) observed that the best effect was achieved by adding 0.5% Na_2O as sulphate to soda-lime-silica batches melted at 1400°C. Either too small or excessive additions could impair the refining process and with 1.5% sulphate refining was improved by adding carbon to assist decomposition of the sulphate.

Lyle (1956) found two ranges of soda-lime-silica compositions with good and bad sulphase refining respectively. At 1450°C 0.3% sulphate improved refining in the range of compositions

$$\%SiO_2 > 2.2(\%Na_2O) + 44.3 \qquad (1.2)$$

Bhuiyan and Cable (1965) confirmed these findings. They also found that sodium peroxide assisted the process in the range of good refining and arsenic improved the bad refining caused by sulphate alone.

Other alkali and earth-alkali sulphates and ammonium sulphate can assist refining (Parkin and co-authors, 1931). Sulphates with relatively low melting points are usually more efficient than sulphates with high melting points (Guy, 1961; Gottardi et al., 1973). Some waste materials (slags) with large sulphate and sulphide contents have also been successfully used to improve the refining behaviour.

Manring and Hopkins (1958) suggested the use of oxidation-reduction numbers to estimate the best sulphur additions to glass batches. The role of sulphate during melting and refining was explained in terms of acting as a surfactant agent below about 1260°C and by sulphate decomposition and interfacial turbulence (surface tension driven flows) at higher temperatures (Conroy et al., 1966).

1.3.3 Halides

Halides are used as refining agents in borosilicates, and there is some evidence that they can assist common soda-lime-silica glasses (Gehlhoff et al., 1930; Hirayama and Camp, 1969; Higham and Cable, 1973; Van Erk et al., 1977).

Volatilization of halides tends to approach equilibrium concentrations in glass melts (Callow, 1949, 1952; Higham and Cable 1973), and it is not clear what role volatilization plays during refining. Halides can also effect a decrease of viscosity and surface tension which might assist refining (Götz, 1974).

1.3.4 Other chemical agents

It was emphasized that nitrate assists the effects of arsenic and antimony on refining but nitrate alone does not play any significant role. Sodium peroxide has similar effects.

CeO_2 can have some effect on the refining of lead glasses. Apak and Cable (1977) investigated the effects of CeO_2, Cr_2O_3, MnO_2 and Fe_2O_3 on the refining of soda-lime-silica glasses, but general conclusions cannot be drawn.

1.4 Other factors which incluence refining

Most work on refining has been done in isothermal conditions but these processes generally come faster as the temperature is raised (Bastick, 1955; Cable, 1960b). The improvement of refining with increasing temperature is usually greater than the corresponding decrease of viscosity (Lyle, 1945). However, a rapid fall of temperature, soon after the melt becomes batch-free, can be more efficient than refining at constant temperature (Zschimmer et al., 1926; Conroy et al., 1963). These results refer to sulphate refined glasses and there is no precise information about other refining agents.

Too fine or too coarse sands in soda-lime-silica batches can have deleterious effects on refining (Cable, 1958a, 1958b). Glass composition as well as batch composition can also affect the refining behaviour. The effect of cullet was studied by Gehlhoff et al. (1930).

Sulphate refining is affected by oxidizing or reducing atmospheres (Shaw and Jones, 1966; Conroy et al., 1963).

Most of the refining studies can only be carried out in laboratory scale. It is believed that large scale melts can behave qualitatively like small scale laboratory melts, but large melts require longer refining times (Cable et al., 1968). However, quantitative comparisons are very difficult to make.

1.5 Behaviour of individual bubbles

Direct observation of bubbles in glass melts is difficult and usually involves conditions not typical of real melting. Most of these experiments were designed to test diffusion mechanisms but their interpretation was frequently poor due to insufficient data about concentration, solubilities and diffusivities, as well as poor mathematical analysis or ill defined experimental conditions.

The most extensive study of this kind was carried out by Greene and co-authors (1959a, 1959b, 1965, 1969, 1974). Glass samples contained in a small cylinder with a bubble in the centre were rotated during the experiment to keep the bubble relatively stationary. The temperatures used did not exceed 1300°C because of experimental difficulties.

Greene and Gaffney (1959) recorded the dissolution of oxygen bubbles in a commercial silicate glass. The radius of the bubble a was plotted against the square root of time $\sqrt{t}$ but the relation was not strictly true. The initial stage was slower than the intermediate stage and a final residual bubble remained undissolved for very long times.

Greene and Kitano (1959) compared the dissolution rates of oxygen bubbles in four different compositions. In three of these compositions the intermediate stage of dissolution was reasonably given by linear relations between a and $t^{\frac{1}{2}}$ with slopes in the range -0.1 to -0.01 mm/min$^{\frac{1}{2}}$. In the fourth composition the dissolution was better fitted by a linear relation between a and t with slopes in the range -0.04, - 0.01 mm/hr. Dissolution rates were enhanced as the temperature was raised.

Arsenic and nitrate affect the behaviour of oxygen bubbles in soda-lime-silica melts (Greene and Lee, 1965). The dissolution was usually faster in glasses which had been melted from batch in an electric furnace than in glasses melted in a gas-fired furnace (table 1.1). This order was reversed in glasses melted from batch with additions of arsenic and nitrate. In glasses melted in an electric furnace with arsenic and nitrate the rate of dissolution reaches a maximum at about 1255°C and decreases at higher temperature.

In one experiment Greene and Lee stopped the dissolution by lowering the temperature from 1160 to 850°C. After a stage at 850°C the temperature was quickly raised to 1160°C and dissolution continued at about the same rate.

Table 1.1

Effects of melting conditions and refining additions on the rates of dissolution of oxygen bubbles in a soda-lime-silica melt (Greene and Lee, 1965).

furnace		electric	gas-fired
temperature (°C)	additions	$-\frac{da}{dt^{1/2}}$ (mm/min$^{\frac{1}{2}}$)	
1065	None	-	0.0029
1080		0.0047	-
1165		0.013	0.0094
1280		0.044	0.027
1080	arsenic	0.047	0.053
1165		-	0.089
1180		0.107	-
1265		-	0.262
1280		0.300	0.273
1065	arsenic	0.044	-
1080	+	-	0.052
1165	nitrate	0.121	0.141
1255		0.255	-
1265		-	0.318
1280		0.240	-

It was also shown that dissolution rates are greatly enhanced by allowing the free rise of the bubble, which demonstrates that diffusion, not reaction controlled the dissolution. Finally it was suggested that the slopes of the relations $\underline{a}$ versus $\sqrt{t}$ can be nearly independent of the initial radius.

The dissolution of bubbles containing SO_2 or $SO_2 + O_2$ mixtures in soda-lime-silica melts can be also enhanced by adding arsenic and nitrate to the glass batch (Greene and Platts, 1969). The dissolution rate of SO_2 bubbles decreased slightly when sulphate was added to the glass batch.

Cable and Haroon (1970) blew CO_2 bubbles in a soda-lime-silica composition at 1200°C and measured the changes of bubble radius and composition in samples cooled after 3 and 18 minutes treatments. Dissolution rates of CO_2 and changes of bubble composition from CO_2 to O_2 were assisted by adding 0.1% arsenic to the glass batch. Similar procedure was used by Mulfinger (1972) in an alkali-barium silicate melt refined with arsenic and antimony. O_2 bubbles dissolved rapidly leaving residues of N_2 and CO_2. The volume fraction of CO_2 in these bubbles increased rapidly, peaked and dropped again while $\%N_2$ increased at first rapidly and then slowly. Counter-diffusion of N_2 and CO_2 was evident as oxygen was replaced. In N_2 bubbles nitrogen remained the major component, while in CO_2 bubbles the $\%N_2$ increased steadily as CO_2 dissolved.

The method of blowing gas was also used by Greene and Davies (1974) to form bubbles containing N_2,O_2 or water vapour in molten boric oxide. These authors used the rotation of the sample to keep the bubbles effectively stationary. Below 800°C N_2 bubbles dissolved but at higher temperatures these bubbles grew steadily. The volume of steam bubbles decreased rapidly by more than 50%, and then the residual bubbles dissolved slowly (below 800°C) or even grew again (above 800°C). These results suggest the counterdiffusion of other gases (because a decrease in solubility made the melt supersaturated

above 800°C) while the highly soluble water vapour dissolves rapidly. The dissolution of oxygen bubbles in molten B_2O_3 was more complex than in silicate melts.

The rapid initial dissolution of water vapour bubbles in silicate glass was also demonstrated by Nemec (1969). Dissolution almost stopped when the bubble size decreased to about half the initial size.

The effects of melting schedule on subsequent behaviour of bubbles was demonstrated by Brown and Doremus (1976). Dissolution rates were greater in molten B_2O_3 previously equilibrated in air at relatively higher temperatures (1000°C) than in melts which had been held at 550°C. These authors used a simplified form of the quasi-stationary approximate solution of diffusion controlled behaviour of one-component spheres while dealing with bubbles containing at least two gases (O_2 and N_2). However, in spite of this doubtful mathematical analysis, these experiments showed that the dissolution times of bubbles containing initially O_2, N_2, or air were nearly proportional to the square initial radius.

The growth of freely-rising bubbles seems to follow linear relations between the radius of the bubble and time (Solinov and Pankova, 1965; Nemec, 1974, 1977a, 1977b). Growth rates were greatly enhanced by adding arsenic and nitrate or sulphate to the batch. Nemec (1974) showed that the proportion of O_2 in bubbles was enhanced as the additions of arsenic to the batch were increased up to 2%, and in glass melts with arsenic the bubbles started redissolving as the temperature was lowered from 1400°C to 1150°C (Nemec, 1974).

The changes of dissolution rates or changes from growth to dissolution which occur with decreasing temperatures demonstrate the misleading results that may be obtained by studying bubble behaviour at temperatures lower than normal melting conditions. Actual studies of dissolution cannot be

extrapolated to higher temperatures because the solubility of some gases involved in may change considerably with temperature. Changes of diffusivity contribute only to changes in rate of dissolution or growth but cannot reverse the behaviour.

Bubble nucleation and its relation with efficient refining are not precisely understood. Solinov and Pankova (1965) found that bubbles nucleate on solid surfaces especially sand grains. For this reason nucleation rates must decrease sharply when the melt becomes batch-free. Solinov and Pankova also suggested that the size of bubbles leaving the nucleation sites and the wetting angle decreased on adding refining agents.

1.6 Composition of bubbles in glass

Slavyanski (1957) published a review of early experimental analysis of bubble composition, by microchemical methods. Carbon dioxide, oxygen, nitrogen and sulphur dioxide were the most important gases.

Decomposition of carbonates gives rise to large volumes of CO_2. This initial step is rapid and later oxygen might replace CO_2 in bubbles in glasses with arsenic or antimony. This change occurs gradually and the average percentages of oxygen in bubbles can be high in melts not yet free from batch particles (Cable et al., 1968). After long times and in the finished glasses oxygen may have been replaced by nitrogen (Slavyanski, 1957). Too large additions of arsenic or antimony may hinder the change $CO_2 \rightarrow O_2$ in bubbles in glass (Cable et al., 1969; Cable and Naqvi, 1975). Cable and Haroon (1970) have shown that change $CO_2 \rightarrow O_2$ can also occur at relatively low melting temperatures (1200°C) in dissolving bubbles, but Greene and Lee (1965) verified that aresenic usually enhances the dissolution rates of oxygen bubbles below 1300°C. CeO_2, Fe_2O_3 and MnO_2 can also assist the change

from CO_2 to O_2 (Apak and Cable, 1977). Slavyanski (1957) reported some measurements of bubble composition which suggested a change $CO_2 \rightarrow N_2$ in glasses containing arsenic and melted below 1200°C. There is no apparent relation between nitrogen in bubbles and the addition of nitrate to the batch (Cable et al., 1969).

SO_2 may be the common main component of bubbles in glass refined by sulphate. The change $CO_2 \rightarrow SO_2$ occurs relatively early and the change $SO_2 - N_2$ is unlikely to occur in those glasses.

The water content in bubbles was usually not measured and indirect estimates suggest up to about 15% vol in the gas (Cable et al., 1969, 1975).

1.7 Gases dissolved in glass melts

Permeation techniques have been used to measure the permeability P of gases in glass

$$P = S.D$$

where S is the solubility and D the diffusivity of the gas. Obviously these measurements were usually performed below the softening points and cannot be used to analyse the refining process (Scholze, 1968). These results show that the solubility increases with decreasing radius of the diffusing particle but only a very small proportion of the possible structural holes in the glass are occupied by dissolved gas.

Uhlig (1937) derived the following relation

$$\ln K_o = - 4\pi a^2 \sigma / RT \qquad (1.3)$$

where K_o denotes the Ostwald coefficient, that is the ratio between the

concentration of gas in the liquid and the concentration in the gas phase, a is the radius of the particle (atom or molecule), σ the surface tension of the glass, R the Boltzmann constant, and T the absolute temperature. Uhlig's equation has not been verified for gases in glass and it only suggests the qualitative dependence of the solubility on the temperature.

Relatively few measurements of solubilities and concentrations of gases in glass have been reported and data are not always reliable. Measurements at very high pressures may be easier to monitor but their extrapolation to 1 atmosphere is not justified because the Henry's law has a limited range of applicability (Faile and Roy, 1966; Weyl, 1931).

1.7.1 Solubility of inert gases

In spite of having little practical interest the solubility of inert gases has possibly been the most accurately measured. Mulfinger and Scholze (1962a) measured the solubility of helium in alkali-silicates and soda-lime-silica melts. Their results were in the range 0.05-0.16 cm^3 STP/mol glass which are equivalent to Ostwald coefficient K_0 of about 0.02. K_0 increased slightly with increasing temperature. The solubility of those gases decreases with increasing radius of the dissolved atom (Mulfinger et al., 1972) and with increasing alkali content (Mulfinger and Scholze, 1962a). The solubility of inert gases in alkali silicates also increases in the order Li-Na-K, which corresponds to increasing size of the alkali ions. Thus the alkali ions might be responsible for the expansion of the structure of the glass creating new cavities.

1.7.2 Solubility of nitrogen

Mulfinger and Meyer (1963) found that nitrogen can dissolve both physically and chemically in glass melts. Reducing conditions enhance the chemical dissolution (Mulfinger, 1966a). Mulfinger and Franz (1965) found that nitrogen can be present in glasses as nitride and as =NH, and/or $-NH_2$ groups, which suggests the following mechanisms of dissolution

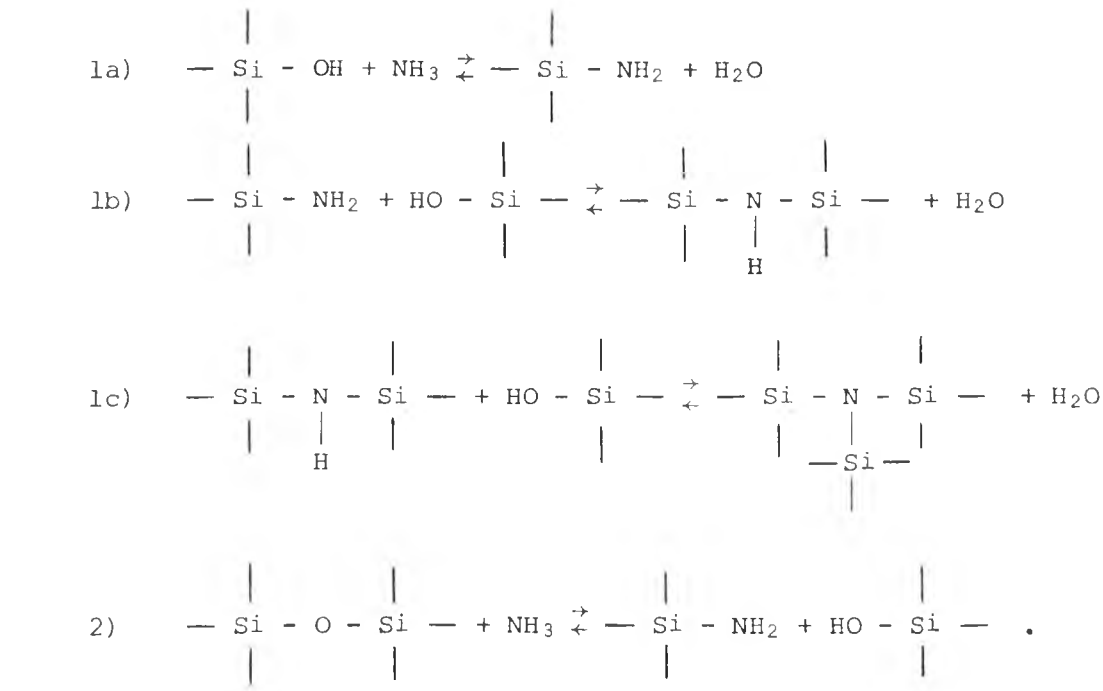

This interpretation agrees with the finding that by bubbling N_2 through a soda-lime-silica melt the resulting equilibrium concentration will be low (about 4.2×10^{-4} cm^3 STP/cm^3 glass at 1400°C) whilst after saturation with ammonia the equilibrium concentration can be as much as about 3.3×10^4 times greater (Mulfinger, 1966a). That value for the saturation with N_2 corresponds to a Ostwald coefficient of about 0.0024.

The solubility of nitrogen in oxidized alkali silicates and soda-lime-silica melts increases slightly with increasing temperature or decreasing basicity (Mulfinger and co-authors, 1972). Similarly the solubility of nitrogen in borate melts increased with decreasing alkali content (Ferrandis

et al., 1972) but decreased in the order Li-Na-K, while the solubility of nitrogen in borate melts was found in the range 0.18-0.27 g N_2/mol B_2O_3, that is much higher than in the silicate with equivalent alkali content.

1.7.3 Solubility of carbon dioxide

Weyl (1931) and Eitel and Weyl (1932) investigated the equilibrium CO_2 content in silicate melts under very high CO_2 pressures. These results did not follow a linear relation between equilibrium CO_2 content in the glass and the CO_2 pressure (Henry's law). The CO_2 content of the glasses increased with increasing basicity and in the order Li-Na-K.

Pearce (1964, 1965) and Strnad (1971) confirmed the effect of basicity of the melt. Pearce's results suggested linear relations between the solubility of CO_2 and the reciprocate of the absolute temperature. His interpretation in terms of ideal behaviour is questionable. Strnad analyzed the soda content of the samples to check volatilization losses and demonstrated that the equilibrium concentration of dissolved CO_2 was proportional to the partial pressure of CO_2 in the gas.

Kroger and Goldman (1962) melted soda-lime-silica glasses (using the ^{14}C isotope to measure the concentration of dissolved CO_2). They found results in the range 4×10^{-5} to 8×10^{-5} wt.% CO_2, which correspond to K_0 in the range 0.0025-0.006. Kroger and Lummerzheim (1965) used the same technique and in a melt with composition about 74 SiO_2-15 Na_2O-11 CaO and found solubilities which are equivalent to Ostwald coefficients 1.38, 0.040, 0.0083 and 0.0085 at 900, 1200, 1300 and 1500°C respectively.

1.7.4 Solubility of oxygen

In spite of its importance the solubility of oxygen in glass melts has received little attention. It is frequently assumed that oxygen participates in reactions of the kind

$$As^{3+}_{(m)} + \frac{1}{2} O_2 \rightleftarrows As^{5+}_{(m)} + O^{2-}_{(m)} \qquad (1.4)$$

$$Sb^{3+}_{(m)} + \frac{1}{2} O_2 \rightleftarrows Sb^{5+}_{(m)} + O^{2-}_{(m)} \qquad (1.5)$$

Other redox pairs may also affect the solubility of oxygen (Douglas et al., 1965).

Thermodynamic data suggest that below 1200°C the pentavalent arsenic or antimony are dominant in glass melts, but at temperatures higher than about 1290°C the equilibrium is shifted and $Sb^{5+}/Sb^{3+} < 1$ (Baak and Hornyak, 1966). $As^{5+}/As^{3+} < 1$ may occur, but usually above 1500°C (Baak, 1959; Kuhl et al., 1938). The fractions of As^{3+} or Sb^{3+} are also nearly unity below 500°C (Kuhl et al., 1938). The exact values of these ratios must depend on glass composition as well as temperature.

Dalton (1933) found that the amount of oxygen extracted from a soda-lime-silica composition which had been refined with 0.5% As_2O_3 was about 0.47 N cm^3 O_2/g glass whereas about 0.56 N cm^3 O_2/g glass could be released by complete conversion of pentavalent to trivalent arsenic. The last quantity represents Ostwald coefficients of about 7 and 8 at 1200°C and 1400°C respectively.

Experiments on the dissolution of oxygen bubbles (Greene and co-authors, 1959) cannot be properly analysed (Doremus, 1960) because none of the values of concentrations, solubility and diffusivity were known.

1.7.5 Solubility of water

Vacuum extraction (Tomlinson, 1956; Russell, 1957, 1958) and infra-red spectroscopy (Scholze, 1959, 1960) were used to determine the water content in glasses. Franz and Scholze (1963) found that the equilibrium water content increases with increasing basicity in silicates which suggests the following mechanism

$$O^{-}_{2\ melt} + H_2O \rightleftarrows 2OH^{-}_{melt}$$

In the range of temperatures 1250-1500°C the Ostwald coefficients of water vapour in soda-lime-silica melts have values of about 20 (Scholze, 1962).

It is believed that water is incorporated as OH^- groups, either free, or hydrogen bonded, with absorption bands at about 2.8 μm and 3.5 μm respectively. This interpretation was confirmed by linear relations between the equilibrium water content and the square root of the partial pressure of water vapour in the atmosphere (Scholze, 1962; Franz, 1965, 1966). Thus the Henry's law does not apply to glass melt-water vapour systems.

The solubility of water in alkali borate melts is usually higher than in silicates with equivalent alkali content. In highly acidic borate melts the solubility of water decreases with increasing alkali content (Franz, 1966) but the solubility is minimum at about 25 mol% K_2O in the system K_2O-B_2O_3 at 900°C. These findings suggested the existence of two different mechanisms of water dissolution in highly acidic and highly basic melts respectively.

The solubility of water increases with increasing temperature in silicate melts (Scholze, 1962) but seems to decrease in borate melts (Franz, 1965).

1.7.6 Solubility of sulphur oxides

A comprehensive study of sulphur in the systems $CaO-Al_2O_3-SiO_2$ and $MgO-SiO_2$ was reported by Fincham and Richardson (1954). These authors found that the solubility of sulphur is strongly dependent on the partial pressure of oxygen and has a minimum at about $P_{O_2} = 10^{-5}$ atm. At high values of P_{O_2} the solubility decreases with increasing temperatures; at very low pressures the solubility rises with increasing temperatures. In oxidizing conditions Fincham and Richardson proposed the following mechanism

$$\frac{1}{2} S_2 + \frac{3}{2} O_2 + O^{2-}_{(m)} \rightleftarrows SO_4{}^{2-}_{(m)} \qquad (1.6)$$

and in reducing conditions

$$\frac{1}{2} S_2 + O^{2-}_{(m)} \rightleftarrows \frac{1}{2} O_2 + S^{2-}_{(m)} \qquad (1.7)$$

In practice the activity coefficients of $SO_4{}^{2-}$, S^{2-} and O^{2-} in glass are not known and the solubility of sulphate or sulphide cannot be estimated from the partial pressures of SO_2 and O_2. Holmquist (1966) produced evidence that the solubility of SO_3 in sodium silicates depends on the product $P_{SO_2}.P_{O_2}{}^{\frac{1}{2}}$, in agreement with equation (1.7). He also showed that the solubility of SO_3 increases with the reciprocal of the temperature and with increasing Na_2O content.

Other authors encountered difficulties when trying to bring the melts to equilibrium with excess Na_2SO_4 (Kordes et al., 1951; Fisher, 1976), or by bubbling SO_2-O_2 gas mixtures through the melts (Papadopoulos, 1973).

1.7.7 Diffusivity of inert gases and nitrogen

Frischat and Oel (1967) found that the diffusivity of inert gases increases very rapidly with the radius of the gas; that is

$$D_{N_2} : D_{Ne} : D_{He} = 1 : 50 : 1000$$

Mulfinger and Scholze (1962b) measured the diffusivity of helium and found it to be in the range 10^{-4} - 4 x 10^{-2} cm^2/sec at temperatures in the range 1200-1500°C. These results show that diffusion is an activated process where the diffusivity is given by

$$D = D_0 \exp(- E/RT) \qquad (1.8)$$

E is the activation energy, R the constant of perfect gas, T the absolute temperature (K) and D_0 the pre-exponential factor. E usually increases with increasing basicity in alkali silicates.

Frischat and Oel (1965) reported measurements of He in soda-lime-silica melts which were consistent with

$$D = 0.0109 \exp[- 14.37 \text{ Kcal mol}^{-1}/RT] \text{ cm}^2 \text{ sec}^{-1} \qquad (1.9)$$

From the dissolution of neon bubbles in similar melts, Frischat and Oel (1967b) obtained a relation

$$D = 4.94 \times 10^{-4} \exp[- 13.7 \text{ Kcal mol}^{-1}/RT] \text{ cm}^2 \text{ sec}^{-1} \qquad (1.10)$$

which suggests that the activation energies are similar in the case of He and Ne.

Measurements of diffusivity of physically dissolved nitrogen in

16 Na_2O-10 CaO-74 SiO_2 in the range 1000-1400°C (Meyer et al., 1977) were described by

$$D_{phys} = 0.43 \exp[-\ 38\ \text{Kcal mol}^{-1}/RT]\ \text{cm}^2\ \text{sec}^{-1} \qquad (1.11)$$

and in a similar composition Frischat et al., (1978) found

$$D_{chem} = 200 \exp[-\ 58\ \text{Kcal mol}^{-1}/RT]\ \text{cm}^2\ \text{sec}^{-1} \qquad (1.12)$$

Their results indicate that diffusivities are equal (about 3.7×10^{-6} $cm^2\ s^{-1}$) at about 1365°C. Physically dissolved N_2 would have the lower diffusivity at higher temperatures. Nitrogen has also a higher temperature coefficient than several other gases, including inert gases and water.

1.7.8 Diffusivity of water

Scholze and Mulfinger (1959) carried out a large number of measurements of diffusivity of water in alkali silicates and other melts. The activation energy was found to increase with increasing basicity but most values of E were close to 20 Kcal mol^{-1}. At 1300°C the diffusivity of water was always in the range 0.65×10^{-6} - 8.4×10^{-6} cm^2/sec.

Garbe (1961) estimated diffusivities of water in sodium silicates at 900°C to be in the range 10^{-7} - 10^{-5} cm^2/sec.

Near the transformation range of a soda-lime-silica composition (522-598°C) Cockram et al., (1969) used a tritium tracer technique and obtained the following relation

$$D = 4.4 \times 10^{-6} \exp[-\ 17200/T]\ \text{cm}^2/\text{sec} \qquad (1.13)$$

Extrapolation to higher temperatures is dubious.

Nemec (1969) used dissolution experiments to estimate the diffusivity of water in soda-lime-silica melts in the range 930-1180°C, but the accuracy of his mathematical analysis is doubtful.

1.7.9 Diffusivity of oxygen

Measurements of self-diffusion of oxygen in glass melts (Terai and Osihi, 1977) may not be useful to analyse the dissolution or growth of bubbles containing oxygen, because it is not clear which species controls the diffusion process. Alternatively Doremus (1960) analysed experimental dissolution of oxygen bubbles to estimate both the diffusivity and a solubility coefficient. For a soda-lime-silica composition at temperatures in the range 1100-1300°C the results were given by $D = 42 \exp(-26.7 \times 10^3/T)$ cm^2/s where T is the absolute temperature (Kelvin). However, the mathematical model used to analyse those experimental measurements may involve significant errors and equally good fitting can be obtained with different combinations of diffusivity and solubility parameter.

1.7.10 Diffusivity of carbon dioxide

Despite being one of the most important gases involved in the refining of glass the diffusivity of carbon dioxide in glass melts has rarely been studied and the data may not be entirely reliable. Kroger and Goldmann (1962) estimated values in the range 10^{-6} - 10^{-4} cm^2 sec^{-1} in silicates at 1100 and 1300°C but their results were based on a very crude analysis.

1.7.11 Diffusivity of sulphur oxides

There are no reliable data in what concerns the diffusivity of products of dissolution of sulphur oxides in glass melts. Absorption or desorption is usually rapid partly due to relatively high solubility of sulphur and

possibly due to flow induced by surface tension gradients (Brückner, 1961, 1962). Mahieux (1956, 1957) showed that SO_3 absorbed from the atmosphere may concentrate in a meniscus. However, Greene and Platts (1969) reported dissolution data which suggest diffusion controlled processes.

1.8 Mathematical analysis of the behaviour of freely rising bubbles

Some experimental studies may suggest that diffusion controlled phenomena control refining but so far its analysis has been hindered by very inadequate knowledge of the relevant physical parameters and by poor mathematical analysis, especially if two or more gases are involved. Direct observation (Solinov and Pankova, 1965; Nemec, 1974) shows that bubbles in glass melts can usually be considered spherical and it is reasonable to assume that their motion is chiefly due to buoyancy. Spherical shape is also expected on theoretical grounds by taking into account the high surface tension of the melt and the small size of most bubbles ($a < 2$ mm).

Free rise of bubbles in glass melts enhances concentration gradients around them by bringing fresh liquid close to the gas-liquid interface. The mathematical analysis of this problem is complex and exact solutions have not been found. Nevertheless such a model is needed for bubbles present in glass melts during refining.

The actual system considered here is an infinite volume of Newtonian liquid surrounding a single spherical bubble. Further simplifications are also assumed:

- the properties of the liquid are uniform and constant,
- there are no reactions in the liquid and transport is exclusively due to diffusion and convection,

- the system is axially symmetric about the vertical axis (direction of motion),
- the bubble contains a single gas with constant concentration C_s,
- the interfacial equilibrium is instantaneously achieved and the concentrations of gas in solution at the interface (C_a) and at infinite distance from the interface (C_∞) are constant,
- the concentration of gas dissolved in the liquid has a negligible effect on its volume and the diffusivity D is constant,
- the flow is controlled by viscosity (in glass melts the Reynolds number is usually much smaller than unity).

In these conditions Levich (1962) proposed solutions for small and medium size spherical bubbles, which should apply to Re << 1 and moderate Re respectively. Levich's solutions were based on quasi steady state approximations (the accumulation term was neglected) and it was assumed that the boundary layers were thin. For Re << 1

$$j_1 = D\left(\frac{\partial C}{\partial r}\right)_a = \sqrt{\frac{3}{2\pi}}\left(\frac{Du}{a}\right)^{\frac{1}{2}} \frac{1 + \cos\theta}{\sqrt{2 + \cos\theta}} (C_\infty - C_a) \qquad (1.15)$$

and for moderate Re

$$j_2 = D\left(\frac{\partial C}{\partial r}\right)_a = \frac{3}{\sqrt{2\pi}}\left(\frac{Du}{a}\right)^{\frac{1}{2}} \frac{1 + \cos\theta}{\sqrt{2 + \cos\theta}} (C_\infty - C_a) \qquad (1.16)$$

where C is the concentration of gas dissolved in the liquid medium, r the radial distance from the centre of the bubble, a the radius of the bubble and the angle θ is measured from the point of incidence of flow. The velocity of motion of the bubble relative to the liquid was given by the

Rubczynski-Hadamard formula, which in the case of gas bubbles reduces to (Levich, 1962).

$$u = \frac{1}{3}\frac{ga^2}{\nu} \tag{1.17}$$

where g is the gravitational acceleration and ν the kinematic viscosity of the liquid medium.

The total diffusional flux is then

$$4\pi a^2 C_s \frac{da}{dt} = 2\pi a^2 D\int_0^{\pi} \sin\theta \left(\frac{\partial C}{\partial r}\right)_a d\theta \tag{1.18}$$

and by combination of equations (1.15), (1.17) and (1.18)

$$\frac{1}{\sqrt{a}}\frac{da}{dt} = \frac{2}{\sqrt{18\pi}}\left(\frac{gD}{\nu}\right)^{\frac{1}{2}}\left(\frac{C_\infty - C_a}{C_s}\right) \tag{1.19}$$

from which it follows that

$$\sqrt{a} - \sqrt{a_0} = \frac{1}{\sqrt{18\pi}}\left(\frac{gD}{\nu}\right)^{\frac{1}{2}}\phi t \tag{1.20}$$

or in dimensionless terms

$$\sqrt{R} = 1 + \left(\frac{A}{18\pi}\right)^{\frac{1}{2}}\phi Z \tag{1.21}$$

where

$$R = a/a_0$$
$$Z = tD/a_0^2$$
$$\phi = (C_\infty - C_a)/C_s \tag{1.22}$$
$$A = g\, a_0^3/(D\nu)$$

and a_0 is the initial radius of the bubble.

Similarly, from equations (1.16), (1.17) and (1.18) the solution for moderate Re values is

$$\sqrt{R} = 1 + \left(\frac{A}{6\pi}\right)^{\frac{1}{2}} \phi Z \tag{1.23}$$

Ruckenstein (1964) suggested a general solution

$$0.849 \left(\frac{u_0}{u}\right)/Sh^2 + 0.662 \left(\frac{3}{2} - 2\,\frac{u_0}{u}\right)/Sh^3 = \left(R_e\, S_c\right)^{-1} \tag{1.24}$$

where u_0 is the tangential component of the velocity at the interface for $\theta = \pi/2$, and

$$Sh = \frac{2a}{\phi D}\frac{da}{dt}$$

$$R_e = 2\, u_a/\nu \tag{1.25}$$

$$S_c = \nu/D$$

For moderate Reynolds numbers Levich (1962) proposed

$$u_0 = \frac{3}{2}\, u \tag{1.26}$$

so that equation (1.24) can be rearranged to

$$\frac{dR}{dZ} = 0.390\,\frac{\phi}{R} + \frac{4.71}{AR\phi^2}\left(\frac{dR}{dZ}\right)^3 \tag{1.27}$$

which, for sufficiently small ϕ, reduces to

$$\sqrt{R} = 1 + 0.230\,\phi\sqrt{A}\, Z \tag{1.28}$$

which is the same as equation (1.23).

For small Re Ruckenstein and Davis (1970) proposed

$$\frac{da}{dt} = \frac{2D}{a}\,\phi\left(\frac{Pe}{3\pi}\right)^{\frac{1}{2}} \tag{1.29}$$

where the Peclet number is

$$Pe = \frac{au}{2D} \,. \tag{1.30}$$

By combination of equations (1.29) with equation (1.17) this solution reduces to equation (1.21).

Some experimental observations of bubbles in glass melts indicate that the radius is proportional to the time (Nemec, 1974). These observations included bubbles containing both oxygen and carbon dioxide so that a two-component model must be used to study these cases. However, the proportions of carbon dioxide in some of those bubbles might have been small and a one-component model for the diffusion of oxygen might be sufficiently accurate. In this case the evidence against equations (1.21) and (1.23) demonstrates the difficulties in formulating sound approximations.

If the bubble is assumed to behave as a solid sphere the diffusion flux becomes (Levich, 1962)

$$j_3 = D\left(\frac{\partial C}{\partial r}\right)_a = \frac{D(C_\infty - C_a)}{1.15}\left(\frac{3u}{4Da^2}\right)^{1/3} \frac{\sin\theta}{\left(\theta - \frac{\sin 2\theta}{2}\right)^{1/3}} \tag{1.31}$$

and

$$2\pi a^2 \int_0^\pi j_3 \sin\theta \, d\theta = 7.98\,(C_\infty - C_a)\left(\frac{D^2 u}{a^2}\right)^{1/3} a^2 \tag{1.32}$$

and if u is given by Stokes's law

$$u = \frac{2}{9}\, ga^2/\nu \quad , \tag{1.33}$$

$$4\pi a^2 \frac{da}{dt} = 4.83 \ (C_\infty - C_a) \left(\frac{D^2 g}{\nu}\right)^{1/3} a^2 \ . \qquad (1.34)$$

Finally after integration and rearranging

$$R = 1 + 0.385 \ \phi \ A^{1/3} \ Z \qquad (1.35)$$

which agrees qualitatively with Menec's findings (1974). Whether that linear relation between radius and time is valid for bubbles of variable composition or only for bubbles of nearly constant composition and containing large proportions of a major component (oxygen) is a question which requires further study.

1.9 Applicability of solutions for rising bubbles

From equation (1.15) the relative boundary layer thickness is

$$\delta_1 = \frac{1}{a}\left[(C_\infty - C_a) \Big/ \left(\frac{\partial C}{\partial r}\right)_a\right] = \sqrt{\frac{2\pi}{3A}} \ \frac{\sqrt{2 + \cos\theta}}{1 + \cos\theta} \ . \qquad (1.36)$$

Similarly from equations (1.16) and (1.31) the equivalent boundary layer thicknesses are

$$\delta_2 = \frac{1}{3} \sqrt{2\pi/A} \ \frac{\sqrt{2 + \cos\theta}}{1 + \cos\theta} \qquad (1.37)$$

$$\delta_3 = \frac{2.09}{R} \ A^{-1/3} \left[\theta - \frac{\sin(2\theta)}{2}\right] \Big/ \sin\theta \ . \qquad (1.38)$$

Equations (1.36), (1.37) and (1.38) provide the means to assess whether the assumption of a thin boundary layer is justified. If $\theta = \pi$ and A is finite δ_1, δ_2 and δ_3 become infinite, so that one has to define a range $\theta < \theta_{max}$ where δ_1, δ_2 or δ_3 are less than a limit δ_{max}. These

conditions impose minimum limits on A (that is size of bubble) and, if a convenient set of physical variables is chosen, the reference radius a_0 must also exceed a minimum value a_{min}. Typical conditions of glass melting can be represented by

$$\text{diffusivity } D = 10^{-6} \text{ cm}^2 \text{ sec}^{-1}$$

$$\text{viscosity } \mu = 92 \text{ poise}$$

$$\text{density of the melt } \rho = 2.3 \times 10^3 \text{ Kg m}^{-3}$$

$$g = 9.8 \text{ m sec}^{-2}$$

By convenient substitution equations (1.36), (1.37) and (1.38) lead to

$$a_0 > a_{min} = 0.04405 \left[\frac{2 + \cos\theta_{max}}{(1 + \cos\theta_{max})^2} \right]^{1/3} \cdot \delta_{max}^{-2/3} \text{ (mm)} \qquad (1.39)$$

$$a_0 > a_{min} = 0.03054 \left[\frac{2 + \cos\theta_{max}}{(1 + \cos\theta_{max})^2} \right]^{1/3} \cdot \delta_{max}^{-2/3} \text{ (mm)} \qquad (1.40)$$

$$a_0 > a_{min} = 0.0720 \left[\theta_{max} - \frac{\sin(2\theta_{max})}{2} \right] \Big/ (\delta_{max} \sin\theta_{max}) \text{ (mm)} . \qquad (1.41)$$

Equation (1.41) has been derived for $a = a_0$, that is $R = 1$.

These relations are represented in fig 1.1 where a_{min} is plotted against θ_{max} for several values of δ_{max}. The full lines denote equation (1.39), the dashed lines equation (1.41) and the dotted-dashed lines equation (1.40). If the boundary layer is kept less than 10% of the radius of the bubble ($\delta_{max} = 0.1$), and $\theta_{max} = \pi/2$ then conditions (1.39), (1.40) and (1.41) will not be fulfilled by bubbles with radius less than about 0.26, 0.18 and 1.1 mm respectively. The fluxes j_1, j_2 or j_3 are

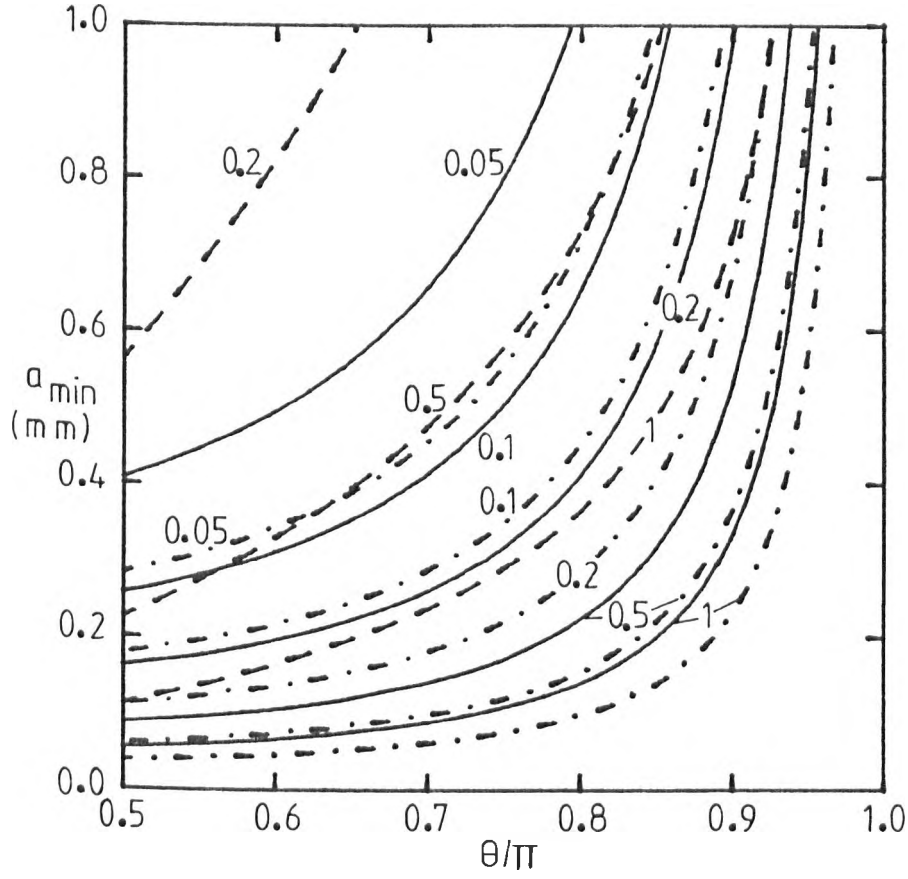

Fig 1.1 : Minimum size of bubbles required to validate Levich's approximations. The full lines represent equation (1.39), the dashed lines equation (1.41), and the dashed-dotted lines equation (1.40). The figures show the values of the ratio δ_{max} of the boundary layer thickness to the radius of the bubble.

larger in the front of the bubble ($\theta < \pi/2$) and the accuracy of predictions $\theta > \pi/2$ will be less important in terms of the overall rate of growth or dissolution. However, those solutions for rising bubbles are not valid for a very important range of bubble sizes ($a < 0.1$ mm) which are common in glass melts and can hardly be removed by rising to the surface of the melt.

Ononato et al. (1981) described the material balances by the following set of equations

$$\frac{\partial C}{\partial t} + V_r \frac{\partial C}{\partial r} + \frac{V_\theta}{r} \frac{\partial C}{\partial \theta} = D\left[\frac{1}{r^2} \frac{\partial}{\partial r} \left(r^2 \frac{\partial C}{\partial r} \right) + \frac{1}{r^2 \sin\theta} \frac{\partial}{\partial \theta} \left(\sin\theta \frac{\partial C}{\partial \theta} \right) \right] \tag{1.42}$$

$$C(r,\theta,t) = C_0 \quad ; \quad r > a_0 \quad ; \quad t = 0 \tag{1.43}$$

$$C(a,\theta,t) = C_a \tag{1.44}$$

$$C(\infty,\theta,t) = C_\infty \tag{1.45}$$

$$\left(\frac{\partial C}{\partial \theta} \right)_{\theta=0} = 0 \tag{1.46}$$

$$\left(\frac{\partial C}{\partial \theta} \right)_{\theta=\pi} = 0 \tag{1.47}$$

$$\frac{d}{dt} \left(\frac{4}{3} \pi a^3 C_s \right) = 2\pi a^2 D \int_0^\pi \left(\frac{\partial C}{\partial r} \right)_{\pi=a} \sin\theta \, d\theta \tag{1.48}$$

$$V_r = u\left(\frac{a}{r} - 1 \right) \cos\theta + \left(\frac{a}{r} \right)^2 \frac{da}{dt} \tag{1.49}$$

$$V_\theta = u\left[\frac{1}{2} \left(\frac{a}{r} \right) - 1 \right] \sin\theta \tag{1.50}$$

which they solved by a finite difference technique. Levich's formulation for $Re << 1$ with constant interfacial concentration C_a is the same as

equations (1.42) to (1.50) when the term $\frac{\partial C}{\partial t}$ is negligible (quasi steady state) and the boundary layer is much thinner than the radius of the sphere. Onorato et al showed that Levich's solutions (equation (1.21)) differ markedly from the numerical solutions of equations (1.42) to (1.50) where u is given by equation (1.17) except for large A, (A > 600). Solutions for stationary bubbles were found to be reasonably good approximations for low A, (A close to unity) but become very poor for large A. Note that A = 1, and 10^3 correspond to a_0 = 0.034 and 0.34 mm respectively when D, μ, ρ and g assume the values indicated previously.

Finite difference solutions might be more accurate than the approximate solutions derived by Levich for rising bubbles, but both methods fail to reproduce the linear relation between radius and time suggested by some experimental observations (Nemec, 1974). Note that the size of bubbles observed by Nemec (usually above 0.5 mm) must be sufficient to make the Levich's approximation (equation (1.20)) reasonably accurate especially taking into account the growth of the bubbles which causes improvement of that approximation. A model based on a solid sphere (equation (1.35)) is apparently more suitable to describe those experimental results. The main reason for those differences might be a poor description of the components V_r and V_θ of the velocity but the hypothesis of a gradual degasification and decrease in bulk concentration of gases dissolved in the melt is also plausible. Such decrease in concentration would cause decrease in growth rate which is in qualitative agreement with a change from $\underline{\sqrt{a}\ \alpha\ t}$ to $\underline{a\ \alpha\ t}$. Finally a multicomponent method is required to describe the behaviour of some bubbles in glass melts. Accurate interpretation of bubble behaviour will not be possible without resolving those questions.

This discussion shows some of the limitations of the solutions available to describe diffusion-controlled behaviour of freely-rising bubbles. The solutions of the diffusion-controlled behaviour of stationary spheres are considerably simpler and the assumptions required to derive reasonably simple balances can be achieved in experimental conditions. In addition, analytical solutions (Scriven, 1959) are available for growth of stationary spheres from zero size and these can be used to test the numerical methods developed to solve other related problems.

CHAPTER II

2.1 Diffusion controlled material transport around stationary spheres

This treatment quantifies the behaviour of spheres which are exchanging material with a surrounding liquid medium. The sphere is assumed to have uniform composition and uniform properties and to be surrounded by an infinite volume of liquid. The only flow in the liquid is assumed to be due to radial convection as the sphere grows or dissolves. The liquid is assumed to have uniform composition and properties at the beginning of the process. Material transport is diffusion controlled with instantaneous interfacial equilibrium and it is assumed that the system remains spherically symmetrical. Different species in the liquid are assumed to diffuse independently, with constant diffusivities. Viscous or inertial forces, surface tension and other external forces are ignored for the present.

The required material balances are considerably simplified in spherically symmetric systems. In addition the liquid medium is assumed to be ideal, that is, with constant partial molar volumes, so that it is possible to define simple relations between the velocity in the liquid and the motion of the interface. It is also possible to derive a simple formulation of Fick's law and to quantify the flux of material across the interface.

Some of these assumptions are only partly fulfilled in real systems and their importance can be investigated by relaxing the corresponding restrictions. Some solutions for cases of concentration dependent diffusivities are reported in Chapter VII. The effects of surface kinetics on growth or dissolution of spheres is discussed in Chapter VIII, and finally the effects of surface tension, viscous and inertial forces are analysed in Chapter IX.

2.2 Continuity with spherical symmetry

A general n+1 component system will be considered with n independent solutes and a solvent denoted by the index n+1. If C_i is the molar concentration of species i and y_i its volume fraction at distance r from the centre of the sphere and at time t,

$$\sum_{i=1}^{n+1} y_i = 1 \tag{2.1}$$

and if the partial molar volume of species i is a constant v_i

$$y_i = v_i C_i \quad ; \quad i=1,\ldots,n \ . \tag{2.2}$$

The velocity $\vec{u}$ is then the sum of fractional contributions of solutes and the contribution of solvent

$$\vec{u} = \sum_{i=1}^{n+1} \vec{u}_i C_i v_i = \sum_{i=1}^{n+1} \vec{u}_i y_i \ . \tag{2.3}$$

$\vec{u}$ is the average volume velocity relative to the fixed coordinate system and can be different from the mass average velocity or molal average velocity (Bird and alia, 1960). In the present circumstances $\vec{u}$ is the more convenient definition of velocity because it reduces the diffusive fluxes to simple forms, even with variable density. In fact, if the only mechanisms of solute transport are convection ($\vec{u}C_i$) and diffusion j_{D_i}, the velocity of species i will be given by

$$\vec{u}_i C_i = \vec{u} C_i + j_{D_i} \ . \tag{2.4}$$

The equivalent relations in terms of mass average velocity or molal average velocity are more complex if the density is variable (Bird and alia, 1960).

Our primary interest is the transfer of individual species so that it is convenient to write the continuity equation for the generic species i

$$\frac{\partial C_i}{\partial t} + (\nabla \cdot \vec{u} C_i) + (\nabla \cdot j_{D_i}) = 0 \tag{2.5}$$

or

$$\frac{\partial C_i}{\partial t} + (\nabla \cdot \vec{u}_i C_i) = 0 \ . \tag{2.6}$$

With spherical symmetry equation (2.6) reduces to (see Appendix 8).

$$\frac{\partial C_i}{\partial t} + \frac{1}{r^2} \frac{\partial}{\partial r} (r^2 u_i C_i) = 0 \tag{2.7}$$

and if the concentration C_i is replaced by the volume fraction y_i with constant partial molar volume,

$$\frac{\partial y_i}{\partial t} + \frac{1}{r^2} \frac{\partial}{\partial r} (r^2 y_i u_i) = 0 \ . \tag{2.8}$$

After summing the n+1 equations (2.8), the overall continuity condition reduces to

$$\frac{\partial}{\partial r} (r^2 u) = 0 \tag{2.9}$$

or

$$u(r) = \left(\frac{a}{r}\right)^2 u(a) \quad ; \quad r \geq a \ , \tag{2.10}$$

where a denotes the radius of the sphere.

Equation (2.10) was previously derived for the case of constant density (Scriven, 1959) and the present formulation extends its validity to more general cases. Notice that constant density, ρ, implies that the partial molar volumes must be equal, this restriction being relaxed in the present treatment.

Equation (2.4) has defined the diffusive flux relative to the velocity of the liquid. Similarly, and in order to maintain the conservation of material the flux J_i of species i into the sphere must be defined relative to the velocity of the interface (da/dt).

$$J_i = -C_i(a)\left[u_i(a) - \frac{da}{dt}\right] \tag{2.11}$$

and from equations (2.2) and (2.11)

$$\sum_{i=1}^{n+1} (v_i J_i) = -\sum_{i=1}^{n+1} y_i(a)\left[u_i(a) - \frac{da}{dt}\right]$$

$$= -u(a) + \frac{da}{dt} \ . \tag{2.12}$$

Also, from equations (2.10) and (2.12)

$$u(r) = \left(\frac{a}{r}\right)^2 \left[\frac{da}{dt} - \sum_{i=1}^{n+1} (v_i J_i)\right] . \tag{2.13}$$

Further simplifications result when the solvent cannot be transferred

into the sphere ($J_{n+1} = 0$) a condition which holds reasonably well for gas bubbles and some crystalline phases. In such cases from equation (2.11)

$$u_{n+1}(a) = \frac{da}{dt} \tag{2.14}$$

and equation (2.13) becomes

$$u(r) = \left(\frac{a}{r}\right)^2 \left[\frac{da}{dt} - \sum_{i=1}^{n} (v_i J_i) \right] , \tag{2.15}$$

that is, the velocity is only dependent on those species being transferred across the interface.

From equations (2.4) and (2.15) with spherical symmetry and assuming that the diffusive flux is given by Fick's law, $\left[j_{D_i} = - D_i \left(\frac{\partial C_i}{\partial r}\right) \right]$,

$$- D_i \left(\frac{\partial C_i}{\partial r}\right)_a = C_i(a) \left[u_i(a) - \frac{da}{dt} + \sum_{j=1}^{n} (v_j J_j) \right] . \tag{2.16}$$

Also, from equations (2.11) and (2.16)

$$J_i = \left[C_i(a) \sum_{\substack{j=1 \\ j \neq i}}^{n} (v_j J_j) + D_i \left(\frac{\partial C_i}{\partial r}\right) \right] \Big/ (1 - C_i(a) v_i) . \tag{2.17}$$

Finally the general material balance with spherical symmetry can be obtained from equations (2.5) and (2.15), with constant diffusivity D_i,

$$D_i \frac{\partial^2 C_i}{\partial r^2} + \left\{ \frac{2}{r} D_i + \left[\sum_{j=1}^{n} (v_j J_j) - \frac{da}{dt} \right] \left(\frac{a}{r}\right)^2 \right\} \frac{\partial C_i}{\partial r} = \frac{\partial C_i}{\partial t} . \tag{2.18}$$

In a uniform medium the initial conditions are

$$C_i(r) = C_{\infty_i} \quad ; \quad r > a \quad ; \quad t = 0 \tag{2.19}$$

and in a infinite medium the boundary condition

$$C_i(\infty) = C_{\infty_i} \quad ; \quad t \geq 0 \ , \tag{2.20}$$

always holds. The concentrations at the interface can vary due to changes of composition in the spherical phase (gas bubble).

2.3 Particular cases

i) One-component spheres

In these cases the pressure and concentration of solute in the sphere (C_s°) can be considered constant and the molar content N of the sphere will be related to the flux J by

$$\frac{dN}{dt} = 4\pi a^2 \, C_s^\circ \, \frac{da}{dt} = 4\pi a^2 J \ , \tag{2.21}$$

where the subscripts are omitted in one-component systems. From equations (2.17) and (2.21)

$$\frac{dN}{dt} = 4\pi a^2 \, D \left[1 - C(a) v \right]^{-1} \left(\frac{\partial C}{\partial r} \right)_a \tag{2.22}$$

and

$$\frac{da}{dt} = D\left[C_s^{\circ}(1 - C(a)v) \right]^{-1} \left(\frac{\partial C}{\partial r}\right)_a . \qquad (2.23)$$

In addition, from equations (2.18) and (2.21)

$$\frac{\partial C}{\partial t} = D\frac{\partial^2 C}{\partial r^2} + \left[\frac{2}{r} D - \varepsilon\left(\frac{a}{r}\right)^2 \frac{da}{dt} \right]\frac{\partial C}{\partial r} \qquad (2.24)$$

where

$$\varepsilon = 1 - C_s^{\circ}v . \qquad (2.25)$$

The term $(1-\varepsilon)$ represents the ratio of the volume occupied by a mole of solute in the liquid medium to that in the sphere. This condition is valid whenever the partial molar volumes in the liquid are constant.

The assumption of instantaneous equilibrium at the interface leads to constant boundary conditions

$$\begin{aligned} C(a) &= C_a \\ C(\infty) &= C_\infty \end{aligned} \qquad t \geq 0 \qquad (2.26)$$

and the initial conditions will be

$$C(r) = C_\infty \quad ; \quad r > a \quad ; \quad t = 0 . \qquad (2.27)$$

Equations (2.23) and (2.24) can be simplified by using dimensionless variables

$$\frac{\partial^2 F}{\partial e^2} + \left[\frac{2}{e} - \varepsilon \left(\frac{R}{e} \right)^2 \frac{dR}{dz} \right] \frac{\partial F}{\partial e} = \frac{\partial F}{\partial z} \tag{2.28}$$

and

$$\frac{dR}{dz} = \left(\frac{\partial F}{\partial e} \right)_R \tag{2.29}$$

where

$$\begin{aligned} e &= r/a_0 \\ R &= a/a_0 \\ z &= t.D/a_0^2 \\ F &= (C - C_\infty)/[C_s^\circ (1 - vC_a)] \end{aligned} \tag{2.30}$$

and a_0 is the reference radius ($a_0 > 0$), which will denote the initial radius of dissolving spheres or of spheres growing from finite size.

In dimensionless form the boundary and initial conditions (2.26) and (2.27) lead to

$$F(R) = F_a = (C_a - C_\infty)/[C_s^\circ (1 - vC_a)] \tag{2.31}$$

$$F(\infty) = 0 \tag{2.32}$$

$$F(e) = 0 \quad ; \quad e > R \quad ; \quad z = 0 \, . \tag{2.33}$$

ii) n-Component gas bubbles

With constant temperature and constant pressure the molar concentration inside an ideal gas bubble can be considered constant at C_s° and therefore

$$\frac{dN_i}{dt} = 4\pi\, C_s^\circ \frac{d}{dt}\,(a^3 g_i) = 4\pi a^2\, J_i \quad , \tag{2.34}$$

where N_i is the number of moles of species i in the bubble and g_i its volume fraction, which is equal to the mole fraction in an ideal gas mixture.

From equation (2.34)

$$J_i v_i = C_s^\circ\, v_i \left[g_i \frac{da}{dt} + \frac{a}{3} \frac{dg_i}{dt} \right] \tag{2.35}$$

and at ordinary temperatures and pressures

$$v_i\, C_s^\circ << 1 \tag{2.36}$$

and

$$y_i(a) = v_i\, C_i(a) << 1 \quad , \tag{2.37}$$

and equations (2.17) and (2.18) reduce to

$$J_i = D_i \left(\frac{\partial C_i}{\partial r} \right)_a \tag{2.38}$$

and

$$D_i \frac{\partial^2 C_i}{\partial r^2} + \left[\frac{2}{r} D_i - \varepsilon \left(\frac{a}{r}\right)^2 \frac{da}{dt} \right] \frac{\partial C_i}{\partial r} = \frac{\partial C_i}{\partial t} \quad , \tag{2.39}$$

with $\varepsilon = 1$ in the case of gas bubbles.

From equations (2.34) and (2.38)

$$\frac{dN_i}{dt} = 4\pi a^2 J_i = 4\pi a^2 D_i \left(\frac{\partial C_i}{\partial r}\right)_a \tag{2.40}$$

and

$$\sum_{i=1}^{n} \frac{dN_i}{dt} = 4\pi a^2 C_s^{\circ} \frac{da}{dt} \tag{2.41}$$

with

$$\sum_{i=1}^{n} g_i = 1 \quad . \tag{2.42}$$

Also from equations (2.40) and (2.41)

$$\frac{da}{dt} = \sum_{i=1}^{n} \left[\frac{D_i}{C_s^{\circ}} \left(\frac{\partial C_i}{\partial r}\right)_a \right] \tag{2.43}$$

and equations (2.35) and (2.40) give

$$\frac{dg_i}{dt} = \frac{3}{a}\left[(D_i/C_s^{\circ}) \left(\frac{\partial C_i}{\partial r}\right)_a - g_i \frac{da}{dt} \right] . \tag{2.44}$$

The equilibrium at the interface may usually be assumed to be given by

Henry's law so that

$$C_i(a) = H_i\, p_i \tag{2.45}$$

where H_i and p_i are the Henry's law constant and the parti al pressure of species i. By combining Henry's law and Dalton's law for ideal gas solutions

$$C_i(a) = H_i\, P\, g_i = C_{p_i}\, g_i \tag{2.46}$$

where C_{p_i} is the interfacial concentration of species i in the liquid in equilibrium with gas at a standard pressure P (e.g. 1 atmosphere).

In dimensionless terms equations (2.39), (2.40), (2.43) and (2.44) become

$$f_i \frac{\partial^2 F_i}{\partial e^2} + \left[\frac{2}{e} f_i - \varepsilon \left(\frac{R}{e}\right)^2 \frac{dR}{dz} \right] \frac{\partial F_i}{\partial e} = \frac{\partial F_i}{\partial z} \tag{2.47}$$

$$\frac{dG_i}{dz} = 4\pi R^2 f_i \left(\frac{\partial F_i}{\partial e}\right)_R , \tag{2.48}$$

$$\frac{dR}{dz} = \sum_{i=1}^{n} \left[f_i \left(\frac{\partial F_i}{\partial e}\right)_R \right] , \tag{2.49}$$

and

$$\frac{dq_i}{dz} = \frac{3}{R}\left[f_i \left(\frac{\partial F_i}{\partial e}\right)_R - q_i \frac{dR}{dz} \right] , \tag{2.50}$$

where

$$z = t\, D_l / a_0^2$$

$$f_i = D_i / D_l \qquad (2.51)$$

$$F_i = (C_i - C_\infty)/C_s^\circ$$

$$G_i = N_i/(a_0^3\, C_s^\circ)$$

Finally the initial (equation (2.19)) and boundary conditions (equations (2.20) and (2.46)) become

$$F_i(e) = 0 \quad ; \quad e > R \quad ; \quad z = 0 \qquad (2.52)$$

$$F_i(\infty) = 0 \quad ; \quad z \geq 0 \qquad (2.53)$$

$$F_i(R) = \alpha_i g_i - F_{o_i} \quad ; \quad z \geq 0 \qquad (2.54)$$

where

$$\alpha_i = C_{p_i}/C_s^\circ$$

$$F_{o_i} = C_{\infty_i}/C_s^\circ \qquad (2.55)$$

2.4 Typical parameters in glass melts

The present formulation of dimensionless balances show that α_i, F_{o_i}, g_i and f_i are the essential parameters. Ostwald solubility coefficient of species i is identical to α_i and from the scarce solubility data available for silicate melts we can expect the following ranges of α_i values to be typical.

0.001-0.01 for nitrogen (dissolved physically),

0.001-0.05 for carbon dioxide,

up to 10 for oxygen,

around 20 for water.

It is reasonable to assume that the bulk concentration C_{∞_i} must be of

the same order of magnitude as C_{p_i}, so that the solubility parameter $[\alpha_i - F_{o_i}]$ will have the order of magnitude of the Ostwald coefficient.

Measurements in silicate glasses showed that the diffusivities of water (Scholze and Mulfinger, 1959) and nitrogen (Meyer and alia, 1977) at about 1400°C are usually in the range 10^{-6}-10^{-5} cm^2 sec^{-1}. Some estimates of the diffusivity of carbon dioxide in glass melts (Kroger and Goldmann, 1962) are based on a crude technique and seem somewhat higher than those of water but this seems rather unlikely. From experimental dissolution of oxygen bubbles in soda-lime-silica melts at temperatures in the range 1100-1300°C Doremus (1960) obtained the relation $D = 42 \exp(-26.7 \times 10^3/T)$ cm^2/sec where T is the absolute temperature (Kelvin). Extrapolation of this relation to 1400°C gives a value of about 5×10^{-6} cm^2/sec for the diffusivity of oxygen. Therefore, the relevant gases are expected to have diffusivities of the same order of magnitude and ratios $0.1 < f_i < 10$ are likely to occur.

2.5 Solutions for one-component spheres

Exact solutions of the relevant partial differential equations governing the growth of spheres from zero size were obtained after Boltzmann transformations (Frank, 1950; Scriven, 1959). These solutions do not describe the growth from finite size and the partial differential equations governing dissolution cannot be cast into the required ordinary differential equations.

Epstein and Plesset (1950) obtained quasi-stationary solutions by neglecting the convective transport of solute. For gas bubbles those approximations were

$$\frac{da}{dt} = D \frac{(C_\infty - C_a)}{C_s^\circ} \left(\frac{1}{a} - \frac{1}{\sqrt{\pi D t}} \right) \tag{2.56}$$

and in dimensionless terms

$$\begin{aligned} \frac{dR}{dz} &= - F_a \left(\frac{1}{R} + \frac{1}{\sqrt{\pi z}} \right) \\ &= \phi \left(\frac{1}{R} + \frac{1}{\sqrt{\pi z}} \right) . \end{aligned} \tag{2.57}$$

Parametric solutions of equation (2.57) were reported by Epstein and Plesset (1950), and Frischat and Oel (1965), and the concentration profiles which correspond to quasi-stationary solutions can be obtained by analogy with the equivalent heat conduction problem (Carslaw and Jaeger, 1959).

$$F(e,z) = F_a \left(\frac{R}{e} \right) \operatorname{erfc} \left(\frac{e - R}{2\sqrt{z}} \right) \quad ; \quad e \geq R \tag{2.58}$$

and

$$\left(\frac{\partial F}{\partial e} \right)_R = - F_a \left(\frac{1}{R} + \frac{1}{\sqrt{\pi z}} \right) . \tag{2.59}$$

A transformed quasi-stationary solution is obtained if equation (2.59) is approximated by

$$\left(\frac{\partial F}{\partial e} \right)_R = - \frac{F_a}{R} \left(1 + \frac{1}{\sqrt{\pi z}} \right) \tag{2.60}$$

which upon combination with equation (2.29) leads to

$$R^2 = 1 + 2\phi z + 4\phi\sqrt{z/\pi} \quad . \tag{2.61}$$

On the contrary, if the interface is kept stationary

$$\left(\frac{\partial F}{\partial e}\right)_R = - F_a\left(\frac{1}{R_0} + \frac{1}{\sqrt{\pi z}}\right) \tag{2 62}$$

and from equations (2.29) and (2.62)

$$R = 1 + \phi z + 2\phi\sqrt{z/\pi} \quad . \tag{2.63}$$

Equation (2.57) was used to analyse the behaviour of bubbles in liquids (Krieger and alia, 1967; Frischat and Oel, 1965). Equally equation (2.61) was also used to analyse experimental data, (Doremus, 1960) and was recovered as the zero order approximation of perturbation series solutions (Duda and Vrentas, 1969; Vrentas and Shin, 1980).

If $R >> \sqrt{\pi z}$ the quasi stationary solution (equation 2.57)) tends to

$$R = 1 + \frac{2}{\sqrt{\pi}}\phi\sqrt{z} \tag{2.64}$$

which can be derived from the one-dimensional diffusion in a semi-infinite medium. In dimensionless form the concentration profile is given by (Crank, 1975)

$$F(e,z) = F_a \operatorname{erfc}[(e - R)/(2/\sqrt{z})] \tag{2.65}$$

and

$$\left(\frac{\partial F}{\partial e}\right)_R = - F_a/\sqrt{\pi z} \quad . \tag{2.66}$$

Thus equation (2.64) results from equations (2.29) and (2.66). As an approximation of the spherically symmetric system equation (2.66) requires very thin boundary layers. During dissolution the role of radial convection prevents that condition, even if the solubility is very large.

A simple quasi steady-state solution was also used to evaluate diffusion coefficients of gases in liquids (Liebermann, 1957; Manley, 1960). The convective transport of solute and the time derivative were ignored in equations (2.24) or (2.28), which reduce to

$$\frac{1}{e^2}\frac{\partial}{\partial e}\left(e^2 \frac{\partial F}{\partial e}\right) = 0 \quad ; \quad e \geq R \quad . \tag{2.67}$$

Equation (2.67) with boundary conditions (2.31), and (2.32) is readily integrated to give

$$\left(\frac{\partial F}{\partial e}\right)_R = - F_a/R = \phi/R \tag{2.68}$$

and

$$F = F_a(R/e) \quad ; \quad e \geq R \quad . \tag{2.69}$$

From equations (2.29) and (2.68) the quasi steady-state solution for the radius of the sphere is

$$\mathbf{R}^2 = 1 + 2\phi z = 1 - 2F_a z \quad . \tag{2.70}$$

Notice that equation (2.70) is equally recovered as the limit of quasi-stationary approximations for $\sqrt{\pi z} >> R$.

From asymptotic expansions Subramanian and Weinberg (1980) derived the following relation

$$R^2 = 1 - \frac{4F_a}{\sqrt{\pi}}\sqrt{z} + 4F_a\left(\frac{5F_a}{3\pi} - \frac{1}{2}\right)z + \frac{8F_a^2}{\sqrt{\pi}}\left(\frac{4}{3} - \frac{16}{5\pi} - \frac{5F_a}{9\pi}\right)z^{3/2} . \qquad (2.71)$$

This equation was found to perform generally better than the quasi steady-state or quasi stationary approximations (Chapter V).

Some predictions of growth were based on the assumption that the boundary layers are sufficiently thin (Barlow and Langlois, 1962). That assumption is generally poor except for growth with large solubility parameters for which exact solutions are available (Scriven, 1959).

Perturbation series solutions (Duda and Vrentas, 1969; Vrentas and Shin, 1980) are tedious to evaluate, except for terms of zero order, which usually reduce to the transformed quasi-stationary approximation (equation (2.61)). First order terms are reasonably good corrections in the range of low solubility parameters.

Numerical solutions were also developed to solve equations (2.23) and (2.24) after normalizing the concentration (Readey and Cooper, 1966; Cable and Evans, 1967). Other authors used transformations of the space variable to immobilize the interface (Duda and Vrentas, 1969; Szekely and Martins, 1971). These techniques did not include sequential optimization of space and time mesh sizes, so that either their accuracy is doubtful or the procedure wasteful of computing facilities.

2.6 Solutions for multicomponent bubbles

The diffusion controlled growth or dissolution of bubbles containing more than one gas has rarely been considered because variable boundary conditions are usually involved. Interactions between the different dissolved species can usually be ignored in the case of very dilute solutions. Gas bubbles can usually be included in this classification and diffusivities can also be considered constant and independent of concentrations. Henry's law is usually assumed to describe the equilibrium gas-liquid, but diatomic gases are sometimes better fitted by the Sievert's law (linear relationship between the concentration of solute in the liquid and the square root of partial pressure of gas). It is widely accepted that the Sievert's law describes the equilibrium for water vapour in glass melts (Scholze, 1962; Franz, 1965 and 1966).

Quasi stationary approximations were used by Kramer (1979) to analyse the behaviour of bubbles containing more than one gas. The limitations of the quasi stationary approximations of the behaviour of multicomponent bubbles are likely to be even greater than in the case of one-component bubbles. Quasi stationary solutions were also used to analyse the behaviour of bubbles containing one diffusing gas and another inert gas (Doremus, 1960; Nemec, 1969; Weinberg and alia, 1980).

Finite difference techniques were occasionally used to solve the behaviour of bubbles containing two gases (Griffin, 1971) or more (Weinberg and Subramanian 1980), but the accuracy of those methods has not been tested.

It will be demonstrated in Chapter VI that an exact asymptotic regime can be derived for bubbles containing two or more gases and growing from zero size. This regime will be used to test the general finite-difference technique described in Chapter III.

CHAPTER III

Finite difference techniques

3.1 Introduction

Analytical solutions of equations (2.47) have limited applicability and the accuracy of published approximate solution has not been systematically tested, except for a few cases usually in the range of moderate or low solubility parameters ϕ or F_a. Numerical solutions are an attractive alternative but very few cases have been computed. In no cases were the efficiency and accuracy of methods used properly established.

The basic partial differential equation (2.47) is parabolic with known initial and boundary conditions but is non-linear due to motion of the interface. Fortunately the diffusion controlled growth of spheres from zero size can be solved analytically so that it is possible to test the convergence of the finite difference equations to these exact solutions of the partial differential equations for those cases provided that computations are continued to large enough sizes.

In practice the finite difference solutions start with a finite size of the sphere ($a_0 > 0$) so that it is necessary to compute large increases of radius ($R >> 1$) to overcome the effects of the initial transient stage. However, another difficulty arises because of the large changes in the radius of the sphere, boundary layer thicknesses and rates of growth or dissolution. The same values of space and time steps cannot be both accurate and efficient in the early stages and much later. For instance if the radius increases by a factor of 1000 it might be convenient to increase the mesh lengths by similar factors for economy of computing.

This difficulty may be partly solved by appropriately transforming

the independent variables (space and time), but it is still convenient to be able to vary the mesh lengths, especially during the transient stages and when the interfacial concentrations vary with time.

Variable interfacial concentrations and variable mesh lengths put an additional constraint on the stability of the difference equations. It is well established (Smith, 1978) that implicit methods with constant δr and δt (or δe and δz) mesh lengths are stable for all positive values of $\delta z/(\delta e)^2$ when used to solve some equations of the parabolic type (Crank and Nicolson, 1947). On the contrary explicit methods usually require $\delta z/(\delta e)^2 < 1/2$.

Readey and Cooper (1966) developed finite difference solutions of the relevant differential equation, with $\delta z/(\delta e)^2 = 0.1$ to guarantee the stability of these solutions. However, they must have experienced the difficulty of having to use fairly large δe increments to prevent the growth of rounding errors, but did so at the expense of the accuracy of the finite difference solutions, especially when the rate of the process is large (thin boundary layers). In addition, this method requires an unduly large number of time steps to compute very slow growth, growth to very large sizes, or very slow dissolution.

Cable and Evans (1967) used a different explicit scheme based on formulae using three time steps proposed by Du Fort and Frankel (1953). The restriction $\delta z/(\delta e)^2 < 1/2$ could be dropped but the mesh lengths were not optimized, so that the convergence of finite difference equations may be poor, especially when the sphere dissolves and the concentration gradients at the interface increase with time during the final stage (Chapter V). Establishing that the results are insensitive to choice of time and space mesh intervals is not sufficient to guarantee accuracy.

Duda and Vrentas (1969, 1971) developed an implicit method and

normalized the space variable accordingly to the following transformations:

$$x = 1 - \exp[-\alpha(r - a)] \qquad (3.1).$$

for dissolution, and

$$x = 1 - \exp\left[-\alpha\left(\frac{r}{a} - 1\right)\right] \qquad (3.2)$$

for growth. The constant α allows some flexibility of the transformation. However, these authors used constant δx increments throughout each run. By varying δx and δt it was established that the difference solutions converged to each other and, though this is not a rigorous proof, it is a good indication that the finite difference equation is convergent to the true solution of the partial differential equation. Computations of large increases in radius are prohibitive in computing time if constant mesh sizes are used, and the convergence of their finite difference solutions to the exact solutions for growth from zero size was not demonstrated.

Szekely and co-authors (1971, 1973) used the transformation of space variable into $x = e - R$ and allowed some adjustment of the space mesh size with a ratio $\delta z/(\delta x)^2$ kept at about 0.4 to ensure stability and economy. A Runge-Kutta method was used to advance from a given time step to the next one. The stability condition was suitable to analyse rapid growth, but is likely to make the computations of low and moderate rates of growth or dissolution prohibitively slow because of the restrictions on δz.

3.2 Immobilization of the interface

It is convenient to immobilize the interface by transforming the space variable. This avoids having to add new mesh points at the interface of dissolving spheres or the elimination of points as the

interface of a growing sphere advances. Besides, without immobilizing the interface, the use of implicit finite difference solutions is inhibited.

A successful transformation is the one which, whenever possible, improves the convergence of the finite difference solutions. For this purpose it is convenient to analyse the nature of the diffusion phenomena involved.

Exact solutions for growth from zero size can be expressed by the dependence of concentrations on a single independent variable $x = r/a = e/R$ (Scriven, 1959). This type of solution has now been extended to multi-component bubbles (see Chapter VI). It is also demonstrated in Chapters IV and VI that the solutions for growth from finite size evolve rapidly to the same type of regime. Therefore, if the space variable is transformed into $x = r/a$, the concentrations become less dependent on a second independent variable (time), which assists the convergence of the finite difference solutions.

Dissolution of spheres is essentially transient and reflects the effects of diffusion and convection in the radial direction (Chapter V). Diffusion is usually dominant but the role of radial convection is very important with large solubility parameters F_a.

For low F_a the actual solutions are reasonably approximated by quasi steady-state predictions which demonstrate the effect of spherical symmetry, and reduce to $F(x) = F_a/x$, (equation (2.69)). Thus the transformation of the space variable into x must be equally convenient for accurately computing dissolution.

If transport is controlled by radial convection the most successful transformation must be the use of the Lagrange coordinate $(r^3 - a^3)$ or $(e^3 - R^3)$ to replace $\underline{r}$ or $\underline{e}$. By use of the Lagrange coordinate the

convergence of finite difference solutions was found to be good for very large solubility parameters ($F_a > 100$) but it was difficult to obtain convergent predictions in the range $F_a < 10$. On the contrary, if the space variable is transformed into x, the solutions converge readily in the entire ranges investigated, $0.0001 < F_a < 1000$, and $0.0001 < \phi < 1000$.

Duda and Vrentas (1969) used a normalized transformed variable to avoid having to truncate the distance over which the computations are carried out. This may be convenient if constant mesh sizes δx are used but is not necessary if the mesh size is allowed to increase in the tail of the profile. Besides, it has been found in this work that with transformation of the space variable into $x = e/R$ the convergence of the finite difference solutions was more easily achieved with moderately low numbers of time steps than in the case of transformation into $1 - 1/x$.

Taking into account these features equations (2.47) to (2.50) were transformed into

$$f_i R^{-2} \frac{\partial^2 F_i}{\partial x^2} + \left[\frac{2}{x} f_i R^{-2} + \frac{1}{R} \frac{dR}{dZ} (x - \varepsilon x^{-2}) \right] \frac{\partial F_i}{\partial x} = \frac{\partial F_i}{\partial Z} \tag{3.3}$$

$$\frac{dG_i}{dZ} = 4\pi R f_i \left(\frac{\partial F_i}{\partial x} \right)_{x=1} \tag{3.4}$$

$$\frac{dR}{dZ} = R^{-1} \sum_{i=1}^{n} \left[f_i \left(\frac{\partial F_i}{\partial x} \right)_{x=1} \right] \tag{3.5}$$

$$\left(\frac{dg_i}{dZ} \right) = 3 \left[f_i R^{-2} \left(\frac{\partial F}{\partial x} \right)_{x=1} - g_i R^{-1} \frac{dR}{dZ} \right] \tag{3.6}$$

where

$$x = e/R \geq 1 \quad .$$

3.3 Solution of concentration profiles

3.3.1 Finite difference equations

The concentrations and their derivatives are single valued, finite and continuous so that Taylor's expansion gives

$$F_{i,j+1,\ell+1} = F_{i,j,\ell} + \delta x_2 \left(\frac{\partial F_i}{\partial x}\right)_{j,\ell} + \frac{1}{2}(\delta x_2)^2 \left(\frac{\partial^2 F_i}{\partial x^2}\right)_{j,\ell} + \ldots \qquad (3.7)$$

$$F_{i,j-1,\ell+1} = F_{i,j,\ell} - \delta x_1 \left(\frac{\partial F_i}{\partial x}\right)_{j,\ell} + \frac{1}{2}(\delta x_1)^2 \left(\frac{\partial^2 F_i}{\partial x^2}\right)_{j,\ell} - \ldots \qquad (3.8)$$

where

$$\delta x_1 = x_j - x_{j-1}$$

$$\delta x_2 = x_{j+1} - x_j \ .$$

The indices i, j and ℓ denote the species i, the radial mesh point x_j, and the time step Z_ℓ.

Using a compromise between the truncation errors involved and the simplicity of algorithms equations (3.7) and (3.8) lead to

$$\left(\frac{\partial F_i}{\partial x}\right)_{j,\ell} = (\delta x_1 + \delta x_2)^{-1} \left[\frac{\delta x_1}{\delta x_2} F_{i,j+1,\ell} + \left(\frac{\delta x_2}{\delta x_1} - \frac{\delta x_1}{\delta x_2}\right) F_{i,j,\ell} - \frac{\delta x_2}{\delta x_1} F_{i,j-1,\ell} \right] \qquad (3.9)$$

and

$$\left(\frac{\partial^2 F_i}{\partial x^2}\right)_{j,\ell} = \frac{2}{\delta x_1 + \delta x_2} \left[\frac{F_{i,j+1,\ell}}{\delta x_2} - \left(\frac{1}{\delta x_2} + \frac{1}{\delta x_1}\right) F_{i,j,\ell} + \frac{F_{i,j-1,\ell}}{\delta x_1} \right] \ . \qquad (3.10)$$

This procedure allows the use of different mesh sizes and makes it possible to optimize the number and distribution of mesh points. By substitution of equations (3.9) and (3.10) into equation (3.3)

$$\left(\frac{\partial F_i}{\partial Z}\right)_{j,\ell} = 2\Big[\, p_1\, F_{i,j-1,\ell} - (p_1 + p_2)\, F_{i,j,\ell} + p_2\, F_{i,j+1,\ell} \,\Big] \qquad (3.11)$$

where

$$p_1 = (f_i/R^2 - \gamma\, \delta x_2)/[\delta x_1(\delta x_1 + \delta x_2)] \qquad (3.12)$$

$$p_2 = (f_i/R^2 + \gamma\, \delta x_1)/[\delta x_2(\delta x_1 + \delta x_2)] \qquad (3.13)$$

$$\gamma = f_i/(x_j\, R^2) + \frac{1}{2R}\frac{dR}{dZ}\left[x_j - \varepsilon\, x_j^{-2}\right] . \qquad (3.14)$$

It is well known that the stability of implicit methods is usually superior to the stability of explicit methods. Let R_{av} be the average radius of the sphere between time steps Z_ℓ and $Z_{\ell+1}$ and $\left(\frac{dR}{dZ}\right)_{av}$ the average time derivative so that

$$\gamma = f_i \Big/ \Big[\, x_j (R^2)_{av} \,\Big] + \frac{1}{2R_{av}}\left(\frac{dR}{dZ}\right)_{av}\left[x_j - \varepsilon\, x_j^{-2}\right] \qquad (3.15)$$

where

$$R_{av} = \Big[\, R_{\ell+1} + R_\ell \,\Big]\Big/2 \quad ; \quad (R^2)_{av} = \frac{R_{\ell+1}^{\,2} + R_\ell\, R_{\ell+1} + R_\ell^{\,2}}{3}$$

$$\left(\frac{dR}{dZ}\right)_{av} = \Big(R_{\ell+1} - R_\ell\Big)\Big/\delta Z$$

and

$$\delta Z = Z_{\ell+1} - Z_\ell \ .$$

Next equation (3.11) is replaced by the finite difference average

$$\left[F_{i,j,\ell+1} - F_{i,j,\ell} \right] / \delta Z = p_1 \left(F_{i,j-1,\ell} + F_{i,j-1,\ell+1} \right) - (p_1 + p_2) \left(F_{i,j,\ell} + F_{i,j,\ell+1} \right) + p_2 \left(F_{i,j+1,\ell} + F_{i,j+1,\ell+1} \right) \tag{3.16}$$

which leads to the implicit scheme

$$b_{1,j} F_{i,j-1,\ell+1} + b_{2,j} F_{i,j,\ell+1} + b_{3,j} F_{i,j+1,\ell+1} = b_{4,j} \tag{3.17}$$

where

$$b_{1,j} = - \delta Z \, p_1 \tag{3.18}$$

$$b_{3,j} = - \delta Z \, p_2 \tag{3.19}$$

$$b_{2,j} = 1 + \delta Z (p_1 + p_2) = 1 - b_{1,j} - b_{3,j} \tag{3.20}$$

$$b_{4,j} = \delta Z \left[p_1 F_{i,j-1,\ell} + p_2 F_{i,j+1,\ell} \right] + \left[1 - \delta Z (p_1 + p_2) \right] F_{i,j,\ell} \, . \tag{3.21}$$

By definition, $F_i(\infty) = 0$ so that the last finite difference equation (3.17) becomes

$$b_{1,n_1-1} F_{i,n_1-2,\ell+1} + b_{2,n_1-1} F_{i,n_1-1,\ell+1} = b_{4,n_1-1} \tag{3.22}$$

where n_1 is the number of radial mesh points. In addition, the first finite difference equation will be written

$$b_{2,1} F_{i,1,\ell+1} + b_{3,1} F_{1,2,\ell+1} = b_{4,1} \tag{3.23}$$

and if the interfacial concentrations are constant

$$F_{i,1,\ell+1} = F_i(R) = -\phi_i \tag{3.24}$$

or

$$b_{2,1} = 1$$

$$b_{3,1} = 0$$

$$b_{4,1} = -\phi_i \quad .$$

A more general formulation of equation (3.23) is derived in section 3.6 for the multicomponent bubbles with a linear relation between the mole fraction of gas i and its equilibrium concentration in the liquid medium.

The system of equations (3.17), (3.22) and (3.23) is suitable for a step-by-step solution, using a non-pivoting elimination method to advance one time step.

3.3.2 Non-pivoting elimination method

Equations (3.17), (3.22) and (3.23) are solved by Gauss's elimination method (Smith, 1978). A back substitution procedure is currently used as follows: the last difference equation (3.22) is used to eliminate $F_{i,n_l-1,\ell+1}$ from the penultimate equation ($j = n_l-2$);

the new penultimate equation is used to eliminate $F_{i,n_l-2,\ell+1}$ from the equation of order $j = n_l-3$ and so on, until $F_{i,2,\ell+1}$ is eliminated from the first equation (3.23),

the new first equation contains a single unknown $F_{i,1,\ell+1}$ which is calculated directly,

the unknown $F_{i,2,\ell+1}$, $F_{i,3,\ell+1}$, ..., $F_{i,n_l-1,\ell+1}$ can now be calculated by forward substitution.

The back substitution elimination can be represented by the generic

scheme involving the original equations of jth order and the new equation of (j+1)th order

$$b_{1,j}\, F_{i,j-1,\ell+1} + b_{2,j}\, F_{i,j,\ell+1} + b_{3,j}\, F_{i,j+1,\ell+1} = b_{4,j} \tag{3.25}$$

$$b_{1,j+1}\, F_{i,j,\ell+1} + b'_{2,j+1}\, F_{i,j+1,\ell+1} = b'_{4,j+1} \tag{3.26}$$

where

$$b'_{2,n_1-1} = b_{2,n_1-1} \quad ; \quad b'_{4,n_1-1} = b_{4,n_1-1} \tag{3.27}$$

Eliminating $F_{i,j+1,\ell+1}$ leads to

$$b_{1,j}\, F_{i,j-1,\ell+1} + b'_{2,j}\, F_{i,j,\ell+1} = b'_{4,j} \tag{3.28}$$

where

$$b'_{2,j} = b_{2,j} - b_{1,j+1}\left[b_{3,j}/b'_{2,j+1}\right] \tag{3.29}$$

$$b'_{4,j} = b_{4,j} - b'_{4,j+1}\left[b_{3,j}/b'_{2,j+1}\right] \quad . \tag{3.30}$$

The last simultaneous equations to be modified are

$$b_{2,1}\, F_{i,1,\ell+1} + b_{3,1}\, F_{i,2,\ell+1} = b_{4,1} \tag{3.31}$$

$$b_{1,2}\, F_{i,1,\ell+1} + b'_{2,2}\, F_{i,2,\ell+1} = b'_{4,2} \tag{3.32}$$

and the elimination of $F_{i,2,\ell+1}$ gives

$$F_{i,1,\ell+1} = \left[\, b_{4,1} - b'_{4,2}\left[b_{3,1}/b'_{2,2}\right] \,\right] \Big/ \left[\, b_{2,1} - b_{1,2}\left[b_{3,1}/b'_{2,2}\right] \,\right] \quad ; \tag{3.33}$$

by forward substitution

$$F_{i,j,\ell+1} = \left[b'_{4,j} - b_{1,j} F_{i,j-1,\ell+1} \right] \Big/ b'_{2,j} \qquad (j = 2,3, \ldots, n_1-1) \; . \tag{3.34}$$

This step completes the operations required to recalculate the concentrations at the standard mesh points. The application of this scheme requires an initial concentration profile which will be based on a quasi-stationary approximation rather than by the singularity expressed by equations (2.52) and (2.54).

3.4 Solution of radius and composition of the sphere

So far only the solution of equation (3.3) has been considered but both R and dR/dZ are required to calculate the non-linear coefficients of equation (3.3). In some cases the interfacial concentrations may vary with the mole fractions of a multi-component bubble. Therefore the radius of the sphere and the composition of bubbles must be solved accurately, which requires an efficient method of solving ordinary differential equations to integrate $\frac{dR}{dZ}$ and $\frac{dg_i}{dZ}$. In the present conditions these derivatives are calculated through the solution of concentration profiles, which represent the slowest part of a generic time step. Therefore multistep methods of solving $\frac{dR}{dZ}$ have advantages over other methods which require several estimates of the derivative per time step (Runge-Kutta methods).

In the present case explicit multistep methods become unstable due to the complex relation between concentration gradients and R, and $\frac{dR}{dZ}$, and strictly implicit methods cannot be used. Alternatively an explicit-implicit scheme is used with some modifications to avoid having to compute the concentrations profiles twice per time step. Four-step formulas are derived in appendix 1 for variable mesh size explicit and implicit methods.

The explicit method is used as a predictor following which the concentration profiles are solved. Finally the new derivative $\frac{dR}{dZ}$ can be obtained and the implicit method is used as a corrector.

The general solution can be summarized as follows:

1. Set the initial conditions ($\ell = 0$).
2. Calculate the concentration gradients $\left(\frac{\partial F_i}{\partial x}\right)_{x=1}$ at time step ℓ equation (3.43)).
3. Calculate the derivatives

$$\left(\frac{dR}{dZ}\right)_\ell = R_\ell^{-1} \sum_{i=1}^{n} \left[f_i \left(\frac{\partial F_i}{\partial x}\right)_{x=1} \right]$$

$$\left(\frac{dG_i}{dZ}\right)_\ell = 4\pi R_\ell \; f_i \left(\frac{\partial F_i}{\partial x}\right)_{x=1} .$$

4. Use the explicit four step formula (described in appendix 1) to predict $R'_{\ell+1}$.

$$R'_{\ell+1} = R_\ell + \delta Z \left[P'_1 \left(\frac{dR}{dZ}\right)_\ell + P'_2 \left(\frac{dR}{dZ}\right)_{\ell-1} + P'_3 \left(\frac{dR}{dZ}\right)_{\ell-2} + P'_4 \left(\frac{dR}{dZ}\right)_{\ell-3} \right] \qquad (3.35)$$

where $\delta Z = Z_{\ell+1} - Z_\ell$.

5. Calculate

$$R_{av} = \left(R'_{\ell+1} - R_\ell\right) / 2$$

$$\left(R^2\right)_{av} = \left[\left(R'_{\ell+1}\right)^2 + R'_{\ell+1} \cdot R_\ell + \left(R_\ell\right)^2 \right] / 3$$

$$\left(\frac{dR}{dZ}\right)_{av} = \left(R'_{\ell+1} - R_\ell\right) / \delta Z .$$

6. Calculate the new concentration profile at time step $\ell+1$ with the above estimates of R_{av}, $\left(R^2\right)_{av}$, and $\left(\frac{dR}{dZ}\right)_{av}$.
7. Calculate the new gradient at the interface $\left(\frac{\partial F_i}{\partial x}\right)_{x=1}$; $(i = 1, \ldots, n)$, (equation (3.43)), and

$$S = \sum_{i=1}^{n} \left[f_i \left(\frac{\partial F_i}{\partial x} \right)_{x=1} \right]_{\ell+1} \quad . \tag{3.36}$$

8. Correct $R_{\ell+1}$ by using the implicit multistep method described in appendix 1.

$$R_{\ell+1} = R_\ell + \delta Z \left[P_0 \left(\frac{dR}{dZ} \right)_{\ell+1} + P_1 \left(\frac{dR}{dZ} \right)_\ell + P_2 \left(\frac{dR}{dZ} \right)_{\ell-1} + P_3 \left(\frac{dR}{dZ} \right)_{\ell-2} + P_4 \left(\frac{dR}{dZ} \right)_{\ell-3} \right] \tag{3.37}$$

where

$$\left(\frac{dR}{dZ} \right)_{\ell+1} = S/R_{\ell+1} \quad . \tag{3.38}$$

After rearranging equation (3.37) becomes

$$R_{\ell+1} = R^*/2 + \sqrt{\frac{(R^*)^2}{4} + S.P_0 \, \delta Z} \tag{3.39}$$

where

$$R^* = R_\ell + \delta Z \left[P_1 \left(\frac{dR}{dZ} \right)_\ell + P_2 \left(\frac{dR}{dZ} \right)_{\ell-1} + P_3 \left(\frac{dR}{dZ} \right)_{\ell-2} + P_4 \left(\frac{dR}{dZ} \right)_{\ell-3} \right] \quad .$$

9. As g_i appears in the derivative $\left(\frac{dg_i}{dZ} \right)$, and the new solution must obey the condition $\sum_{i=1}^{n} g_i = 1$, it is preferable to integrate the numbers of moles of the individual components of a bubble. This is equivalent to integrating the dimensionless variables G_i ; $i = 1, \ldots, n$.

$$G_{i,\ell+1} = G_{i,\ell} + \left[\left(\frac{dG_i}{dZ} \right)_{\ell+1} .P_0 + \left(\frac{dG_i}{dZ} \right)_\ell .P_1 + \left(\frac{dG_i}{dZ} \right)_{\ell-1} .P_2 + \left(\frac{dG_i}{dZ} \right)_{\ell-2} .P_3 + \left(\frac{dG_i}{dZ} \right)_{\ell-3} .P_4 \right] \quad . \tag{3.40}$$

Then the mole fractions $g_{i,\ell+1}$ (i = 1, ..., n) are given by

$$g_{i,\ell+1} = \frac{N_i}{\sum_{k=1}^{n} N_K} = \frac{G_{i,\ell+1}}{\sum_{k=1}^{n} G_{K,\ell+1}} \qquad (3.41)$$

where N_i represents the number of moles of species i. A second correction of $R_{\ell+1}$ is also possible taking into account the definition of $G_{i,\ell+1}$ terms (formulas (2.51)). Thus

$$R_{\ell+1} = \left[\frac{3}{4\pi} \sum_{i=1}^{n} G_{i,\ell+1} \right]^{1/3} . \qquad (3.42)$$

If the final conditions have been reached stop; otherwise make $\ell = \ell+1$ and return to step 3.

3.5 Calculation of concentration gradients at the interface

The accuracy of the estimates of concentration gradients is dependent on the space mesh size. Excessively large mesh sizes are prevented by periodically readjusting the mesh points and a four point Lagrange interpolation formula is used to improve the estimate of the concentration gradient. If

$$\zeta = x - 1$$

$$\zeta_j = x_j - 1 \quad ; \quad (j = 1,2,3,4)$$

$$F_{i,j} = F_i(\zeta_j)$$

then we can write

$$F_i(\zeta) = P_1(\zeta)\, F_{i,1} + P_2(\zeta)\, F_{i,2} + P_3(\zeta)\, F_{i,3} + P_4(\zeta)_{i,4}$$

where

$$P_j(\zeta) = \prod_{K \neq j}^{4} \left(\frac{\zeta - \zeta_K}{\zeta_j - \zeta_K} \right) \qquad (j = 1, \ldots, 4) \quad .$$

By expansion of the $P_j(\zeta)$ terms and differentiation the gradient at the interface reduces to

$$\left(\frac{\partial F_i}{\partial x} \right)_{x=1} = \left(\frac{\partial F_i}{\partial \zeta} \right)_{\zeta=0} = d_1\, F_{i,1} + d_2\, F_{i,2} + d_3\, F_{i,3} + d_4\, F_{i,4} \tag{3.43}$$

where

$$d_1 = -\,(1/\zeta_2 + 1/\zeta_3 + 1/\zeta_4)$$

$$d_2 = 1/[(\zeta_2 - \zeta_2^2/\zeta_3)(1 - \zeta_2/\zeta_4)]$$

$$d_3 = 1/[(\zeta_3^2/\zeta_2 - \zeta_3)(\zeta_3/\zeta_4 - 1)]$$

$$d_4 = 1/[(\zeta_4^2/\zeta_3 - \zeta_4)(\zeta_4/\zeta_2 - 1)] = -\,d_1 - d_2 - d_3 \quad .$$

3.6 Variable interfacial concentrations

It can be easily recognized that a sudden perturbation of the interfacial concentrations may cause relatively greater errors in the next estimate of concentration gradients at the interface. This relation may cause oscillatory instabilities of the finite difference solution if the concentrations of the solutes at the interface vary with the composition of n-component bubbles.

During the initial stage the gas composition may vary rapidly and evolve towards equilibrium. Therefore, if changes of gas composition are rapid, a small perturbation will be negligible if compared with the correct changes of gas composition predicted by equation (3.6), and the errors tend to oscillate with decreasing amplitude and vanish. On the contrary, if the gas composition comes close to equilibrium the changes of gas composition may be almost exclusively due to abnormal perturbations. Thus a scheme which uses concentration gradients at step ℓ to compute the gas composition (equation (3.6)) and interfacial concentrations (equations (2.54)) at step $\ell+1$ leads to oscillatory propagation of errors with increasing amplitude.

To solve this type of difficulty the diffusion equation is also solved at the interface and this requires the introduction of a fictitious mesh point (which falls inside the bubble). In addition the relations between concentration gradients at the interface, gas composition, and interfacial concentrations are used to formulate a second equation required to eliminate the unknown concentration at the fictitious point.

Let x_o be space variable at the fictitious point so that $x_o = x_1 - \delta x = 1 - \delta x$, where $x_1 = 1$, $\delta x = x_2 - x_1 = x_2 - 1$. If the index ℓ is temporarily omitted from equations (3.9) and (3.10)

$$\left(\frac{\partial F_i}{\partial x}\right)_{x=1} = \frac{F_{i,2} - F_{i,o}}{2\delta x} \tag{3.44}$$

$$\left(\frac{\partial^2 F_i}{\partial x^2}\right)_{x=1} = \frac{F_{i,2} - 2F_{i,1} + F_{i,o}}{(\delta x)^2} \tag{3.45}$$

In addition, as $\varepsilon = 1$ in the case of a gas bubble, the material balance (equation (3.3)) at the interface reduces to

$$\frac{\partial^2 F_i}{\partial x^2} + 2\frac{\partial F_i}{\partial x} = \frac{R^2}{f_i}\left(\frac{\partial F_i}{\partial Z}\right) \quad ; \quad x = 1 \ . \tag{3.46}$$

The concentration gradient $J_{i,\ell} = \left[\left(\frac{\partial F_i}{\partial x}\right)_{x=1}\right]_\ell$ can be calculated from the last computed concentration profile. Therefore, from equation (3.44)

$$F_{i,o,\ell} = F_{i,2,\ell} - 2\delta x \, J_{i,\ell} \tag{3.47}$$

A similar relationship is needed for time step $\ell+1$ in order to eliminate the concentration at the fictitious point. On integrating equation (3.4) by multistep implicit formula (appendix 1)

$$\frac{4\pi}{3} R_{\ell+1}^3 \, g_{i,\ell+1} = G_{i,\ell+1}$$

$$= G_{i,\ell} + \delta Z \left[P_1\left(\frac{dG_i}{dZ}\right)_\ell + P_2\left(\frac{dG_i}{dZ}\right)_{\ell-1} + P_3\left(\frac{dG_i}{dZ}\right)_{\ell-2} + P_4\left(\frac{dG_i}{dZ}\right)_{\ell-3} \right]$$

$$+ \delta Z \, P_o \, R_\ell \left[\left(\frac{\partial F_i}{\partial x}\right)_{x=1}\right]_{\ell+1} \tag{3.48}$$

and on rearranging

$$\left[\left(\frac{\partial F_i}{\partial x}\right)_{x=1}\right]_{\ell+1} = - d_o + d_1 \, g_{i,\ell+1} \tag{3.49}$$

where

$$d_o = \left[G_{i,\ell}/\delta Z + P_1\left(\frac{dG_i}{dZ}\right)_\ell + P_2\left(\frac{dG}{dZ}\right)_{\ell-1} + P_3\left(\frac{dG_i}{dZ}\right)_{\ell-2} + P_4\left(\frac{dG_i}{dZ}\right)_{\ell-3}\right] \Big/ \left[P_o \, R_{\ell+1} \right]$$

$$d_1 = \frac{4\pi}{3} R_{\ell+1}^2 \Big/ \left[P_o \, \delta Z \right] \ .$$

From equations (3.49) and (2.54), ($F_i(R) = \alpha_i g_i - F_{o_i}$),

$$\left(\frac{\partial F_i}{\partial x}\right)_{\substack{x=1 \\ \ell+1}} = d_o' + d_1' F_{i,1,\ell+1} \tag{3.50}$$

where

$$F_{i,1,\ell+1} = F_i(R)$$

$$d_o' = - d_o + d_1 F_{o_i}/\alpha i$$

$$d_1' = d_1/\alpha_i$$

and from equations (3.44) and (3.50)

$$F_{i,o,\ell+1} = F_{i,2,\ell+1} - 2(\delta x)\, d_o' - 2\delta x\, d_1' F_{i,1,\ell+1} \quad . \tag{3.51}$$

Finally the time derivative can be replaced by

$$\left(\frac{\partial F_i}{\partial Z}\right)_{x=1} = \left(F_{i,1,\ell+1} - F_{i,1,\ell}\right) / \delta Z \tag{3.52}$$

and on combining equations (3.44) to (3.47), and (3.50) to (3.52) one obtains

$$b_{2,1} F_{i,1,\ell+1} + F_{i,2,\ell+1} = b_{4,1} \tag{3.53}$$

where

$$b_{2,1} = - 1 - \frac{(\delta x)^2 (R^2)_{av}}{f_i\, \delta Z} - \delta x(1 - \delta x) d_1'$$

$$b_{4,1} = \delta x(1 - \delta x) \left[J_{i,\ell} + d_o' \right] + \left(1 - \frac{(\delta x)^2 (R^2)_{av}}{f_i\, \delta Z}\right) F_{i,1,\ell} - F_{i,2,\ell} \quad .$$

Equation (3.53) assumes the form required for the boundary conditions of the finite difference implicit scheme, and resolves oscillatory instabilities of computed interfacial concentrations. A similar formulation was used by Crank and Nicolson (1947) to solve diffusion phenomena with surface kinetics acting as a boundary condition.

3.7 Starting conditions for the numerical scheme

3.7.1 Concentration profiles

Equations (2.52) and (2.54) express a singularity so that it is convenient to use the quasi-stationary approximation (equation (2.58)), which holds reasonably well for relatively small initial changes of content and radius of the sphere. For this purpose starting time Z_O and starting radius R_O must be estimated and equation (2.58) is expressed by

$$F_i(e,Z_O) = F_i(R_O,Z_O)\cdot\left(\frac{R_O}{e}\right)\cdot \operatorname{erfc}\left[\frac{e - R_O}{2\sqrt{f_i\, Z_O}}\right] \qquad (3.54)$$

with $e \geq R_O$.

3.7.2 Relation between concentration profiles and content of the sphere

Considering an element of volume V of liquid medium containing m_i moles of species i, the corresponding volume contribution of that species is $(m_i \cdot v_i)$ and the volume fraction $(v_i \cdot C_i)$. (These definitions may not be exact if the partial molar volumes v_i (i=1, ..., n+1) are not constant.). Here (n+1) refers to the solvent.

Taking the volume V_O of solvent as the frame of reference

$$V_O = m_{n+1}\, v_{n+1} = V\left[\, 1 - \sum_{i=1}^{n} (v_i\, C_i) \,\right] \qquad (3.55)$$

$$= V_\infty\left[\, 1 - \sum_{i=1}^{n} (v_i\, C_{\infty_i}) \,\right] .$$

The volume fraction of solvent is $y_{n+1} = [1 - \sum_{i=1}^{n} y_i] = [1 - \sum_{i=1}^{n} (v_i \cdot C_i)]$ and V_∞ denotes the initial volume of the element of solution containing volume V_o of solvent and concentrations C_{∞_i} (i=1, ..., n+1). Due to the change of concentrations from C_{∞_i} to C_i the number of moles can vary from m_{∞_i} to m_i so that

$$m_{\infty_i} - m_i = V_\infty C_{\infty_i} - V C_i \ , \tag{3.56}$$

and combination of equations (3.55) and (3.56) leads to the change in concentration being expressed by

$$X_i = \frac{(m_{\infty_i} - m_i)}{V} = \frac{\left[C_{\infty_i} - C_i + C_i \sum_{j=1}^{n} (v_j C_{\infty_j}) - C_{\infty_i} \sum_{j=1}^{n} (v_j C_j) \right]}{\left[1 - \sum_{j=1}^{n} (C_{\infty_j} v_j \right]} \ . \tag{3.57}$$

In the case of one-component spheres equation (3.57) reduces to

$$X_1 = (C_\infty - C)/(1 - C_\infty v) \tag{3.58}$$

and in the case of gas bubbles the terms $(v_j \cdot C_j)$ (j=1, ..., n) can be neglected which simplifies equation (3.57) to

$$X_i = C_{\infty_i} - C_i \ ; \quad (i=1, \ldots, n) \ . \tag{3.59}$$

The changes of solute content of the sphere can now be worked out from the changes on the concentration profiles, that is, from equation (3.58)

$$4\pi \int_a^\infty r^2 X_1 \, dr = 4\pi \int_a^\infty r^2 \frac{C_\infty - C}{(1 - C_\infty v)} \, dr = \frac{4\pi}{3} C_s^\circ (a^3 - a_o^3) \tag{3.60}$$

where the concentration C_s° in the sphere is considered constant. Equation (3.60) can be made dimensionless and after simplification

$$3X_o \int_R^\infty e^2 F \, de = 1 - R^3 \tag{3.61}$$

where

$$X_o = (1 - C_a v)/(1 - C_\infty v) \, . \tag{3.62}$$

Similarly from equation (3.59) the case of n-component gas bubbles reduces to

$$3 \int_R^\infty e^2 F_i \, de = g_i(0) - g_i R^3 \tag{3.63}$$

where $g_i(0)$ and g_i are the initial and actual volume fractions of species i in the gas mixture. (In ideal gas mixtures g_i is also the mole fraction of species i.)

In some conditions F_i may be a simple function of e so that it will be possible to integrate equations (3.61) or (3.63) analytically. Otherwise numerical solution is needed and truncation is inevitable. In these cases the truncation also makes it possible to restrict the integration to significant ranges of e values whilst avoiding the computing for large values of e where insignificant errors of F_i invalidate the solution of equations (3.61) or (3.63).

3.7.3 Starting time Z_o

The dimensionless starting time Z_o must be small to reduce the errors involved in assuming initial quasi-stationary approximations. For this purpose it is sufficient to consider the simplified form (equation (2.61)) of

the quasi-stationary solution, which holds during the initial stage. Thus from equation (2.61), for one-component cases,

$$R_O^2 - 1 = 2\,\phi\,Z_O + 4\,\phi\,\sqrt{Z_O/\pi} \tag{3.64}$$

or

$$Z_O = \left[\left(\frac{1}{\pi} + (\delta R_O)/\phi \right)^{\frac{1}{2}} - \frac{1}{\sqrt{\pi}} \right]^2 \tag{3.65}$$

where, as $R_O \simeq 1$ and $|R_O^2 - 1| \ll 1$

$$R_O^2 - 1 \simeq 2(R_O - 1) = 2(\delta R_O) \ .$$

Similarly for a general n-component bubble taking into account the possibility of transport in both directions

$$Z_O = \left[\left(\frac{1}{\pi} + |\delta R_O| / \sum_{i=1}^{n} |F_i(1,O)| \right)^{\frac{1}{2}} - \frac{1}{\sqrt{\pi}} \right]^2 \ . \tag{3.66}$$

This initial stage ($O < Z < Z_O$) is not covered by the finite difference solution. Thus, it must be short, and its duration can be varied by varying δR_O. Accurate predictions are usually achieved with $|\delta R_O| < 0.025$ (see tables 3.1 and 3.2) .

3.7.4 Starting radius and composition of the sphere

Conbination of equations (3.54) and (3.61) or (3.63) leads to

$$\Delta G_i = g_i R_O - g_i(O) = -\,4\pi X_O \int_{R_O}^{\infty} e^2 F_i \, de$$

$$= -\,8\pi \cdot F_i(R_O, Z_O) \cdot R_O \cdot (f_i \cdot Z_O)^{\frac{1}{2}} \cdot \int_O^{\infty} [2w \cdot (f_i \cdot Z_O)^{\frac{1}{2}} + R_O] \operatorname{erfc}(w)\, dw \tag{3.67}$$

where $X_O = 1$ in the case of gas bubbles, $F_i(R_O, Z_O) \simeq F_i(1, Z_O)$ and

$$w = (e - R_O) \Big/ \left[2(f_i \cdot Z_O)^{\frac{1}{2}} \right]$$

with

$$\int_0^\infty w \, \mathrm{erfc}(w) \, dw = 1/4$$

and

$$\int_0^\infty \mathrm{erfc}(w) \, dw = 1/\sqrt{\pi} \, .$$

Thus, on integrating equation (3.67)

$$\Delta G_i = - X_O \cdot R_O \cdot F_i(R_O, Z_O) \cdot [4\pi \cdot f_i \cdot Z_O + 8\sqrt{\pi} \cdot R_O \cdot (f_i \cdot Z_O)^{\frac{1}{2}}] \qquad (3.68)$$

and

$$G_i(Z_O) = G_i(O) + \Delta G_i$$

$$\sum_{i=1}^{n} G_i(Z_O) = \frac{4\pi}{3} \cdot R_O^{\,3} \, ,$$

from which it follows that

$$R_O = \left[\frac{3}{4\pi} \sum_{i=1}^{n} [G_i(Z_O)] \right]^{1/3} \, . \qquad (3.69)$$

Also taking into account that G_i represents the dimensionless number of moles of gas i

$$g_i(Z_O) = G_i(Z_O) \Big/ \sum_{j=1}^{n} G_j(Z_O) \, . \qquad (3.70)$$

The interfacial concentrations can also be corrected by taking into account the mole fractions $g_i(Z_O)$ and equation (2.54), that is

$$F_i(R_O, Z_O) = \alpha_i \cdot g_i(Z_O) - F_{O_i} \, . \qquad (3.71)$$

3.8 Distribution of space mesh points

Equally spaced distributions are commonly used in finite difference methods, regardless of the changes of the shape of concentration profiles (Readey and Cooper, 1966; Cable and Evans, 1967; Duda and Vrentas, 1969). Szekely and co-authors (1971, 1973) doubled the spacing of mesh points each time the concentration gradient at the interface had decreased by a factor of 0.5. (See also Martins, 1969). However constant mesh sizes were used at every time step. The present method uses redistribution of mesh points from time to time but also variable spacing at any particular time step, to ensure accuracy and economy and also to cover large values of the space variable without undue numbers of mesh points.

It is difficult to predict the evolution of concentration profiles with time, especially if the concentrations at the interface vary with time. A possible way of taking into account these changes is to allow larger space mesh where the concentrations vary smoothly with increasing radial distance from the centre.

For a convenient redistribution of existing x_j ; $F_{i,j}$ pairs, where $F_{i,j} = F_i(x_j)$, the following $S(x)$ function is used

$$S(x) = \sum_{i=1}^{n} \left[\int_{F(R)}^{F(x)} d\left|F_i(x)\right| \right] \tag{3.72}$$

or its discrete form

$$S_j = S(x_j) = \sum_{i=1}^{n} \left[\sum_{k=2}^{j} \left|F_{i,k} - F_{i,k-1}\right| \right] ; \; j=2,\ldots,n_1 \tag{3.73}$$

and a new δS increment

$$\delta S = S(\infty)/n_2 = S_{n_1}/n_1 \tag{3.74}$$

so that the new space mesh points x_j' will be interpolated from previous x_j; $F_{i,j}$, where the function $S(x)$ assumes the new discrete values

$$S_j' = S_{j-1}' + \delta S \qquad j \geqslant 2$$

with $S_1' = 0$

and

$$x_j' = x(S_j') \ .$$

The new x_j' can be obtained by simple linear interpolation because the redistribution of point does not need to be rigorous. Polynomial interpolations were only used to recalculate the concentrations $F_{i,j}' = F_i(x_j')$ at these points.

In the tail of the profile the concentrations tend to vary smoothly and it is necessary to control the ratio λ between the size of adjacent mesh units, that is

$$\lambda = \left(x_{j+1}' - x_j'\right) / \left(x_j' - x_{j-1}'\right) \leqslant \lambda_{max} \ . \qquad (3.76)$$

In tables 3.1 and 3.2 it is shown that accurate results are achieved with $\lambda_{max} \leqslant 1.5$. The range $1.1 \leqslant \lambda_{max} \leqslant 1.5$ is a useful compromise between accuracy and the need to cover large ranges of x values without undue numbers of mesh points.

Truncation of the space variable can be based on the formula

$$x_{max} = x_a + q_1 \ (x_a - x_b) \qquad (3.77)$$

where x_a and x_b are obtained by interpolation from existing $(x_j;\ S_j)$ pairs, so that

$$S'(x_a) = 0.975\ S_{n_1}$$

$$S'(x_b) = 0.95\ S_{n_1} \quad .$$

The factor q_1 has very little effect on the final solutions provided $q_1 \geq 5$ (tables 3.1 and 3.2). This demonstrates the soundness of the truncation criterion.

Redistribution is not needed after every time step. Besides extra computing is involved in the redistribution of mesh points as well as errors due to interpolations. A compromise is achieved by redistributing the space mesh points every ten time steps. The stability of the finite difference method will then ensure that errors which are due to interpolations will tend to vanish.

3.9 Amplitude of time intervals

The non-linear coefficients of equation (3.3) are functions of both the radius of the sphere and its time derivative, so that the convergence of the finite difference solutions may be hindered by excessive values of $|\delta R/R|$.

Rapid changes of concentration profiles are the other cause of poor convergence. To overcome this difficulty it is necessary to control the relative changes of interfacial concentrations and the relative amount of material transferred per time step. The last quantity can be controlled by preventing large $|(\delta R)/R|$ values, but this restriction is insufficient when different species diffuse in opposite directions, causing relatively rapid changes of composition in multi-component bubbles. This interdependence allows a second control by restricting the changes of mole fractions of gas per time step in n-component bubbles. Thus, the proposed controls can be written

$$\underset{\sim}{R}^{-1} \left| \left(\frac{dR}{dZ} \right)_{\ell} \right| (\delta Z)_{\ell+1} \leq \delta_1 \tag{3.78}$$

$$\left| \left(\frac{dg_i}{dZ} \right)_{\ell} \right| (\delta Z)_{\ell+1} \leq \delta_2 \tag{3.79}$$

$$\left| \left(\frac{dF_i(R)}{dZ} \right) / F_i(R) \right|_{\ell} (\delta Z)_{\ell+1} \leq \delta_3 \ . \tag{3.80}$$

The derivatives $\left(\frac{dR}{dZ}\right)$ and $\left(\frac{dg_i}{dZ}\right)$ at time step ℓ can be used to estimate the new time increment because the procedure is controlled step by step and those time derivatives do not vary significantly between two consecutive time steps.

The effect of varying δ_1 is illustrated in tables 3.1 and 3.2 and is discussed next. The restriction (3.79) is effective with δ_2 in the range 0.002-0.01. For the species having the maximum absolute numerical values of the "driving force", $|F_i(R)| = \phi_{max}$, it is convenient to use δ_3 in the range 0.001 - 0.005; otherwise it is sufficient to use $\delta_3 = 0.01$ and restriction (3.80) can be dropped if $|F_i(R)/\phi_{max}| < 0.05$.

During the initial stage the boundary layers are thin and small quantities of material transferred in any direction can produce significant changes of shape of concentration profiles. It is then convenient to add an additional restriction, relating the actual changes per time step to the changes which have happened since the beginning of the process. This restriction should not be too severe and can be expressed by

$$(\delta Z)_{\ell+1} \leq 0.02 \ Z_{\ell} \ . \tag{3.81}$$

3.10 Convergence of finite difference solutions

It has been emphasized that the best way of assessing the convergence of finite difference solutions was to compare asymptotic regimes of growth. Growth from zero size has been solved analytically by assuming a unique form for $C(s) = C(r,t)$ where $s = r/(2\sqrt{tD})$ (Scriven, 1959) and can be expressed by

$$a = 2 \beta \sqrt{tD}$$

or in dimensionless terms

$$R = 2 \beta \sqrt{Z}$$

where the characteristic growth constant β is a function of the solubility parameter $\phi = (C_\infty - C_a)/[C_s^\circ (1 - v C_a)]$ and $\varepsilon = (1 - v C_s^\circ)$ which accounts for the changes in volume of the system (see Chapter II). This analysis was derived for one-component spheres, but has now been extended to multicomponent bubbles (Chapter VI).

The evolution of growth from finite size towards the same type of solution is largely illustrated in Chapters IV and VI and it was found that with $R \geq 100$ the ratios $\beta_n = R/2\sqrt{Z}$ given by the (R,Z) pairs computed numerically by finite difference solution remain constant (to at least the fourth significant figure).

If $\phi = 0.6977$ and $\varepsilon = 1$ the analytical solution is $\beta = 1$. The same values of ϕ and ε were chosen for solution by the finite difference method to obtain the numerical values β_n. Several sets of n_1, δ_1, λ_{max} and q_1 were used as indicated to give the results included in table 3.1. In all these cases the accuracy of the finite difference solutions was very good taking into account the existence of non-linear coefficients which must be solved simultaneously. It is clear from table 3.1 that the ratio between adjacent

Table : 3.1

Effect of the number of space mesh points n_1, relative changes in radius δ_1 (restriction (3-78)), maximum ratio λ_{max} between the size of adjacent space mesh units (restriction (3-76)), and truncation factor q_1 (restriction (3-77)) on the finite difference predictions of growth constant for one-component bubbles β_n. In all these cases $\varepsilon = 1$ and the β_n predictions are constant for $R \geq 100$. $(\delta R) = 0.01$.

			ϕ	0.001	1	100
n_1	δ_1	λ_{max}	q_1		β_n	
50	0.01	1.1	10	0.02284	1.001	98.30
100	0.01	1.1	10	0.02283	1.001	98.25
200	0.01	1.1	10	0.02281	1.000	95.22
100	0.005	1.1	10	0.02282	1.001	98.25
100	0.02	1.1	10	0.02283	1.001	98.25
100	0.01	1.05	10	0.02281	1.000	98.20
100	0.01	1.25	10	0.02286	1.002	98.39
100	0.01	1.5	10	0.02290	1.005	98.72
100	0.01	2.0	10	0.02305	1.014	99.78
100	0.01	1.1	5	0.02285	1.001	98.27
100	0.01	1.1	20	0.02283	1.001	98.25

Table : 3.2

Effects of $n_1, \delta_1, \lambda_{max}, q_1, \delta R_o$ (equation (3.65)) on the finite difference predictions of dimensionless time required to decrease to half the initial size $Z_{0.5}$ ($\varepsilon=1$).

				F_a	0.001	1	100
n_1	δ_1	λ_{max}	q_1	(δR_o)	$Z_{0.5}$		$F_a^2 . Z_{0.5}$
50	0.01	1.1	10	0.01	359.5	0.1265	0.3212
100	0.01	1.1	10	0.01	360.0	0.1263	0.3204
200	0.01	1.1	10	0.01	360.2	0.1263	0.3204
100	0.005	1.1	10	0.01	360.1	0.1263	0.3204
100	0.02	1.1	10	0.01	359.8	0.1263	0.3204
100	0.01	1.05	10	0.01	360.3	0.1263	0.3205
100	0.01	1.25	10	0.01	359.4	0.1262	0.3203
100	0.01	1.5	10	0.01	358.4	0.1259	0.3195
100	0.01	2.0	10	0.01	355.2	0.1250	0.3166
100	0.01	1.1	5	0.01	359.8	0.1261	0.3198
100	0.01	1.1	20	0.01	360.0	0.1263	0.3204
100	0.01	1.1	10	0.005	360.1	0.1263	0.3206
100	0.01	1.1	10	0.025	359.8	0.1259	0.3189
100	0.01	1.1	10	0.05	359.4	0.1243	0.3133

space mesh units λ is the parameter most likely to affect the convergence of the finite difference solutions, but the errors remain below about 0.5% with λ_{max} up to 1.5. Changing the number of space mesh points n_1 does not have a significant effect on the accuracy of the finite difference solutions, within the range used, and the same can be said of the relative change in radius (restriction (3.78)), provided $\delta_1 < 0.02$, and truncation factor $q_1 > 5$ (equation (3.77)). The solutions reported in the next three chapters were usually computed with $\lambda_{max} = 1.1$, $n_1 = 100$, $\delta_1 = 0.01$ and $q_1 = 10$.

Two extreme cases $\phi = 0.001$ and $\phi = 100$ ($\varepsilon = 1$) are also included in table 3.1. The finite difference solutions for the usual parameters ($n_1 = 100$; $\delta_1 = 0.01$; $\lambda_{max} = 1.1$; and $q_1 = 10$) are $\beta_n = 0.02283$ for $\phi = 0.001$ and $\beta = 98.25$ for $\phi = 100$. The corresponding analytical solutions for these values of β in terms of $\phi(\beta,\varepsilon)$ are $\phi(0.02283,1) = 0.001002$, and $\phi(98.25,1) = 100.1$. The use of other combinations of the parameters n_1, δ_1, λ_{max} and q_1 gave only trivially different solutions, all probably of greater accuracy than the experimental determination of concentrations and solubility (ϕ) in any practical case. Thus, the finite difference method is accurate over a very large range of values of solubility parameters, which covers virtually any spherical phase in a sufficiently large volume of liquid.

The effects of the number of space mesh points n_1, relative increase in radius per time step δ_1,(restriction (3.78)), and parameters λ_{max},(restriction (3.76)), q_1,(restriction (3.77)), and δR_o,(equation (3.65)) on the dimensionless time $Z_{0.5}$ required to reach half the initial size have been investigated and are illustrated in table 3.2. If $n_1 > 50$, $\delta_1 < 0.02$, $q_1 > 5$, and $\lambda_{max} < 1.5$ the finite difference solutions do not vary significantly by varying any of those parameters. The largest differences occur for $\lambda_{max} \geq 2$ and $|\delta R_o| \geq 0.05$.

As analytical solution is impossible for a dissolving sphere it is more

difficult to prove the accuracy of numerical methods for dissolving bubbles. The greatest problems would often occur as size approaches zero, especially in cases when the rate of dissolution $\left|\frac{dR}{dZ}\right|$ increases with decreasing size. This difficulty is solved by redistribution of the space mesh points and control of the relative changes in radius per time step,(restriction (3.78)). Then the accuracy of the finite difference method is not poorer during the last stage than it is during the intermediate stage of dissolution.

3.11 Comparison of the present method and previous finite difference solutions

It was earlier noted that Readey and Cooper's (1966) explicit method could require excessively large space mesh sizes to ensure stability but at the expense of convergence. Their solutions for the case $F_a = 0.5$ (dissolution) with $\varepsilon = 0$ and 0.5 were about $Z_o = 1$ and 0.93 respectively where Z_o denotes the time required for complete dissolution. For those cases our solutions are $Z_o = 0.834$ and 0.742 respectively. Solutions for slower dissolution were not reported in Readey and Cooper's work (1966) which suggests that the method was not suitable for slow processes due to restrictions on the time increments making computing times very long.

Cable and Evans (1967) reported a fairly large number of solutions but their results seem to be inaccurate, especially the predictions of dissolution. This may be due to the decrease of boundary layer thickness during dissolution without correspondingly decreasing the mesh size δe. The differences between our results and Cable and Evans predictions of dissolution times can be as much as 82% (table 3.3). Besides, there is evidence that the differences are not exclusively due to different time scales (figure 3.1).

Another shortcoming of Cable and Evans method is that it would be very

Table 3.3

Comparison between the present predictions and Cable and Evans' predictions of dimensionless dissolution time, Z_o

	Cable and Evans		Present work	
ε	0	1	0	1
F_a	Z_o			
0.01	67.44	67.25	46.48	46.25
0.1	5.83	5.68	4.214	3.994
0.5	1.090	0.966	0.834	0.644
1	0.540	0.441	0.451	0.2828
2	0.281	0.192	0.2670	0.1214
4	0.149	0.093	0.1726	0.0512

inefficient to compute large increases of radius because a constant mesh size was used.

Duda and Vrentas (1969, 1971) used N_A and N_B to characterize the behaviour of one-component spheres where $N_A = F_a$ is a solubility parameter and N_B is related to ε by the relation

$$\varepsilon = 1 - N_B/N_A \quad .$$

Table 3.4

Comparison between the present predictions and Duda and Vrentas' predictions of dimensionless dissolution time, Z_O

			Duda and Vrentas (1971)	Present work
F_a	N_B	ε	$F_a \cdot Z_O$	
0.01	0.01	0	0.465	0.465
0.01	0.1	-9	0.486	0.486
0.1	0.01	0.9	0.402	0.402
0.1	0.1	0	0.422	0.421
0.1	1	-9	0.601	0.601
1	0.1	0.9	0.302	0.3011
1	1	0	0.451	0.451
10	1	0.9	0.271	0.2742
100	1	0.99	0.143	0.1464
1000	1	0.999	0.0726	0.0742

Figures 3.2a to 3.2d show some of the present finite difference solutions and the corresponding predictions by Duda and Vrentas (1969, 1971). Comparisons of times required for complete dissolution are also shown in table 3.4 and the differences between the actual predictions and Duda and Vrentas' results (1971) are usually less than 1% which represents a remarkable agreement taking into account that the techniques are quite different. The largest differences in times occur for large solubility parameter F_a but are always less than 2.5%. Duda and Vrentas investigated the effect of varying the space and time mesh sizes and this might explain the accuracy of their predictions. They also found that accuracy of solutions and economy of computing can only be achieved by decreasing the amplitude of time intervals

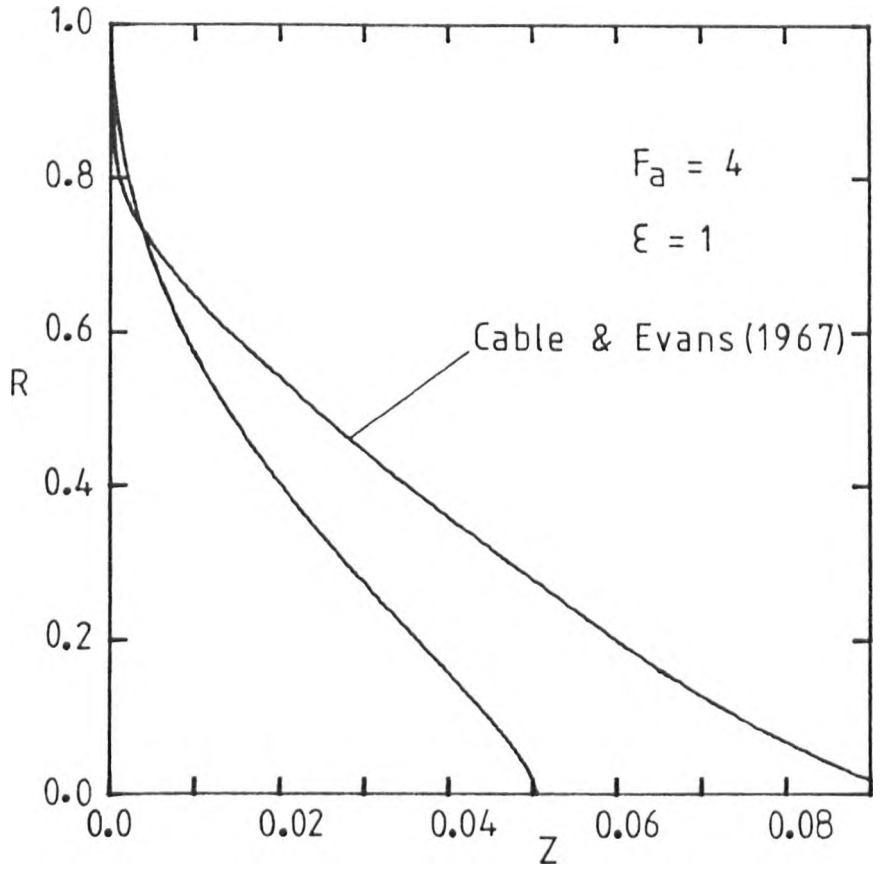

Fig 3.1 : Comparison between the present finite difference solutions for the one-component case $F_a = 4$; $\varepsilon = 1$ and the corresponding finite difference predictions by Cable and Evans (1967).

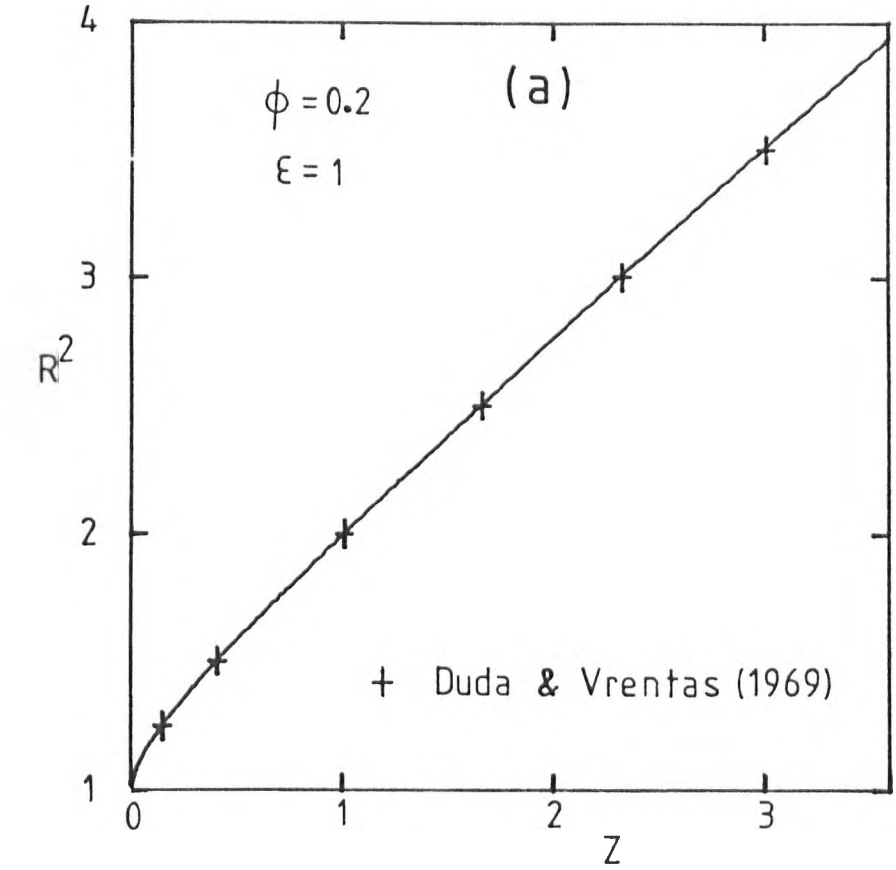

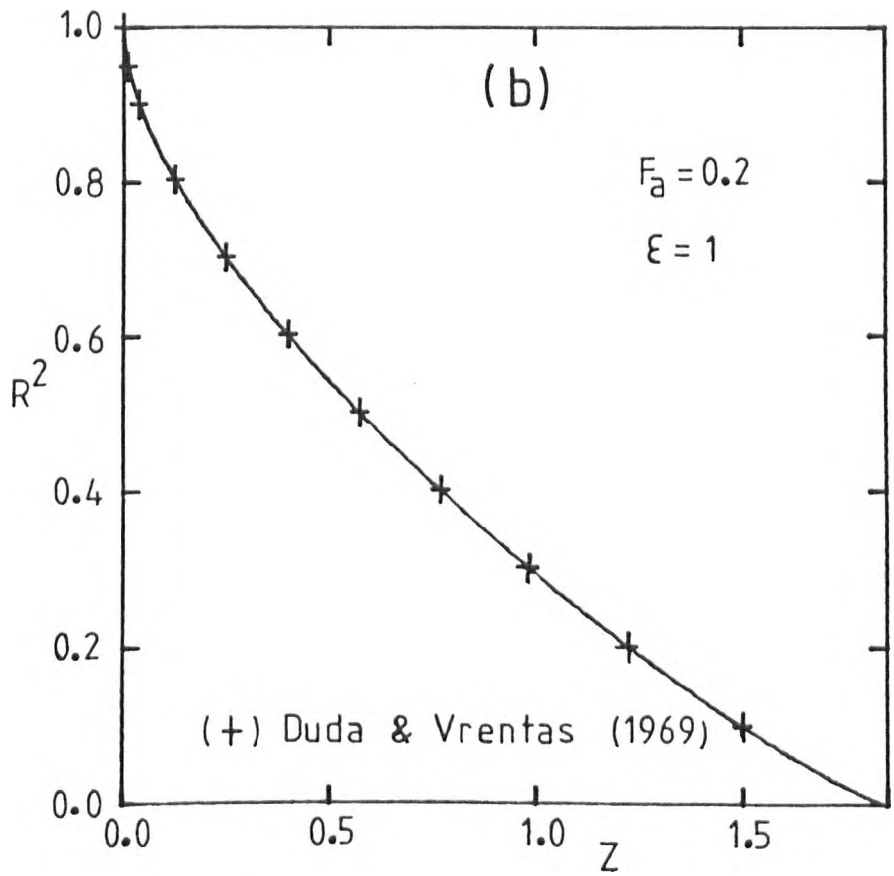

Figs 3.2a to 3.2d : Comparison between the present finite difference solutions for one-component cases and the corresponding finite difference predictions by Duda and Vrentas (1969, 1971).

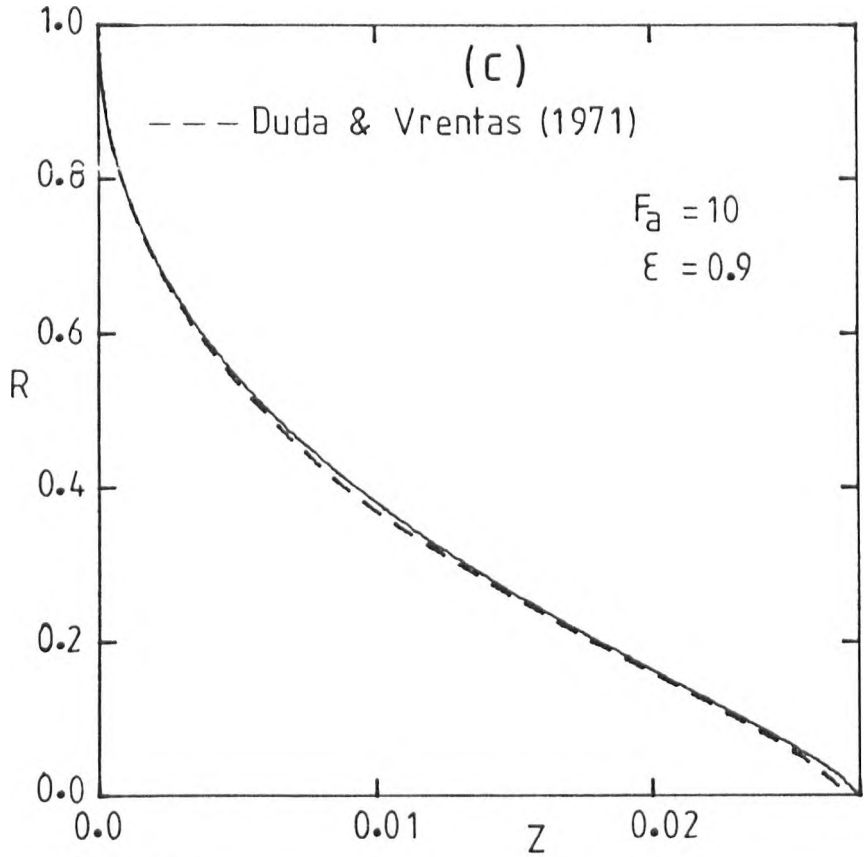

Fig 3.2c

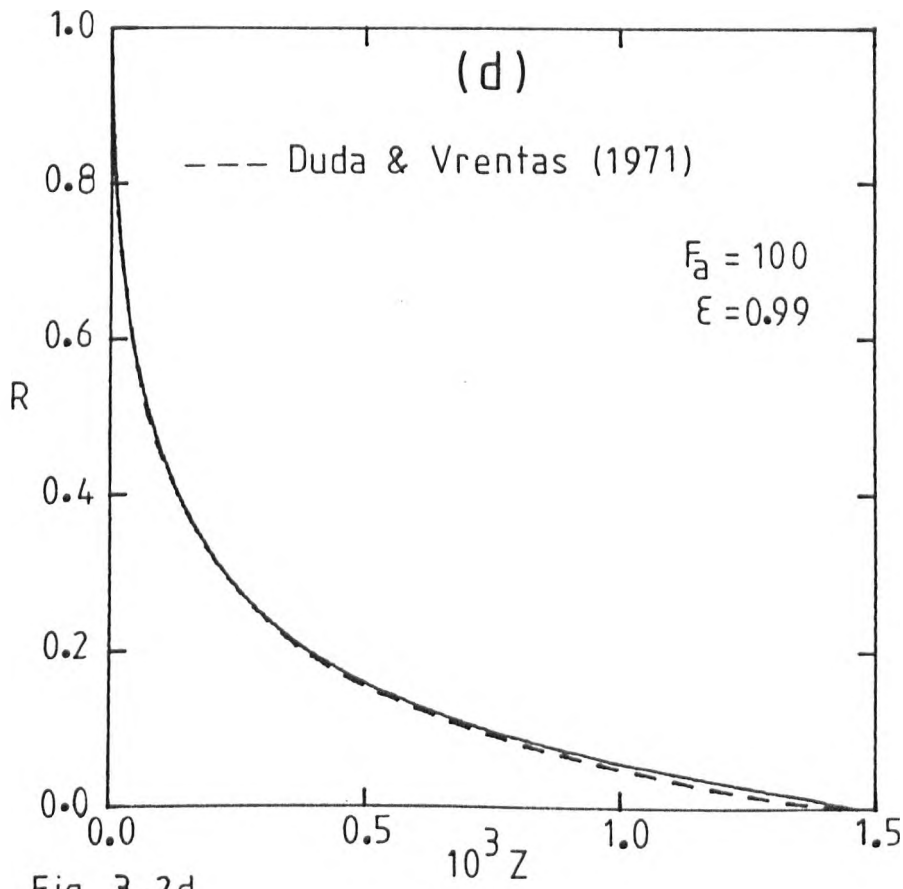

Fig 3.2d

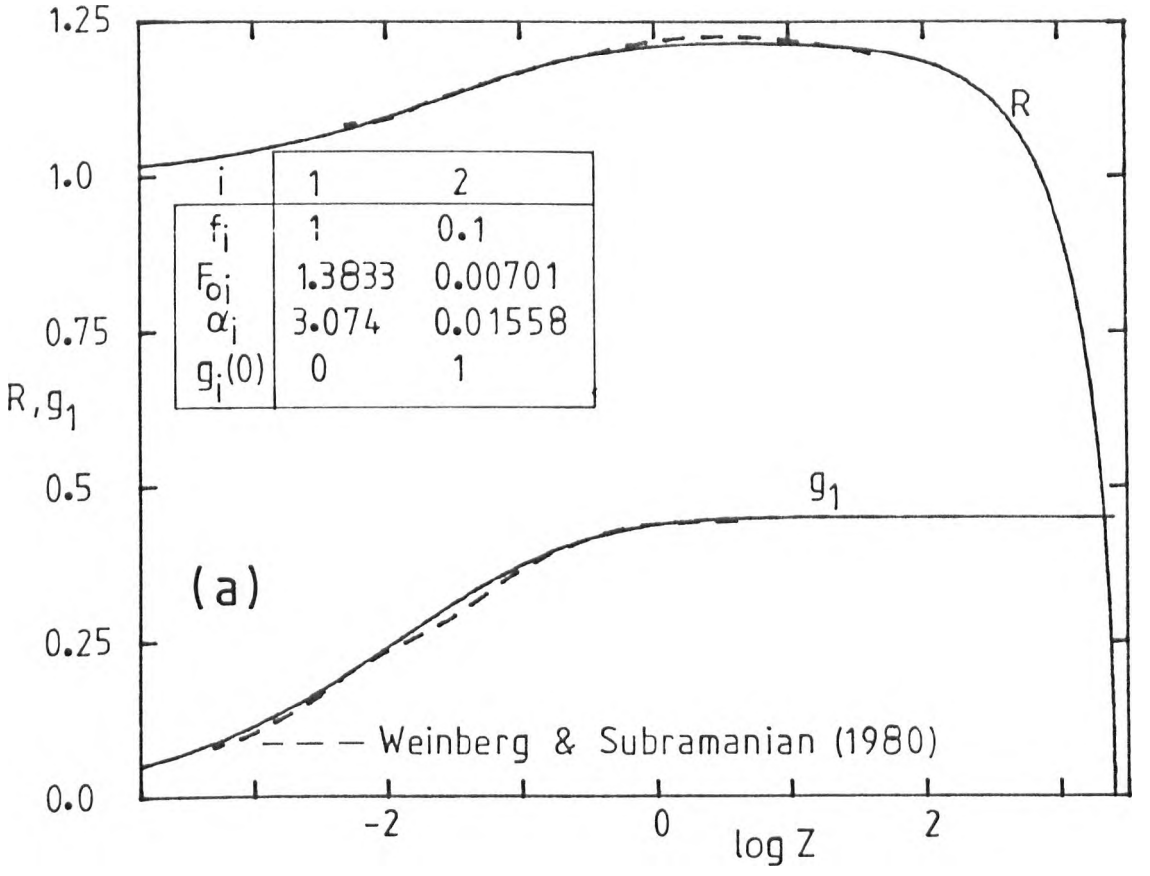

i	1	2
f_i	1	0.1
F_{oi}	1.3833	0.00701
α_i	3.074	0.01558
$g_i(0)$	0	1

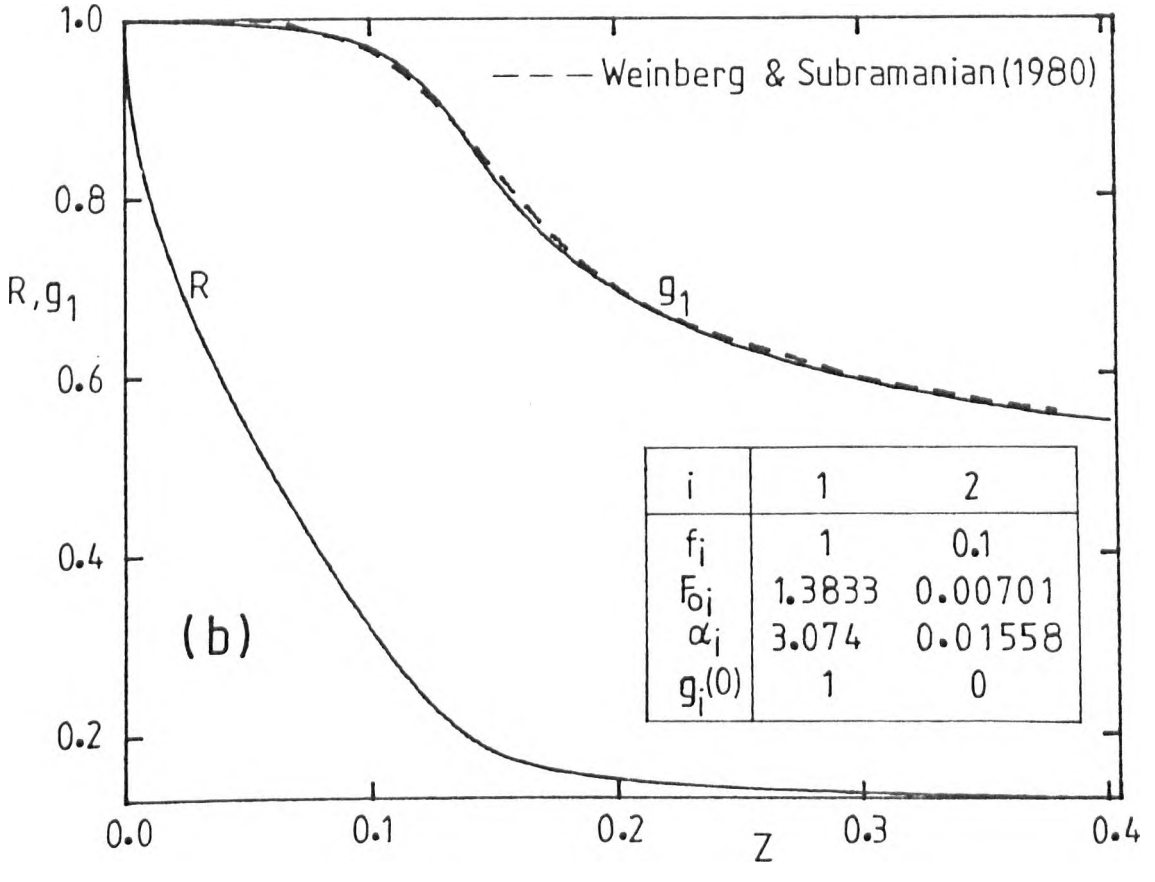

i	1	2
f_i	1	0.1
F_{oi}	1.3833	0.00701
α_i	3.074	0.01558
$g_i(0)$	1	0

Figs 3.3a and 3.3b : Comparison between the present finite difference solutions for two-component cases and the corresponding finite difference predictions by Weinberg and Subramanian (1980) (shown dashed).

during the initial stage of dissolution and during the final stage for the cases when the dissolution rate increases with time (low F_a). However, they failed to provide a general criterion or algorithms to control the time intervals. In addition they did not include algorithms to readjust the space mesh points which may be necessary as the boundary layer thicknesses vary considerably during transient regimes.

Having published a comprehensive set of predictions for dissolution Duda and Vrentas failed to do the same for growth and did not compare finite difference predictions to the only class of exact solutions available for growth from zero size (Scriven, 1959). It has been pointed out that comparison is possible provided that sufficiently large increases in size are computed by the finite difference technique, so that the effect of the initial transient stage becomes negligible. This requires unduly large numbers of time steps if sequential control of time intervals is not used.

Another limitation of Duda and Vrentas' techniques is that they were not conceived for use with multicomponent bubbles, especially when rapid changes of interfacial concentrations are involved and when there is a need for models to describe unusual bubble behaviour (see Chapter VI). Weinberg and Subramanian (1980), used a technique similar to Duda and Vrentas's finite difference method to solve the behaviour of two-component stationary bubbles. However they reported only two examples which is clearly insufficient to demonstrate the performance of their method. They also failed to show comparison with alternative exact solutions to test their predictions of behaviour of multicomponent bubbles.

Figures 3.3a and 3.3b show the predictions reported by Weinberg and Subramanian (1980) and the corresponding actual predictions. These cases were computed with arbitrarily chosen solubilities, diffusivities and concentrations in the bulk liquid so that it is more significant to use only

dimensionless variables instead of the real time used by Weinberg and Subramanian. These authors might have been unable to solve the final stage of the process illustrated in figure 3.3b. Also they computed only a relatively short initial stage in the case shown in figure 3.3a, stopping before the direction of transfer of species 1 (which corresponded to oxygen) had changed. During the initial stage species 1 diffuses into the bubble whilst the interfacial concentration increases and approaches the value of the solute concentration C_{∞_i} in the bulk liquid medium. At $g_1 = 0.45$ the interfacial concentration exceeds C_{∞_1} and $F_1(R)$ changes from negative to positive. This points out that the normalized dimensionless concentration $C_i^* = [(C_i(r,t) - C_{\infty_i})/(C_i(a,t) - C_{\infty_i})]$ used by those authors is not suitable for this type of problem because of the discontinuity which occurs when $C_i(a,t) < C_{\infty_i}$ is reversed to become $C_i(a,t) > C_{\infty_i}$ or vice-versa. These examples also show that the changes of interfacial concentrations per time step must be controlled.

During the last stage of the example shown in figure 3.3b $F_2(R)$ also changes sign at $g_2 = 0.45$. Again the computations reported by Weinberg and Subramanian (1980) did not reach this stage. This supports the previous arguments. Weinberg and Subramanian's prediction of the R versus Z curve is not included because the R scale is not properly shown in the original article.

Szekely and co-authors (1971, 1973) showed good agreement between their finite difference predictions for large ϕ and the corresponding asymptotic regime for growth from zero size (Scriven, 1959). However, that finite difference technique was not used to compute growth with low or moderate ϕ, or dissolution. The restriction on the amplitude of time intervals which was needed to ensure stability might prevent efficient use of such methods for all ranges of the parameters.

CHAPTER IV

4.1 Growth of one-component spheres

Equations (2.28) and (2.29) illustrate that one-component spheres can be characterized in terms of only two variables ϕ and ε. The solubility parameter accounts for concentrations of solute in both phases and ε accounts for the partial molar volumes of the solute. It is not necessary to include the diffusivity, D, in the dimensionless balances, so that the dynamics of the process can be studied independently of D. It is therefore reasonable to use the terms slow and rapid growth to denote small ($\phi < 0.01$) and large ($\phi > 10$) values of ϕ respectively.

The relevant material balances (equations (2.28) and (2.29)) can be solved by using the finite difference technique outlined in Chapter III. Exact solutions cannot quantify the growth of spheres from finite (non-zero) size. However those analytical solutions have vital importance in testing the accuracy of numerical techniques.

The study of nucleation and growth of spherical phases is important in the science of materials, in glass technology and in many chemical engineering processes. In some systems analytical solutions of growth from zero size can be useful. Otherwise, alternative methods are required to quantify the growth from a nucleus with significant finite radius. The limitations of various approximate solutions must also be discussed.

4.2 Analytical solutions for the growth of one-component spheres from zero size

Equations (2.28) and (2.29), with boundary conditions (2.31), (2.32) and initial conditions (2.33) were solved by Frank (1950), for the case $\varepsilon = 0$, that is when $u(r) = 0$ and the volume of the system remains constant because the partial molar volumes of solute in the liquid and in the sphere are equal (equation (2.25)). Frank's solutions were extended by Scriven (1959) to cover the general cases $\varepsilon \neq 0$. Both authors used Boltzmann transformations by assuming the unique variable

$$C(s) = C(r,t) \tag{4.1}$$

with

$$s = r/2\sqrt{Dt} = e/2\sqrt{Z} \tag{4.2}$$

and

$$a = 2\beta\sqrt{Dt} \tag{4.3}$$

for growth from zero size. β is a characteristic constant dependent on both ϕ and ε.

Accordingly to such transformation the concentration profile is given by

$$C(r/a) = C_\infty - 2\beta^2 C_s^\circ (1-C_a v) \int_{1-\frac{a}{r}}^{1} \exp\left(\beta^2 \left[1 + 2\varepsilon x - (1-x)^{-2}\right]\right) dx \tag{4.4}$$

and on introducing the boundary conditions

$$\phi = \frac{C_\infty - C_a}{C_s^\circ (1 - C_a v)} = 2\beta^2 \int_0^1 \exp\left(\beta^2 \left[1 + 2\varepsilon x - (1-x)^{-2} \right] \right) dx \quad . \qquad (4.5)$$

The transformation of the partial differential equations leads to simple ordinary differential equation which is easy to integrate by using numerical methods. Fourth-order Runge-Kutta and fourth-order Runge-Kutta-Fehlberg (Fehlberg, 1970) techniques were used for that purpose (appendix 2).

These analytical solutions rely on the existence of unique self similar profiles, which can be used to confirm the material conservation, by integration of the changes of solute content in the liquid medium. This confirmation also serves to verify the continuity equations formulated in Chapter II and the velocity profile in the liquid medium (equation (2.10)).

Analytical solutions are also the best test of comparison for general numerical solutions of the partial differential equations and other simple approximate solutions. Reliable numerical techniques must produce convergence of numerically predicted growth rates and concentration profiles to the equivalent analytical predictions for sufficiently large spheres. Computing algorithms which fulfil these conditions can be intended for use in more general conditions, when analytical solutions are not available.

4.3 Concentration profiles and material conservation

Mass conservation after growth from zero size requires

$$4\pi \int_a^\infty r^2 \frac{C_\infty - C}{(1 - C_\infty v)} dr = \frac{4}{3} \pi a^3 C_s^\circ \qquad (4.6)$$

and by substitution of equation (4.4) into equation (4.6) and transformation of variable r into $w = 1 - a/r$,

$$I = 6\beta^2 \left(\frac{1 - C_a v}{1 - C_\infty v} \right) \int_0^1 (1-w)^{-4} \int_w^1 \exp\left(\beta^2 \left[1 + 2\varepsilon x - (1-x)^{-2} \right] \right) dx \, dw = 1 \quad . \qquad (4.7)$$

The integral I was evaluated numerically (appendix 3) for wide ranges of β and ε in the range 0-2. Some results are listed in table 4.1, for the case $C_a = 0$, and show that the deviations from equation (4.7) remain negligible. The mole fractions of solute in the bulk liquid medium, $y_\infty = v\, C_\infty$, are also indicated to demonstrate that deviations from equation (4.7) can only be detected with very large values of the factor $(1 - C_\infty\, v)^{-1}$, which make the numerical integration of equation (4.7) very dependent on apparently negligible differences of the concentration C_∞ (obtained by numerical integration of equation (4.4)).

The excellent agreement between concentration profiles and the overall material conservation is a conclusive proof of the correctness of the differential balances. It also confirms that the rate of the process is dependent on the partial molar volume of solute, rather than on the density of the liquid medium.

Table 4.1

Confirmation of material conservation

according to equation (4.7)

ε	0		1	
β	y_∞	I	y_∞	I
0.01	0.0002	1.000	0	1.000
0.1	0.0168	1.000	0	1.000
1	0.484	1.000	0	1.000
10	0.985	1.000	0	1.000
20	0.996	0.998	0	1.000

4.4 Numerical solutions of growth from finite size

Computations of growth of one-component spheres were carried out by using the technique outlined in Chapter III. Wide ranges of ϕ were covered and different values of ε, special emphasis being given to the cases $\varepsilon = 1$ and $\varepsilon = 0$. With $\varepsilon = 1$ the volume of liquid medium remains constant, whilst if $\varepsilon = 0$ transfer of solute across the interface between sphere and liquid causes no change in volume and the volume of the system remains constant.

Equation (4.3) can be written in dimensionless form

$$R = 2\beta\sqrt{Z} \tag{4.8}$$

or

$$\log R = \frac{1}{2} \log Z + \log(2\beta) \tag{4.9}$$

and the plotting of numerically computed results in logarithmic scales allows a ready confirmation of the convergence of numerical solutions to their equivalent asymptotic regime of growth from zero size. This convergence is illustrated in figures 4.1, 4.2 and 4.3 for the cases $\varepsilon = 1$, $\varepsilon = 0.5$ and $\varepsilon = 0$ respectively. The dashed lines represent analytical predictions of growth from zero size (equation (4.8)) for the smallest and largest ϕ values respectively.

The convergence of numerical solutions to equation (4.8) is also confirmed in table 4.2. After an increase to 10 times the initial size ($R = 10$) the ratio $R/2\sqrt{Z}$ is already less than 1.5% greater than the final limiting values for $R = 10^5$.

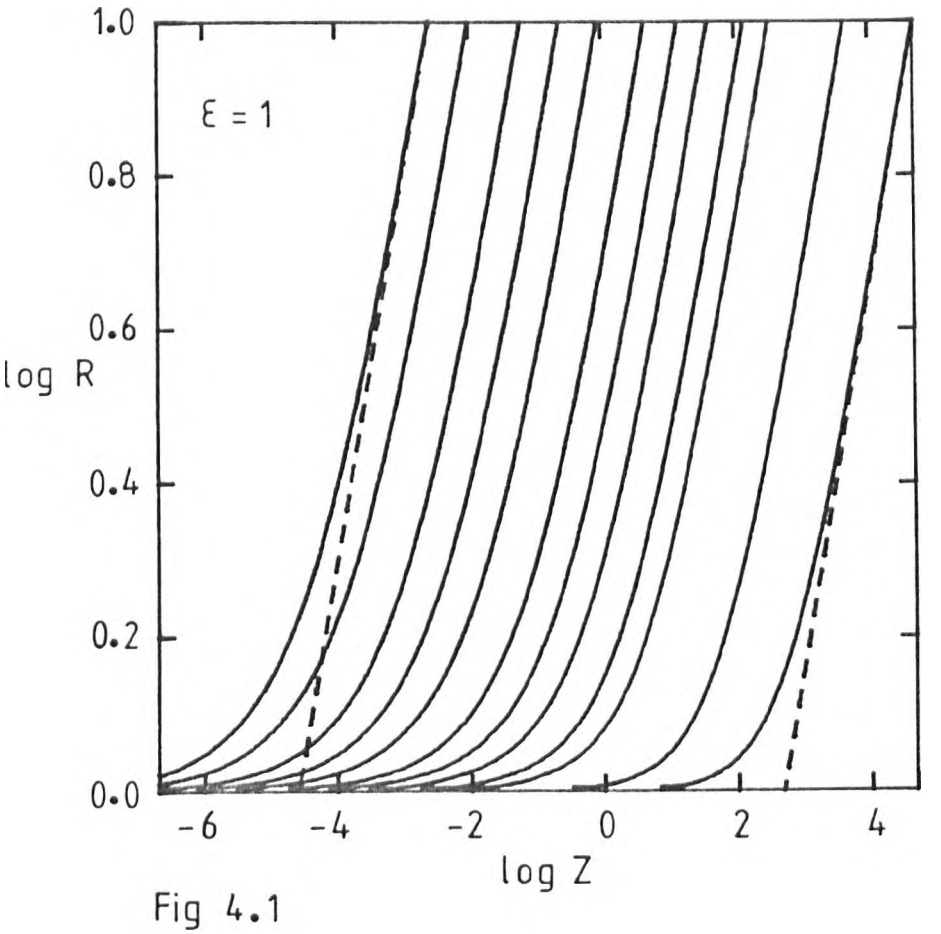

Fig 4.1

Figs 4.1, 4.2 and 4.3 : Convergence of growth from finite size towards the asymptotic regime. The values of ε are shown in the figures. The dashed lines represent growth from zero size for the smallest and largest values of ϕ shown in each figure. The solubility parameters are, from right to left,

in fig 4.1 : ϕ = 0.001, 0.01, 0.1, 0.2, 0.5, 1, 2, 5, 10, 20, 50 and 100 respectively.

in fig 4.2 : ϕ = 0.001, 0.01, 0.1, 0.2, 0.5, 1, 1.5, 1.75 and 1.9 respectively.

in fig 4.3 : ϕ = 0.001, 0.01, 0.1, 0.2, 0.5, 0.75, 0.9 and 0.95 respectively.

Table 4.2

Evolution of growth rates towards the asymptotic regime for the case $\varepsilon = 1$

ϕ	0.001	0.01	0.1	1	10	100
R	$R/2\sqrt{Z}$					
2	0.02647	0.0885	0.3330	1.745	14.30	139.5
5	0.02333	0.0771	0.2816	1.378	10.78	104.1
10	0.02295	0.0758	0.2757	1.336	10.37	99.9
10^2	0.02280	0.0753	0.2739	1.320	10.21	98.3
10^3	0.02279	0.0753	0.2738	1.320	10.20	98.2
10^5	0.02279	0.0753	0.2738	1.320	10.20	98.2

Computations were carried out until $a = (10^5 \cdot a_0)$, $(R = 10^5)$, and these numerical predictions were used to estimate the growth constant β. The numerical predictions of β values were then put into equation (4.5) to recover the analytically predicted values of solubility parameter $\phi(\beta,\varepsilon)$ (see table 4.3). These computed ϕ values differ by less than 1% even with very large growth rates. Experimental methods are very unlikely to measure concentrations within 1% error.

4.5 Concentration profiles

Analytical solutions for growth from zero size require a unique concentration profile as predicted by equation (4.4). Valid numerical predictions of concentration profiles during growth from finite size must converge to those solutions of growth from zero size and provide further confirmation of both numerical and analytical solutions of the relevant partial differential equations.

In figures 4.4 to 4.8 the concentrations have been normalized and the

Table 4.3

Comparison between finite difference predictions of the asymptotic regime of growth from finite size and the corresponding analytical solutions for growth from zero size.

ε	0		0.5		1	
ϕ	β	$\phi(\beta,\varepsilon)$	β	$\phi(\beta,\varepsilon)$	β	$\phi(\beta,\varepsilon)$
0.001	0.02284	0.001002	0.02283	0.001002	0.02283	0.001002
0.01	0.0756	0.01002	0.0755	0.01002	0.0753	0.01000
0.1	0.2827	0.1000	0.2779	0.1000	0.2734	0.1000
0.2	0.4541	0.2000	0.4360	0.2000	0.4206	0.2001
0.5	1.038	0.5000	0.880	0.5000	0.783	0.5001
0.75	1.958	0.7501				
0.9	3.564	0.9004				
0.95	5.263	0.9502				
1	-		1.819	1.000	1.320	1.001
1.5			3.654	1.500		
1.75			6.003	1.750		
1.9			10.36	1.900		
2			-		2.334	2.001
5					5.30	5.005
10					10.20	10.01
20					19.99	20.02
50					49.33	50.04
100					98.2	100.1

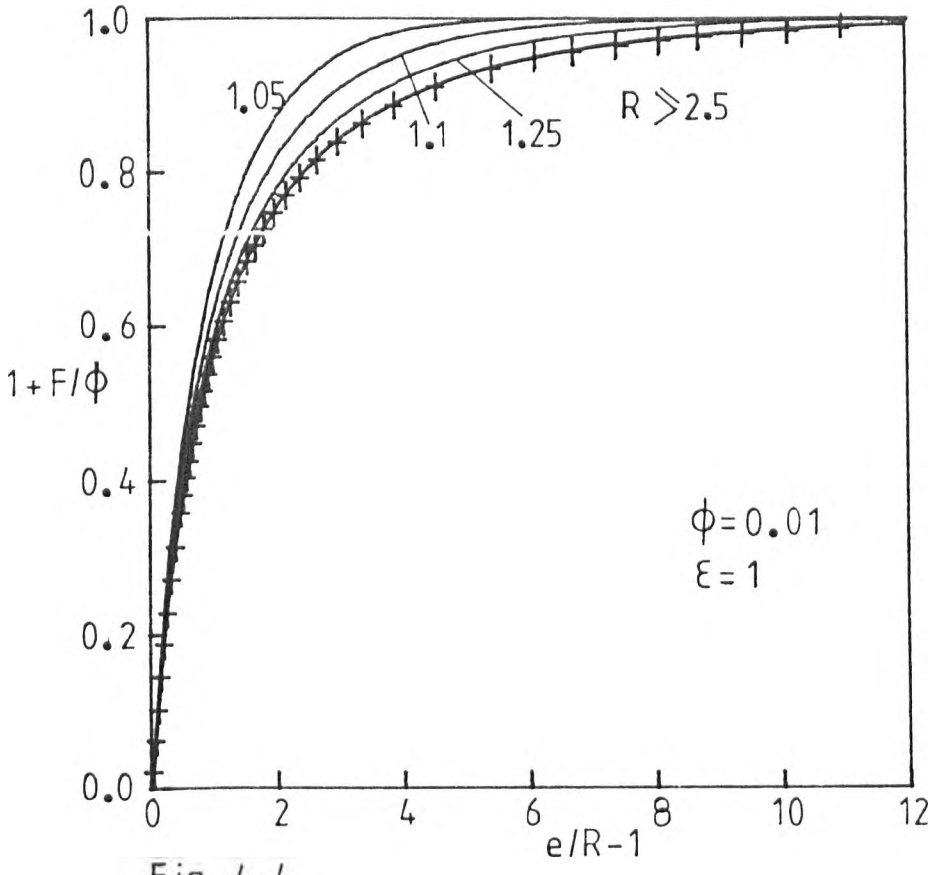

Fig 4.4

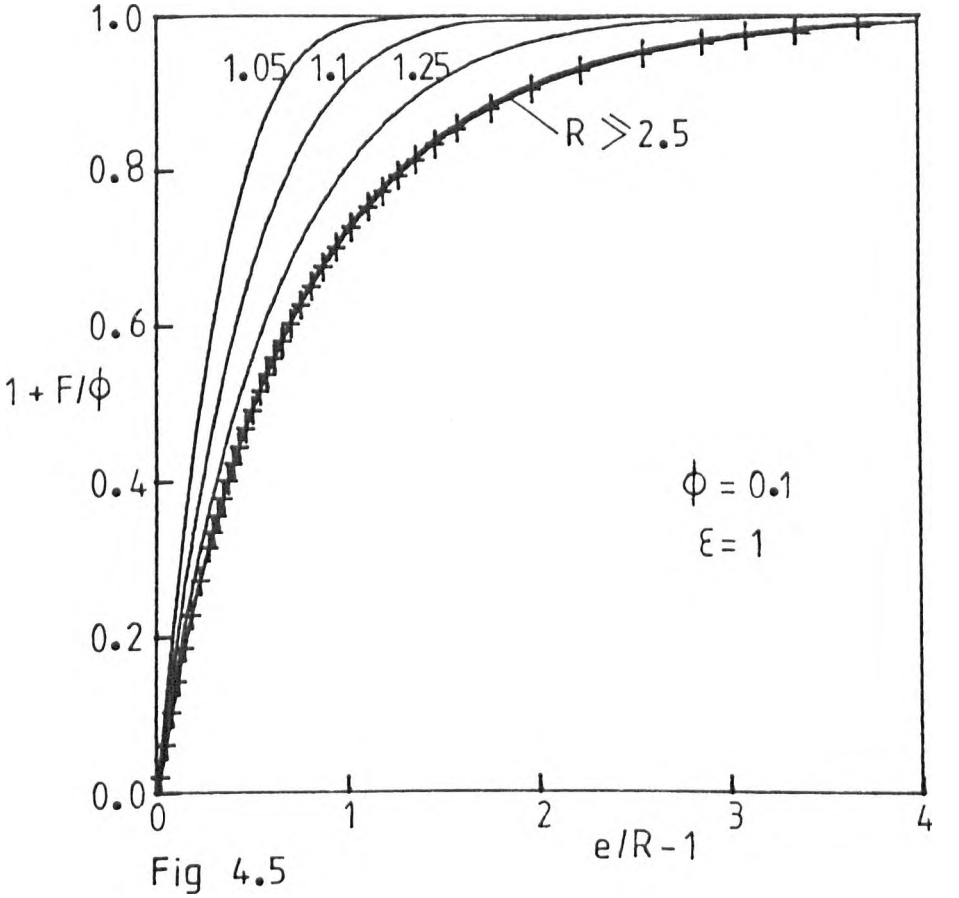

Fig 4.5

Figs 4.4 to 4.7 : Finite difference predictions of concentration profiles during growth from finite size. The numbers show the corresponding dimensionless radius R. The discrete symbols (+) represent the analytical solutions for growth from zero size (equation (4.4)). The relevant values of ε and ϕ are shown in the figures.

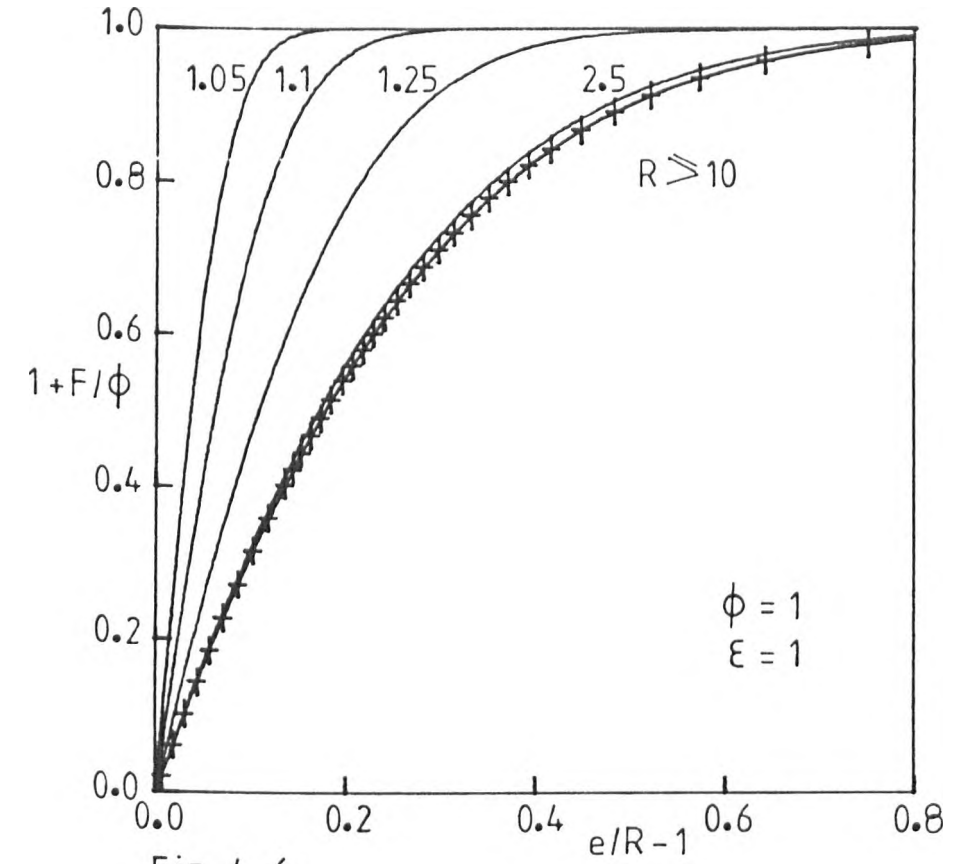
1.0
0.8
0.6
0.4
0.2
0.0
1+F/ϕ
1.05
1.1
1.25
2.5
R ⩾ 10
ϕ = 1
ε = 1
0.0
0.2
0.4
0.6
0.8
e/R-1

Fig 4.6

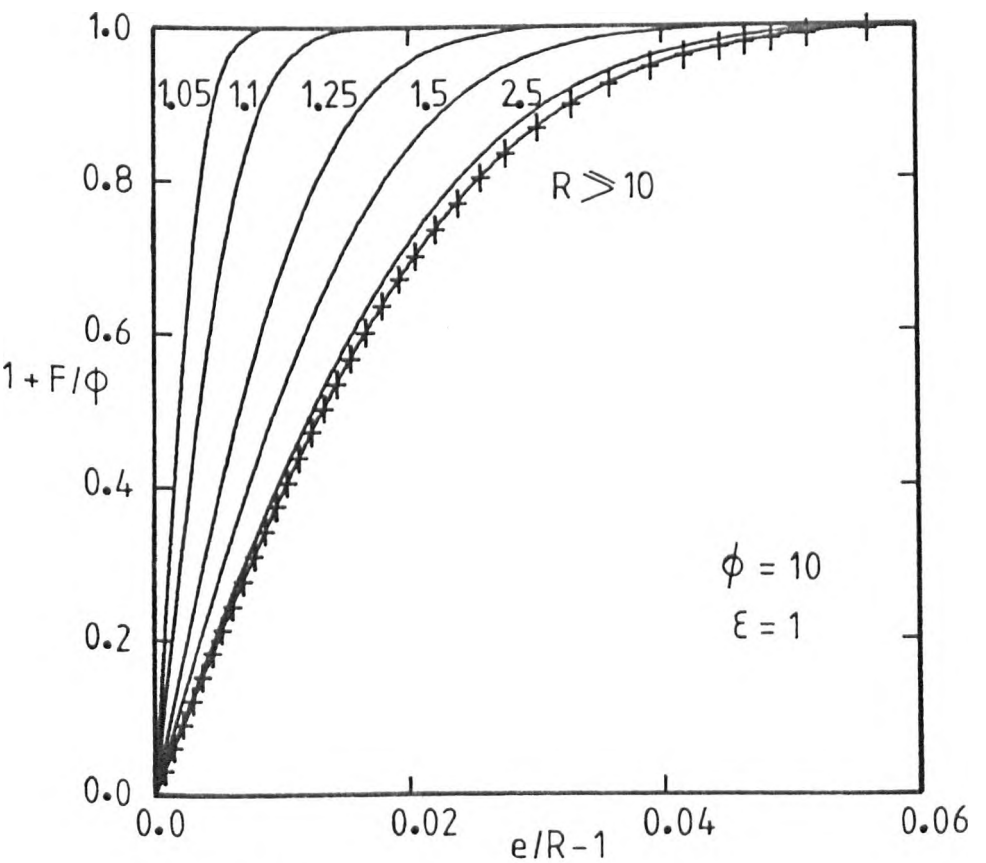
1.0
0.8
0.6
0.4
0.2
0.0
1+F/ϕ
1.05
1.1
1.25
1.5
2.5
R ⩾ 10
ϕ = 10
ε = 1
0.0
0.02
0.04
0.06
e/R-1

Fig 4.7

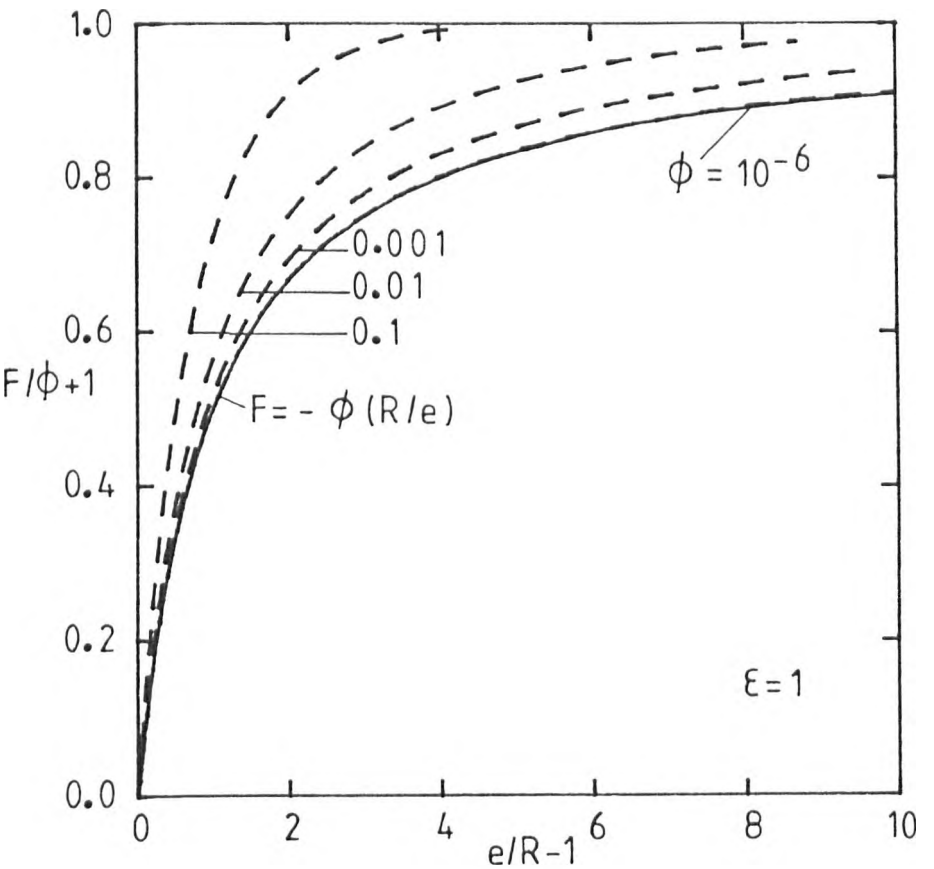

Fig 4.8 : Analytical solutions of concentration profiles for growth from zero size (equation (4.4)) for low values of ϕ (dashed lines). The full line represents the limiting quasi steady-state prediction (equation (2.69)). The numbers show the values of the solubility parameter ϕ.

radial distance from the centre of the sphere transformed as suggested by the analytical solutions (equation (4.4)). The evolution of numerically computed profiles in these figures is illustrated at several stages of the transient regime, namely with R = 1.05, 1.1, 1.25, 2.5 and 10.

In figure 4.4 (ϕ = 0.01 and ε = 1), the numerical predictions evolve rapidly towards the final asymptotic profile. The solution for R = 2.5 is indistinguishable from the final profile for R = 10^5, and is also indistinguished from the analytical predictions. The concentration gradient near the interface converges even more rapidly to the final solution than the tail of the profile. This must be due to the fact that very little material is needed to saturate the boundary layer while the tail of the profile requires larger times to be built up by diffusion.

The evolution of profiles with moderate and large solubility parameters (figures 4.5, 4.6 and 4.7) show the increasing importance of the transient stage. With ϕ = 1 and ε = 1, (figure 4.6), or ϕ = 10 and ε = 1 (figure 4.7) the profile for R = 2.5 is still distinguishable from the final one, but profiles for R = 10 and R = 10^5 cannot be distinguished. Again these final profiles are almost coincident with the equivalent analytical solutions of equation (4.4).

The evolution of concentration profiles shows that the transient stage is usually important until about R = 2.5, that is when the radius of the sphere is about 2.5 times the initial radius. This stage may include the most important part of the process, and analytical solutions cannot then be used.

By comparison between figures 4.4, 4.5, 4.6 and 4.7 it is evident that the boundary layer thicknesses increase with decreasing solubility parameters. Asymptotic profiles are shown in figure 4.8 in the range of very low ϕ. The actual solutions converge towards the quasi steady-state

which is nearly indistinguishable from the solution for $\phi = 10^{-6}$. Growth rates also confirm the quasi-steady state approximation as the limit of actual solutions in the range of very low ϕ.

4.6 Comparison between analytical solutions and approximate predictions of bubble growth

Gas bubbles can be characterized by only a single parameter ϕ, with $\varepsilon = 1$. For these cases it is possible to find precise limits of asymptotic regimes (Scriven, 1959), that is for very low ϕ

$$\phi = 2\beta^2 \tag{4.10}$$

and

$$R = (2\ \phi Z)^{\frac{1}{2}} \tag{4.11}$$

and for very large ϕ

$$\phi = \sqrt{\pi/3}\ \beta \tag{4.12}$$

or

$$R = 2\phi\sqrt{3/\pi}\ \sqrt{Z}\ . \tag{4.13}$$

For sufficiently long times the quasi-stationary equation (2.57) and quasi steady state equation (2.70) each leads to

$$R \simeq 2\ \beta\ \sqrt{Z} = (2\ \phi Z)^{\frac{1}{2}} \tag{4.14}$$

which is also the limit of analytical solutions of growth from zero size, (equation (4.11), for very low ϕ.

The other limit of quasi-stationary solutions for large ϕ (equation

(2.64)) may be expected to hold better in the range of very small Z, that is with large β. Therefore, for large R equation (2.64) becomes

$$R \simeq 2 \beta \sqrt{Z} = 2 \phi \sqrt{Z/\pi} \tag{4.15}$$

or

$$\phi = \sqrt{\pi} \beta \ . \tag{4.16}$$

However, these predictions of solubility parameters are about 73% in excess of those given by the analytical solutions (equation (4.12)).

By substitution of asymptotic dependence of R on $\sqrt{Z}$, (equation (4.8)), into the quasi-stationary equation (2.57) one obtains for large R

$$R = 2 \phi \left(\frac{1}{2\beta} + \frac{1}{\sqrt{\pi}} \right) \sqrt{Z} \tag{4.17}$$

and therefore the asymptotic quasi-stationary regime leads to

$$\phi = \beta \Big/ \left(\frac{1}{2\beta} + \frac{1}{\sqrt{\pi}} \right) \ . \tag{4.18}$$

In an attempt to find a generally acceptable approximation to the true analytical solutions equation (4.18) can be replaced by

$$\phi = \beta \Big/ \left(\frac{1}{2\beta} + \sqrt{\frac{3}{\pi}} \right) \tag{4.19}$$

so that its limits for very low and very large growth rates will be coincident with the corresponding limits of analytical solutions (equations (4.10) and (4.12) respectively).

The ratios ϕ_{ap}/ϕ are plotted versus log β in figure 4.9, where ϕ_{ap} is the approximate prediction of solubility parameter and ϕ the equivalent analytical solution of equation (4.5) with $\varepsilon = 1$. Both quasi steady state

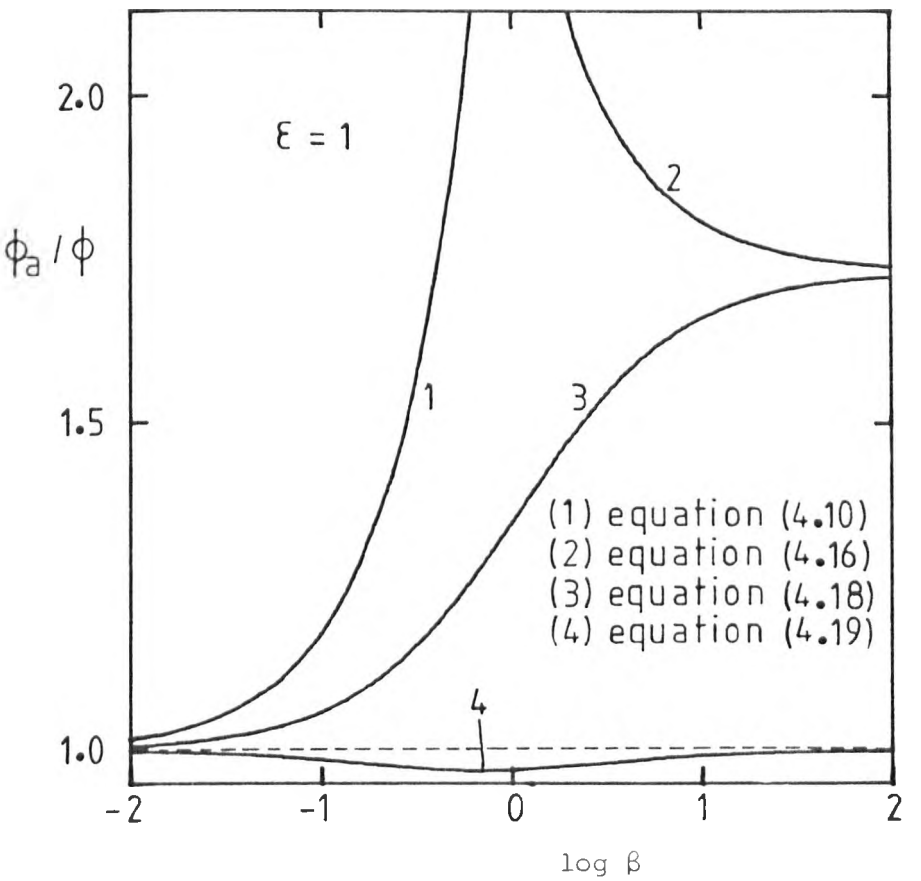

Fig 4.9 : Relation between the approximate values of solubility parameters ϕ_{ap} predicted by
1 - equation (4.10)
2 - equation (4.16)
3 - equation (4.18)
4 - equation (4.19)
and the equivalent analytical values of ϕ.

(equation (4.10)) and quasi-stationary solutions (equation (4.18)) are reasonably good in the range of very low growth rates. Equation (4.16) is generally very poor even in the range of rapid growth. The failure of this flat slab model is possibly due to the role of boundary motion. Finally equation (4.19) is an excellent approximation in the ranges $\beta < 0.05$ and $\beta > 10$ where the differences are less than 1% of the analytical $\phi(\beta)$ values. It is still generally acceptable for $0.05 < \beta < 10$ where the differences are $< 3\%$.

4.7 Comparison between approximate and numerical solutions of the transient initial stage

The simple form of quasi steady-state approximations suggests a useful representation of the relation between the square radius and time (figure 4.10) for growth from finite size. All the solutions represented in figure 4.10 reproduce nearly linear relations between R^2 and Z. These results also confirm the gradual convergence of actual solutions to the quasi steady-state limit, (dashed line in figure 4.10), for low solubility parameter. It has already been shown that quasi-stationary solutions converge to the quasi steady-state approximations for very low ϕ and that other approximate predictions are poorer in this region.

The quasi-stationary approximation suggests a different representation for very large solubility parameters (equations (4.13) and (2.64)). In the asymptotic regime R becomes a unique function of the transformed time $\phi^2 Z$. This unique dependence can be extended to growth from finite size (figure 4.11), where the solutions for $\phi = 100$ and $\phi = 1000$ are almost indistinguishable. Therefore the case $\phi = 100$, $\varepsilon = 1$ is good representation of growth of all bubbles with very large solubility parameters. The limiting

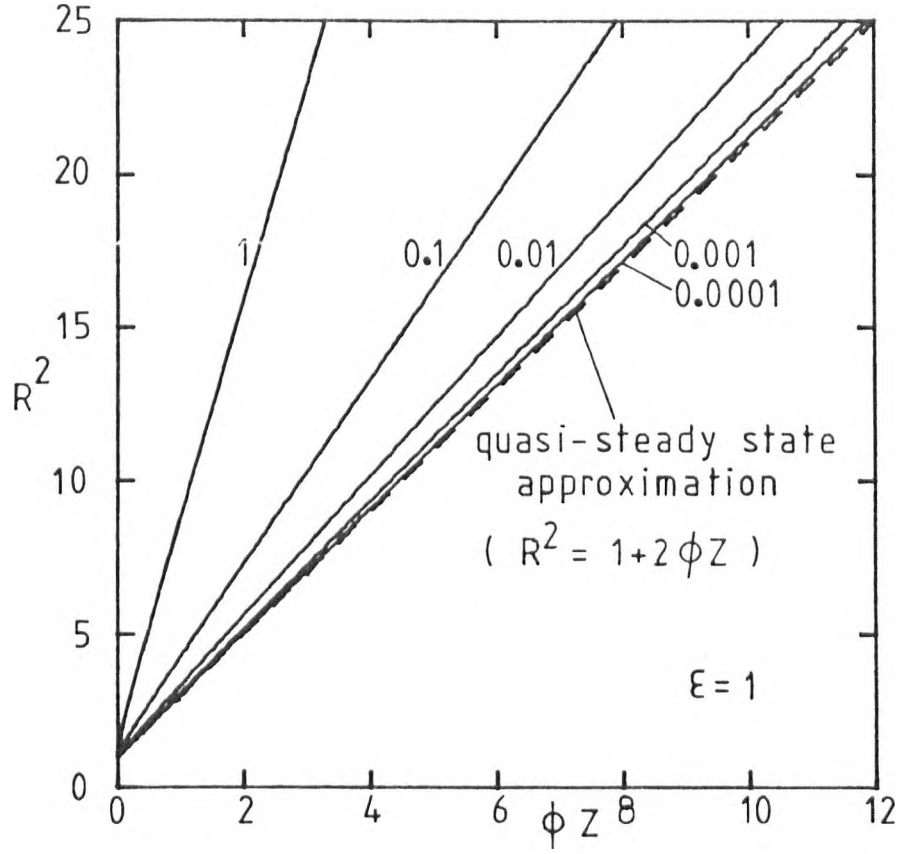

Fig 4.10 : Initial stage of growth from finite size for low and moderate solubility parameters ϕ. The numbers show the values of ϕ. The dashed line represents the quasi steady-state approximation (equation (2.70)).

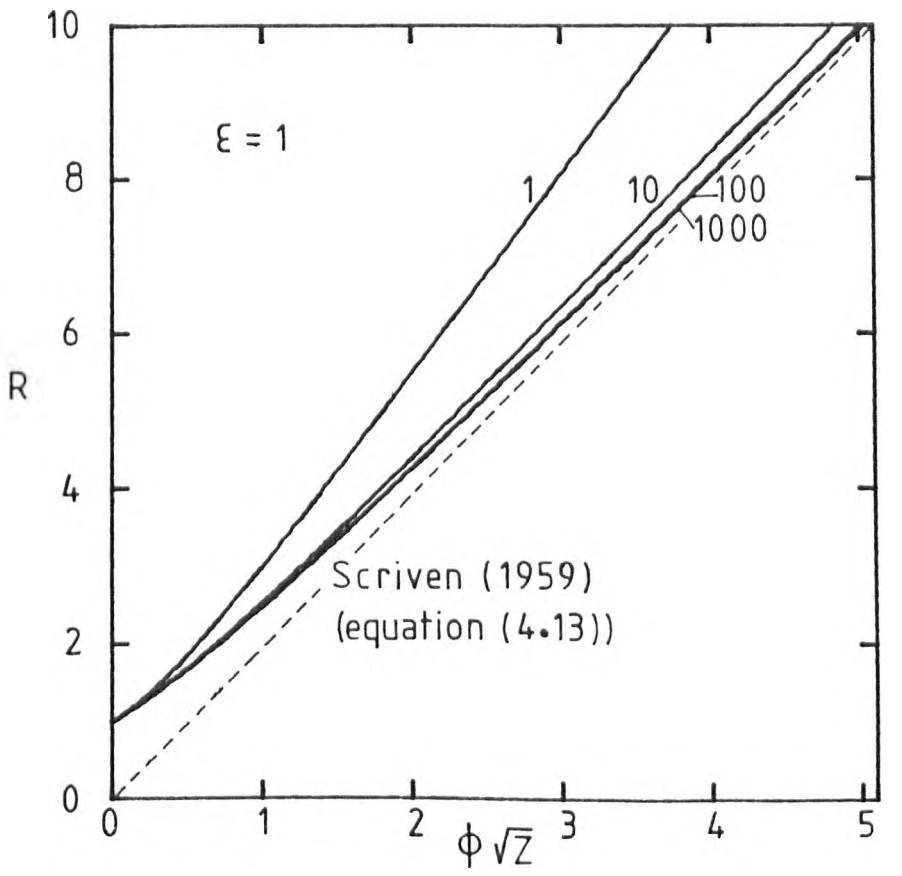

Fig 4.11 : Initial stage of growth from finite size for moderate and large ϕ. The numbers indicate the values of ϕ.

growth from zero size (equation (4.13)) is also shown in figure 4.11 (dashed line).

Other simple approximate solutions have been proposed in the literature to quantify the initial transient stage of growth from finite size. Martins (1969) proposed the following transformation of equation (4.13) into

$$R = 1 + 2\phi\sqrt{3/\pi}\ \sqrt{Z} \ . \tag{4.20}$$

A different approximation was obtained by Rosner and Epstein (1972) by assuming a simple approximate form of concentration profiles.

$$\frac{1}{2}\,(R^2 - 1) - (1 - 1/R) = 2\phi^2\, Z \ . \tag{4.21}$$

Equation (4.21) leads to the asymptotic regime

$$R = 2\phi\sqrt{Z} \tag{4.22}$$

which is about 2.33% in excess of analytical predictions of R in the range of large ϕ (equation (4.13)). However, equation (4.21) fails for low and moderate ϕ.

In figure 4.12 it is shown that equation (4.21) is reasonably accurate for large ϕ even during the initial transient stage. Spherical symmetry must be relatively insignificant whenever the boundary layer is very thin, which explains the agreement between the actual numerical solutions (ϕ = 100) and the flat-slab model (equation (2.64)) during the very early stage. Equations (4.13) and (4.20) are poor approximations of the initial stage of growth from finite size.

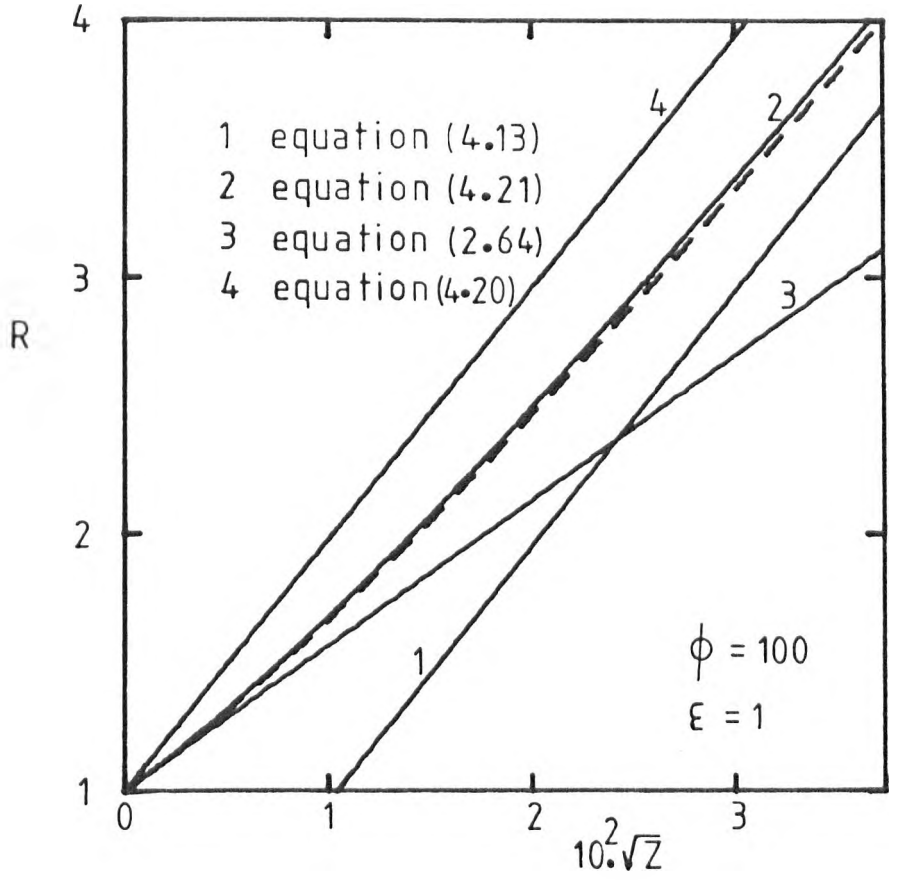

Figure 4.12 : Comparison between the actual finite difference predictions (dashed line) and approximate predictions for the case $\phi = 100$, $\varepsilon = 1$.

4.8 The transient stage of growth from finite size

Figure 4.10 has shown that in the range of low and moderate solubility parameters the actual solutions converge to quasi steady-state approximations. In the limit this unique solution reduces to a linear relation between the square radius and the transformed time ϕZ. Besides, even with moderate ϕ values the growth from finite size is reasonably given by

$$R^2 = 1 + 4\,\beta^2\,Z\ , \tag{4.23}$$

where β is the characteristic growth constant for the asymptotic regime.

From equation (4.8) it is possible to write for the analytical solutions of growth from zero size

$$\frac{dR}{dZ} = \beta/\sqrt{Z} = 2\beta^2/R\ . \tag{4.24}$$

Numerical predictions of $\left(\frac{dR}{dZ}\right)_n$ for the growth from finite size $R(0) = 1$ are compared to $2\beta^2/R$ in table 4.4. These results include a wide range of values of ϕ for the case $\varepsilon = 1$. The values of β used in the table were obtained from numerical results for $R = 10^5$. By the time the radius of the sphere is twice the initial size growth rates for growth from finite size are usually not significantly different from the rates for the growth from zero size. These differences vanish before an increase of ten times the initial size of the sphere.

It is worth noticing that equation (4.23) is reproduced by integration of equation (4.24) from $Z = 0$; $R = 1$. This condition requires a very short transient evolution of concentration profiles towards the unique asymptotic dependence expressed by equation (4.4). Figure 4.4 demonstrates that low values of ϕ satisfy that requirement.

Table 4.4

Relation between the rates of growth from finite size, $(dR/dZ)_n$, and the rates of growth from zero size for $\varepsilon = 1$.

ϕ	0.001	0.01	0.1	1	10
R	$\left(\frac{dR}{dZ}\right)_n \Big/ \left(\frac{2\beta^2}{R}\right)$				
1.1	1.052	1.118	1.428	2.634	3.759
1.25	1.027	1.054	1.152	1.559	1.953
1.5	1.015	1.031	1.060	1.220	1.394
2	1.010	1.018	1.021	1.073	1.128
5	1.000	1.001	1.002	1.004	1.008
10	1.000	1.000	1.000	1.000	1.000
100	1.000	1.000	1.000	1.000	1.000
10^5	1.000	1.000	1.000	1.000	1.000

This analysis of growth rates is based on the evolution of concentration profiles that is to say the values of $\left(\frac{\partial C}{\partial r}\right)_a$ which is more significant than fitting R, Z data into equation (4.8). This explains why the convergence to asymptotic conditions is quicker in table 4.4, than in table 4.2. The differences are mostly due to an initial quantity $Z(1) = 1/(4\beta^2)$, that is, the time required for a sphere to grow from zero size to the reference size ($R = 1$); that quantity is non existent in growth from finite size. For $R >> 1$, Z becomes nearly proportional to R^2 and $Z(1)$ represents a negligible fraction of the actual dimensionless time Z.

4.9 The role of spherical symmetry in the diffusion controlled growth of spheres

It was shown that in the range of very low solubility parameters, ϕ, the actual solutions for growth converge to quasi steady-state conditions, (equations (2.67) and (2.68)) which lead to

$$\left(\frac{e}{R}\right)^2 \cdot \frac{\partial F}{\partial\left(\frac{e}{R}\right)} = - F_a = \phi \ . \tag{4.25}$$

Equation (4.25) shows that the concentration gradients are very steep near the interface because the area available for the spherically symmetric transport increases as $(e/R)^2$.

Quasi steady-state and quasi-stationary approximations converge in the range of very low ϕ. The effect of spherical symmetry on concentration profiles in that range can then be easily estimated by comparing quasi-stationary profiles (equation (2.58)) with the flat slab model (equation (2.65)). The contribution of spherical symmetry to the rate of the process can also be established by comparing the quasi steady-state (equation (2.70)) and flat slab approximations (equation (2.64)). The latter proves to be a very poor description.

With large ϕ the boundary layer (obtained by extrapolation of the concentration gradient at the interface) is thin and spherical symmetry is expected to become much less important than with low ϕ. This conclusion is confirmed by the fact that quasi-stationary and flat slab approximations converge in the range of large ϕ. Both approximations are based on ignoring the convective transport of solute and, in spite of spherical symmetry, the quasi-stationary solutions converge to flat slab approximations (figure 4.9).

However the actual finite difference predictions of the time required to reach a generic radius R can be as little as 1/3 of the equivalent quasi-stationary predictions. The differences are the result of radial convection and this is dependent on the spherical symmetry of the system.

In the intermediate range of ϕ values, $(0.1 < \phi < 10)$, spherical symmetry remains very important, but its role decreases with increasing ϕ. On the contrary the radial convection can be ignored in the range of very low ϕ but its role is gradually enhanced as ϕ increases and accounts for the differences between actual solutions and quasi-stationary approximations.

4.10 Conclusions

The analysis of diffusion controlled growth of spheres with constant conditions at the interface was simplified by making the material balances dimensionless. The dynamics of the process is then completely specified by two parameters, ϕ, and ε. The role of the diffusivity, D, is readily obtained by recovering the real time t from the definition of the dimensionless time Z. During the asymptotic regime the growth rate is proportional to the square root of D, that is $(da/dt) = \beta\sqrt{D}/\sqrt{t}$. In the range of very low solubility parameters the growth constant β is nearly proportional to $\phi^{\frac{1}{2}}$, so that similar effects can be obtained by corresponding changes of either diffusivity or solubility parameter. On the contrary, β is proportional to ϕ for very large values of solubility parameter and the growth rate is then more sensitive to changes of solubility parameter than to changes of D. The empirical equation (4.19) provides reasonably good predictions for the complete range of ϕ values, and illustrates the transition between those limiting conditions.

Whenever $\varepsilon < 1$ the partial molar volume of solute represents a positive contribution to the volume of the liquid medium by the solute. During growth the transfer of material from the liquid into the sphere is responsible for a decrease of volume of the solution which opposes the expansion of the boundary layer. Growth rates are then enhanced relative to the case when the volume contribution of solute is negligible. With low ϕ that volume contribution is negligible except for unrealistically large partial molar volumes of solute.

The nature of limiting regimes for very low and very large ϕ was clarified and the limitations of some approximate solutions were investigated. The numerical finite difference technique developed in this work was successfully tested by comparison with exact solutions over wide ranges of all the relevant parameters and can therefore be expected to perform equally well with dissolution and for other more complex systems.

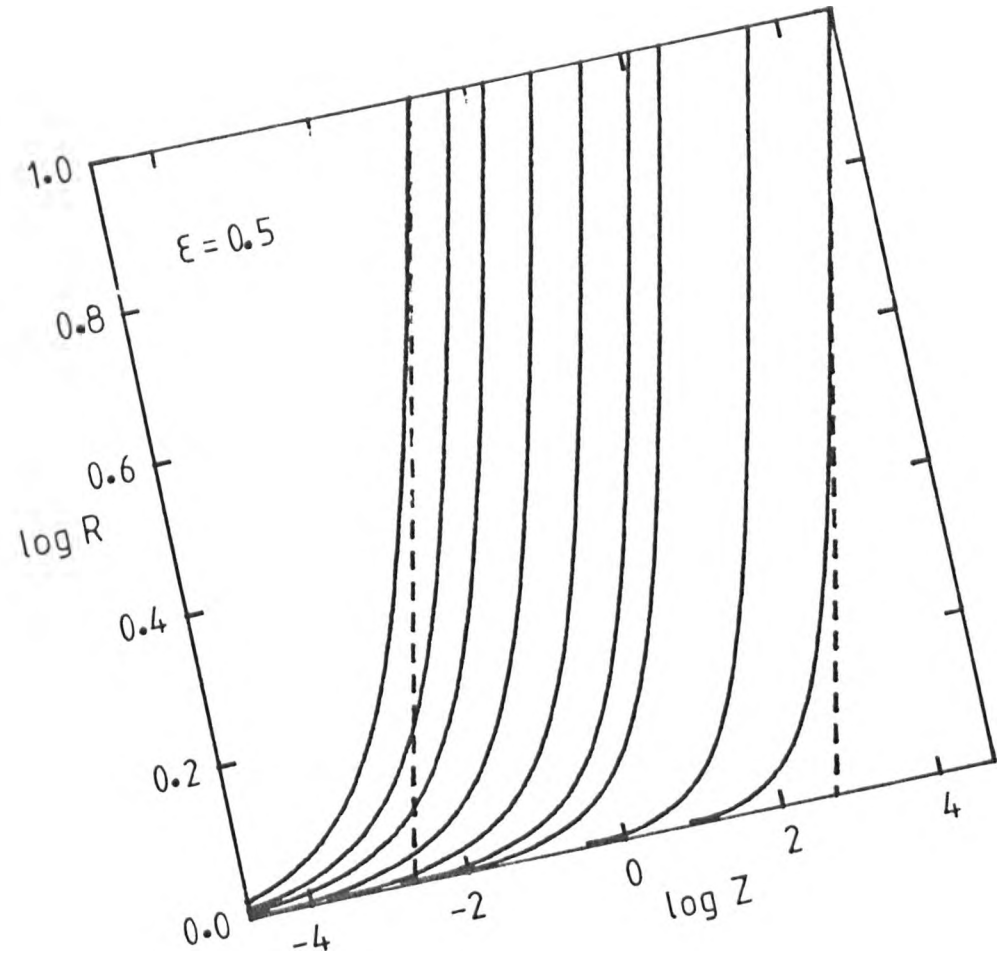
1.0
0.8
0.6
0.4
0.2
0.0
log R
ε = 0.5
-4
-2
0
2
4
log Z

Fig 4.2

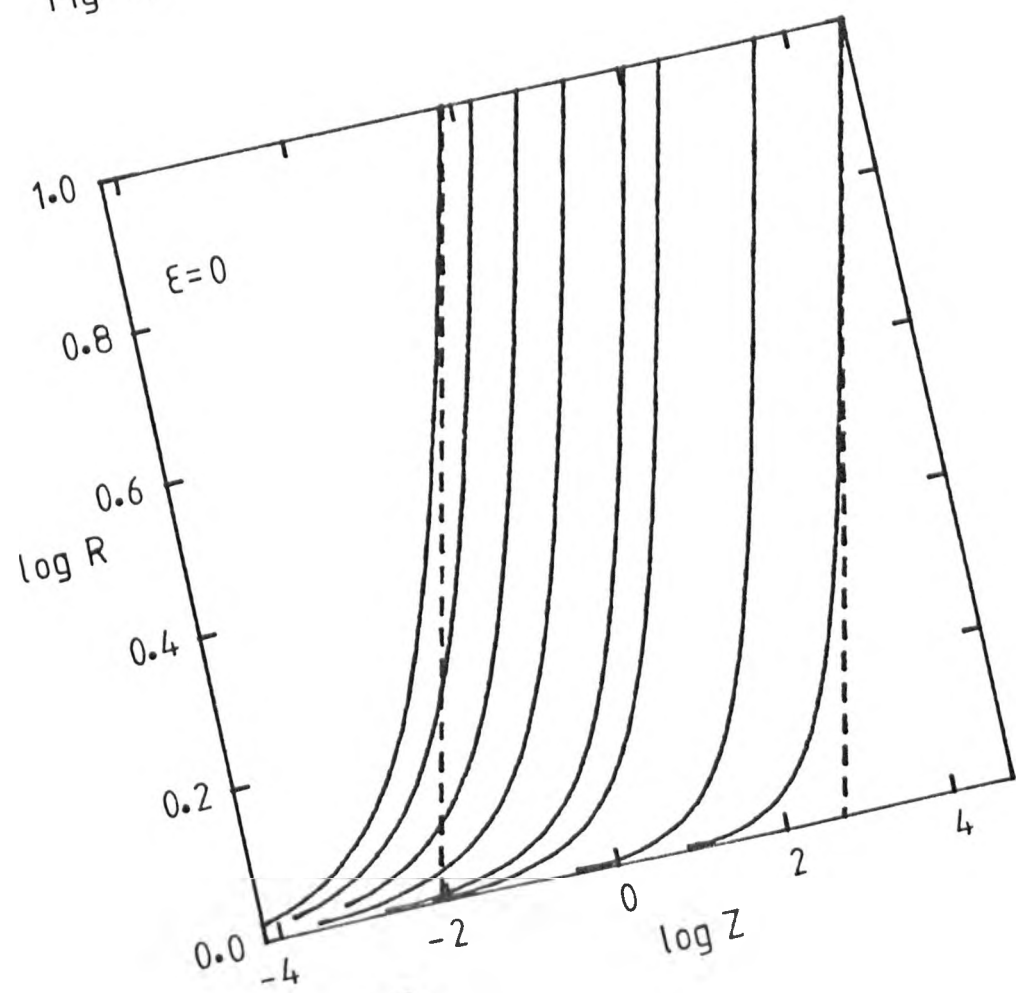
1.0
0.8
0.6
0.4
0.2
0.0
log R
ε=0
-4
-2
0
2
4
log Z

Fig 4.3

CHAPTER V

5.1 Dissolution of one-component spheres

It was demonstrated in Chapter IV that growth tends to an asymptotic regime, which was solved analytically. This tendency assists the development and testing of accurate numerical techniques. However for all cases of growth from finite initial size transient behaviour is important at least until the sphere has doubled in size (volume of precipitate increased by a factor of 8). This at once suggests that dissolution must be considered a transient regime. In general the partial differential balances cannot be solved analytically and the accuracy of simple approximate solutions is rather doubtful. Numerical solutions are also susceptible to poor accuracy and efficiency unless the method includes algorithms to optimize the finite differences.

The mathematical analysis of dissolution is of interest to some problems of glass technology and chemical engineering. The primary objective is to obtain the relationship between the radius of the sphere and time, but the analysis of concentration profiles is essential for the interpretation of mechanisms. It is equally important to identify the similarities and general solutions especially in the ranges of very low and very large "driving-forces".

It is convenient to use a positive solubility parameter F_a to characterize the rate of dissolution. The diffusivity can be excluded from the basic analysis of the dynamics of one-component spheres so that throughout this chapter the terms slow and rapid dissolution will refer to small ($F_a < 0.01$) and large values of Fa ($F_a > 10$) respectively.

5.2 Numerical solutions

The numerical technique developed in this work was described in Chapter III and tested in detail for growing spheres as described in Chapter IV. The results given here were obtained by this method.

In table 5.1 and figure 5.1 the dimensionless time required for complete dissolution, Z_o is related to the solubility parameter F_a. The curves in figure 5.1 represent the following values of parameter ε = 0, 0.5, 1, 1.5, 2. In the range of very low F_a the dissolution time converges to

$$Z_o = 1/(2\ F_a) \tag{5.1}$$

and becomes nearly independent of the value of parameter ε, except for unrealistically high or low ε, that is $\varepsilon \gg 2$ or $\varepsilon \ll 0$ (see table 3.4). In the case $\varepsilon = 1$ dissolution becomes quicker than the predictions of equation (5.1) and the deviations increase with F_a. The parameter ε plays an important role in the range of moderate and large F_a values.

From the definition of $F_a = \dfrac{C_a - C_\infty}{C_s^\circ(1 - C_a\ v)}$ it follows that

$$\lim_{C_a \cdot v \to 1} F_a = \infty \ . \tag{5.2}$$

As $\varepsilon = 1 - C_s^\circ \cdot v$ it also follows from the definition of F_a that for $\varepsilon > 1$

$$\lim_{C_a \to \infty} F_a = 1/(\varepsilon - 1) \ . \tag{5.3}$$

This last condition is shown in figure 5.1 where Z_o decreases very rapidly as F_a approaches 1 for $\varepsilon = 2$ and 2 for $\varepsilon = 1.5$ respectively.

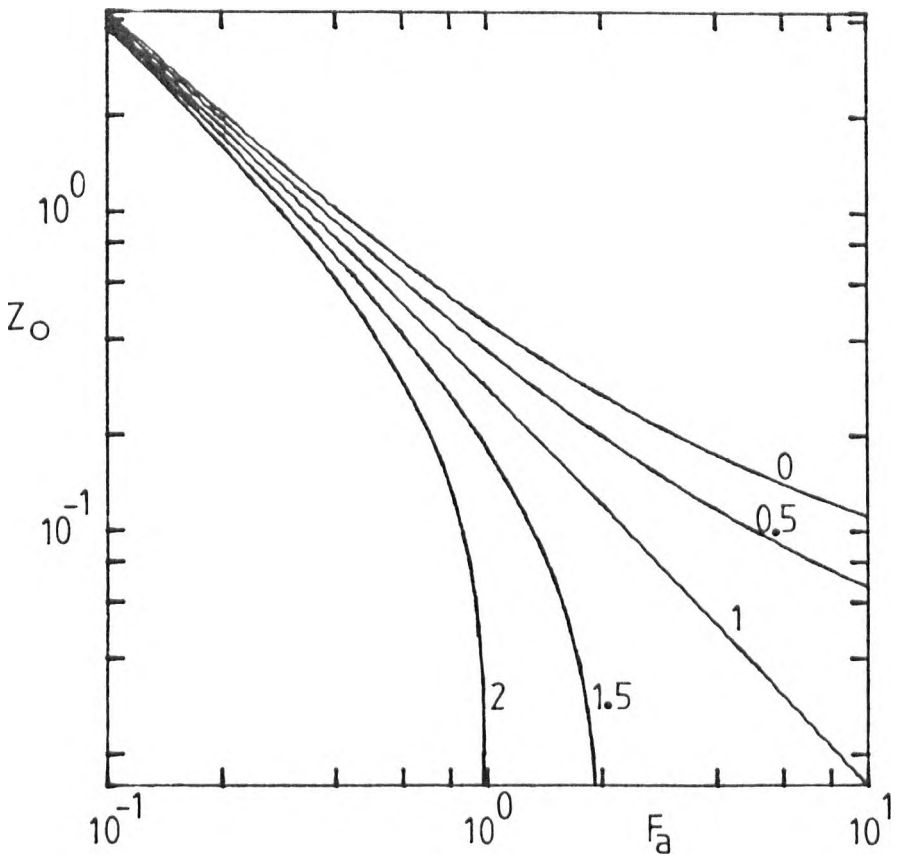

Fig 5.1 : Relation between finite difference predictions of dimensionless time required for complete dissolution, Z_o, and solubility parameter F_a. The figures show the values of ε.

Table : 5.1

Dimensionless times required for complete dissolution, Z_o.

ε	0	0.5	1	1.5	2
F_a			Z_o		
0.001	486.6	486.5	486.4	486.3	486.2
0.01	46.48	46.40	46.25	46.11	45.99
0.1	4.214	4.106	3.994	3.880	3.764
0.2	2.057	1.953	1.846	1.737	1.623
0.5	0.834	0.742	0.644	0.539	0.4230
0.75					0.1709
0.9					0.0792
0.95					0.0492
1	0.451	0.3707	0.2828	0.1815	-
1.5				0.0707	
1.75				0.03769	
1.9				0.01919	
2	0.2670	0.1987	0.1214	-	
5	0.1536	0.1003	0.03861		
10	0.1111	0.0669	0.01599		
20	0.0855	0.0483	0.00656		
50	0.0651	0.03473	0.002006		
100	0.0546	0.02835	0.000814		

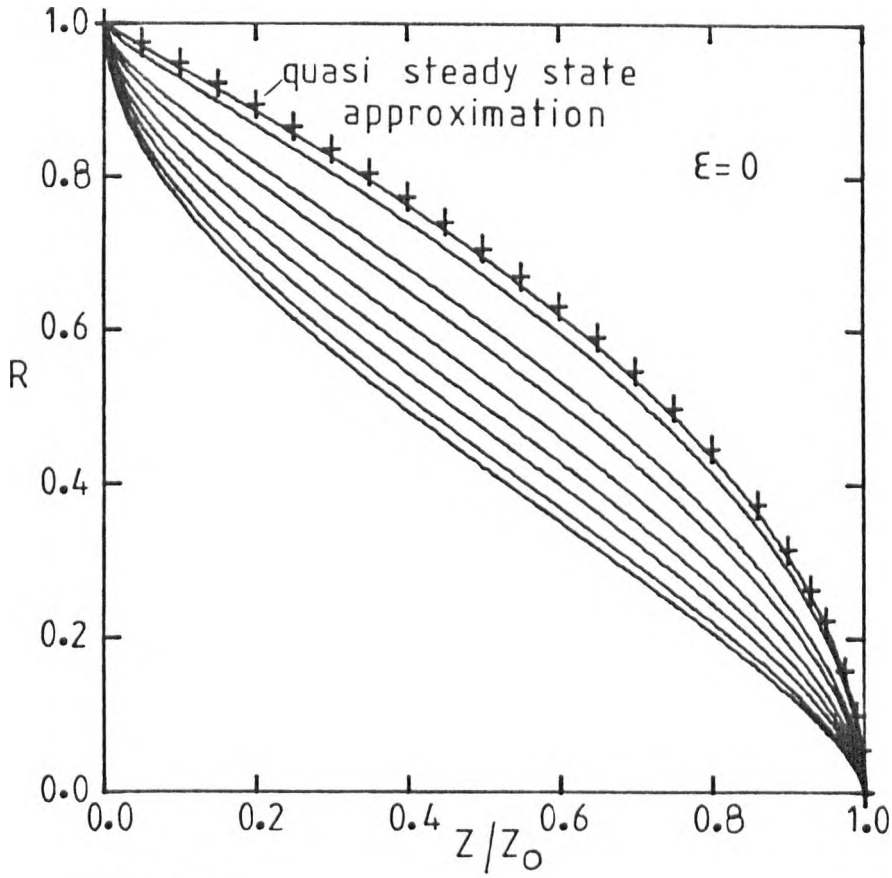

Fig 5.2

Figs 5.2 to 5.6 : Finite difference predictions of dissolution. The symbols (+) represent the quasi steady-state approximation (equation (2.70)). The values of ε are shown in these figures and the values of solubility parameter are, from top to bottom,

in fig 5.2 : F_a = 0.001, 0.01, 0.1, 0.2, 0.5, 1, 2, 5 and 10

in fig 5.3 : F_a = 0.001, 0.01, 0.1, 0.2, 0.5, 1, 2, 5 and 10

in fig 5.4 : F_a = 0.001, 0.01, 0.1, 0.2, 0.5, 1, 2, 5, 10, 20, 50, 100 and 1000.

in fig 5.5 : F_a = 0.001, 0.01, 0.1, 0.2, 0.5, 1, 1.5, 1.75 and 1.9.

in fig 5.6 : F_a = 0.001, 0.01, 0.1, 0.2, 0.5, 0.75, 0.9 and 0.95.

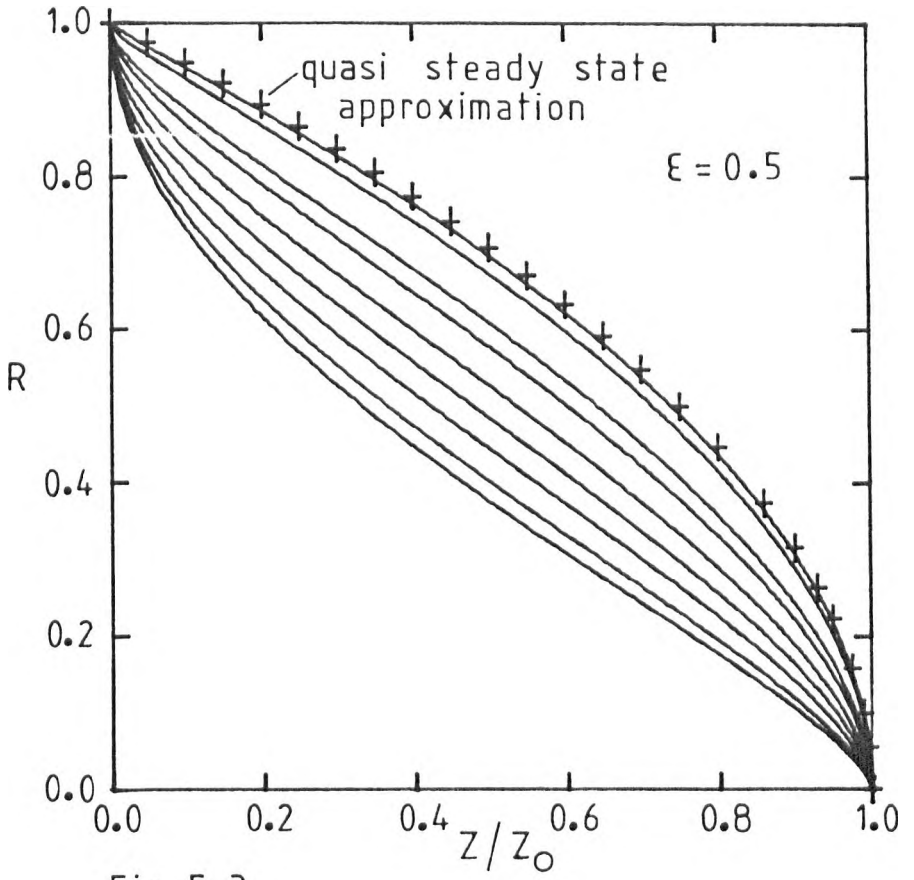
quasi steady state
approximation
ε = 0.5
R
Z/Z_o
1.0
0.8
0.6
0.4
0.2
0.0
0.0
0.2
0.4
0.6
0.8
1.0

Fig 5.3

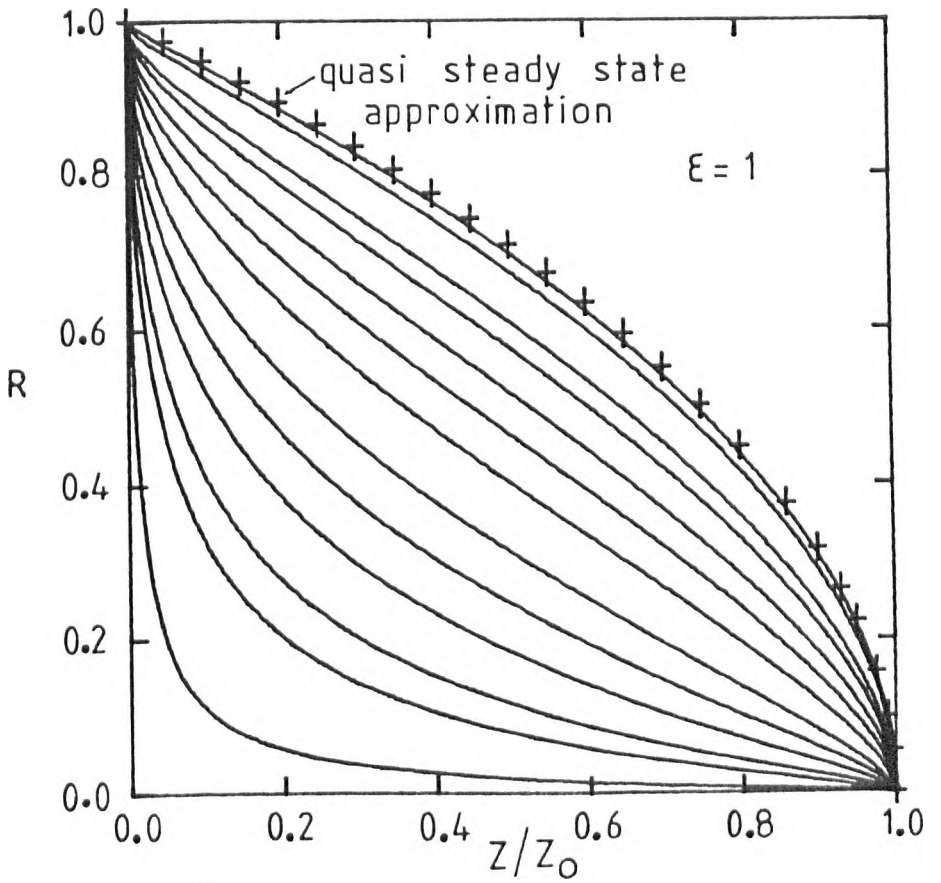
quasi steady state
approximation
ε = 1
R
Z/Z_o
1.0
0.8
0.6
0.4
0.2
0.0
0.0
0.2
0.4
0.6
0.8
1.0

Fig 5.4

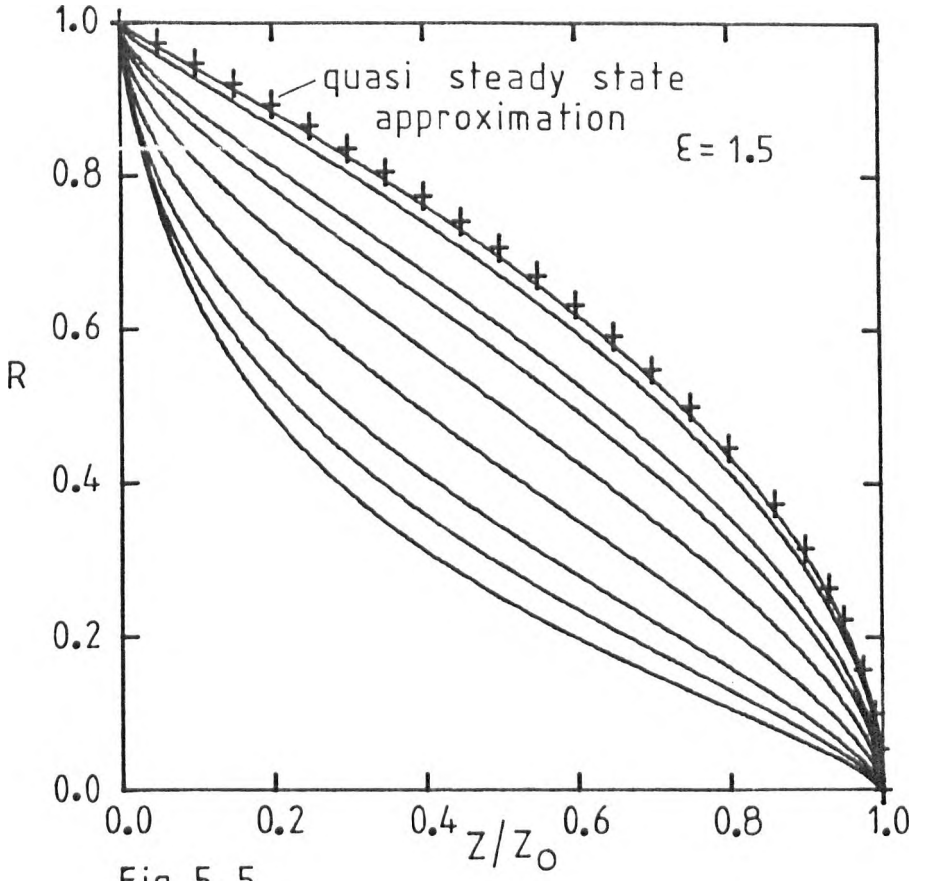
quasi steady state
approximation
ε = 1.5
R
1.0
0.8
0.6
0.4
0.2
0.0
0.0
0.2
0.4
0.6
0.8
1.0
Z/Z_o

Fig 5.5

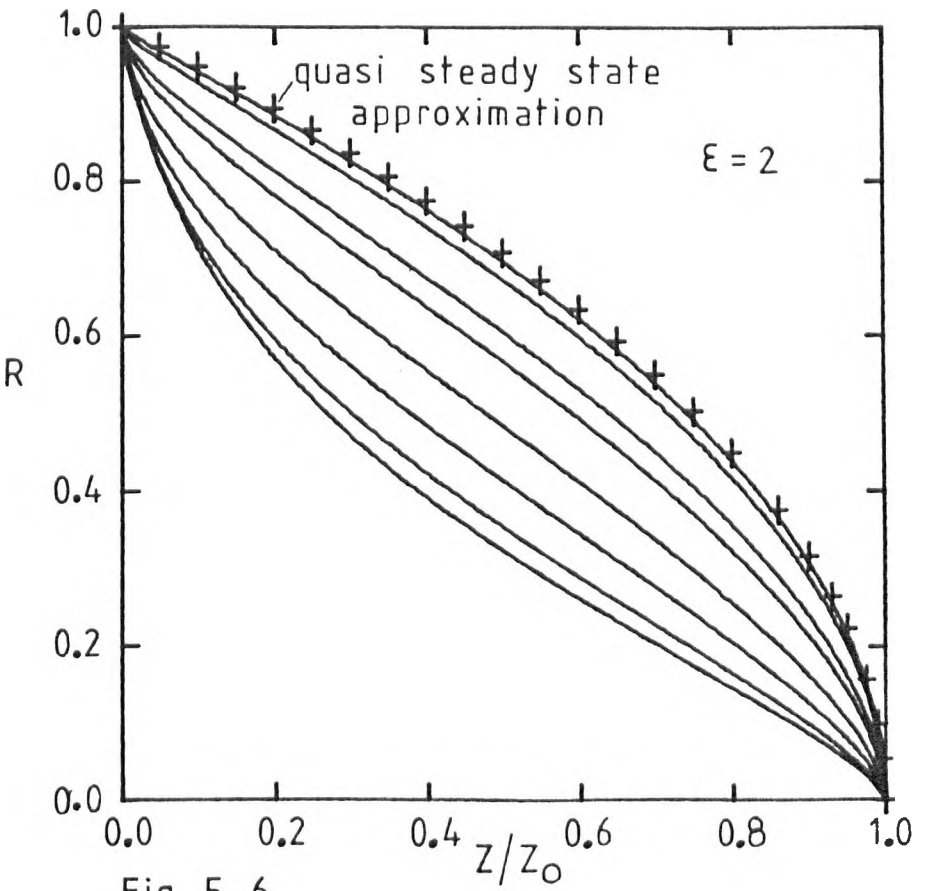
quasi steady state
approximation
ε = 2
R
1.0
0.8
0.6
0.4
0.2
0.0
0.0
0.2
0.4
0.6
0.8
1.0
Z/Z_o

Fig 5.6

The computed relations between the dimensionless radius, R, and the dimensionless time Z are shown in figures 5.2 to 5.6 for several values of ε from 0 to 2. The time was normalized in terms of Z_o to allow the simultaneous representation of a wide range of F_a values.

For very low solubility parameters ($F_a < 0.001$) the actual numerical solutions converge to the quasi steady-state approximations (equation (2.70)), and become independent of ε. Equation (2.70) illustrates the limiting regime with increasing rate of dissolution throughout the whole process. As F_a increases the solutions diverge progressively from that limiting case. The dissolution rates decrease during the early stages but increase again during the final stages. The point at which this inflection occurs is progressively shifted from relatively close to the beginning (R=1), for very low solubility parameters F_a, to almost complete dissolution (R=0) for high values of F_a.

Figures 5.4 demonstrate the existence of a unique limiting solution, (equation (2.70)), for low solubility. On the contrary, there is no such limiting behaviour in the range of very large F_a. In these conditions the last stage of the process becomes very much slower than the initial and intermediate stages. For example, with $F_a = 1000$; $\varepsilon = 1$ the sphere decreases to 10% of the initial size (R=0.1) in only about 11% of the total dissolution time.

5.3 Concentration profiles

Concentration profiles are illustrated in figures 5.7 to 5.9 for the case $\varepsilon = 1$ (gas bubbles) and F_a from 0.0001 to 100. This series assists understanding of the evolution of boundary layers and of the factors and mechanisms which are likely to influence their shape. In addition the cases $F_a = 10$; $\varepsilon = 0$, and $F_a = 0.95$; $\varepsilon = 2$ are illustrated in figures 5.10 and 5.11 respectively and serve the purpose of analysing the effects of the partial molar volume of solute.

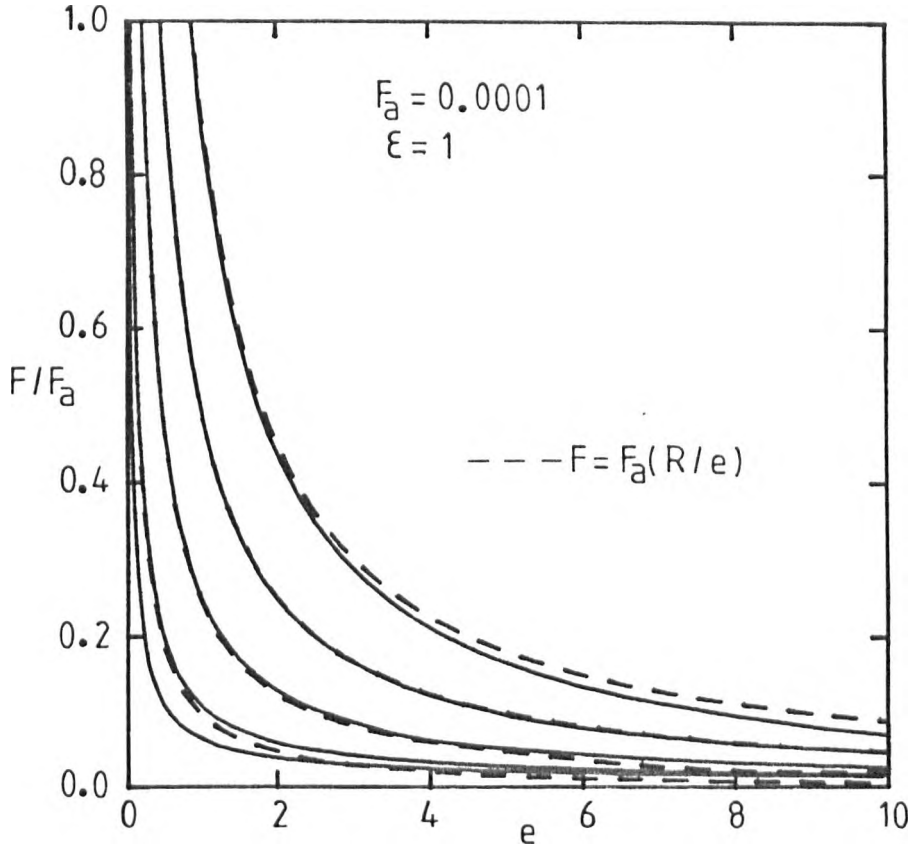

Fig 5.7 : Finite difference prediction of concentration profiles for the case F_a = 0.0001, ε = 1 at several stages of dissolution which correspond, from right to left, to R = 0.9, 0.5, 0.25, 0.1 and 0.05. The dashed lines represent the quasi steady-state (equation (2.69)).

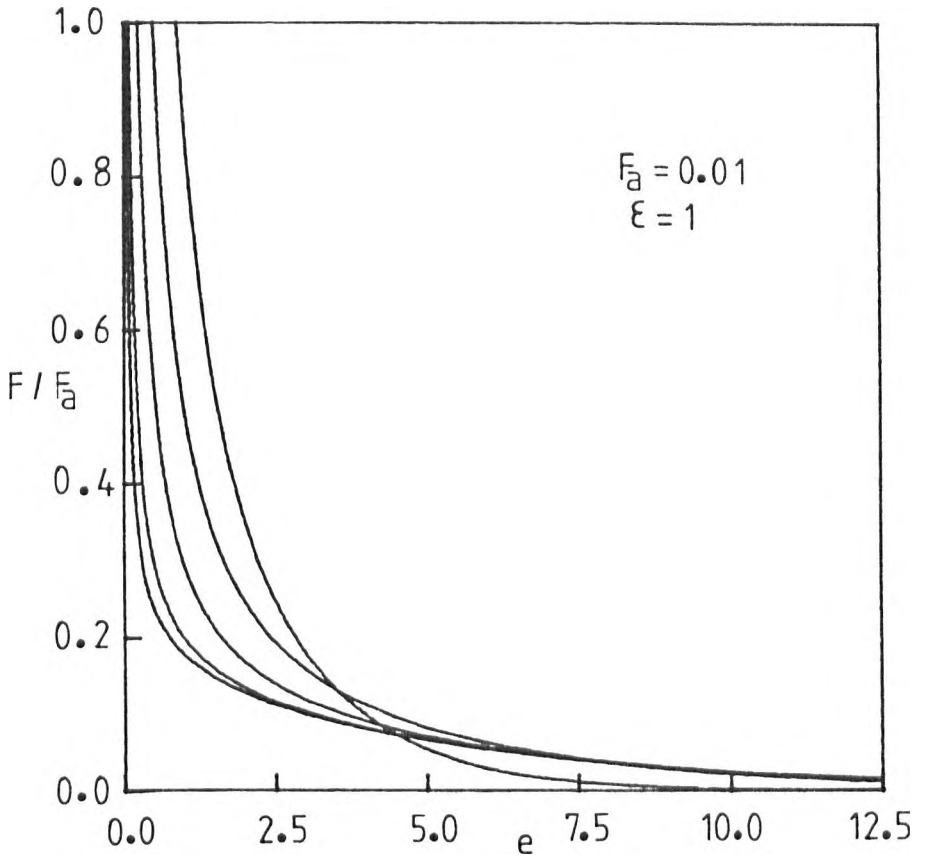

Fig 5.8a

Figs 5.8a to 5.8e : Finite difference predictions of concentration profiles at several stages of dissolution corresponding (from right to left) to R = 0.9, 0.5,0.25, 0.1 and 0.05 respectively. The values of ε and F_a are shown in the figures.

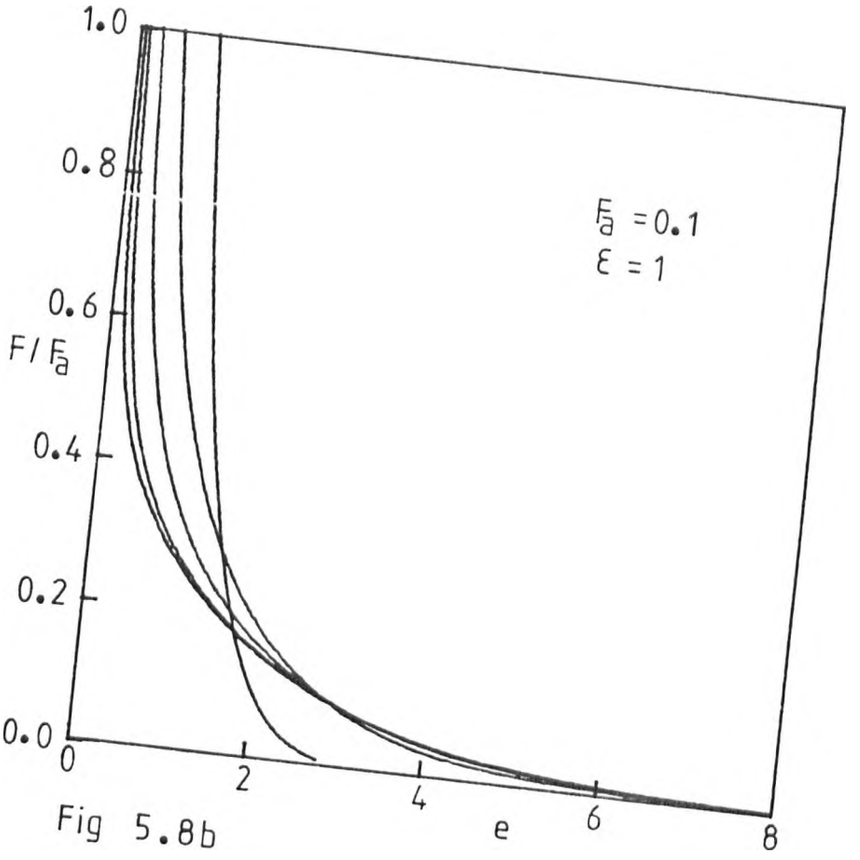

Fig 5.8b

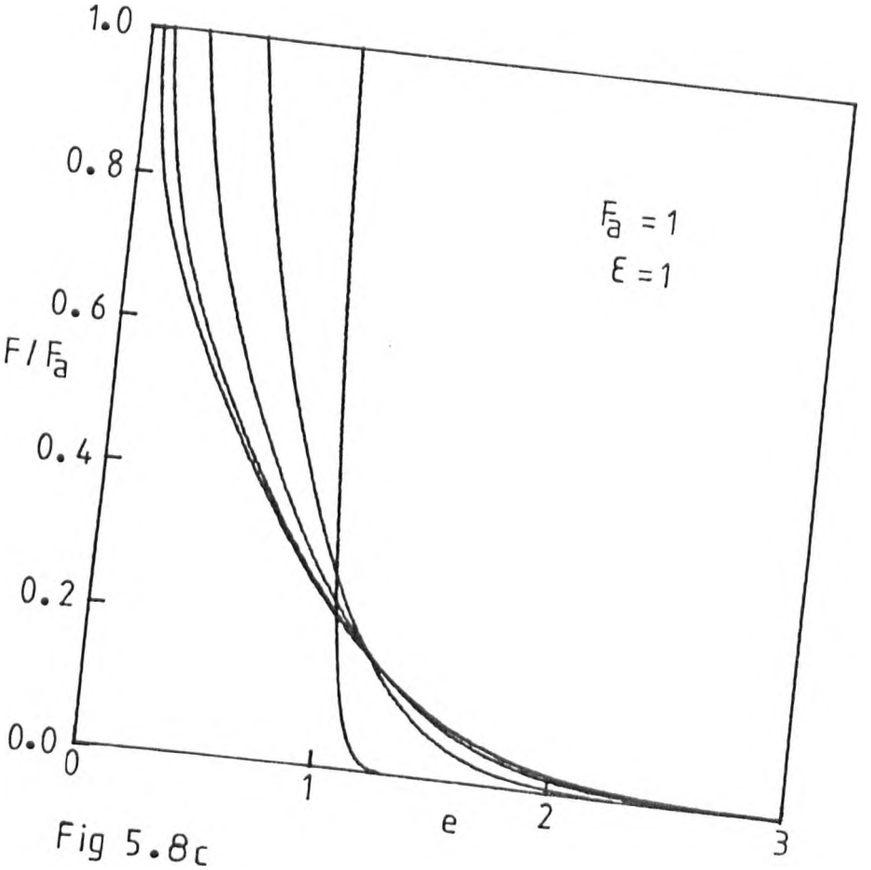

Fig 5.8c

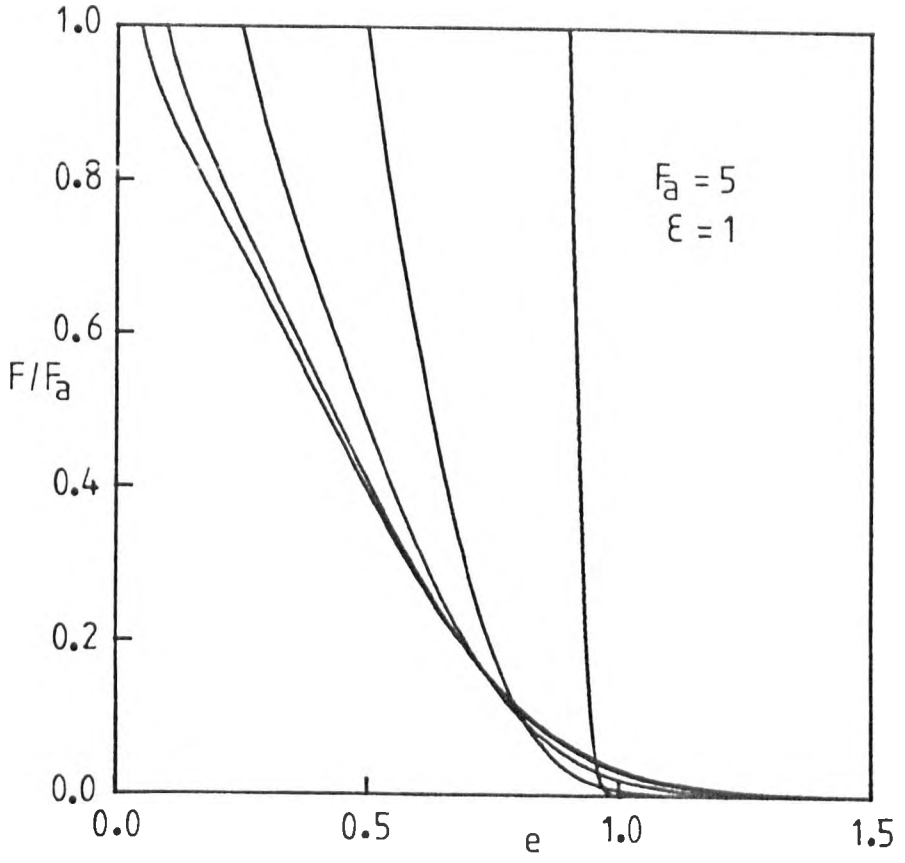

Fig 5.8d

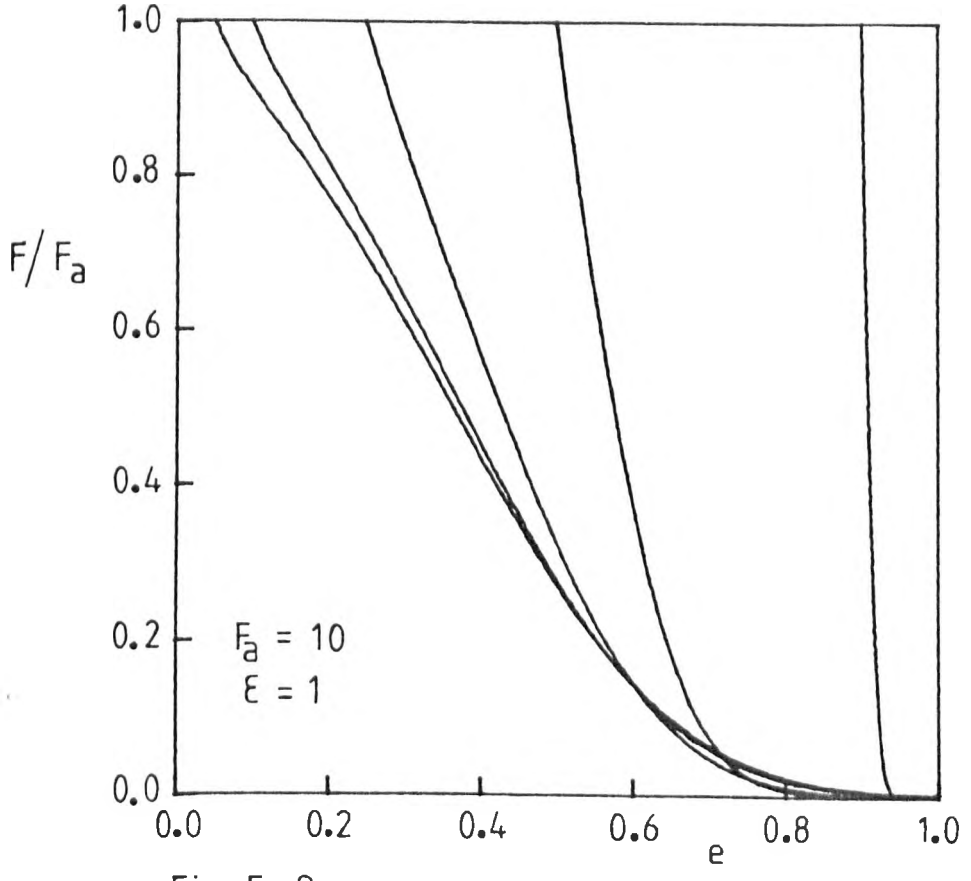

Fig 5.8e

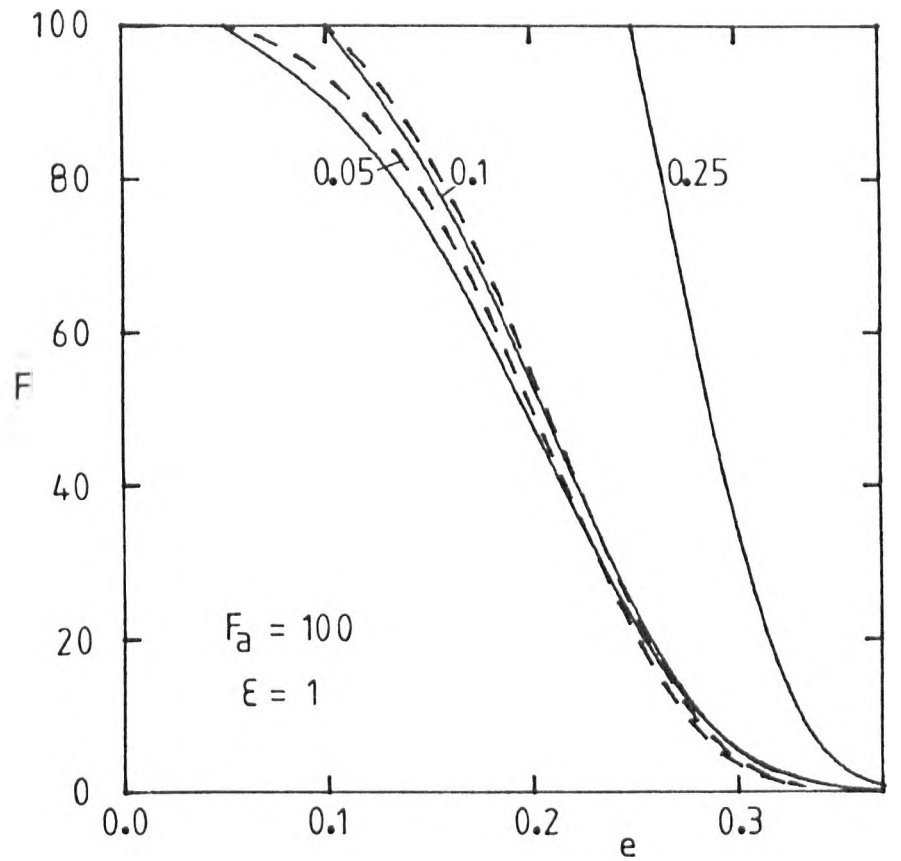

Fig 5.9 : Concentration profiles during dissolution. The full lines represent the finite difference predictions corresponding to the dimensionless radii R = 0.25, 0.1 and 0.05. The dashed lines represent the transformation from R = 0.25 to R = 0.1 and 0.05 due only to radial convection (equation (5.6)).

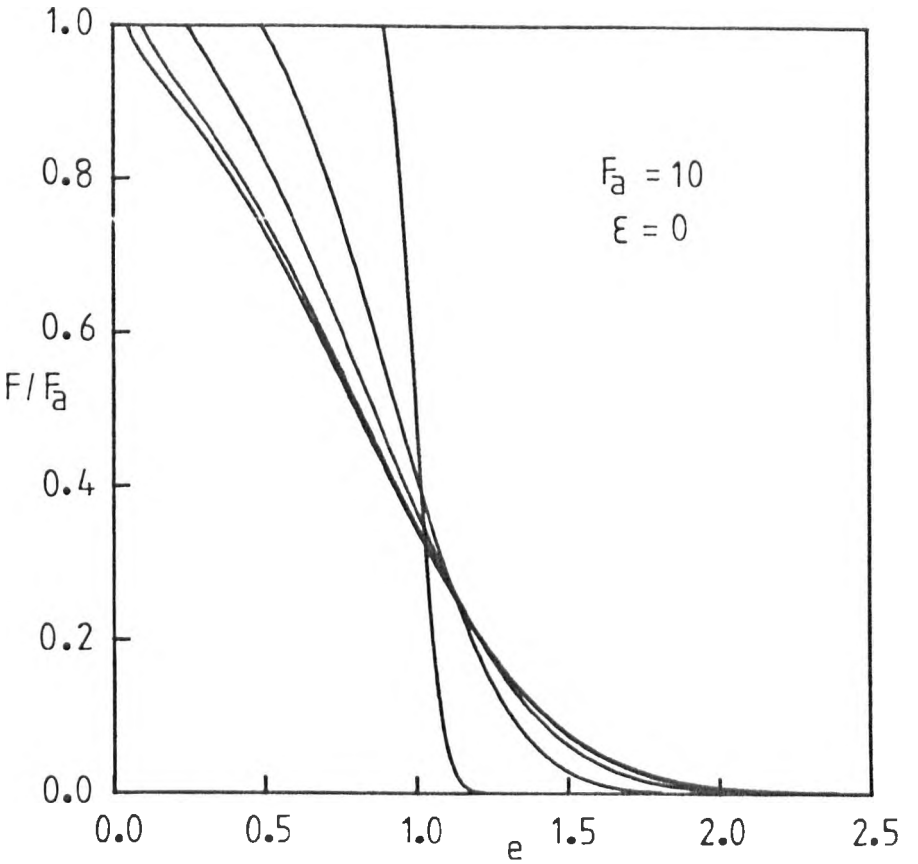

Fig 5.10

Figs 5.10 and 5.11 : Finite difference predictions of concentration profiles at several stages of dissolution corresponding from right to left to R = 0.9, 0.5, 0.25, 0.1 and 0.05 respectively for the cases
F_a = 10, ε = 0 in figure 5.10.
F_a = 0.95, ε = 2 in figure 5.11.

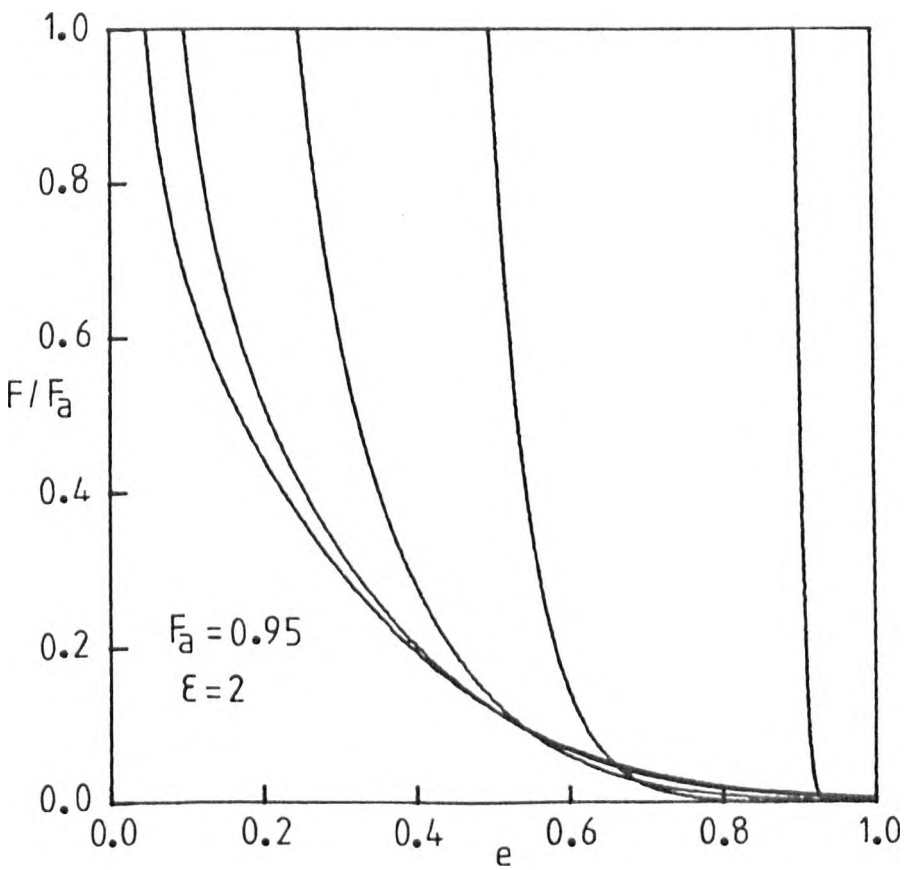

Fig 5.11

The dashed lines in figure 5.7 represent the quasi steady state approximation (equation (2.69)). Near the interface the approximate and numerical predictions are indistinguishable. During the initial stage the material dissolved is insufficient to produce the concentrations predicted as the tail of quasi steady-state profiles. The agreement is generally good by the middle of the process (R=0.5) but the tail of numerically computed profiles contains higher concentrations than quasi steady-state predictions. This relation must reflect insufficient time for the diffusive transport to be effective throughout large distances.

The sequence of figures 5.8a to 5.8e shows that the boundary layer thicknesses increase during the initial stage of the process due to accumulation of material. However, this trend is reversed during the later stages of dissolution due to the effect of spherical symmetry which makes the volume of shell of any given thickness dr increase rapidly. That transition occurs relatively early with slow dissolution (figure 5.8a) but is hardly noticed with rapid dissolution (figure 5.8e). Inflection points shown by the relationships between the radius and time are a direct consequence of the inflection of concentration gradients at the interface.

With large dissolution rates ($F_a > 5$) the intermediate region of the concentration profiles tends to develop inflections and the second radial derivative of the concentrations can become negative. These features are uncommon in dissolution processes except possibly if the diffusivity is strongly dependent on concentration (Crank, 1975). In the present conditions it is believed to be a consequence of the radial convection being very important and this effect persists throughout the range of very large solubility parameters (full lines in figure 5.9). The interpretation of the last pheneomenon has to take into consideration its development relatively late during dissolution ($R < 0.25$) when less than 2% of the

original content of the sphere is left to dissolve. Accumulation of solute reduces the diffusion rate, while a relatively rapid motion of the boundary combined with the spherical symmetry and decreasing radius will have important effects on the concentration profiles.

To clarify the actual behaviour it is convenient to analyse the effect of pure radial convection due to contraction of the sphere. If transport of solute is assumed to be exclusively due to the motion of liquid, decrease in radius of the sphere will make the concentration F(e,R) a function of the Lagrangian coordinate

$$r^3 - a^3 = r_o^3 - a_o^3 \tag{5.4}$$

or

$$e^3 - R^3 = e_o^3 - R_o^3 \tag{5.5}$$

A point originally at distance e_o with concentration $F_o = F(e_o, R_o)$ moves to e due to a decrease of radius from R_o to R so that

$$e(F_o) = (e_o^3 - R_o^3 + R^3)^{1/3} \tag{5.6}$$

This relation was used to simulate the effect of pure radial convection on the first profile in fig. 5.9 for R = 0.25 when the radius had further decreased to 0.1 and 0.05; these curves are shown dashed. The actual concentration profiles for the finite difference solution at these same values of R are also shown (full lines); these differ only slightly from the effect of radial convection alone.

For radial convection to be effective the motion of the boundary must be sufficiently rapid, and the boundary layer thickness must be sufficiently large for the velocity of the liquid to vary throughout that region (equation (2.10)). The first condition is not met for very samll F_a, which

justifies dropping the convective term from equation (2.28) so that the quasi-stationary and quasi steady-state approximations hold reasonably well. On the contrary the second condition is not fulfilled during the initial stage of rapid and moderately rapid dissolution (fig. 5.8e).

Unless the dissolution rate is small and diffusion can transport the solute to relatively large distances, the accumulation of solute becomes increasingly severe. With large solubility parameters the amount of solute dissolved is initially accommodated in a thin layer due to the high level of concentrations. However the thickness of that layer increases with decreasing radius and becomes very important during the last stage of the process.

If $\varepsilon < 1$ the volume of liquid increases as the dissolution proceeds. This contribution by the solute is an extra factor for expanding the boundary layer, especially near the interface. Therefore the boundary layer thicknesses are greater than for the case $\varepsilon = 1$ and the intermediate region of the concentration profiles shows negative gradients $\frac{\partial^2 F}{\partial e^2}$ relatively early (R=0.9), (see fig. 5.10).

On the contrary if $\varepsilon > 1$ the partial molar volume of solute is negative which causes a decrease of the volume of liquid as dissolution proceeds. The tendency to increase boundary layer thicknesses is then somewhat restricted especially near the interface (see the case $F_a = 0.95$; $\varepsilon = 2$ in fig. 5.11).

5.4 Role of spherical symmetry

The spherical symmetry of the system affects the two competing mechanisms of transport of solute, namely diffusion and radial convection.

It was found that for very low solubility parameters the dissolution of spheres is almost exclusively dependent on the diffusion of solute in the surrounding liquid. This class of solutions converges to quasi steady-state

approximations which provide a simple understanding of the limiting role of spherical symmetry on the concentration profiles (equation (2.67)). The concentration drops relatively rapidly near the interface to compensate the rapid increase in the area available for diffusion and the volume available to store the solute. In consequence the dissolution rates increase with time (equation (2.70)). These features do not happen with different geometries or in diffusion processes involving constant or increasing radius of the sphere.

In practice the quasi steady-state approximation has no use in predicting the exact behaviour of real systems, its importance being restricted to the clarification of limiting conditions. A slightly better description is provided by quasi stationary approximations which include the accumulation of solute in the boundary layer around a sphere of constant radius. Equation (2.58), ($F(e,Z) = F_a(R/e)\cdot\mathrm{erfc}[(e-R)/(2\sqrt{Z})]$), is then the illustration of the role of spherical symmetry on concentration profiles and can be compared to the one-dimensional equivalent profile, $F(e,Z) = F_a\cdot\mathrm{erfc}[(e-R)/(2\sqrt{Z})]$, [equation (2.65)] .

With increasing F_a the radial convection and accumulation are enhanced and the boundary layer thickness increases as dissolution proceeds. Radial convection is then accounted for by Lagrangian coordinates, (equations (5.5) and (5.6)), which demonstrate the role of spherical symmetry.

5.5 Comparisons between approximate predictions and numerical solutions

A preliminary analysis of the accuracy of several approximate solutions is shown in figure 5.12, where Z_d represents the dimensionless time given by the approximations and Z_o the equivalent numerical solution.

If the dimensionless time Z is sufficiently low the quasi-stationary solution reduces to $R = 1 - 2F_a\sqrt{Z/\pi}$, (equation (2.64)), and can be derived

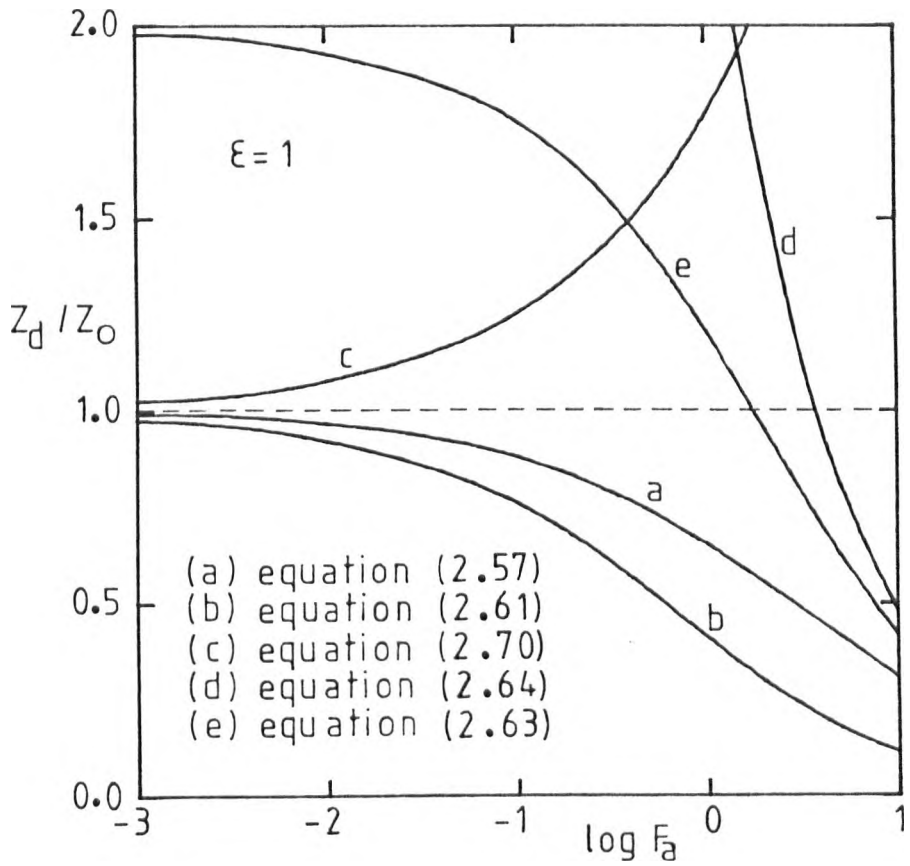

Fig 5.12 : Comparison between finite difference predictions of dimensionless time required for complete dissolution, Z_o, and the corresponding approximate predictions Z_d given by

a - equation (2.57) (quasi-stationary solutions)
b - equation (2.61)
c - equation (2.70) (quasi steady-state)
d - equation (2.64) (flat slab model)
e - equation (2.63)

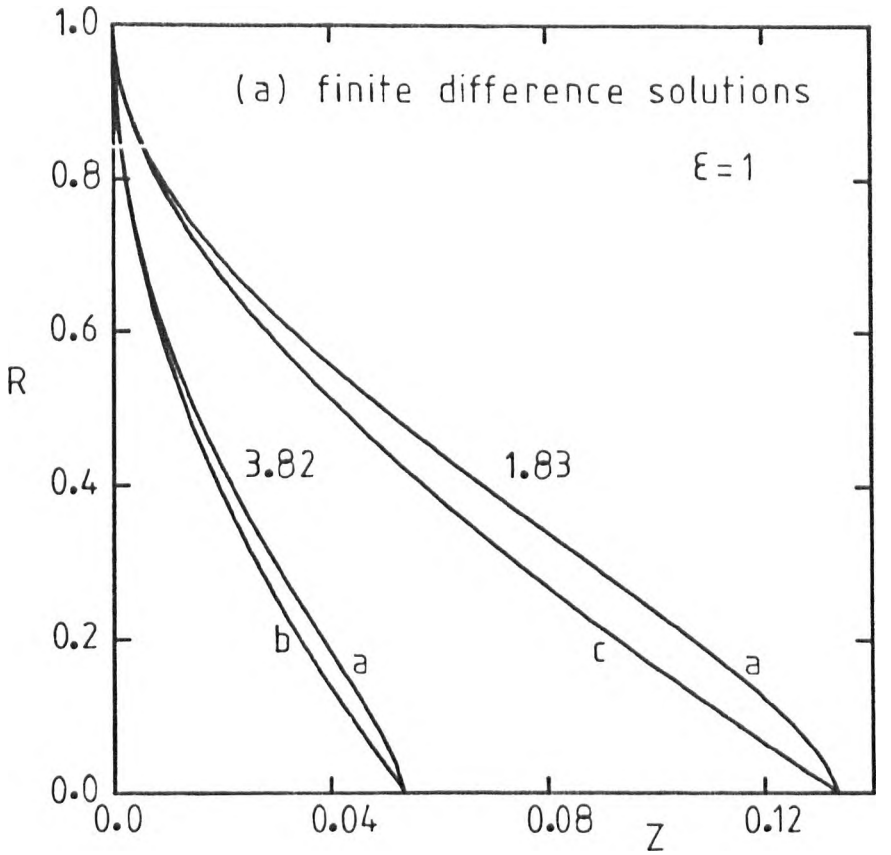

Figure 5.13 - Comparison between finite difference predictions of dissolution (a) and the corresponding predictions by
(b) equation (2.64) (flat slab)
(c) equation (2.63)
The figures show the solubility parameter F_a.

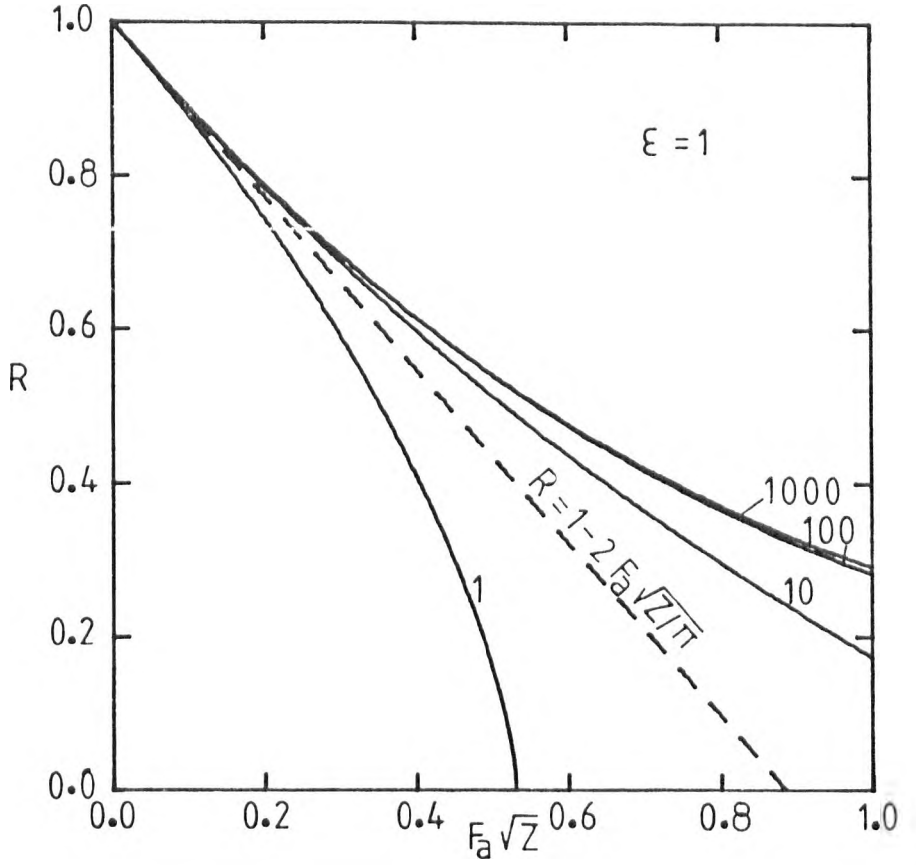

Fig 5.14 : Finite difference predictions of dissolution for moderate and large values of F_a. The figures show the values of F_a. The dashed line represents the flat slab model (equation (2.64)).

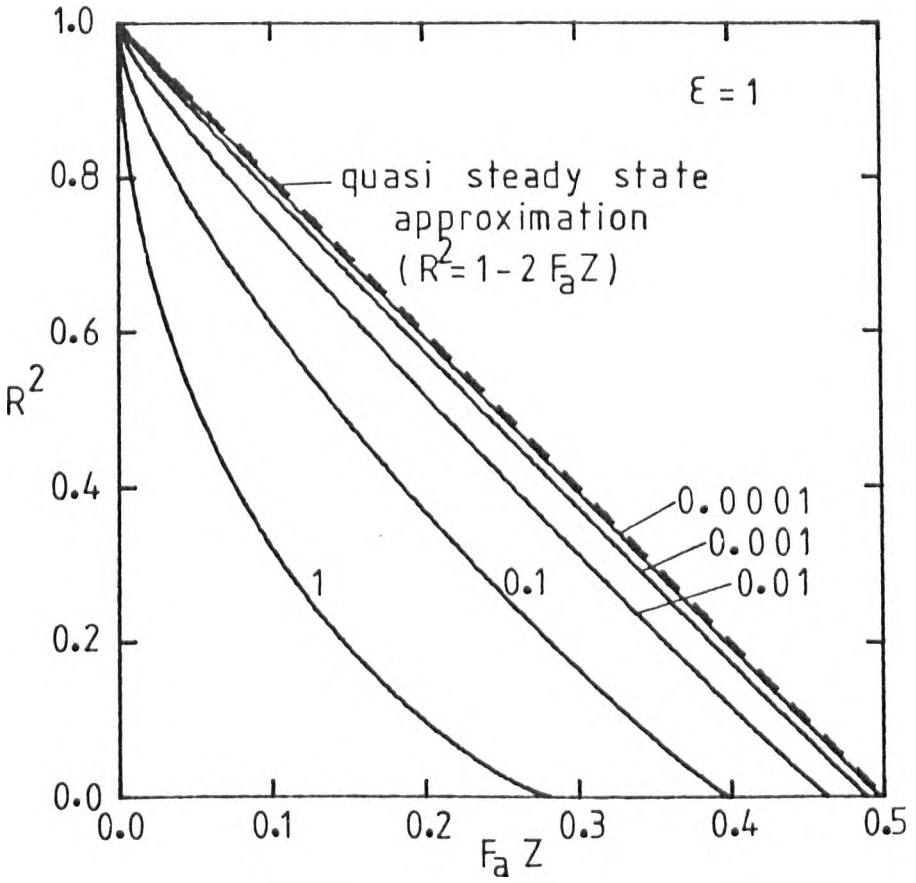

Fig 5.15 : Finite difference predictions of dissolution for low and moderate values of F_a. The figures show the values of F_a. The dashed line represents the quasi steady-state (equation (2.70)).

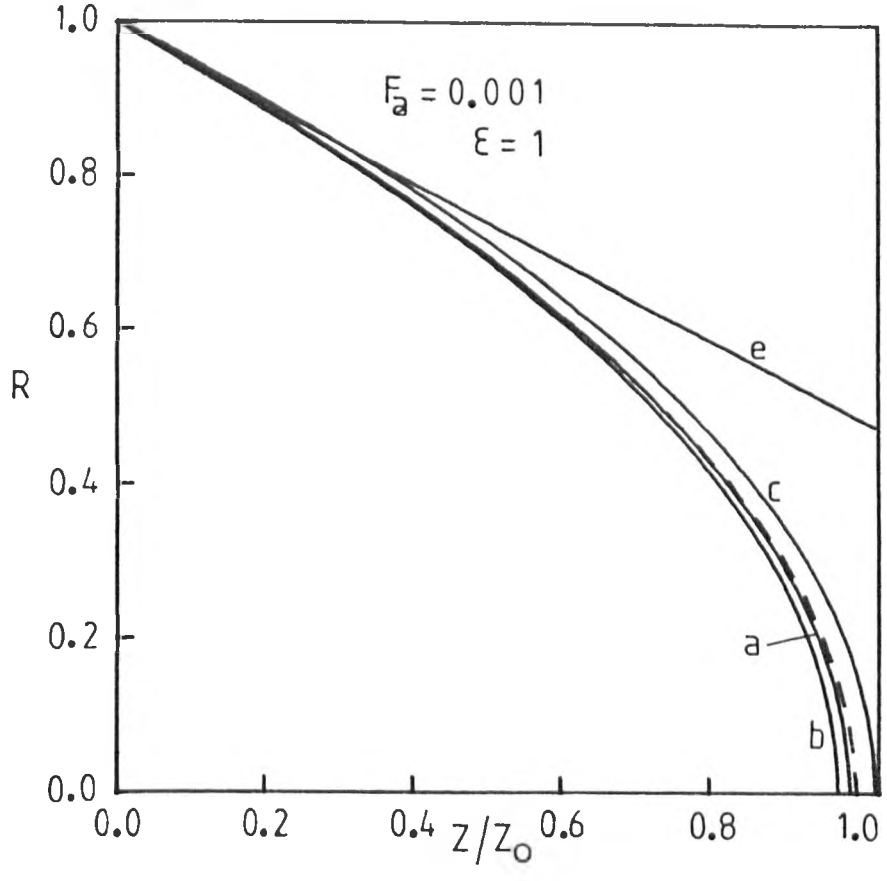

Fig 5.16

Figs 5.16, 5.17 and 5.18 : Comparison between finite difference predictions of dissolution (dashed lines) and the corresponding predictions by

a) equation (2.57),
b) equation (2.61),
c) equation (2.70),
d) equation (2.64),
e) equation (2.63).

The values of ε and F_a are shown in these figures.

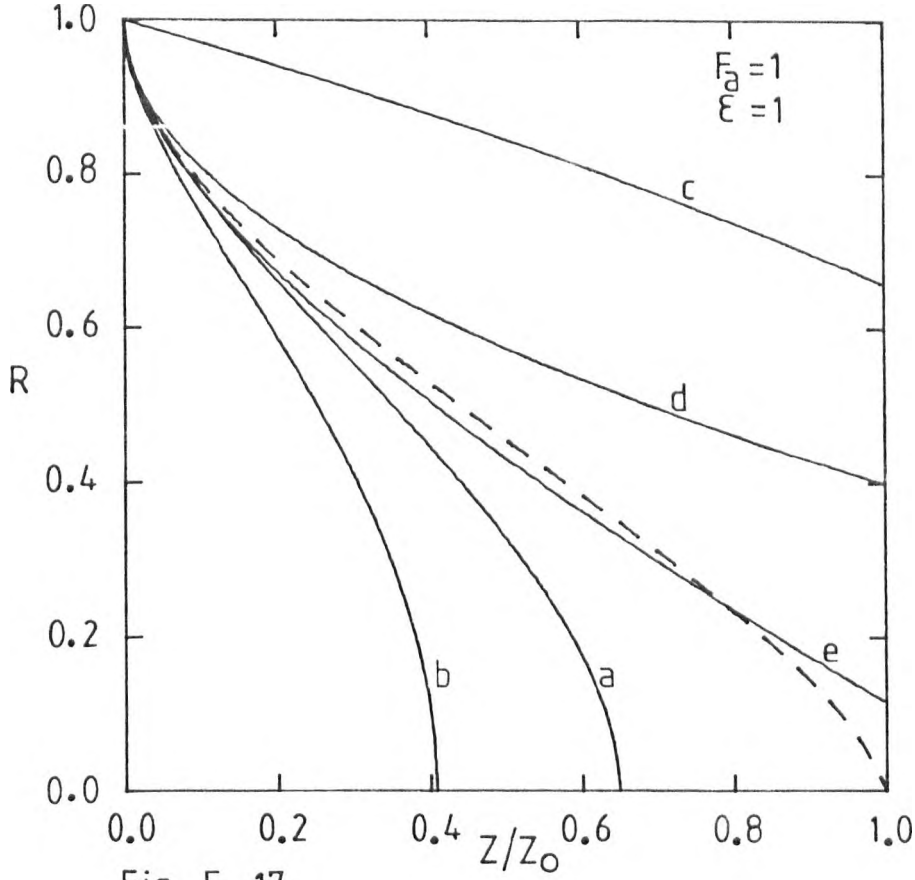

Fig 5.17

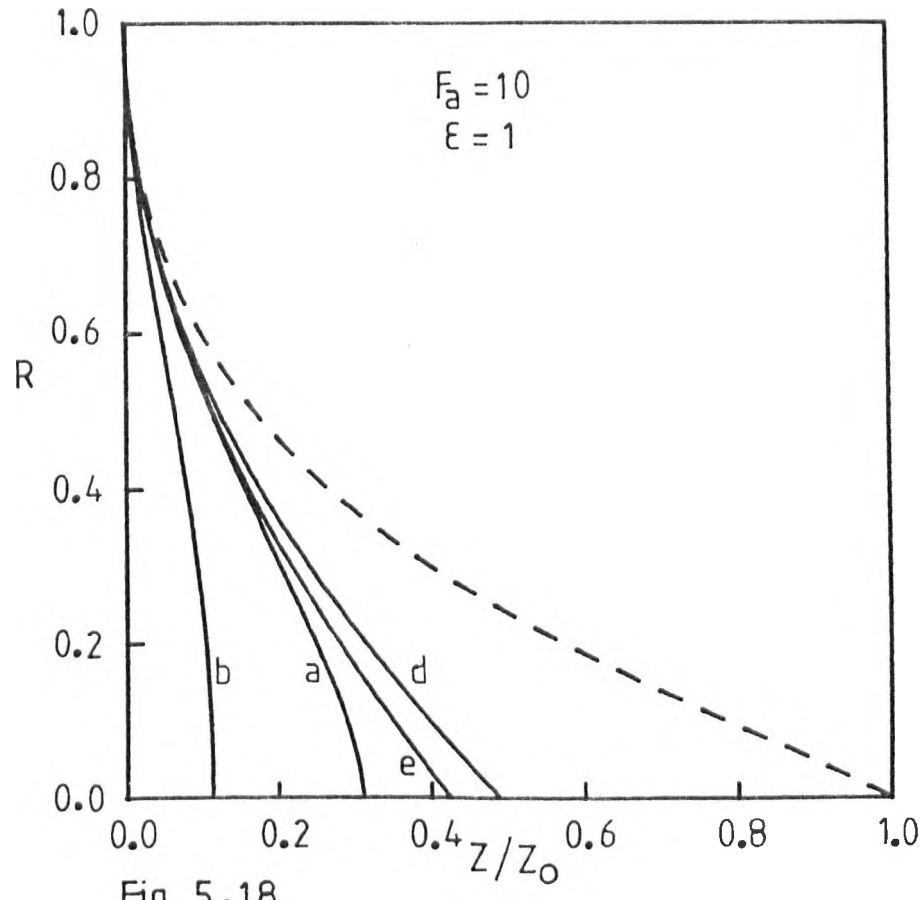

Fig 5.18

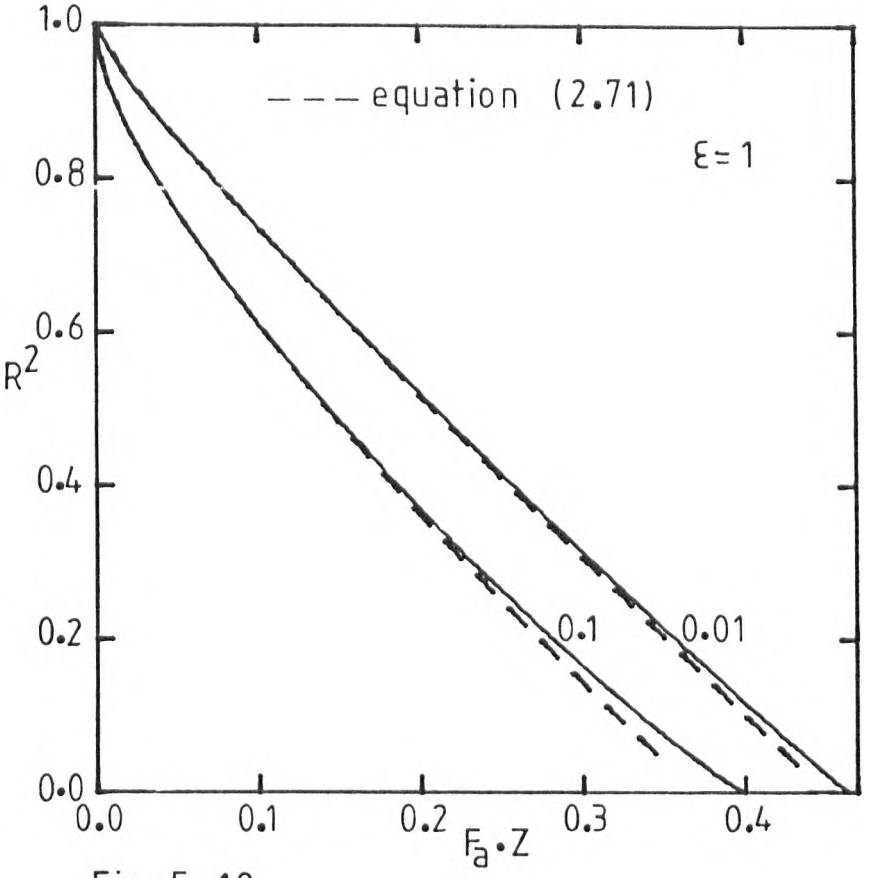

Fig 5.19

Figs 5.19 and 5.20 : Comparisons between finite difference solutions (full lines) and the corresponding predictions given by equation (2.71), (dashed lines). The numbers show the values of F_a.

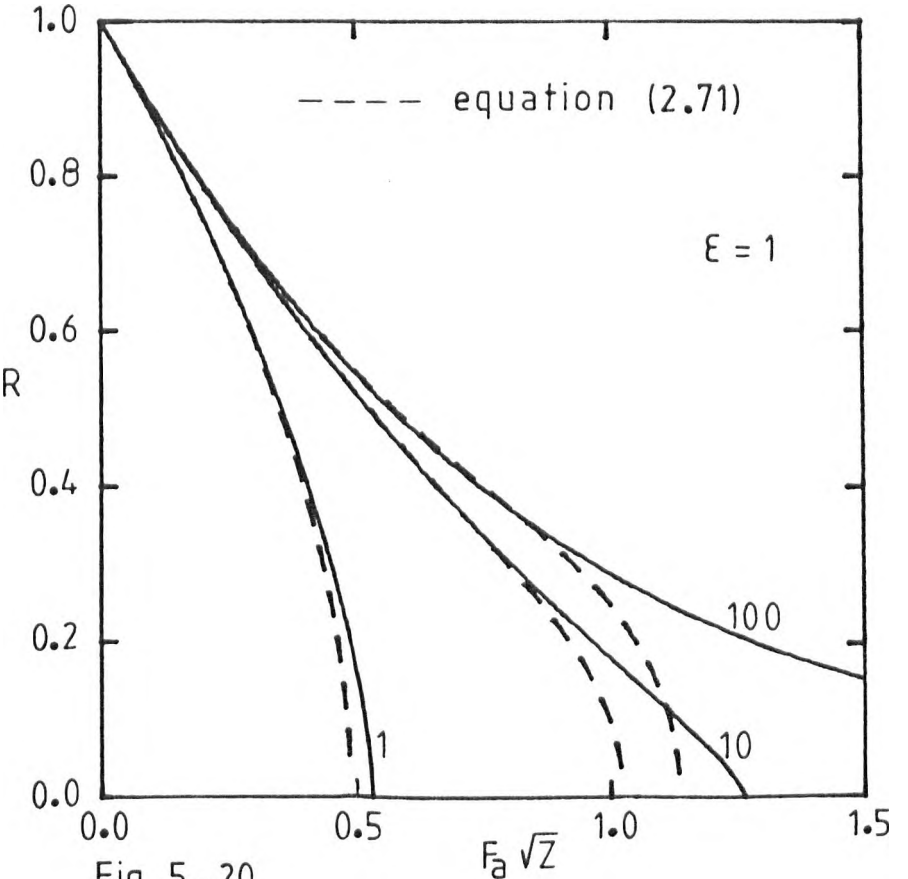

Fig 5.20

from the one-dimensional diffusion (flat slab). Equation (2.64) is very inaccurate for both very low and very large values of the solubility parameter F_a because the roles of spherical symmetry and radial convection are not recognized. The ratio Z_d/Z_o predicted by equation (2.64) is unity at about $F_a = 3.8$ but complete coincidence is not verified even for that case (figure 5.13) because the shapes of R(Z) are somewhat different. Figure 5.14 shows that for moderate and large values of F_a equation (2.64) is reasonably accurate during the first 20% of the process ($R > 0.8$) when boundary layers are relatively thin.

Equation (2.63), $\left(R = 1 - F_a \cdot Z - 2F_a \cdot \sqrt{Z/\pi}\right)$, is also poor (figure 5.12) and only at about $F_a = 1.8$ does $Z_d = Z_o$ again without complete coincidence of the solutions (figure 5.13).

Quasi steady-state, (equation (2.70)), and quasi-stationary approximations, (equation (2.57)), are reasonable in the range of very low solubility parameters (figures 5.12 and 5.15), but are increasingly poor in a range of common practical interest ($F_a > 0.01$). Quasi steady-state approximations predict linear relations between the square radius and time, and these have been used to analyse some experimental results (Liebermann, 1957; Manley, 1960). These authors interpreted the final deviations from linearity as the effect of an organic deposit at the interface. Figure 5.15 shows that actual diffusion controlled solutions can account for that final stage of dissolution.

Both quasi steady-state and quasi-stationary approximations become increasingly poor as F_a increases. Quasi-stationary solutions are generally better but predict too rapid dissolution whilst quasi steady-state solutions predict excessively slow dissolution.

The transformed quasi-stationary equation (2.61), ($R^2 = 1 - 2F_a \cdot Z -$

$4F_a \cdot \sqrt{Z/\pi}$), is generally worse than the original quasi-stationary equation (2.57), ($dR/dZ = - F_a[1/R + 1/\sqrt{\pi Z}]$).

The illustration of approximate solutions in the ranges of very low, moderate and large F_a is shown in figures 5.16, 5.17 and 5.18 respectively. The quasi-stationary equation (2.57) and the quasi steady-state equation (2.70) perform well for low F_a. The transformed quasi-stationary equation (2.61) is also reasonably accurate for low F_a, whilst equation (2.63), ($R = 1 + \phi Z + 2\phi\sqrt{Z/\pi}$), is reasonable during the initial stage but fails for $R < 0.8$.

Figure 5.17 shows that none of the approximations is accurate for moderate values of F_a. Equation (2.63) is much closer to the numerical predictions for $R(Z)$ between $1 \geqslant R \geqslant 0.2$ than any of the other approximations. However it was shown in figure 5.12 that equation (2.63) cannot be considered a useful general approximation because its range of application is so narrow.

Finally none of those approximations is acceptable in the range of very large F_a (figure 5.18).

Equation (2.71) (Subramanian and Weinberg, 1980) is more accurate than quasi steady-state or quasi-stationary approximations, especially during the initial and intermediate stages. Figures 5.19 and 5.20 show that equation (2.71) is accurate for low and large solubility parameters F_a, and fails only for $R < 0.3$. Notice that radial convection was included in the derivation of equation (2.71) and its failure is only due to inclusion of insufficient terms of the asymptotic expansion.

5.6 Limiting solutions for low and high solubility parameters

The convergence of actual solutions to a quasi steady-state limit for low F_a was illustrated in figure 5.15. The time was transformed into $F_a \cdot Z$ to recover the limiting dependence suggested by equation (2.70). This

relation is reasonably good in the range $F_a < 0.001$ but with $F_a = 0.01$ the quasi steady-state prediction of dissolution time is already about 8% larger than the equivalent finite difference solution. Figure 5.15 also demonstrates the progressive deviation from linearity between the square radius and time. With moderately low solubility parameters, $F_a < 0.1$, these deviations are chiefly due to the initial stage which is required to accumulate sufficient material to build up the boundary layer thickness characteristics of quasi steady-state profiles with spherical symmetry (equations (2.68) and (2.69)). That limiting thickness is equal to the radius of the sphere. For moderate F_a values the deviations from linearity in figure 5.15 are initially due to insufficient accumulation, but during the final stage $\left[\frac{d(R^2)}{d(F_a Z)}\right] < 0.5$, which reflects the excessive accumulation and larger boundary layer thicknesses than for quasi steady-state limits.

Equation (2.64) results from thin boundary layer assumptions and is expected to hold reasonably during the initial stage of dissolution with large F_a. For these limiting cases the time is conveniently transformed into $(F_a^2 . Z)$ (figure 5.14). Actual predictions of rate $\left(\frac{dR}{dZ}\right)$ are larger than the solutions of equation (2.64) in the range of low and moderate solubility parameters ($F_a < 3.8$). The spherical symmetry accounts for those differences. For large F_a the assumption of thin boundary layers fails due to accumulation and radial convection. Actual dissolution times are then larger than the equivalent predictions given by equation (2.64).

Figure 5.14 also shows a characteristic coincidence of solutions for rapid dissolution of bubbles which has not been identified previously. The solutions for the cases $F_a = 100$ and $F_a = 1000$ are almost indistinguishable excepting during the last stage of dissolution ($R < 0.3$). With increasing F_a the solutions diverge at progressively later stages. It is unfortunate that such large values of F_a are of little practical interest. However,

this solution is still reasonably accurate in the range $1 \geqslant R \geqslant 0.7$ for $F_a > 4$.

5.7 Design of experiments

In Chapter III the liquid medium surrounding the sphere is assumed to be infinite. In practice it must be restricted and it is usually easier to monitor the experiments if the size of the system is as small as possible. Thus, it is convenient to establish an approximate criterion to select the minimum ratio between the size of the whole system and the size of the sphere, especially for dissolving spheres. For that purpose the actual shapes of the concentration profiles which develop under the assumption that the liquid medium is infinite was used to estimate at what distance r_m from the centre the concentration of solute C_m remains sufficiently close to the bulk concentration. In the present conditions r_m was chosen to be $C(r_m,t) \leq [C_\infty + 0.01\ (C_a - C_\infty)]$. In practice by the time the radius is 5% of the initial size ($R = 0.05$) only 0.125% of the initial content is left to dissolve, so that there is no need to impose strict conditions during the final stage ($R < 0.05$). In addition r_m increases with time as the boundary layer becomes thicker, except possibly for large F_a (during the intermediate stage). Therefore all the values shown in table 5.2 refer to $R = 0.05$ and should provide approximate values for the r_m/a_o. In the case $F_a = 10$; $\varepsilon = 1$, r_m/a_o only exceeds 1 during the initial stage but never exceeds 1.1. All the remaining values are the maxima for $1 \geqslant R \geqslant 0.05$.

The ratio r_m/a_o was obtained by taking into account the shape of concentration profiles. However, radial convection might cause change in volume of the system. In this case the system must be sufficiently large to make those changes negligible; otherwise convection is not strictly radial.

Table 5.2

Estimates of the ratio r_m/a_o where a_o denotes the initial size of the sphere and r_m the minimum size of the system required to justify the assumption that the liquid medium can be considered infinite.

ε	0	1
F_a	r_m/a_o	
0.01	13.7	13.7
0.02	11.1	10.9
0.05	7.81	7.77
0.1	6.03	5.93
0.2	4.70	4.48
0.5	3.47	3.06
1	2.86	2.28
2	2.45	1.69
5	2.11	1.14
10	1.95	< 1

5.8 Discussion

Dimensionless treatment minimized the number of relevant variables of the system, which is characterized by F_a and ε. The effect of diffusivity on the actual behaviour of a particular sphere is obtained by a straight recovery of the real time. Diffusivity affects the basic dynamics of the system, only if the diffusivity is dependent on concentrations or time. The solubility parameter F_a combines in a single variable the effects of concentrations in both phases. Similarly ε takes into account the effects of partial molar volumes of solute in the sphere and in the liquid.

The dimensionless time required for complete dissolution Z_O, varies more rapidly than the reciprocal of the solubility parameter, whereas Z_O is proportional to the reciprocal of diffusivity. Therefore the rate of the process varies more rapidly with F_a than with D.

If the partial molar volume of solute is positive the dissolution causes a positive volume contribution in the liquid and consequently the boundary layer expands and dissolution rates decrease. Those volume changes are insignificant if F_a is sufficiently low and the rate of dissolution is then almost independent of ε.

Spherical symmetry and radial convection are both extremely important during the diffusion controlled dissolution of stationary spheres. The role of radial convection is insignificant if $F_a < 0.01$ but is progressively enhanced with increasing F_a. In the range of very high solubility parameters ($F_a > 10$) radial convection is responsible for a very slow final stage, which requires most of the total time required for complete dissolution. Accumulation causes a gradual departure from the flat slab model, even with extremely large F_a. It was also pointed out that accumulation of solute and spherical symmetry are necessary for radial convection to become dominant during the last stage of dissolution.

For low F_a the accumulation near the interface remains relatively low forcing the solute to diffuse further and the spherical symmetry is then responsible for nearly linear relations between the square radius and time.

In the range of moderate solubility parameters ($0.1 < F_a < 1$) none of the limiting cases is appropriate, both diffusion and convection are important and this explains the failure of all approximate solutions.

The design of dissolution experiments must take into account the volume occupied by concentration profiles around the sphere, in order to satisfy the boundary conditions. It is convenient to minimize that volume to avoid

natural convection and to make it easy to control the experiment. Numerically computed concentration profiles have been used to determine the minimum ratio of the size of the whole system (sphere and liquid) to the size of the initial sphere.

CHAPTER VI

6.1 Diffusion controlled behaviour of multicomponent bubbles

The equations to describe behaviour of multicomponent bubbles were set up in Chapter II and can be solved by using the finite difference techniques described in Chapter III. These systems involve variable boundary conditions which makes the stability of the solutions somewhat critical. The numerical technique used for that purpose is based on the simultaneous solution of the discrete local balances. New concentration profiles are then computed step-by-step without the need for slow iterative schemes.

Analytical solutions for such multicomponent systems have not previously been available because of the complexity of the problem, especially difficulties due to variable interfacial concentrations. However, it will be demonstrated how the basic procedure used to derive analytical solutions for growth of one component spheres from zero size can be extended to the growth of multicomponent systems. The essential question involves verification that bubbles growing from finite size always lead to an asymptotic regime with an equilibrium bubble composition and a linear relation between the bubble radius and the square root of time. Thus, it is possible to test the accuracy of numerical solutions by comparison between their asymptotic regime and exact solutions for growth from zero size.

The behaviour of multicomponent bubbles depends on the relations between the diffusivities of individual species. When the diffusivities of the species are different their influence cannot be removed by putting the equations into dimensionless form. Therefore, a considerably larger number

of parameters is needed to characterize those systems than might seem necessary at first sight.

The evolution of gas composition in the bubble is closely related to interfacial concentrations and consequently the "driving forces" may vary throughout the process. Uncommon types of behaviour may occur and are easily simulated.

It has been shown that dissolution of one-component spheres is more complex than growth. One must similarly expect even more complex dissolution of multicomponent bubbles whereas growth leads to an asymptotic regime, which is similar to the equivalent growth of one-component spheres.

6.2 Constant composition of multi-component bubbles

From equation (2.50) it can be seen that equilibrium gas composition requires

$$g_{i,eq} = J_i^* = f_i \left(\frac{\partial F_i}{\partial e}\right)_R \Big/ \sum_{j=1}^{n} \left[f_j \left(\frac{\partial F_j}{\partial e}\right)_R \right] \qquad (6.1)$$

$$i = 1, \ldots, n$$

that is, every mole fraction of each species i must be equal to the ratio of its molar flux to the overall molar flux across the interface. This condition can be fulfilled by a constant (time invariant) concentration gradient but this case is exceptionally rare; otherwise all the concentration gradients may vary but must do so according to equation (6.1).

Only exceptionally will equation (6.1) be valid from the beginning of the process. A transient stage is thus generally expected regardless of the eventual evolution towards equilibrium gas composition. The relation between the gas composition and solute interfacial concentrations imposes a tendency to reduce the differences between the actual mole fraction g_i and its equilibrium value J_i^* (equation (6.1)).

If the Henry's law is valid the interfacial concentration $C_i(a)$ is proportional to g_i. Thus, if $g_i < J_i^*$, $C_i(a) < C_{a_i}^{\,o}$ where $C_{a_i}^{\,o}$ is the interfacial concentration in equilibrium when $g_i = J_i^*$. During growth $[C_{\infty_i} - C_i(a)]$ will be higher than the equilibrium "driving-force" $[C_{\infty_i} - C_{a_i}^{\,o}]$. This relation is always true provided the interfacial concentration $C_i(a)$ increases with the corresponding mole fraction g_i.

In a two-component growing bubble if $g_1 < J_1^*$ it must follow that $g_2 > J_2^*$ and $C_2(a) > C_{a_2}^{\,o}$. Therefore $[C_{\infty_2} - C_2(a)] < [C_{\infty_2} - C_{a_2}^{\,o}]$, and g_2 decreases while the corresponding flux of species 2 into the bubble is increasing. Meanwhile g_1 is increasing and the composition of the bubble approaches equilibrium. In a bubble with more than three components the situation is slightly more complex during that transient stage, but similar arguments clarify why the composition of growing bubbles always converges to equilibrium.

Similarly, during the dissolution of two-component spheres if $g_1 > J_1^*$, $C_1(a) > C_{a_1}^{\,o}$ and species 1 is dissolving quicker than if the gas composition was in equilibrium, which causes a decrease of g_1. On the contrary, as $g_2 < J_2^*$, g_2 is increasing, which shows that the composition of dissolving bubbles also tends to converge to the corresponding ratios between material fluxes (equation (6.1)). However the complex evolution of concentration profiles around dissolving spheres can prevent the existence of equilibrium ratios between those fluxes. The tendency to approach equilibrium gas composition is then not general.

6.3 Exact solutions for growth from zero size

It was shown in Chapter IV that the existence of analytical solutions is based on Boltzmann transformation of variables. This transformation implies that the concentration must become a unique function of a single

variable and that the boundary conditions must be constant. These restrictions apply equally to multicomponent gas bubbles which, in addition, must have constant gas composition because of the relation between the gas phase and interfacial solute concentrations. In these conditions we assume

$$F_i(s) = F_i(e,Z) \tag{6.2}$$

where $s = r/(2\sqrt{Dt}) = e/(2\sqrt{Z})$. From equation (2.47)

$$f_i \frac{d^2F_i}{ds^2} + \frac{2}{s} f_i \frac{dF_i}{ds} - \frac{2\beta^3}{s^2} \frac{dF_i}{ds} = -2s \frac{dF_i}{ds} , \tag{6.3}$$

with $\varepsilon = 1$ in the case of gas bubbles. In addition, equation (2.49) is transformed into

$$2\beta = \sum_{i=1}^{n} \left[f_i \left(\frac{dF_i}{ds} \right)_\beta \right] \tag{6.4}$$

where R and β are still related by equation (4.8), $R = 2\beta\sqrt{Z}$, and at the interface $s = \beta$.

The boundary conditions (equations (2.53) and (2.54)) can now be written

$$F_i(\infty) = 0 \tag{6.5}$$

$$F_i(\beta) = \alpha_i g_{i,eq} - F_{O_i} = -\phi_i \tag{6.6}$$

and after a first integration of equation (6.3)

$$\frac{dF_i}{ds} = A_i \cdot s^{-2} \cdot \exp\left[-\left(s^2 + 2\beta^3/s \right) / f_i \right] \qquad (6.7)$$

where A_i is the constant of integration. After a second integration from $s = \beta$ to infinity

$$\phi_i = A_i \int_{\beta}^{\infty} x^{-2} \cdot \exp\left[-\left(x^2 + 2\beta^3/x \right) / f_i \right] dx \qquad (6.8)$$

and by convenient transformation of the independent variable,

$$\phi_i = \frac{A_i}{\beta} \int_0^1 \exp\left\{ -\beta_i^2 \left[2(1 - w) + (1 - w)^{-2} \right] \right\} dw$$

$$= A_i \left[2\beta \cdot \beta_i^2 \cdot \exp(3\beta_i^2) \right]^{-1} \phi(\beta_i) \qquad (6.9)$$

where

$$w = 1 - \beta/x \qquad (6.10)$$

$$\beta_i = \beta/f_i^{\frac{1}{2}} \qquad (6.11)$$

and

$$\phi(\beta_i) = 2\beta_i^2 \int_0^1 \exp\left\{ \beta_i^2 \left[1 + 2w - (1 - w)^{-2} \right] \right\} dw \; . \qquad (6.12)$$

Equation (6.12) is the same as the solution for growth of one-component spheres with $\varepsilon = 1$ (gas bubbles), (Scriven, 1959).

From equations (6.4) and (6.7)

$$\sum_{i=1}^{n} A_i \Big/ \left[2\beta \cdot \beta_i^2 \cdot \exp(3\beta_i^2) \right] = 1 \qquad (6.13)$$

and by combination of equations (6.9) and (6.13)

$$\sum_{i=1}^{n} \left[\phi_i / \phi(\beta_i) \right] = 1 \ . \qquad (6.14)$$

Equation (6.1) expresses the general condition required for equilibrium gas composition. After Boltzmann transformation equation (6.1) becomes

$$g_{i,eq} = f_i \left[\frac{dF_i}{ds}\right] / \sum_{j=1}^{n} \left[f_j . \frac{dF_j}{ds} \right]_{\beta} \qquad (6.15)$$

or from equations (6.4), (6.7) and (6.15)

$$g_{i,eq} = \frac{A_i}{2\beta . \beta_i^{\,2} . \exp(3\beta_i^{\,2})} \ , \qquad (6.16)$$

then from equations (6.9) and (6.16)

$$g_{i,eq} = \phi_i / \phi(\beta_i) \ . \qquad (6.17)$$

The final solutions show that the solubility parameters, ϕ_i, are functions of fictive growth constants, β_i. This mathematical formulation proves that Boltzmann transformation and analytical solutions are possible for bubbles growing from zero size with the equilibrium composition given by equation (6.1). Transient stages of growth from finite size cannot be solved except by numerical techniques, but these solutions must converge asymptotically to the analytical solutions given by equations (6.14) and (6.17). A method of solving these equations is described in appendix 4.

6.4 Particular cases

6.4.1 Equal diffusivities

If all the dissolved gases have equal diffusivity

$$f_i = 1 \quad ; \quad i = 1, \ldots, n \tag{6.18}$$

and we have the simplest possible case. Equations (6.14) and (6.17) now reduce to

$$\phi(\beta) = \sum_{i=1}^{n} \phi_i \tag{6.19}$$

and

$$g_{i,eq} = \phi_i / \sum_{j=1}^{n} \phi_j \quad ; \quad i = 1, \ldots, n \quad . \tag{6.20}$$

The growth constant β is then directly obtained from data referring to one-component systems, where the sum of the n individual solubility parameters is the equivalent solubility parameter for the n-component system. The composition of the bubble growing from zero size is readily obtained from equation (6.20).

6.4.2 Limiting regime for low growth rates

For very low solubility parameters the analytical solutions for one-component bubbles (Scriven, 1959) tend to

$$\phi = 2\beta^2 \tag{6.21}$$

and therefore

$$\phi(\beta/f_i^{\frac{1}{2}}) = 2\beta^2 / f_i \quad . \tag{6.22}$$

Thus, equation (6.14) converges to

$$\sum_{i=1}^{n} \left[f_i \cdot \phi_i \right] = 2\beta^2 \qquad (6.23)$$

and from equations (6.17) and (6.22)

$$g_{i,eq} = f_i \cdot \phi_i \; / \; \sum_{j=1}^{n} \left(f_j \cdot \phi_j \right) . \qquad (6.24)$$

If β_r is the growth constant for a sphere containing pure species i = 1, from equation (6.21)

$$\phi_1 = 2\beta_r^{\,2} \qquad (6.25)$$

and

$$\beta/\beta_r = \left[\sum_{i=1}^{n} \left(f_i \cdot \phi_i \right) \; / \; \phi_1 \right]^{\frac{1}{2}} . \qquad (6.26)$$

Equation (6.26) relates the growth rate of the n-component bubble to the growth rate of a bubble containing exclusively the reference component (i=1).

6.4.3 Limiting regime for large growth rates

According to Scriven (1959) the limit for large solubility parameters is

$$\phi = \beta \sqrt{\pi/3} . \qquad (6.27)$$

Therefore, from equations (6.14) and (6.17)

$$\beta = \sqrt{3/\pi} \sum_{i=1}^{n} \left(\phi_i \cdot f_i^{\frac{1}{2}} \right) \qquad (6.28)$$

and

$$g_{i,eq} = f_i^{\frac{1}{2}} \cdot \phi_i \; / \; \sum_{j=1}^{n} \left(\phi_j \cdot f_j^{\frac{1}{2}} \right) \tag{6.29}$$

also from equation (6.27),

$$\phi_1 = \beta_r \sqrt{\pi/3} \; . \tag{6.30}$$

Finally from equation (6.28) and (6.30)

$$\beta/\beta_r = \sum_{i=1}^{n} \left(\phi_i \cdot \sqrt{f_i} \right) \; / \; \phi_1 \; . \tag{6.31}$$

6.5 Analytical solutions

In the case of gas bubbles $\varepsilon = 1$ and the pairs $[\beta_i ; \; \phi(\beta_i)]$ required to satisfy equation (6.14) can be obtained from Scriven's data (1959). The solubility parameter $\phi(\beta')$ for one-component systems increases monotonically with the growth constant β', so that the problem reduces to the minimization of the square deviation from equation (6.14)

$$\varepsilon_s(\beta) = \left[\sum_{i=1}^{n} \left(\phi_i / \phi(\beta/f_i^{\frac{1}{2}}) \right) - 1 \right]^2 \tag{6.32}$$

and polynomial interpolations can be used to estimate the actual $\phi(\beta/f_i^{\frac{1}{2}})$ values.

The Fibonacci method (see appendix 4) provides an efficient process for rapidly finding the correct β and g_i values. This method requires the previous knowledge of lower limit, β_ℓ, and upper limit, β_u, of the growth constant, which in the present conditions can be

$$\beta_\ell = \beta(\phi_1) \tag{6.33}$$

and

$$\beta_u = f_m^{\frac{1}{2}} \beta(\phi_T) \quad . \tag{6.34}$$

It is useful to define an initial range of β values where the correct solution is to be found. The growth rate will necessarily be greater than the growth rate of a bubble due to diffusion of a single component. Therefore

$$\beta > \beta_\ell = \beta(F_{O_1} - \alpha_1) \tag{6.36}$$

or

$$\beta_\ell = 0 \quad \text{if } F_{O_1} < \alpha_1 \quad .$$

Also the actual growth rate cannot exceed the rate of growth of a one-component bubble with solubility parameter $\phi_T = \sum_{i=1}^{n} (F_{O_i})$ and diffusivity equal to the maximum individual diffusivity of the n-component case. Thus

$$\beta < \beta_u = \sqrt{f_m} \cdot \beta(\phi_T) \tag{6.37}$$

where

$$f_m = \max(f_1; f_2; \ldots; f_n) \quad .$$

The parameters describing growth of two-component bubbles from zero size are illustrated in figures 6.1 and 6.2. The ratio β/β_r represents the relation between the actual growth rate and the growth rate of the reference one-component bubble with solubility parameter $\phi_r = \phi_1$. In table 6.1, 1 to 7 identify the corresponding curves in figures 6.1 and 6.2.

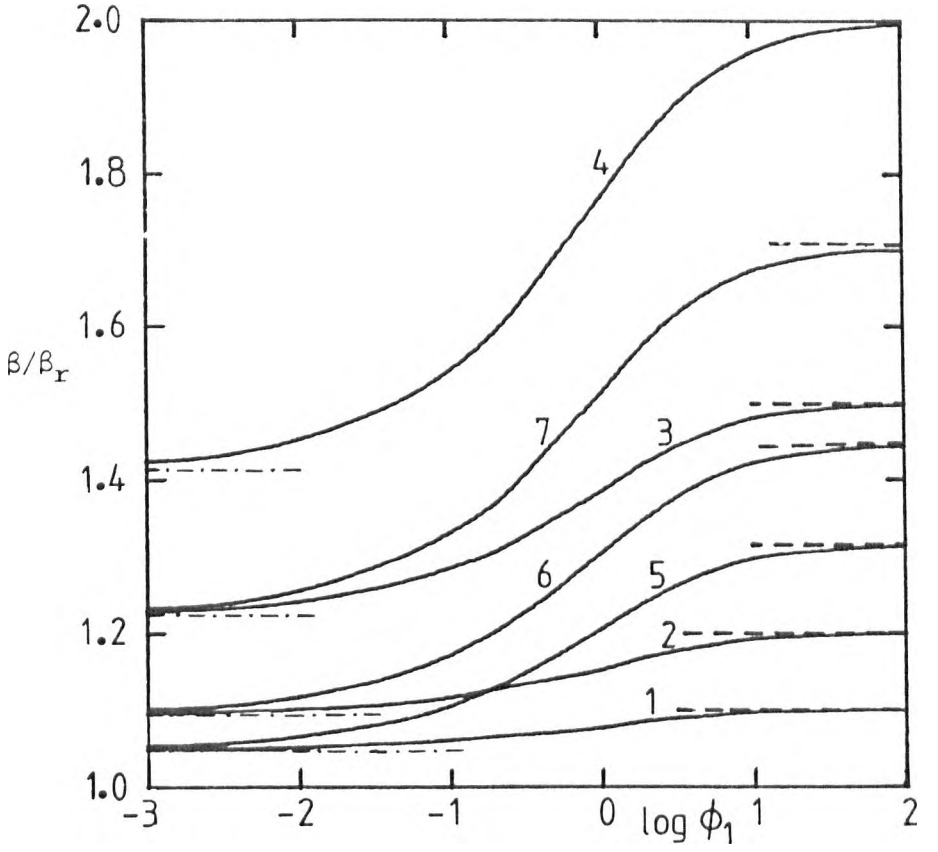

Fig 6.1 : Relation between growth constants for two component bubbles (β) and one-component solutions [$\beta_r(\phi,\varepsilon)$] for the case $\phi = \phi_1$ $\varepsilon = 1$. The figures show the case given in table 6.1. The dashed lines represent equation (6.31) and the dashed-dotted lines represent equation (6.26).

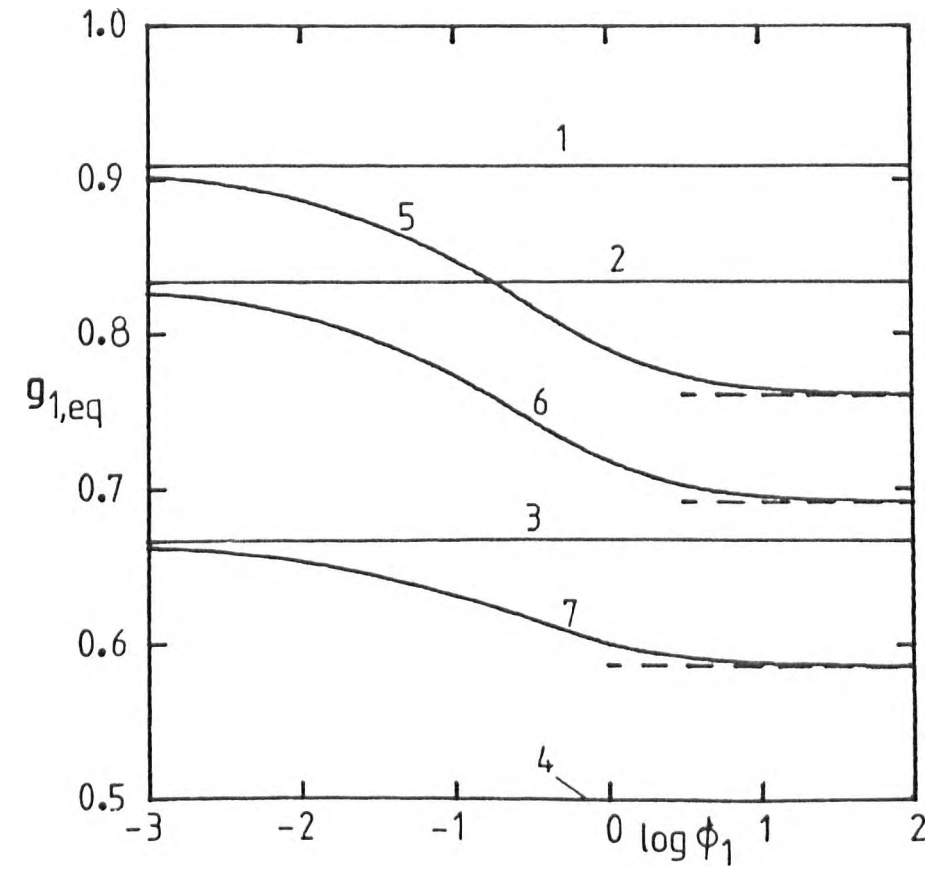

Fig 6.2 : Mole fractions of species 1 for two component growing bubbles. The figures show the cases in table 6.1. The dashed lines represent equation (6.29).

Table 6.1
Parameters for examples shown
in figures 6.1 and 6.2

Curve	f_1	f_2	ϕ_2/ϕ_1
1	1	1	0.1
2	1	1	0.2
3	1	1	0.5
4	1	1	1
5	1	0.1	1
6	1	0.2	1
7	1	0.5	1

The dashed lines in figures 6.1 and 6.2 represent the lower and upper limits according to equations (6.24) and (6.26) for very low solubility parameters or equations (6.29) and (6.31) for very large solubility parameters. These limiting conditions for the curves 1 and 5 are equal with very low solubility parameter and the same occurs with equal values of the factor $f_2(\phi_2/\phi_1)$, (Cases 2 and 6, or 3 and 7). In these cases the effects of the second component depend on the product $f_2 \cdot \phi_2$, which is equivalent to a relative permeability. With large ϕ values the ratio of solubility parameters (ϕ_2/ϕ_1) is more important than the ratio of diffusivities f_2.

If the diffusivities are equal the composition only depends on the ratio of solubility parameters, (cases 1, 2 and 3); otherwise ($f_2 = 1$) the composition varies with ϕ even if the ratio ϕ_2/ϕ_1 remains constant.

This basic discussion of two-component systems could easily be extended to systems with more than two components but the details obviously become increasingly complex. The growth rate and gas composition are again more dependent on the relative values of solubility parameters than on the relative values of diffusivities.

Table : 6.2

Comparison of analytical solutions for growth from zero and numerical solutions for growth from finite size for two-component bubbles when $R \geqslant 100$.

			Analytical solutions		Numerical solutions	
ϕ_1	ϕ_2	f_2	β	$g_{1,eq}$	β'	$g_{1,eq}$
0.001	0.001	1	0.03252	0.5000	0.03260	0.5000
0.01	0.01	1	0.1093	0.5000	0.1095	0.5000
0.1	0.1	1	0.4205	0.5000	0.4212	0.5000
1	10	1	2.333	0.5000	2.340	0.5000
10	10	1	19.97	0.5000	20.04	0.5000
100	100	1	195.9	0.5000	196.6	0.5000
0.001	0.0005	1	0.02806	0.6667	0.02811	0.6667
0.01	0.005	1	0.0936	0.6667	0.0937	0.6667
0.1	0.05	1	0.3505	0.6667	0.3510	0.6667
1	0.5	1	1.831	0.6667	1.835	0.6667
10	5	1	15.09	0.6667	15.13	0.6667
100	50	1	147.0	0.6667	147.5	0.6667
0.001	0.0002	1	0.02500	0.8333	0.02508	0.8333
0.01	0.002	1	0.0830	0.8333	0.0831	0.8333
0.1	0.02	1	0.3053	0.8333	0.3058	0.8333
1	0.2	1	1.526	0.8333	1.529	0.8333
10	2	1	12.15	0.8333	12.19	0.8333
100	20	1	117.7	0.8333	118.1	0.8333
0.001	0.0001	1	0.02400	0.9091	0.02401	0.9091
0.01	0.001	1	0.0792	0.9091	0.0793	0.9091
0.1	0.01	1	0.2896	0.9091	0.2900	0.9091
1	0.1	1	1.423	0.9091	1.426	0.9091
10	1	1	11.17	0.9091	11.21	0.9091
100	10	1	107.9	0.9091	108.3	0.9091
0.001	0.001	0.5	0.02812	0.663	0.02816	0.665
0.01	0.01	0.5	0.0946	0.654	0.0946	0.656
0.1	0.1	0.5	0.3628	0.631	0.3632	0.632
1	1	0.5	2.000	0.600	2.006	0.600
10	10	0.5	17.06	0.588	17.12	0.588
100	100	0.5	167.2	0.586	167.8	0.586
0.001	0.001	0.2	0.02511	0.827	0.02514	0.830
0.01	0.01	0.2	0.0842	0.811	0.0844	0.812
0.1	0.1	0.2	0.3198	0.773	0.3200	0.775
1	1	0.2	1.724	0.717	1.728	0.719
10	10	0.2	14.50	0.694	14.55	0.695
100	100	0.2	141.7	0.691	142.3	0.692
0.001	0.001	0.1	0.02403	0.903	0.02407	0.905
0.01	0.01	0.1	0.0803	0.887	0.0804	0.888
0.1	0.1	0.1	0.3022	0.848	0.3025	0.849
1	1	0.1	1.594	0.789	1.598	0.790
10	10	0.1	13.22	0.764	13.26	0.764
100	100	0.1	129.0	0.760	129.4	0.761

Table : 6.3

Comparison between finite difference solutions and analytical solutions of growth of three-component bubbles.

a) Parameters chosen

case	1	2	3	4
f_1	1.0	1.0	1.0	1.0
f_2	1.0	0.5	0.5	0.1
f_3	1.0	0.2	0.2	10.0
α_1	1.0	1.0	1.0	1.0
α_2	0.5	1.0	0.5	10.0
α_3	0.2	1.0	0.2	0.1
F_{O_1}	1.0	1.0	1.0	1.0
F_{O_2}	0.5	1.0	0.5	10.0
F_{O_3}	0.2	1.0	0.2	0.1

b) Results for $R \gg 100$.

	Analytical solutions			Finite difference solutions		
case	β	$g_{1,eq}$	$g_{2,eq}$	β'	$g_{1,eq}$	$g_{2,eq}$
1	1.319	0.5000	0.3333	1.320	0.5000	0.3333
2	1.634	0.4336	0.3357	1.636	0.4336	0.3357
3	0.997	0.5899	0.3148	0.998	0.5900	0.3147
4	2.674	0.2989	0.5487	2.678	0.2991	0.5485

6.6 Comparison between numerical and analytical solutions

A sphere growing from finite size always converges to asymptotic growth rate and equilibrium gas composition. After a sufficiently large increase of radius the effect of the initial stage must become negligible and the asymptotes of growth from finite size must become indistinguishable from the equivalent analytical predictions of growth from zero size. The composition of the bubble is then given by $g_{i,eq}$ and these satisfy equation (6.1), while the interfacial concentrations, (equation (2.54)), become

$$\left[F_i(R) \right]_{eq} = - \phi_i = \alpha_i \, g_{i,eq} - F_{O_i} \, .$$

Numerically computed (Z,R) pairs were inserted into equation (4.8), $(R = 2\beta\sqrt{Z})$, to obtain the apparent value of β, i.e. β', for computations with $R = 10^5$ to confirm the convergence to the asymptotic regime. This regime was in excellent agreement with the corresponding analytical solutions, see table 6.2. The numerical predictions of $\beta' = R/(2\sqrt{Z})$ are in fact almost identical for any value $R \geq 100$.

The set of 2-component systems reported in table 6.2 covers a very wide range of solubility parameters and several different ratios of diffusivities. The difference between the two values of β is always less than 1%, with β' usually slightly larger than the analytical value, β. The time required for a bubble to grow from zero size to $R = 1$, $\left[Z_1 = (1/2\beta)^2 \right]$, is only a very small fraction of the time required to reach $R = 10^5$, $\left[Z = (10^5/2\beta)^2 = 10^{10} \, Z_1 \right]$, and therefore the initial transient stage of growth from finite size might not explain the differences between β and β'. Truncation errors involved in formulating the finite difference

equations may easily cause those differences. In many cases the analytical and numerical predictions of the compositions $g_{1,eq}$ differ by less than 0.1%.

For all the results reported in table 6.2 $\phi_i = - F_{O_i}$ for simplicity of presentation. Equally good accuracy of finite difference predictions is achieved with more complex systems, including bubbles which contain more than two different gases. Table 6.3 gives some results for three components. These examples are sufficiently general to exemplify the performance of the method independently of the combination of the parameters involved (concentrations, solubilities, and diffusivities).

The asymptotic regimes described in tables 6.2 and 6.3 are independent of the initial composition of bubbles growing from finite size. Examples of the transient regimes are described in the next section.

6.7 Transient regimes

The asymptotic stage of growth was reasonably well understood and interpreted in the previous section. Transient regimes are much more complex and this makes it difficult to illustrate all the interesting trends that can occur. The additional complexity results from the evolution of concentration profiles during the initial stage of dissolution or growth from finite size. There is a time dependent evolution even with constant boundary conditions as illustrated in Chapters IV and V, but there are now changes strongly dependent on the changes of interfacial concentrations. Commonly the individual rate of diffusion of a species i will be dependent on the dimensionless interfacial concentration $F_i(R)$ and on the dimensionless diffusivity f_i, but these relations cannot be easily quantified. However, on assuming a relation such as Henry's law, $F_i(R)$ is easily calculated from

the composition of the bubble. Thus $[F_i(R)]$ will be occasionally designated as "driving-force".

On assuming that the different species diffuse independently, they may sometimes be transferred in opposite directions which causes rapid changes of gas compositions. These changes introduce "feed-back" effects on the interfacial concentrations (equation (2.46)) and also on the rates of transport, which are responsible for bringing the system closer to equilibrium. This interdependence between gas composition and interfacial concentrations explains why growth always tends to asymptotic behaviour, regardless of the initial composition of the bubble (except when the initial growth is a transient effect but leads to dissolution). During dissolution the evolution of gas composition may be less regular because the time dependence of concentration profiles affects the whole course of dissolution. For instance, it is believed that dissolution is generally controlled by the less soluble species or by the species with the lowest diffusivity and that small fractions of a poorly soluble gas lead the bubble to a standstill with an almost insoluble residue (Greene and co-authors, 1959a, 1959b; Doremus, 1960; Nemec, 1969).

The bulk concentration of gases dissolved in the liquid medium may also influence strongly the behaviour of bubbles. In some cases the bulk concentration of species i may be in equilibrium with a particular value of mole fraction g_i^*, so that the "driving-force" $F_i(R) = (\alpha_i\, g_i^* - F_{O_i}) = 0$ or $g_i^* = F_{O_i}/\alpha_i$. In these conditions, unless there is a maximum in the concentration profile, the species i will dissolve if $F_i(R) > 0$. Similarly if $F_i(R) < 0$ this species will diffuse into the bubble unless there is a minimum in the concentration distribution. Thus, if the mole fraction increases from $g_i < g_i^*$ to the upper range $g_i > g_i^*$, the "driving-force" will change from $F_i(R) < 0$ to $F_i(R) > 0$. Species i was initially diffusing

into the bubble but will later reverse and aid dissolution.

From equation (2.49) if initially

$$J_t = \sum_{j=1}^{n} \left[f_j \left(\frac{\partial F_j}{\partial e} \right)_R \right] > 0$$

or

$$f_i \left(\frac{\partial F_i}{\partial e} \right) > - \sum_{\substack{j=1 \\ j \neq i}}^{n} \left[f_j \left(\frac{\partial F_j}{\partial e} \right)_R \right]$$

the bubble starts growing but the changes of the flux of species i may be sufficient to lead to a final condition $J_t < 0$ and the bubble will eventually dissolve completely.

A change from $g_i > g_i^*$ to $g_i < g_i^*$ causes the opposite inversion from dissolution of species i to its diffusion into the bubble. If, in addition, the total flux varies from $J_t < 0$ to $J_t > 0$, the bubble radius initially decreases, then reaches a minimum value and finally increases again.

6.8 Transient stage of growth from finite size

Figure 6.3 illustrates behaviour in a three component system where the products $F_{O_i} . f_i = 0.01$, and $\alpha_i = F_{O_i}$. The bubble composition always evolves towards equilibrium ($g_{1,eq} = 0.2288$; $g_{2,eq} = 0.3026$; $g_{3,eq} = 0.4686$). In case (a) the initial bubble contains pure species 1, so that $F_1(R) = 0$ (equation (2.54)) while $F_2(R) = F_{O_2}$ and $F_3(R) = F_{O_3}$. Diffusion of gases 2 and 3 dilutes gas 1 which causes an increase of g_2 and g_3 and a decrease of g_1. Meanwhile the "driving-forces" of species 2 and 3 decrease and the "driving-force" of species 1 increases until equilibrium is reached. Similar interpretation can be made of cases b or c, which start with pure gas 2 or pure gas 3 respectively. The radius-time relations are only

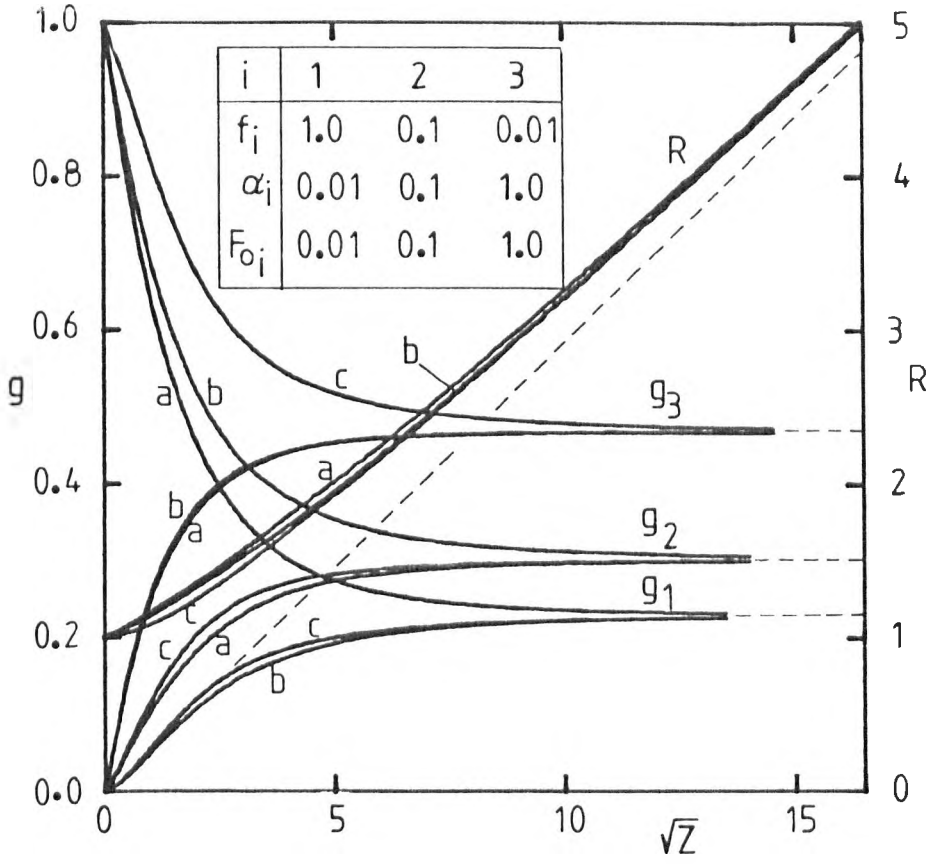

Fig 6.3 : Transient growth of three-component bubbles from finite size. The dashed lines represent the asymptotic regime (equations (6.14) and (6.16)). The initial bubbles contain
a - pure species 1
b - pure species 2
c - pure species 3 .

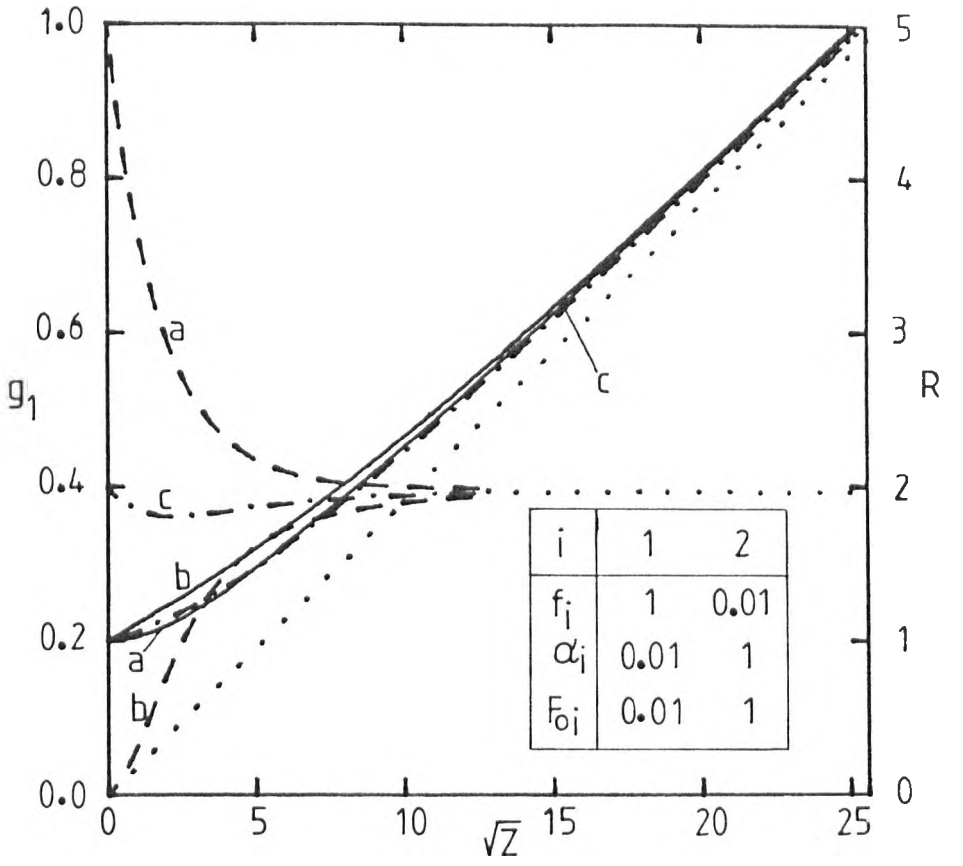

Fig 6.4 : Transient growth of two-component bubbles from finite size. The dashed lines represent the mole fractions of species 1, g_1, for cases a and b. The dashed-dotted lines represent R and g_1 for case c. The dotted lines represent the asymptotic regime.
The initial bubbles contain
a - pure species 1
b - pure species 2
c - g_1 = 0.3939 and g_2 = 0.6061.

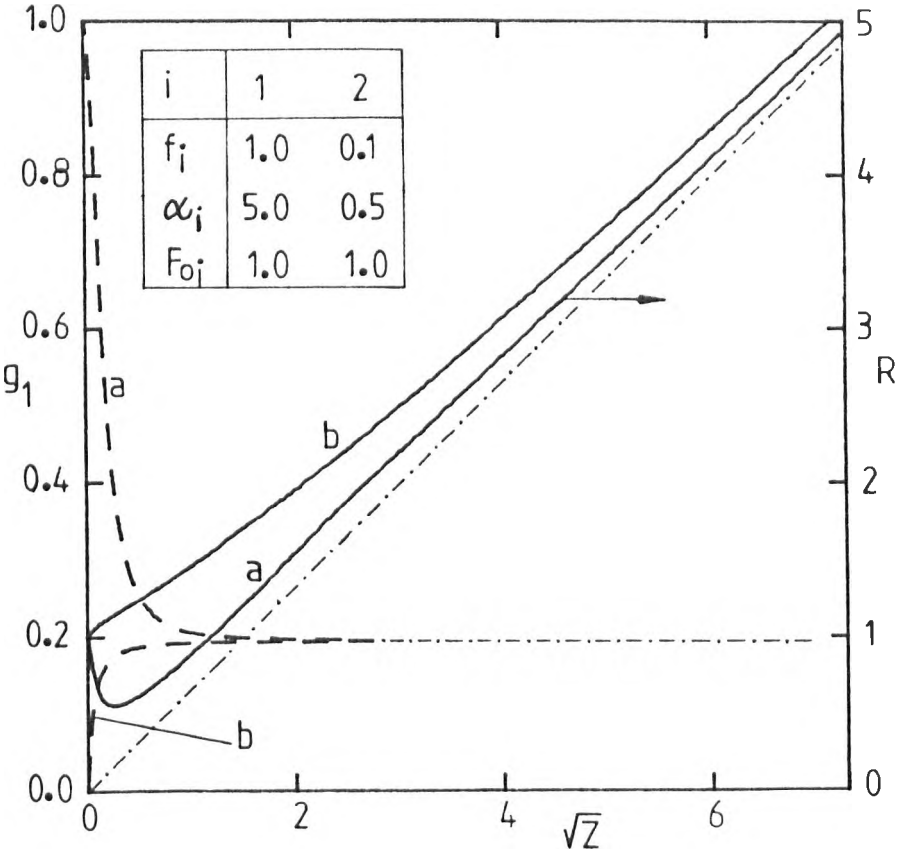

Fig 6.5 : Effect of the initial composition of a bubble on the transient regime. The dashed lines represent g_1 and the dashed-dotted lines represent the asymptotic regime.
The initial bubble contains
a - pure species 1
b - pure species 2.

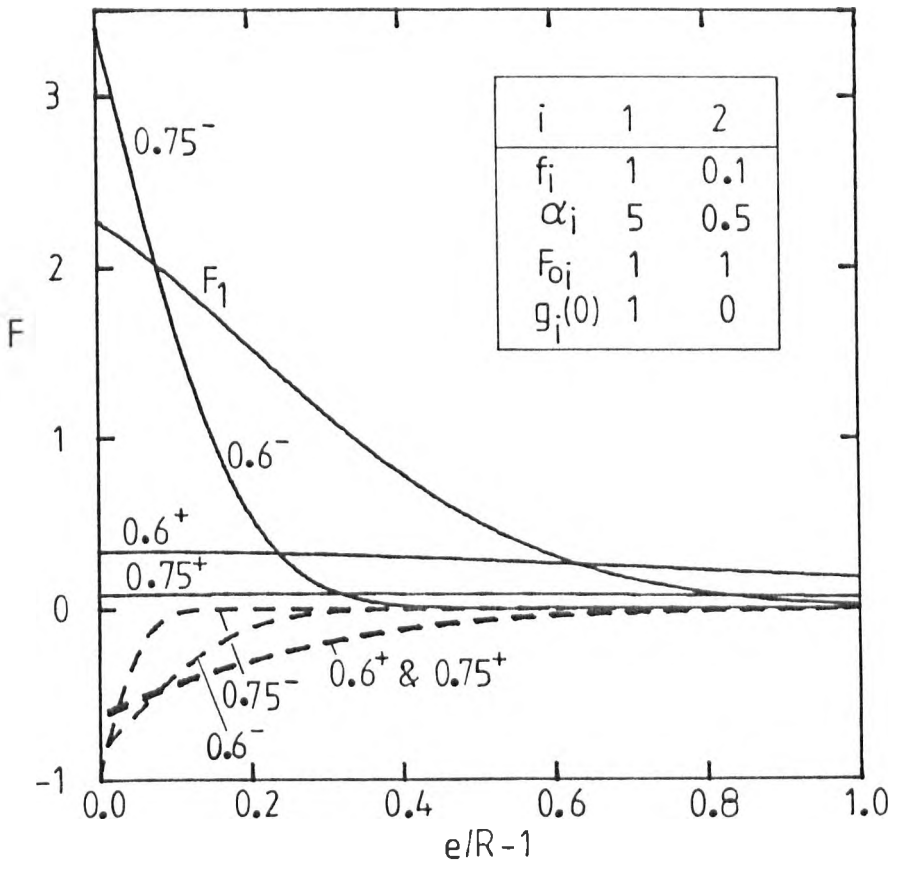

Fig 6.6 : Concentration profiles for the case (a) illustrated in fig 6.5. The full lines represent species 1 and the dashed lines species 2. The figures show the corresponding values of the dimensionless radius R and are marked - during the initial decrease in radius and marked + during the increase in radius.

Table : 6.4

Summary of two component systems represented in figures 6.4, 6.5, 6.7, 6.8, and 6.9, and their asymptotic regimes.

Fig.	F_{O_1}	F_{O_2}	α_1	α_2	f_2	g_1	β
6.4	0.01	1	0.01	1	0.01	0.3939	0.0948
6.5	1	1	5	0.5	0.1	0.1947	0.3312
6.7	1	1	0.5	0.5	1	0.500	1.831
6.7	1	0.01	0.5	0.005	100	0.684	1.280
6.7	1	100	0.5	50	0.01	0.1463	6.60
6.8	1	1	0.5	0.5	0.5	0.578	1.557
6.8	1	1	0.5	0.5	0.2	0.675	1.299
6.8	1	1	0.5	0.5	0.1	0.741	1.162
6.8	1	1	0.5	0.5	0.01	0.894	0.914
6.8	1	1	0.5	0.5	0.001	0.963	0.826
6.9	1	0.5	0.5	0.25	1	0.628	1.416
6.9	1	0.2	0.5	0.1	1	0.775	1.099
6.9	1	0.1	0.5	0.05	1	0.860	0.963
6.9	1	0.01	0.5	0.005	1	0.981	0.805

slightly different during the initial stage, but converge rapidly to each other and gradually approach the analytical prediction of growth from zero size (β = 0.1458) (dashed line).

Figure 6.4 shows a two-component system with the two extreme initial gas compositions (a and b). In both cases the composition of gas converges to the equilibrium $g_{1,eq}$ = 0.3939; $g_{2,eq}$ = 0.6061, which is represented by the horizontal dotted line. In case (c) $g_1(0)$ = 0.3939 but the bubble composition changes during the transient stage, because of large differences in diffusivities, before recovering the equilibrium condition. The radius versus time curves gradually approach the asymptotic regime given by the growth constant β = 0.0948.

The changes of gas composition in case (c) are due to transient changes of concentration profiles. A species with high diffusivity must respond more quickly than one of low diffusivity (species 2). Thus the change in size before the asymptotic concentration profile is achieved is smaller for the highest diffusivity, whilst during a somewhat longer stage the concentration profiles for the other species remain steeper than expected for the asymptotic conditions. This explains the transient increase in g_2.

A more complex transient regime is shown in figure 6.5. In case (a) the initial bubble contains pure species 1, which is highly soluble (α_1 = 5) and its diffusivity is also much higher than the diffusivity of species 2. Thus gas 1 initially dissolves relatively rapidly while the diffusion of gas 2 into the bubble is insufficient to reverse the process. At about Z = 0.068, R = 0.55 and g_1 = 0.39, $\frac{dR}{dZ}$ is reversed, showing that the rate of diffusion of gas 2 begins to exceed the rate of dissolution of gas 1. At this point $F_1(R)$ = 0.969 and $F_2(R)$ = - 0.697 so that the product $\left[f_1.F_1(R)\right]$ = 0.969 is still much larger than $\left[-f_2.F_2(R)\right]$ = 0.0697. The products $f_i.F_i(R)$

suggest that a significant amount of dissolved gas 1 could not diffuse away from the boundary layer and is hindering further dissolution.

This interpretation can be confirmed by examination of the concentration profiles shown in figure 6.6. Initially the interfacial concentration $F_1(R)$ decreases rapidly and $\frac{\partial^2 F_i}{\partial e^2}$ becomes negative near the interface. After the minimum radius, when growth is established, the profiles (marked +) at $R = 0.6$ and $R = 0.75$ show that $F_1(e)$ varies very smoothly in a relatively thick layer.

For a bubble of pure species 2 ((b) in figure 6.5) the rate of diffusion of species 1 into the bubble decreases rapidly as its mole fraction increases towards equilibrium at $g_{i,eq} = 0.1947$ (dashed-dotted line).

Both curves of radius versus time are distinguished from the asymptotic growth from zero size, ($\beta = 0.3312$ (see table 6.4)), but by the time the radius has increased by a factor of 10 the differences between the times required for growth from zero size and growth from finite size are only about 0.7% and 2.6% in cases (a) and (b) respectively.

Figures 6.3 and 6.4 demonstrated that if the products $F_{O_i} . f_i$ and the ratios α_i/F_{O_i} are constant the species with higher bulk concentration F_{O_i} will be transferred into the bubble faster. This trend is confirmed by the three results shown in figure 6.7, $F_{O_2} = 0.01, 1$, and 100, where $F_{O_i} . f_i = 1$, and $\alpha_i/F_{O_i} = 1/2$. The rate of transfer of species 2 increases with increasing F_{O_2} and is responsible for the increase of the equilibrium mole fraction of that species ($g_{2,eq} = 0.316$, 0.500 and 0.854 for the cases $F_{O_2} = 0.01$, 1, and 100 respectively). The enhancement of the rate of transfer of species 2 also causes the increase in growth rates ($\beta = 1.280$, 1.831 and 6.60 for cases $F_{O_2} = 0.01$, 1, and 100 respectively).

In figure 6.8 f_2 varies from 0.001 to 1 whilst $\alpha_2 = \alpha_1 = 0.5$; $F_{O_2} = F_{O_1} = 1$ and $f_1 = 1$ in all cases. The asymptotic regimes are shown in table

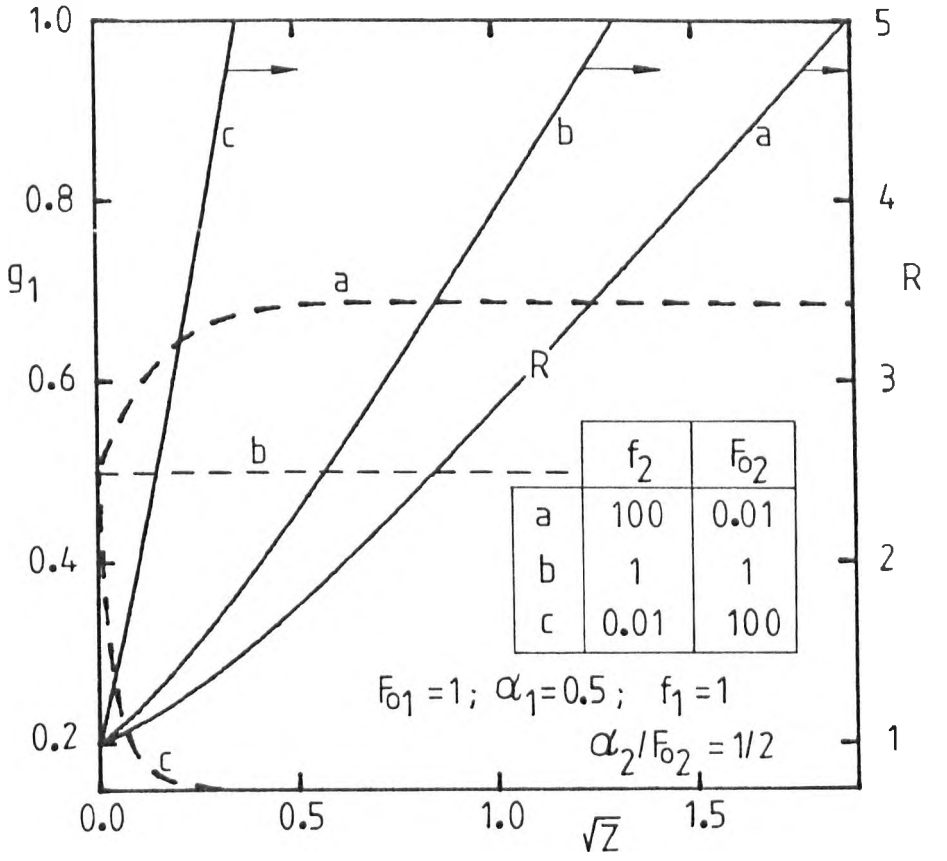

Fig 6.7 : Effect of varying the diffusivity of species 2 with $f_2.F_{O_2} = 1$ and $\alpha_2/F_{O_2} = 1/2$.

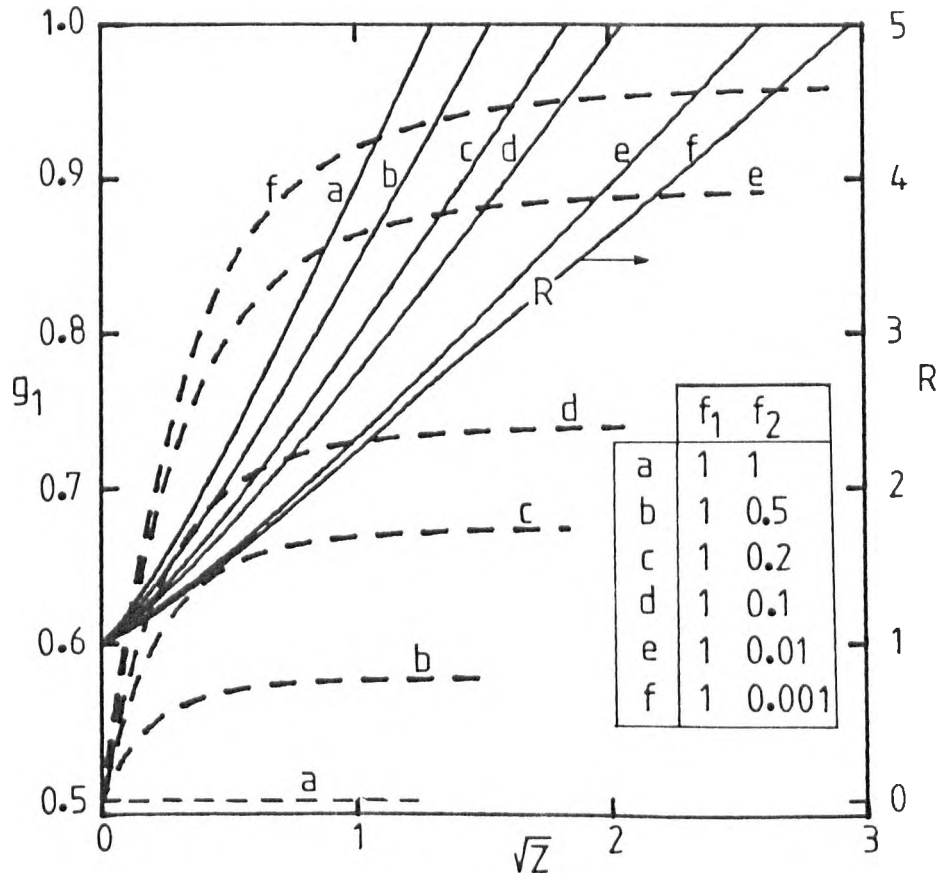

Fig 6.8 : Effect of varying the diffusivity of species 2 with $F_{O_1} = F_{O_2} = 1$ and $\alpha_1 = \alpha_2 = 1/2$.

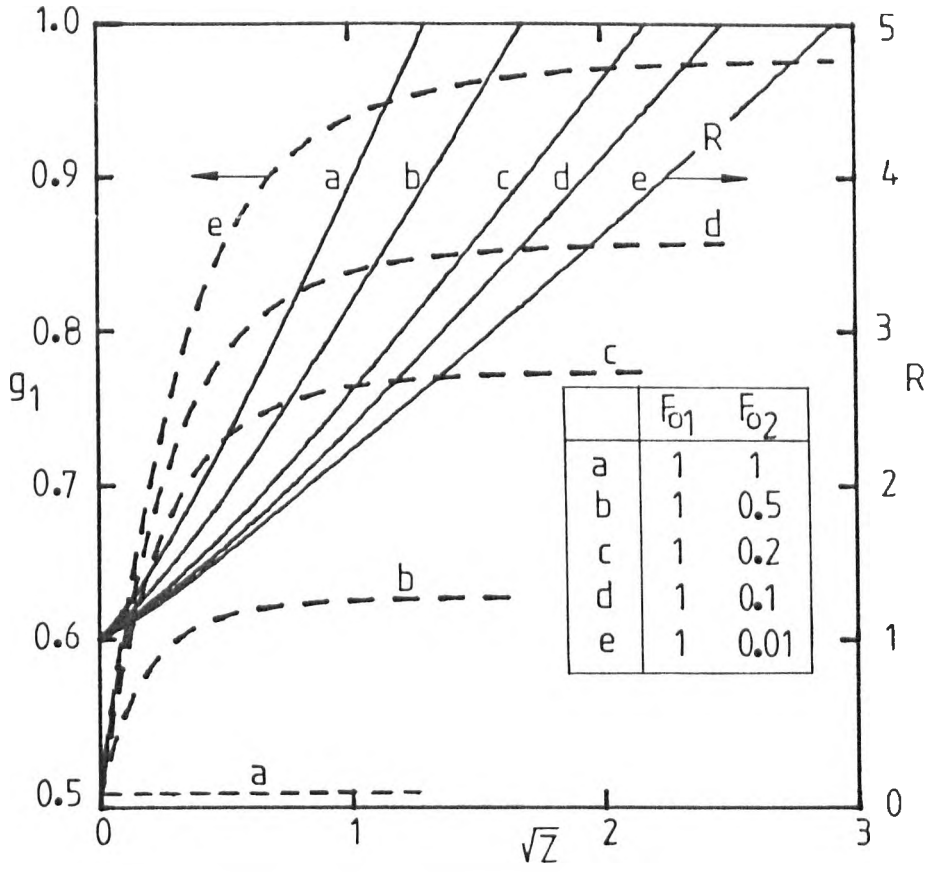

Fig. 6.9 : Effect of varying the bulk concentration of species 2 with $D_1 = D_2$, $F_{o_1} = 1$; $\alpha_1 = 0.5$ and $\alpha_2/F_{o_2} = 1/2$.

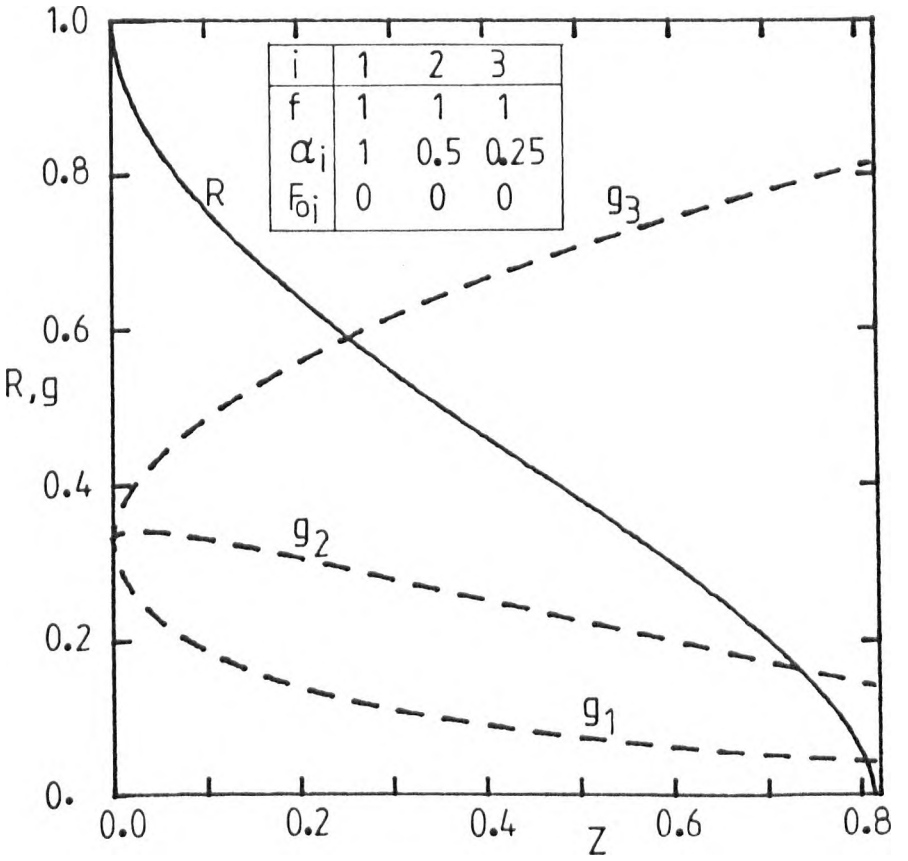

Fig 6.10 : Dissolution of a three-component bubble with equal initial mole fractions, equal diffusivities but different solubilities.

6.4 and show that $(g_{2,eq}/g_{1,eq}) = (1/g_{1,eq} - 1)$ is almost proportional to $f_2^{\frac{1}{2}}$ (f_2 represents the ratio of diffusivities).

Figure 6.9 shows a set of results for F_{O_2} = 0.01, 0.1, 0.2, 0.5 and 1, whilst $F_{O_1} = 1$; $\alpha_1 = 0.5$; $\alpha_2/F_{O_2} = 1/2$ and $f_2 = f_1 = 1$. Although the behaviour is qualitatively very like that in figure 6-8 the details are rather different. The rates of transfer of species 2 here drop more rapidly as F_{O_2} decreases than in the previous cases of decreasing diffusivity (see table 6.4.).

Changes in diffusivity and solubility or bulk concentration can roughly cancel each other but cannot be exactly equivalent because the diffusivity affects coefficients in the partial differential equation (2.47) whilst the solubility and bulk concentration affect the boundary conditions.

6.9 Dissolution

Demonstration of the behaviour of multi-component bubbles must include the effects of solubilities and diffusivities on the dissolution rates and on the composition of the gas phase. The initial concentrations of dissolved gases in the liquid medium may also play a significant role.

The solubilities and diffusivities of gases in glass melts may cover relatively large ranges of values, so that it is important to analyse the behaviour of bubbles containing gases with very different diffusivities or solubilities.

The composition of growing bubbles always converges asymptotically to equilibrium and this regime was solved analytically. Concentration profiles around dissolving species do not evolve towards self-similar regimes, and vary until the dissolution is complete, under the combination of effects of diffusion and radial convection (Chapter V). This situation must be even more complex in the case of bubbles containing several gases which diffuse independently.

6.9.1 Bubble containing gases with different solubilities but the same diffusivities

Figure 6.10 illustrates a 3-component system with equal diffusivities and solubilities given by $\alpha_1 = 1$; $\alpha_2 = 1/2$; $\alpha_3 = 1/4$, with $F_{O_i} = 0$; (i=1, 2, 3). Initially the gas composition varies rapidly due to the differences between solubilities. Species 2 having an intermediate solubility undergoes smaller changes of mole fraction than either 1 or 3. There is no indication of equilibrium composition before the end of the process. The conditions required for a dissolving sphere to tend to equilibrium gas composition will be discussed later.

Figure 6.11 shows the effects of larger ratios between solubilities α_1/α_2 in two-component bubbles. The mole fraction of the most soluble gas (species 1) decreases progressively and becomes lower than 0.01, long before complete dissolution of the bubble. Dissolution of the least soluble gas controls the total dissolution time and in the limit, ($\alpha_2 = 0$), a residual bubble is left (R = 0.794) after complete dissolution of species 1. In general these results confirm that equilibrium composition is rarely achieved in dissolving bubbles containing gases with different solubilities.

The dashed-dotted line in figure 6.11 represents the change in size controlled by dissolution of species 2 after instantaneous (and complete) dissolution of species 1. This causes instantaneous decrease of real radius from a_O to a_i, so that only species 2 is left and

$$\frac{4}{3}\pi a_i^3 C_s = \frac{4\pi}{3} a_O^3 C_s g_2(0)$$

or

$$R_i(0) = (a_i/a_O) = [g_2(0)]^{1/3} \quad . \tag{6.38}$$

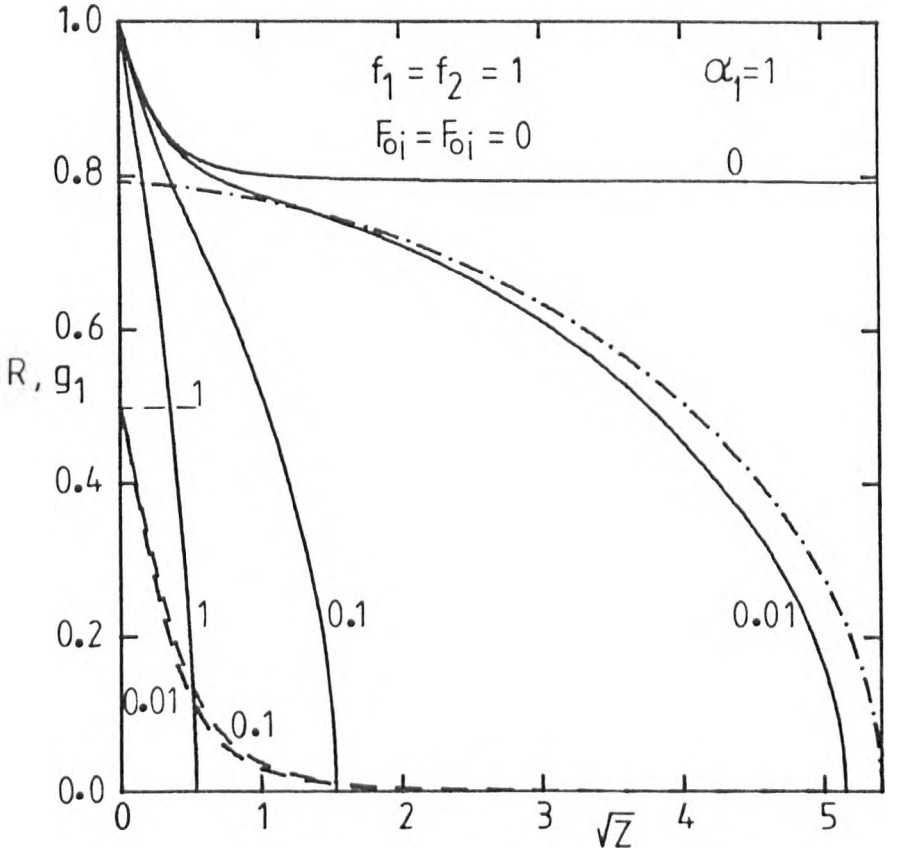

Fig 6.11 : Dissolution of two-component bubbles with gases of different solubilities but the same diffusivities. The dashed lines represent g_1 and the dashed-dotted line represents the dissolution of species 2 after instantaneous dissolution of species 1. The figures show the values of α_2.

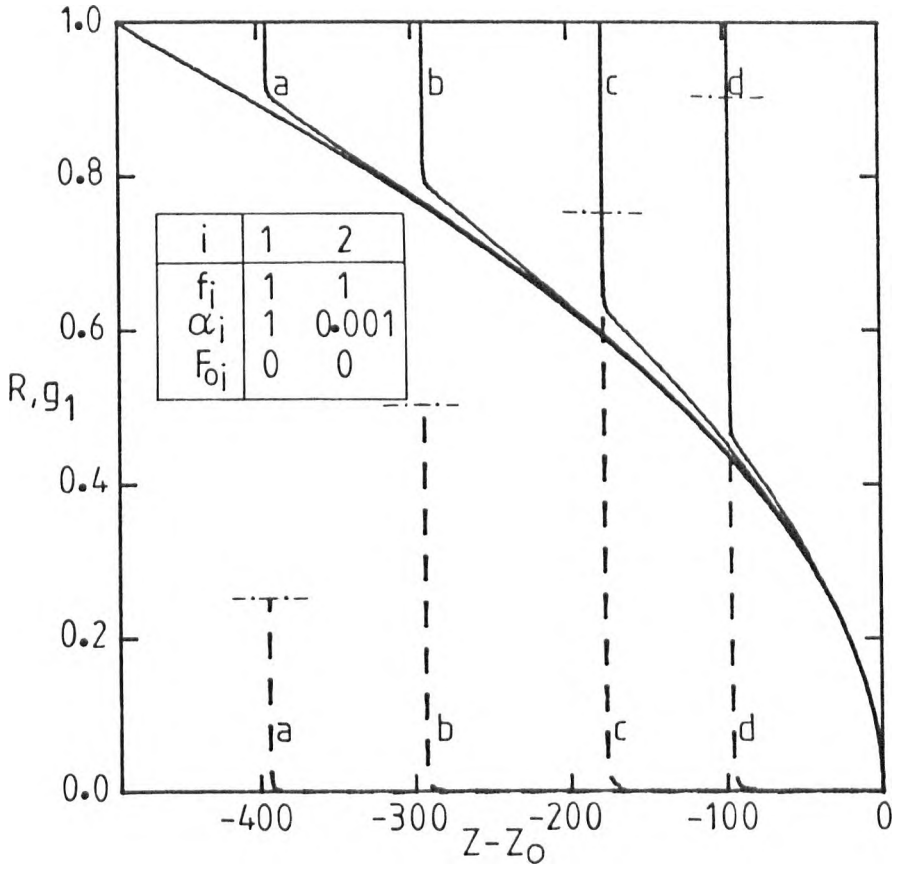

Fig 6.12 : Effect of the initial composition of gas on the dissolution of a two-component bubble containing gases of very different solubilities and the same diffusivities. The dashed lines represent the mole fraction of species 1, g_1 with initial values 0.25, 0.5, 0.75 and 0.9 in cases a, b, c and d.

In the case of figure 6.11 $R_i(0) = 0.7937$. The actual two component solution for $\alpha_2 = 0.01$ is already close to the limiting solution (dashed-dotted line) predicted by assuming that the most soluble species dissolves instantaneously.

From figure 6.11 it is also clear that the shape of the radius-time curves changes markedly as the solubility of the less soluble gas varies.

Confirmation that dissolution is controlled by the less soluble gas is shown in figure 6.12. The initial mole fraction of species 2 is varied ($\varsigma_2(0) = 1$, 0.75, 0.5, 0.25 and 0.1) and the times of dissolution are matched so that it is possible to compare the final stages. All cases show almost instantaneous dissolution of gas 1 (relative to the time scale) and after this stage the residual radii are about $R_i = 0.909$, 0.794, 0.630 and 0.464. Those values would represent the final radius of the bubble if species 2 were completely inert.

That the first stage is due to the dissolution of the species 1 is shown by the rapid drop of its mole fraction in the gas (dashed lines).

The fact that after the initial stage the curves become similar suggests that the rates of dissolution are almost exclusively dependent on the actual size of the bubble. This type of regime is characteristic of very low solubility parameters ($F_a \ll 1$ if the notation of Chapter V is used) and the limit converges to quasi steady state approximations (equation (2.68)).

It must be emphasized that if α_2/α_1 remains very low but the solubility of species 2 is moderate or large ($\alpha_2 > 0.1$) the final stages (after the rapid dissolution of species 1) cannot be matched. The rates of dissolution are then not exclusively dependent on the actual radius but also on the residual radius, R_i, after the initial stage.

6.9.2 Bubble containing gases with different diffusivities but the same solubilities

In the system illustrated in figure 6.13 the diffusivities follow the relation $D_1:D_2:D_3 = 1:\frac{1}{2}:\frac{1}{4}$ and the solubility is constant ($\alpha_i = 1$, $F_{O_i} = 0$, i=1, 2, 3). The changes of gas composition are similar to those observed in figure 6.10 (due to similar differences in solubilities). However the dissolution time is slightly longer when the solubilities differ than when the diffusivities differ.

Figure 6.14 illustrates the effects of further extending the range of diffusivities in two component bubbles. Here the numbers on the curves are the values of f_2. Again the species with the largest diffusivity dissolves almost completely before the end of the process. This is indicated by the decreasing values of the mole fraction g_1 (dashed lines).

The dashed-dotted line in figure 6.14 represents the case when gas 1 is assumed to dissolve instantaneously before species 2 starts dissolving. In this case $f_2 = 0.01$, $F_a = (\alpha_2 - F_{O_2}) = 1$ and the radius-time curve does not differ significantly from the actual two-component solution except during the initial stage. These examples show that dissolution is also controlled by the dissolution of the species which has the lowest diffusivity, provided the bulk concentrations F_{O_i} are zero and the solubilities are equal.

Figure 6.15 shows computed results for bubbles containing initial mole fractions of low diffusivity gas (species 2) $g_2(0) = 0.75$, 0.5, 0.25 and 0.10 which confirm the controlling role of the species with the lowest diffusivity. Again the initial stage is very rapid and finishes at about $R_i = 0.909$; 0.794, 0.630 and 0.464 which are the sizes of bubbles expected if gas 1 disappeared instantaneously. The unmarked curve is the result for pure species 2.

The data represented by (+) in figure 6.15 also corresponds to the

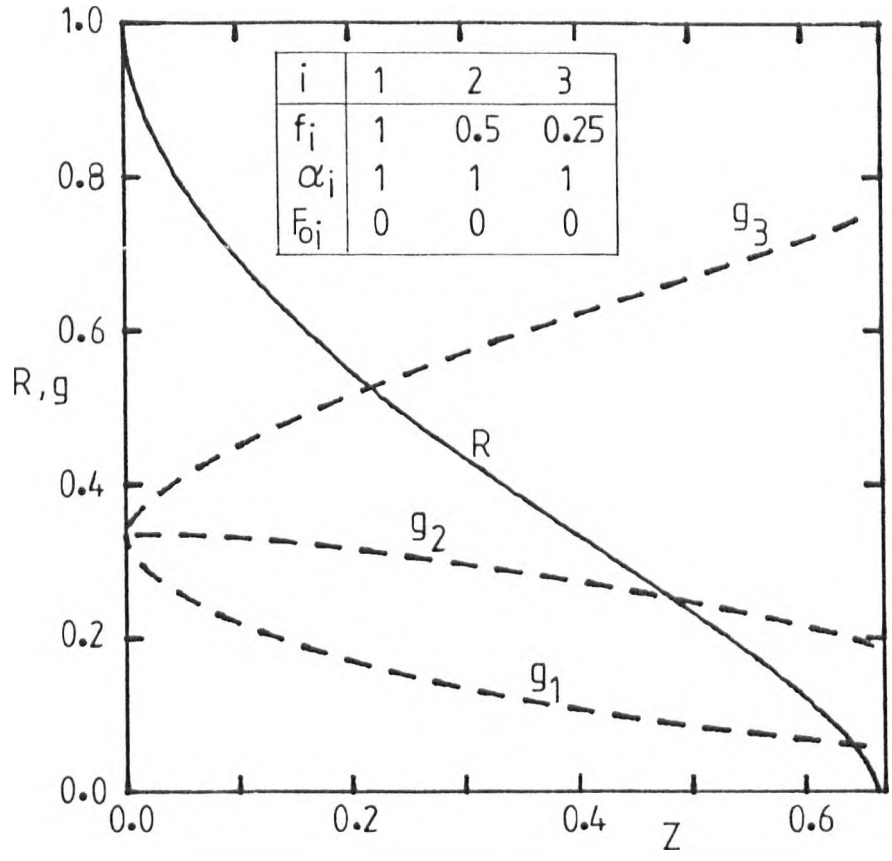

Fig 6.13 : Dissolution of a three-component bubble containing gases with equal initial mole fractions, equal solubilities but different diffusivities.

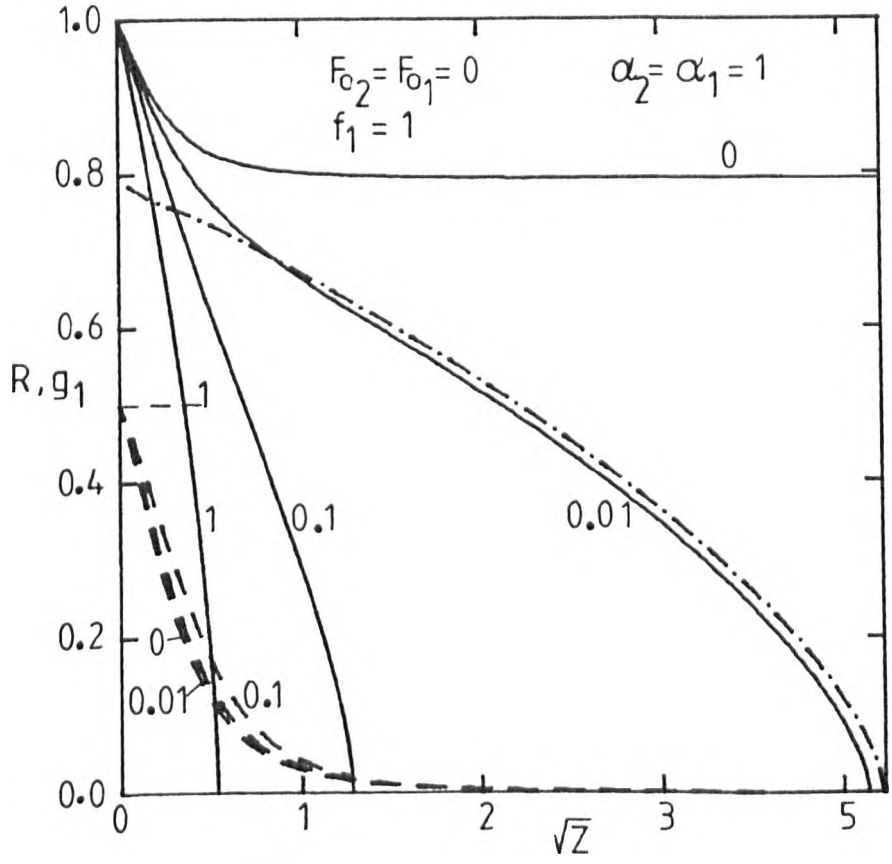

Fig 6.14 : Dissolution of two-component bubbles with gases of different diffusivities and the same solubilities. The dashed lines represent g_1 and the dashed-dotted lines represent the dissolution of species 2 after instantaneous dissolution of species 1. The figures show the values of $f_2 = D_2/D_1$.

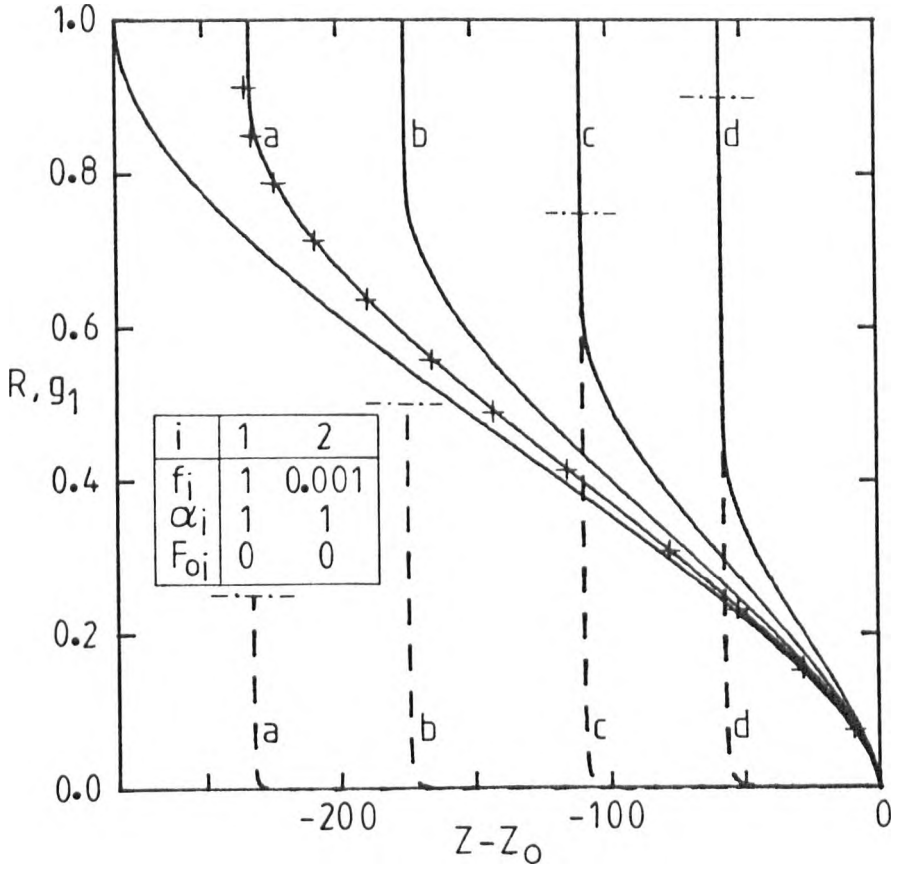

Fig 6.15 : Effect of the initial composition of gas on the dissolution of a two-component bubble containing gases of very different diffusivities and the same solubilities. The dashed lines represent the mole fraction of species 1 with initial values g_1 = 0.25, 0.5, 0.75 and 0.9 in cases a, b, c and d respectively. The symbols (+) represent the dissolution of species 2 after instantaneous dissolution of gas 1 for the case $g_1(0)$ = 0.25.

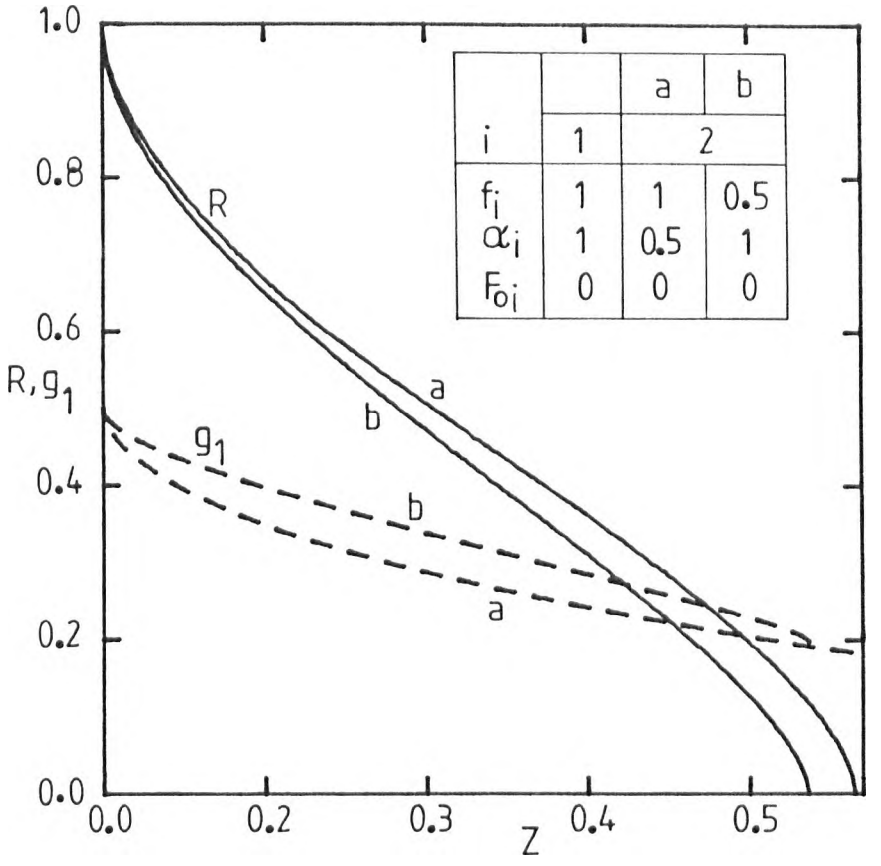

Fig 6.16 : Dissolution of two-component bubbles containing gases with the same permeability $\alpha_1 f_1 = \alpha_2 f_2 = 0.5$ but different solubilities.

instantaneous dissolution of gas 1 and is obtained from one-component solutions of the case $F_a = \alpha_2 - F_{O_2} = 1$ with $f_2 = 0.001$ and $g_2(0) = 0.75$. The agreement of such curves with the actual solution is equally good with the other initial compositions of gas. In these cases the dissolution behaviour can be reasonably predicted from the solutions of a residual bubble containing only the gas with low diffusivity.

In both cases shown in figure 6.16 the permeability of species 2 is the same $\alpha_2 \cdot f_2 = 1/2$ but in case (a), (lower solubility of species 2), the dissolution is slightly quicker. This finding is not surprising by taking into account that the dissolution time changes more rapidly with variable solubility than with variable diffusivity (Chapter V).

6.9.3 Dissolution of bubbles containing gases with equal permeabilities

It has been shown that one-component (i=1) of the gas mixture can dissolve almost completely making the residual bubble become almost pure species 2. This behaviour requires zero bulk concentration of species 1 ($F_{O_1} = 0$) and the solubility or the diffusivity of the rapidly dissolving species 1 must be much higher than the corresponding property of the other species. At this stage it is useful to analyse the behaviour of bubbles containing gases with equal permeabilities (constant $\alpha_i \cdot f_i$ values) when both solubility and diffusivity vary.

Figure 6.17 shows four examples in which the individual properties vary by factors of 1000 and $g_1(0) = g_2(0) = 0.5$; the reference component (i=1) has the same properties in every case ($\alpha_1 = 1$ and $f_1 = 1$) whilst $\alpha_2 \cdot f_2 = 1$ and both bulk concentrations are zero ($F_{O_1} = F_{O_2} = 0$), so that the bubble composition is not *a priori* restricted by equilibrium between the gas phase and the liquid medium. The component with high solubility and low diffusivity always dissolves more rapidly than the reference component in

spite of the fact that both gases have equal permeabilities. This explains why the bubbles with the largest values of solubility (α_1 and α_2) dissolve fastest. It also explains the initial drop of the mole fraction of the species with larger solubility and lower diffusivity. Meanwhile the interfacial concentration of this component also decreases and the same happens to the absolute value of the concentration gradient and to the rate of dissolution. This leads to a temporary "equilibrium" between the individual dissolution rates and the gas composition. However, there are clear signs that the initial tendency is reversed during the final stage of dissolution. There is no simple explanation for this tendency except the fact that, if $\left(-\frac{dR}{dZ}\right)$ is sufficiently large during the initial and intermediate stage of the process, the accumulation of solute near the interface hinders the final stage of dissolution and that this effect is increasingly severe as the diffusivity decreases. In case (a) (figure 6.17) the solubility α_2 is very high and the mole fraction g_2 is relatively low during the intermediate and final stages. Therefore a small change in g_2 causes a significant increase of the "driving-force" $F_2(R)$ which is sufficient to correct the deviations from a final quasi-equilibrium condition.

Bubbles containing equal proportions of more than two gases with equal permeabilities (figure 6.18) behave similarly. Initially the individual rates of dissolution increase with increasing solubility of the species which is being considered. However, because they have smaller diffusivities the dissolved species 1 and 2 may not diffuse to large distances from the interface. Accumulation of dissolved material must then be the reason for the final increase of mole fractions g_1 and g_2.

Other important characteristics of bubbles containing two gases with equal permeabilities but different diffusivities are illustrated in figure 6.19. The dissolution rate is here significantly affected by the

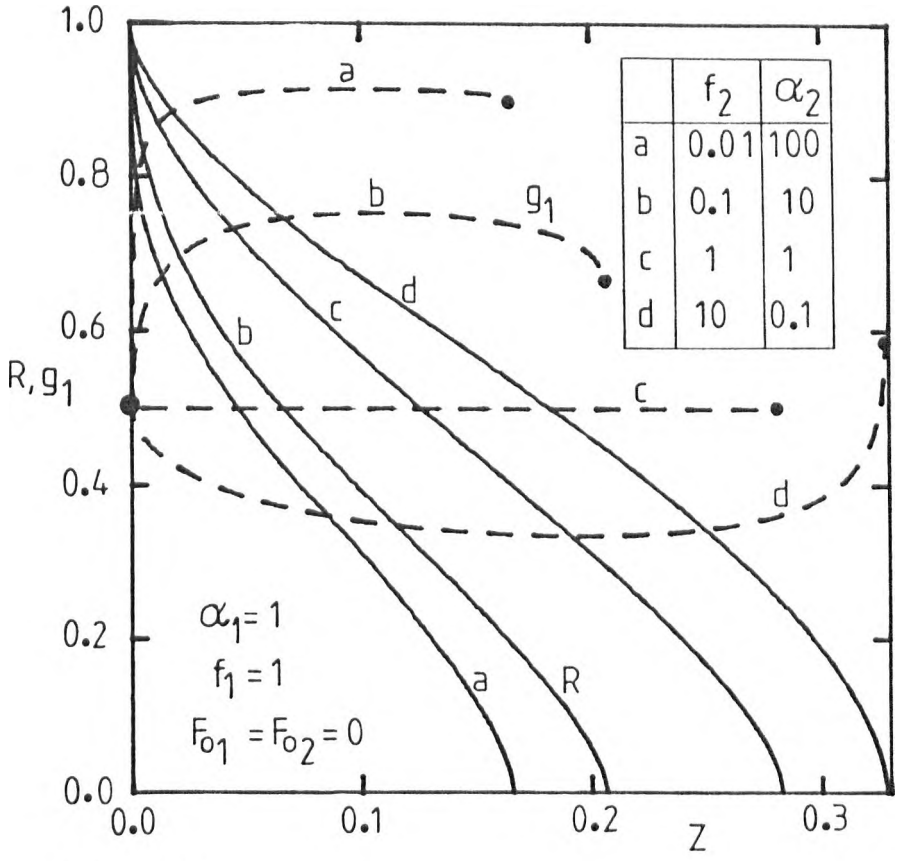

Fig 6.17

Figs 6.17 and 6.18 : Dissolution of bubbles containing gases with the same permeability but very different solubilities.

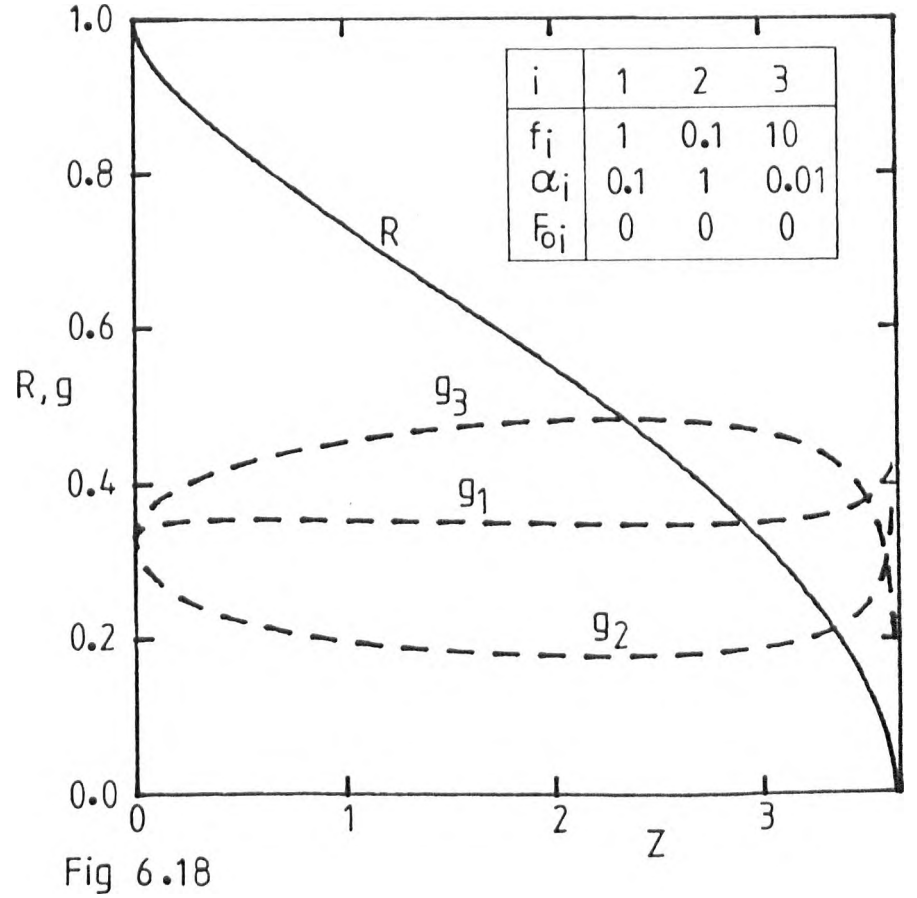

Fig 6.18

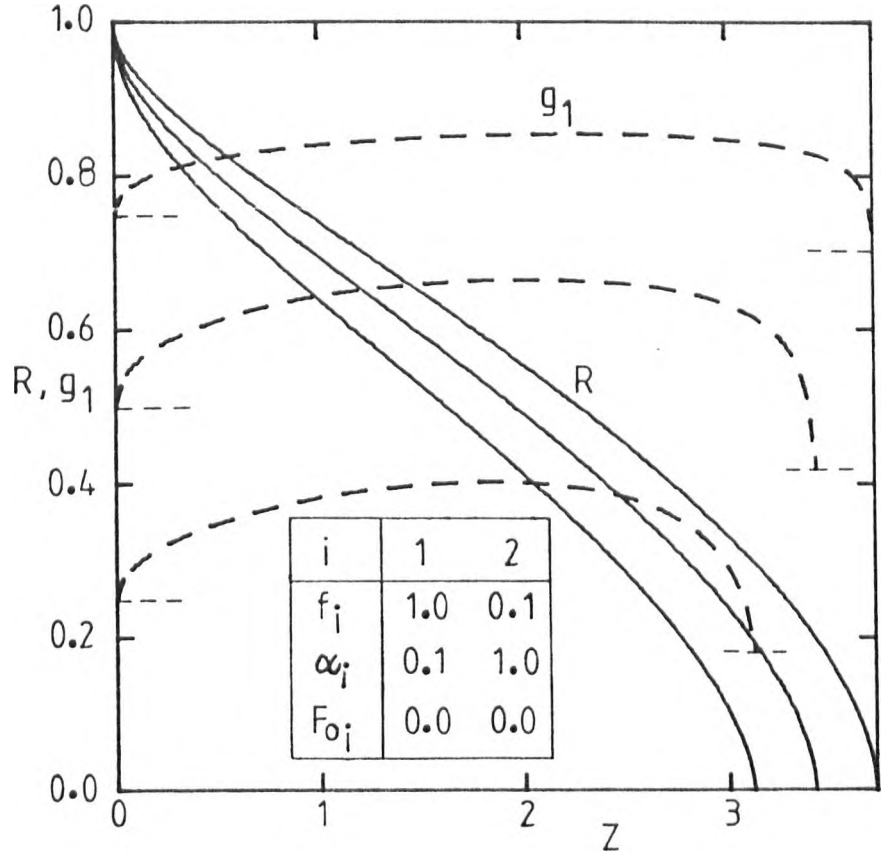

Fig 6.19 : Effect of the initial composition of gas on the dissolution of a bubble containing two gases with the same permeability but different solubilities.

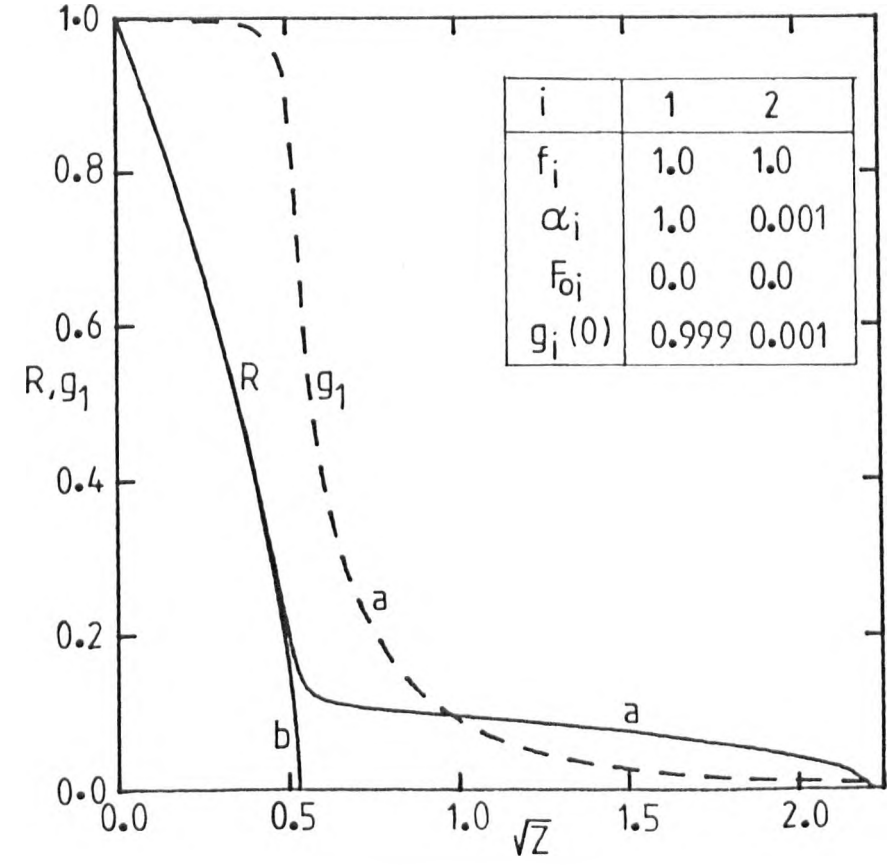

Fig 6.20 : Effect of a poorly soluble impurity in the initial gas composition on the dissolution of a bubble. Case b represents dissolution of a bubble of pure species 1.

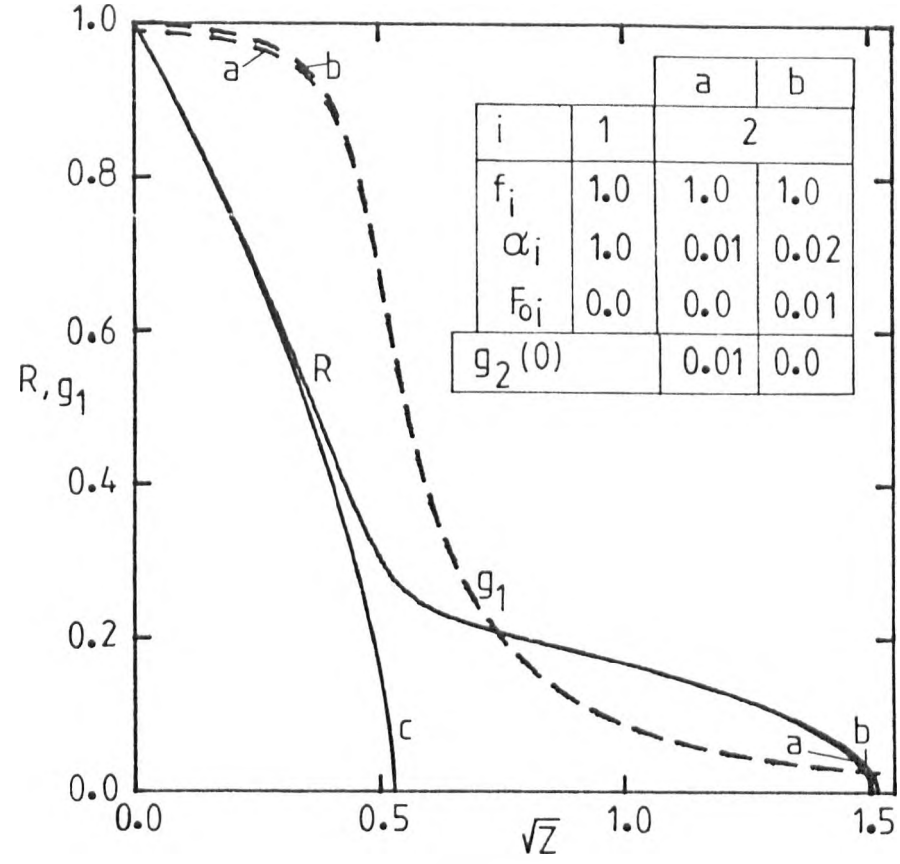

Fig 6.21a : Effect of poorly soluble impurities in the liquid or in the gas phase on the dissolution of bubbles. Case c represents dissolution of a bubble containing pure gas 1.

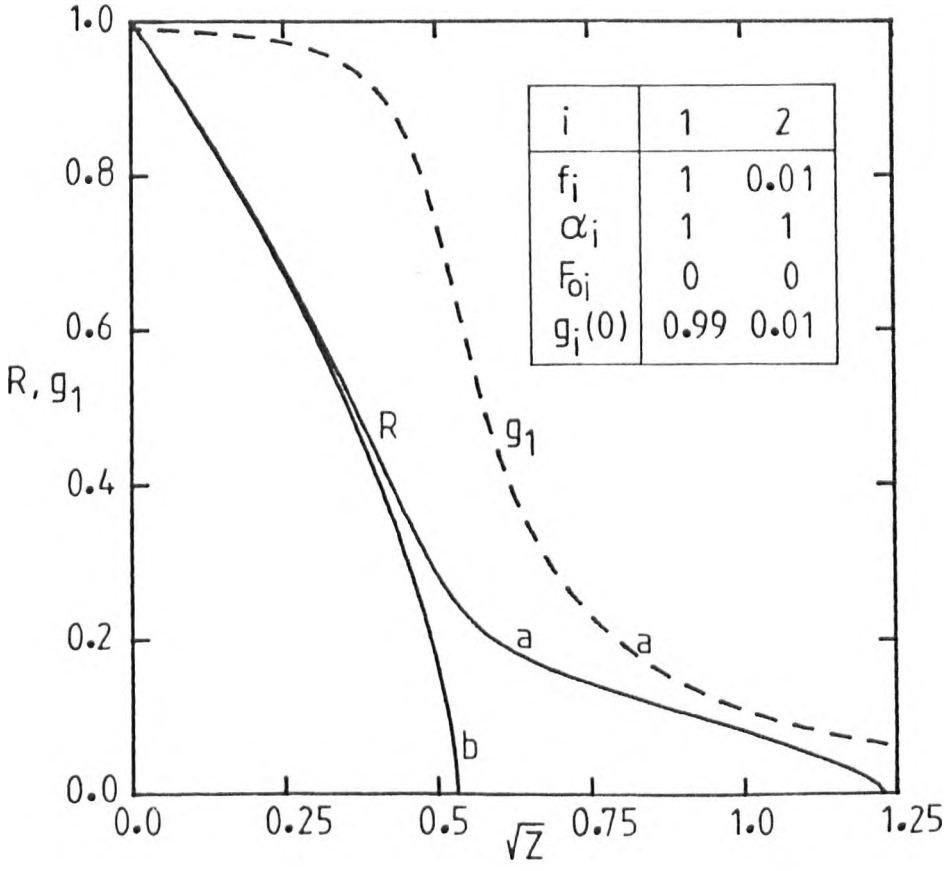

Fig 6.21b : Effect of impurity of relatively low diffusivity on the dissolution of a bubble. Case b represents dissolution of a bubble containing pure gas 1.

initial composition of the bubble and the temporary "equilibrium" composition varies with that composition. The final composition is also very dependent on the initial composition of the gas. In all cases the mole fraction of the least soluble species (g_1) drops significantly during the last stage of the process.

6.9.4 Effect of impurities in the gas or dissolved in the liquid

It has already been shown that the time required for complete dissolution of bubbles containing two or more gases depends greatly on the species which has the lower diffusivity or the lower solubility. That dissolution time decreases with decreasing mole fractions of the less soluble gas in the initial bubble. However, even very small mole fractions of a relatively inert species (low solubility, low diffusivity or both) cause a very slow final stage. In figure 6.20 (case (a)) the initial bubble contains only 0.1% of a poorly soluble gas ($\alpha_2 = 0.001$). Case (b) corresponds to the dissolution of a bubble containing pure gas 1 and both radius-time curves are almost coincident down to R = 0.1, that is, when the bubble is only 10% of the initial radius. By this stage the bubble (a) is only 0.1% of its initial volume and contains a large percentage of the inert gas, which requires a much longer dissolution time. If species 1 did dissolve completely before any dissolution of gas 2 then the residual radius would be R = 0.1. Times for complete dissolution can be greatly affected by low levels of impurity in the original gas.

Case (a) in figure 6.21a confirms the effect of minor proportions of a relatively inert gas in the original bubble ($\alpha_2 = 0.01$). Again this case leads to a slow final stage when the bubble radius is slightly greater than the residual radius R = 0.215. Case (c) is the solution for the bubble containing pure species 1.

In case (b) the initial bubble is free of impurity but the liquid is slightly contaminated so that species 2 can diffuse slowly into the bubble while gas 1 diffuses out. The "driving-force" for this process was initially $F_2(R) = - F_{O_2} = - 0.01$. Rather surprisingly beyond this initial stage ($R < 0.85$) cases (a) and (b) become almost indistinguishable. Notice that during the final stage $F_2(R)$ is similar in both cases.

So far we have been concerned with small proportions of relatively insoluble impurities in the gas or in the surrounding liquid. Similar effect can be predicted by considering that the impurity has much lower diffusivity than the main gas. In the case (a) shown in figure 6.21b the ratio of diffusivities is $f_2 = D_2/D_1 = 0.01$. The main difference between this case and the case(a) shown in figure 6.21a is the time scale for the final stage. Decreasing the solubility of species 2 causes a slower final stage than decreasing the diffusivity.

6.9.5 Changes from growth to dissolution

The relation between the mole fractions and concentrations at the interface suggest that by varying the gas composition it is possible to reverse the direction of diffusion of a particular species. If the initial rate of diffusion of this component (independently of the direction) is much larger than the other individual rates of diffusion, then the behaviour of the bubble may eventually be reversed. A change from dissolution to growth was illustrated in figure 6.5 and the opposite type of changes is exemplified in figure 6.22. The solubility of species 1 is much higher than the solubility of species 2 but the bulk concentration F_{O_1} is also quite high so that species 1 will diffuse into the bubble if its initial mole fraction, $g_1(0)$, is lower than 0.8.

The initial dissolution of species 2 further assists the rapid increase

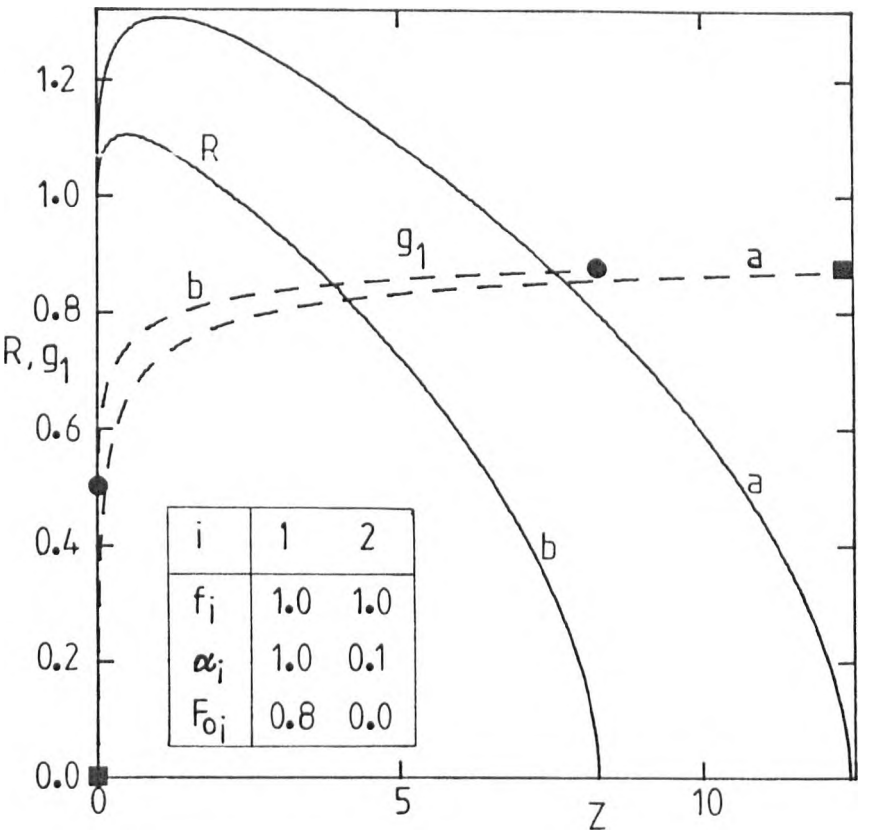

Fig 6.22 : Complete dissolution after an initial increase in radius.

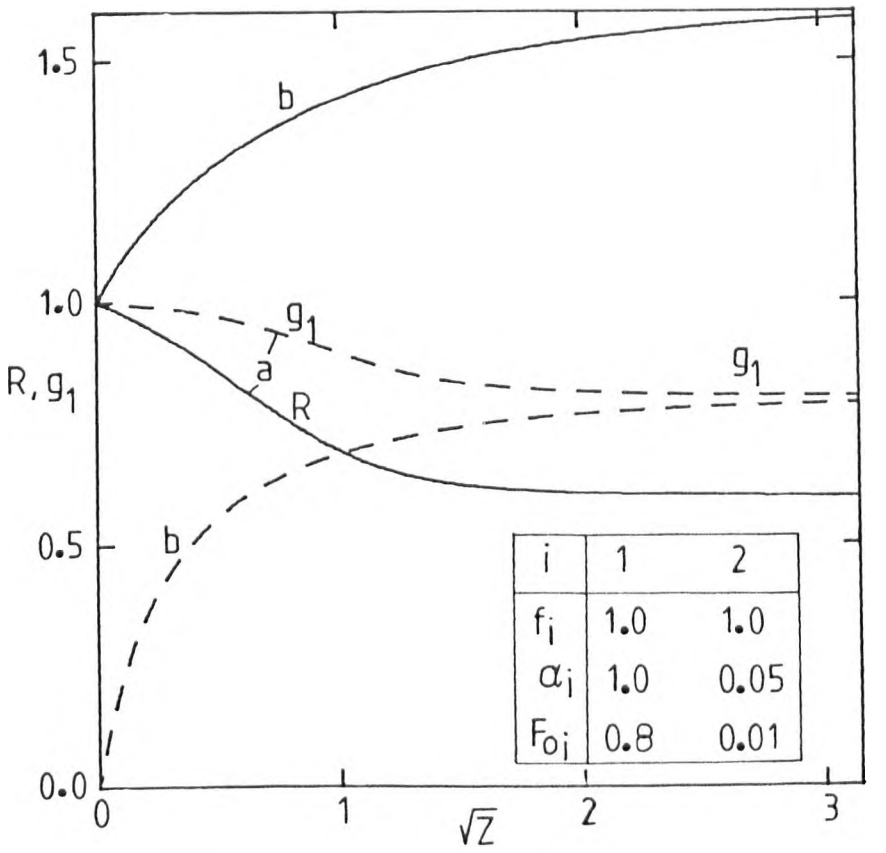

Fig 6.23 : Evolution of bubble behaviour towards equilibrium size and gas composition.

in g_1 but is insufficient to prevent the growth of the bubble. The diffusion rate of species 1 into the bubble inevitably decreases because of the increase in its interfacial concentration. Dissolution of the bubble starts when the dissolution rate of gas 2 exceeds the rate of diffusion of gas 1 into the bubble.

6.9.6 Evolution of size and composition of bubbles towards equilibrium

Figure 6.23 illustrates some cases when the size and composition of the bubble evolve towards equilibrium. The "driving-forces" of both components vanish as the bubble composition approach the point $g_1 = 0.80$, $g_2 = 0.20$. If the initial bubble contains pure species 1 (relatively high solubility) the size will decrease to about $R = 0.59$ as g_1 decreases to 0.80. On the contrary if the initial bubble contains species 2, of low solubility, its rate of dissolution is relatively small and is exceeded by the diffusion of species 1 into the bubble. In this case the size increases to about 1.6 times the initial size as g_1 again approaches 0.80.

These examples demonstrate that the equilibrium gas composition is not dependent on the initial composition of the bubble although the radius of the bubble increases if $g_1(0) < 0.8$ and decreases if $g_1(0) > 0.8$. By varying the initial composition of the gas it is possible to reach different final radii R_f of the bubble, but always in the range $0.5928 < R_f < 1.609$.

6.9.7 Changes of composition in dissolving bubbles

It has been shown that when the liquid is initially free of solutes ($F_{Oi} = 0$, i=1, ..., n) the bubble composition evolves continuously towards complete dissolution of the species which has the highest solubility, the highest diffusivity or both. If the ratios of solubilities or diffusivities

are sufficiently large the most inert gas may remain almost undissolved for a relatively long time, while the quickly diffusing species dissolves almost completely. Otherwise the composition of gas may still be varying when the bubble disappears.

If the permeabilities of the individual gases are equal but their diffusivities differ considerably, the mole fraction of the least soluble component increases during the initial stage, remains nearly constant during the intermediate stage and finally decreases again as seen in figure 6.17. Apparently the condition of quasi-equilibrium between individual material fluxes across the interface and the corresponding mole fractions fails during the final stage due to accumulation of dissolved material around the bubble. The accumulation of a particular species i must be increasingly severe as its diffusivity becomes much smaller than the diffusivity of the other gases.

Examples of complex evolution of gas composition are shown in figures 6.24 and 6.25. In figure 6.24 the three gases have equal diffusivities but markedly different solubilities. The dissolution can then be divided into three stages which correspond to control by each of the gases present in the bubble. Logarithmic time scale was used to distinguish these stages.

In figure 6.24 species 1 dissolves almost completely before significant dissolution of any of the less soluble gases occurs. The mole fractions g_2 and g_3 thus increase almost identically during this first stage.

After almost complete dissolution of gas 1 the process is controlled by species 2 which dissolves at a much greater rate than does species 3; as a result the ratio g_2/g_3 decreases. It then follows that the value of g_2 must reach a maximum then decrease. During the last stage g_2 is almost zero and dissolution is governed by species 3.

The residual bubble containing only gas 3 (if it were inert) would have

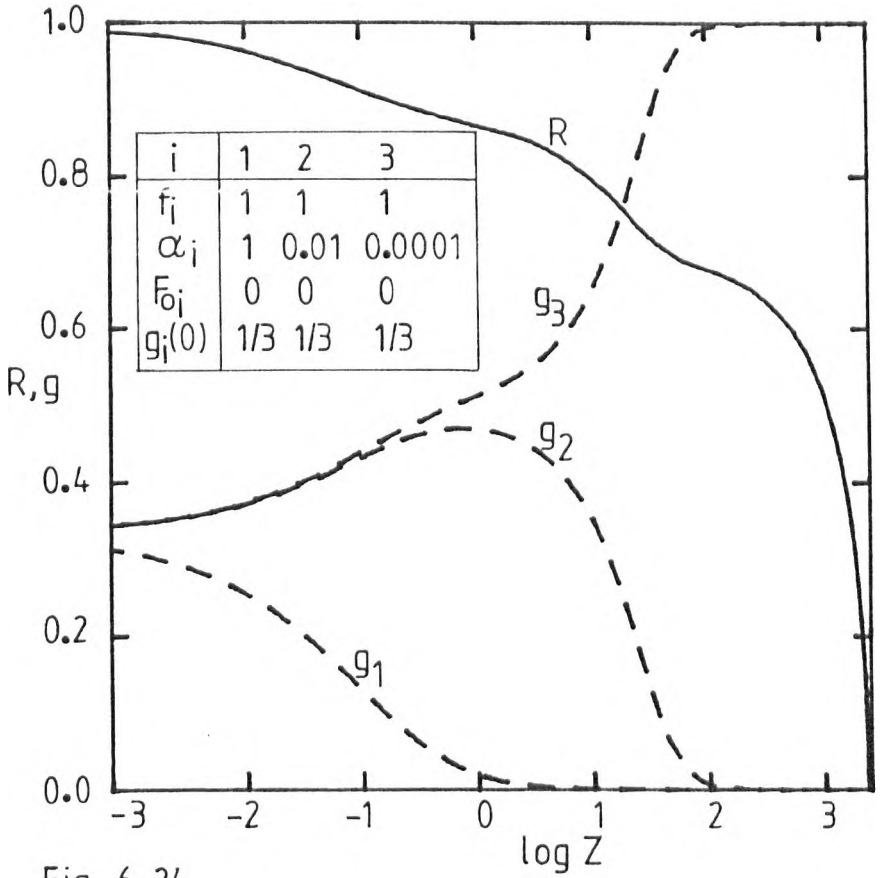

Fig 6.24

Figs 6.24 and 6.25 : Dissolution of three component bubbles showing three distinct stages corresponding to each of those species.

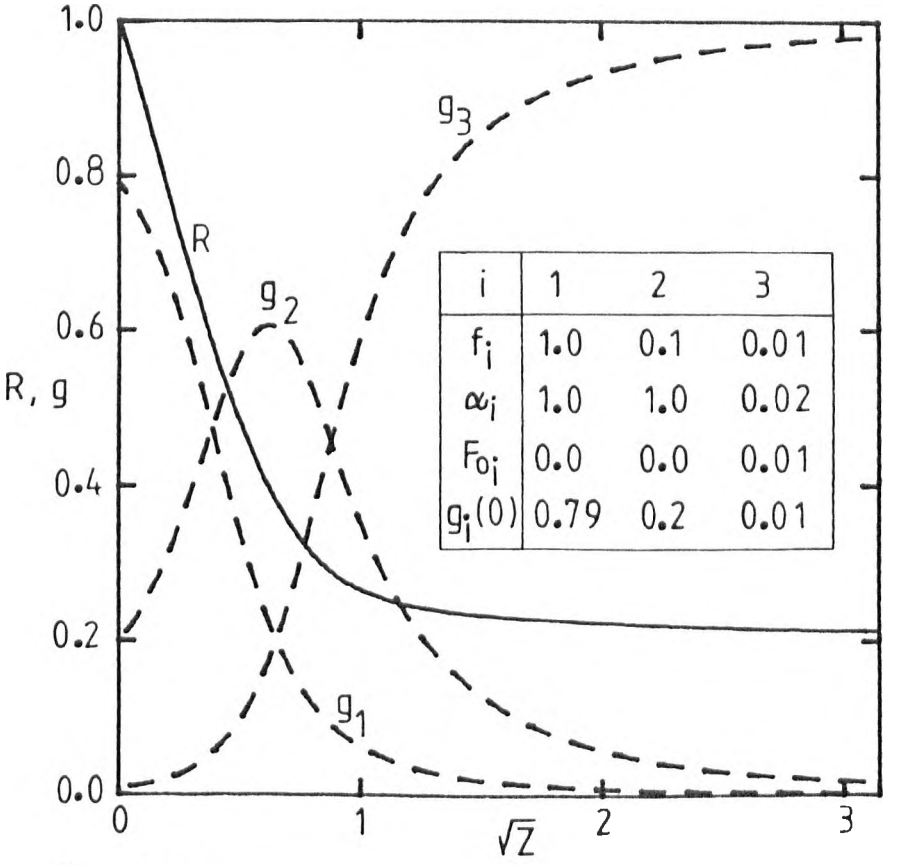

Fig 6.25

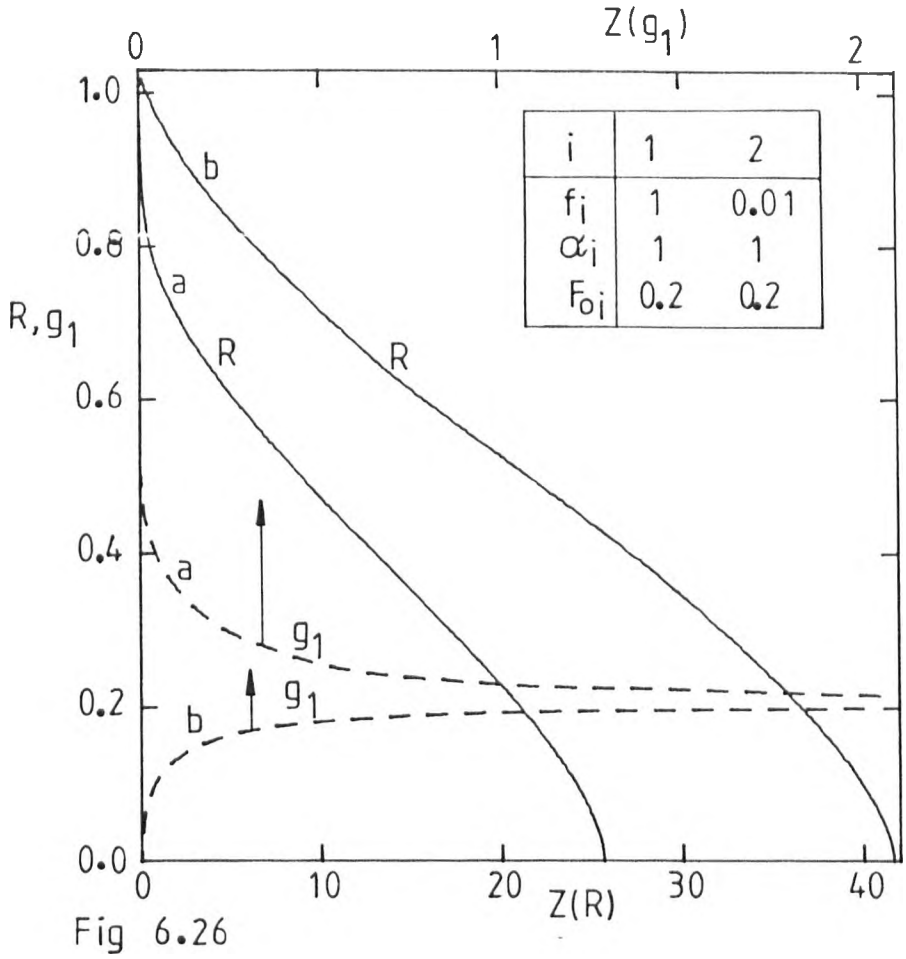

Fig 6.26

Figs 6.26 and 6.27 : Tendency to approach equilibrium gas composition during dissolution of two-component bubbles.

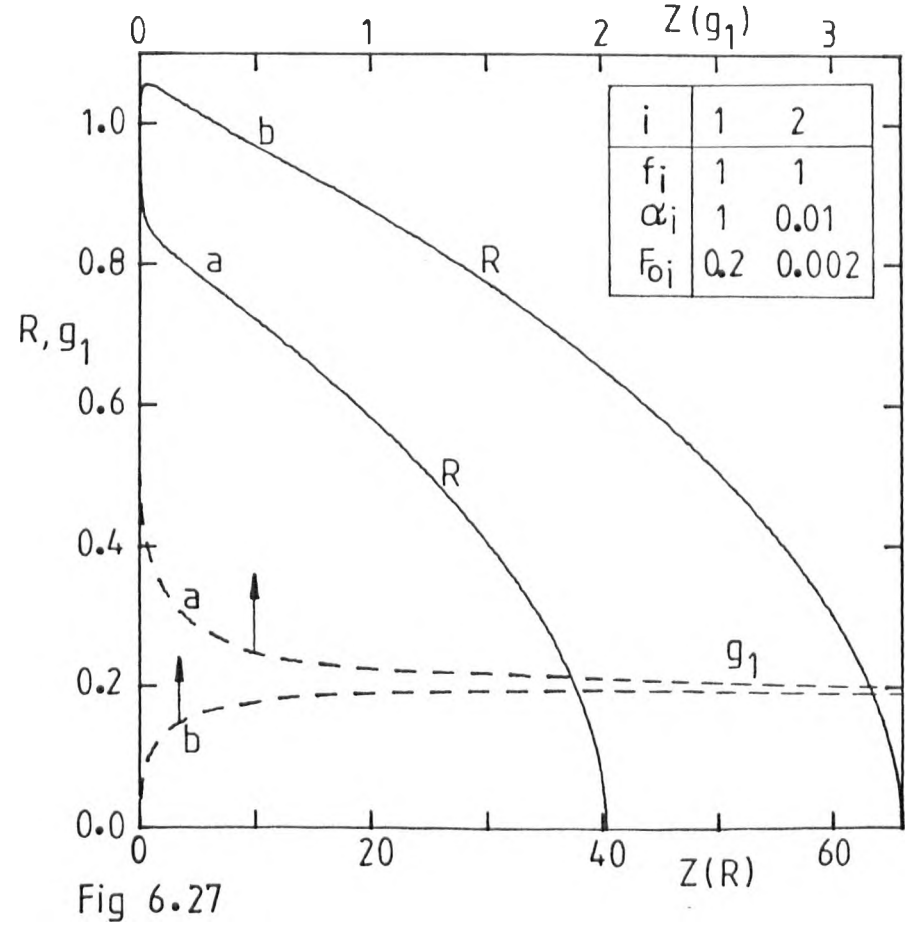

Fig 6.27

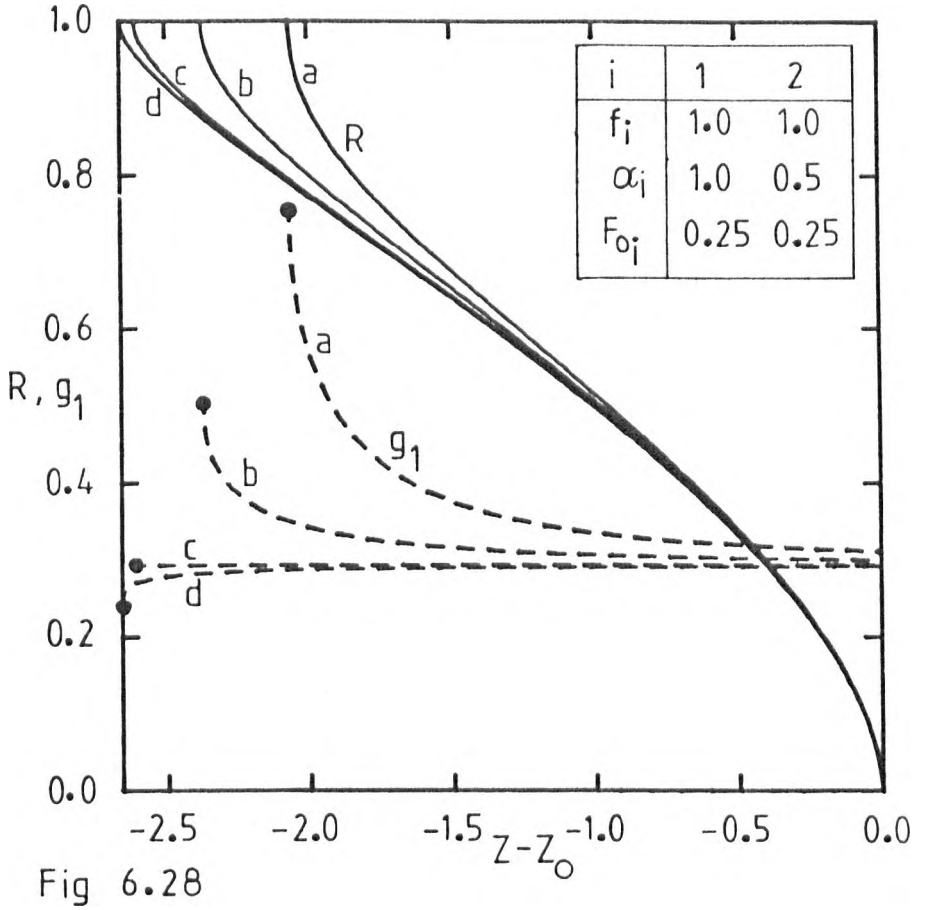

Fig 6.28

Figs 6.28 and 6.29 : Effect of the solute concentration on the tendency to approach equilibrium during dissolution of two-component bubbles.

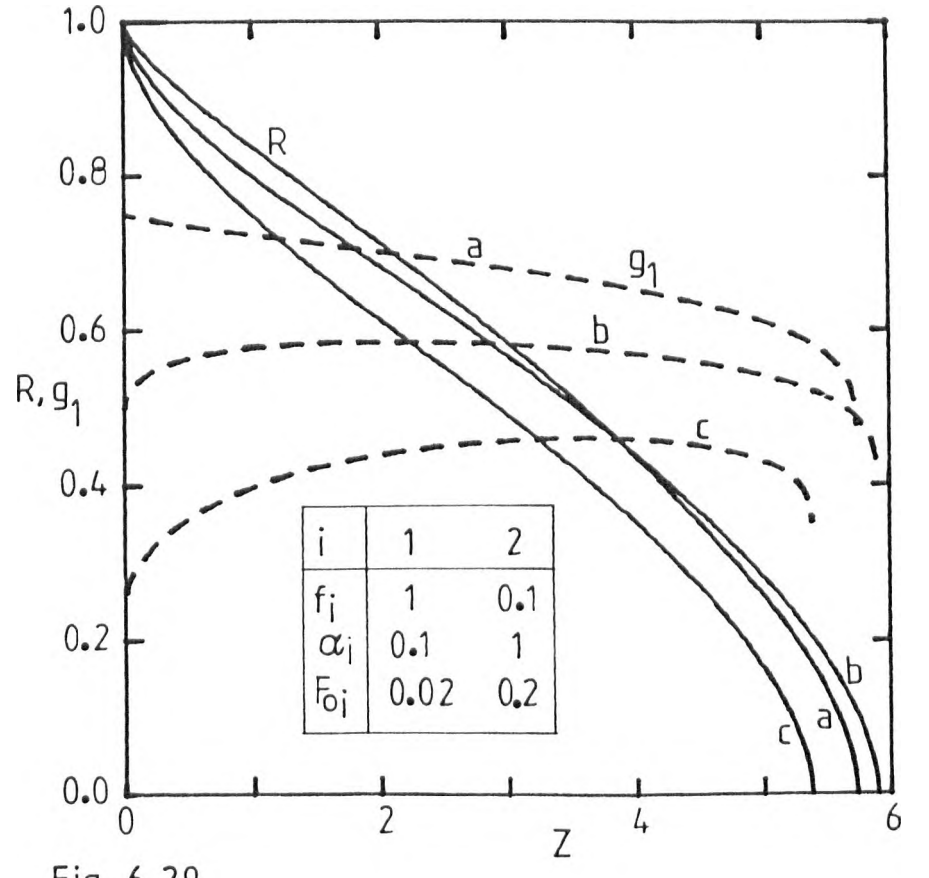

Fig 6.29

a radius R = 0.693. This radius can be taken as the beginning of the final stage.

In figure 6.25 the initial gas composition was chosen so that the composition passes through three distinct stages. Species 1 has relatively large solubility and large diffusivity so that its behaviour is initially the most important and the mole fraction decreases rapidly from an initial value of $g_1(0) = 0.79$.

At first both g_2 and g_3 increase as gas 1 dissolves rapidly but the ratio g_2/g_3 decreases continuously because species 2 has both larger diffusivity and larger solubility than species 3. Therefore g_2 peaks then progressively gives place to large mole fractions of the least soluble species.

The final stage is very slow and the bubble disappears at dimensionless time of about 220. The beginning of this stage is close to the point $R = R_i = 0.2154$ where R_i represents the residual bubble in the case of complete dissolution of gases 1 and 2 before gas 3 starts dissolving.

In some conditions the composition of dissolving bubbles can also evolve towards equilibrium. This always occurs if there is a composition at which all the "driving-forces", $F_i(R)$, vanish (figure 6.23). Other conditions can be formulated from figures 6.26 and 6.27. In both cases the bubble composition tends to a range where the "driving-force" of at least one of the gases varies rapidly with its mole fraction in the bubble. This range is close to the point $g_1 = F_{O1}/\alpha_1 = 0.2$ where $F_1(R)$ vanishes for both these figures.

The time scales used to represent the changes of mole fractions (dashed lines) were expanded to emphasize that those changes occur relatively early. In cases (a) in both figures species 1 initially dissolves at a much greater rate than species 2 causing a relatively rapid contraction of the bubble while the mole fraction g_1 decreases. Much smaller rates of dissolution of

gas 2 may be due to a small ratio of solubilities, α_2/α_1, or a small ratio of diffusivities, f_2, or both.

$F_1(R)$ drops sharply as g_1 approaches 0.2 and the product $f_2.F_2(R)$ remains relatively low. Consequently the rate of bubble contraction decreases considerably. At Z = 2 in case (a) of figure 6.26 $g_1 \simeq 0.2156$ so that

$$\frac{1}{F_1(R)} \cdot \frac{d[F_1(R,g_1)]}{dg_1} = \frac{1}{0.0156} \simeq 64 .$$

Rapid changes of gas composition are then unlikely to occur because the "driving-force" of species 1 varies rapidly with small changes of gas composition and this interdependence acts as an efficient control. Thus g_1 decreases slowly towards a minimum reaching $g_1 \simeq 0.2007$ at the end of the process. Similar arguments can be found for the remaining cases in figures 6.26 and 6.27.

As $g_1(0) = 0$ in cases (b) in figures 6.26 and 6.27, $F_1(R) < 0$ and $|f_1.F_1(R)| > f_2F_2(R)$. Thus the bubbles grow during a short initial stage while g_1 is increasing and approaches the point $g_1 = 0.2$ when $F_1(R) = 0$. By the end of the process g_1 is slightly greater than 0.2 so that $F_1(R) > 0$ and this species can redissolve.

Generally speaking, if species i has the maximum permeability among the n-components of a bubble, and species j has the lowest permeability with a large ratio between permeabilities ($\alpha_i f_i/\alpha_j f_j \gg 1$), the mole fraction of species i tends relatively rapidly to $g_i^* = F_{O_i}/\alpha_i$. If the ratio of permeabilities is close to unity, then the composition of gas may evolve to nearly equilibrium conditions provided the "driving-forces" ($F_i(R)$; i=1, ..., n) vary rapidly in that range of compositions. In practice this occurs when the "equilibrium" mole fractions $g_{i,eq}$ are close to $g_i^* = F_{O_i}/\alpha_i$ and this condition is verified when $\sum_{i=1}^{n} g_i^*$ is reasonably close to unity, (or in

some cases greater than unity).

It was shown in figure 6.23 that if $\sum_{i=1}^{n} g_i^* = 1$, $(g_i^* = F_{O_i}/\alpha_i)$, the bubble composition tends to $g_i = g_i^*$ (i=1, ..., n) and dissolution or growth stops at that point.

In figure 6.28 $g_i^* + g_2^* = 0.75$ and the tendency to approach a unique equilibrium composition is approximate but not rigorous. In this case the times of dissolution are matched to enhance the similarities between the final stages. The agreement between the different radius-time curves is even better than between the corresponding mole fraction-time curves. This is related to the fact that the "driving-force" of the major component during the final stages is similar in all cases at the moment when the bubble disappears ($F_2(R) = 0.0945$, 0.1005, 0.1035 and 0.1040 for cases (a), (b), (c) and (d) respectively). In case (c) the initial composition of gas is $g_1 = 0.295$ and its final value $g_1 = 0.293$ and the composition of the bubble varies very little during dissolution.

The components of the system illustrated in figure 6.29 have equal permeabilities, but quite different diffusivities. It has already been demonstrated that, if $g_i^* = 0$ (i=1, ..., n) (figure 6.19), these systems do not converge to "equilibrium" gas composition and significant changes of gas composition may occur during the final stage of dissolution. In the present case $g_1^* + g_2^* = 0.4$ so that the restrictions on the final composition of the gas must not be severe. However, the initial level of concentrations in the bulk liquid has some effect, especially on case (a), which does not show the usual increase of mole fraction of the less soluble component during the initial stage (compare figures 6.19 and 6.29).

6.10 Unusual concentration profiles

So far it seems that the behaviour of n-component bubbles is greatly affected by changes of gas composition and corresponding changes of concentrations of gases dissolved in the liquid at the interface. However, this crude criterion alone cannot explain some characteristics of transient behaviour. For instance $F_i(R) > 0$, (that is $C_i(a) > C_{\infty_i}$), does not ensure that species i is dissolving. Similarly species i may dissolve temporarily while $F_i(R) < 0$, but then reverse its direction of diffusion and there is no simple relation between $F_i(R)$ and the magnitude of the dimensionless material flux.

In figure 6.30a the original bubble contains a highly soluble gas (i=2) which also has lower diffusivity than species 1. For the latter reason species 1 is transferred at greater rate into the bubble than the rate of dissolution of species 2. Therefore the bubble grows from the beginning and the gas composition changes rapidly and finally levels at about $g_1 = 0.9007$. At the same time the interfacial concentrations, especially $F_2(R)$, change rapidly and the concentration profiles reflect those changes (figure 6.30b).

As the diffusivity of species 1 is much higher than that of species 2, this species diffuses relatively slowly which causes accumulation not far from the interface. The absolute numerical value of its concentration gradient $\left(\frac{\partial F_2}{\partial e}\right)_R$ at the interface decreases rapidly so that later changes of interfacial concentration ($F_2(R)$) are essentially due to a relatively rapid rate of diffusion of species 1. As the mole fraction g_2 continues to decrease $F_2(R)$ also decreases giving rise to a temporary local maximum in the curves F_2 versus $x = e/R$ (profile corresponding to R = 1.5). The numbers which denote the curves in figure 6.30b show the relevant values of the dimensionless radius R.

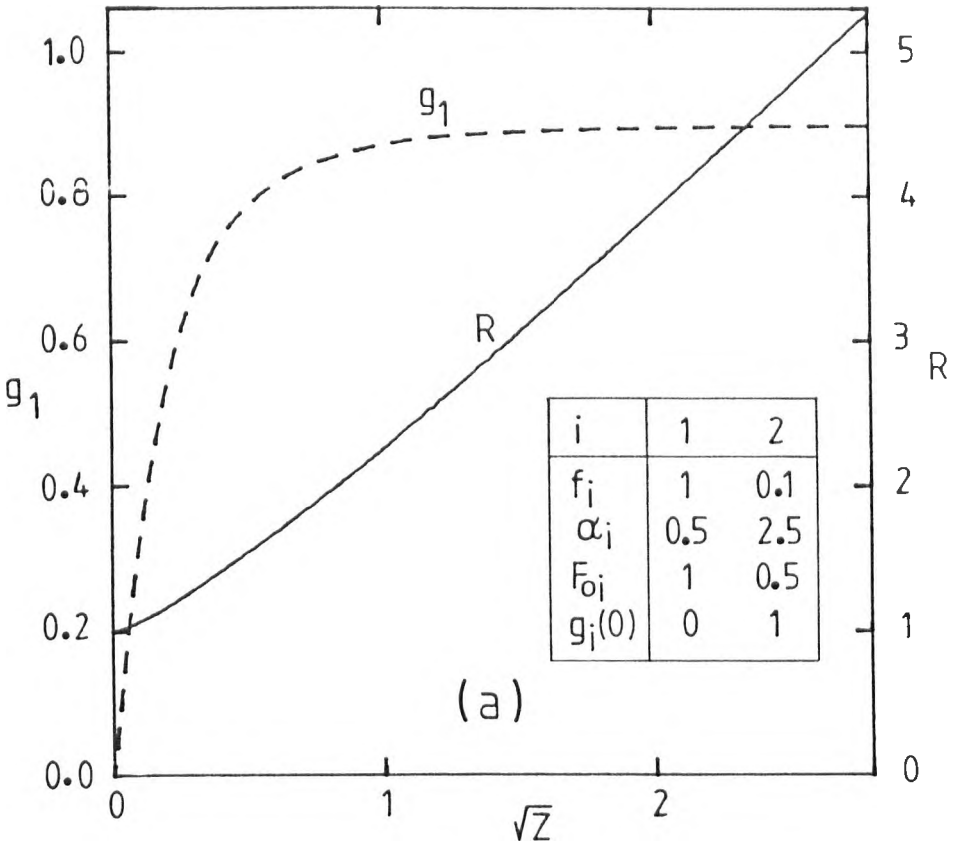

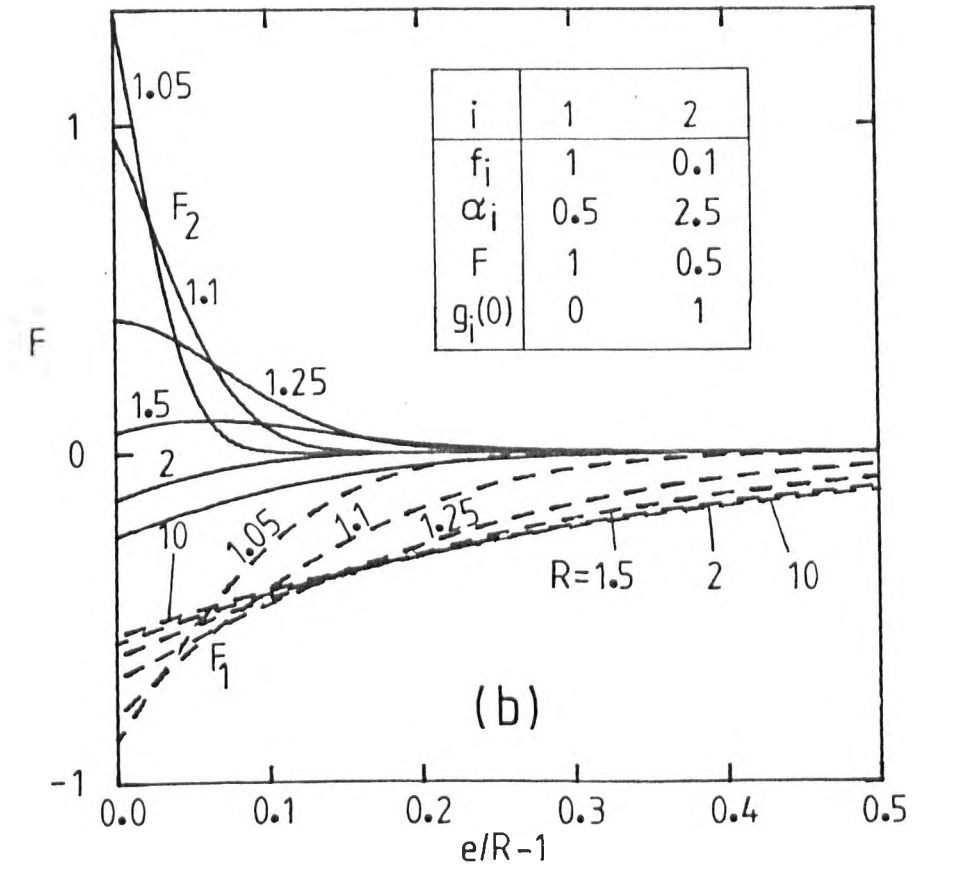

Fig 6.30 : Growth of a two-component bubble showing rapid changes of interfacial concentrations and local maxima in the concentration-distance curve for species 2 (full lines in fig 6.30b).

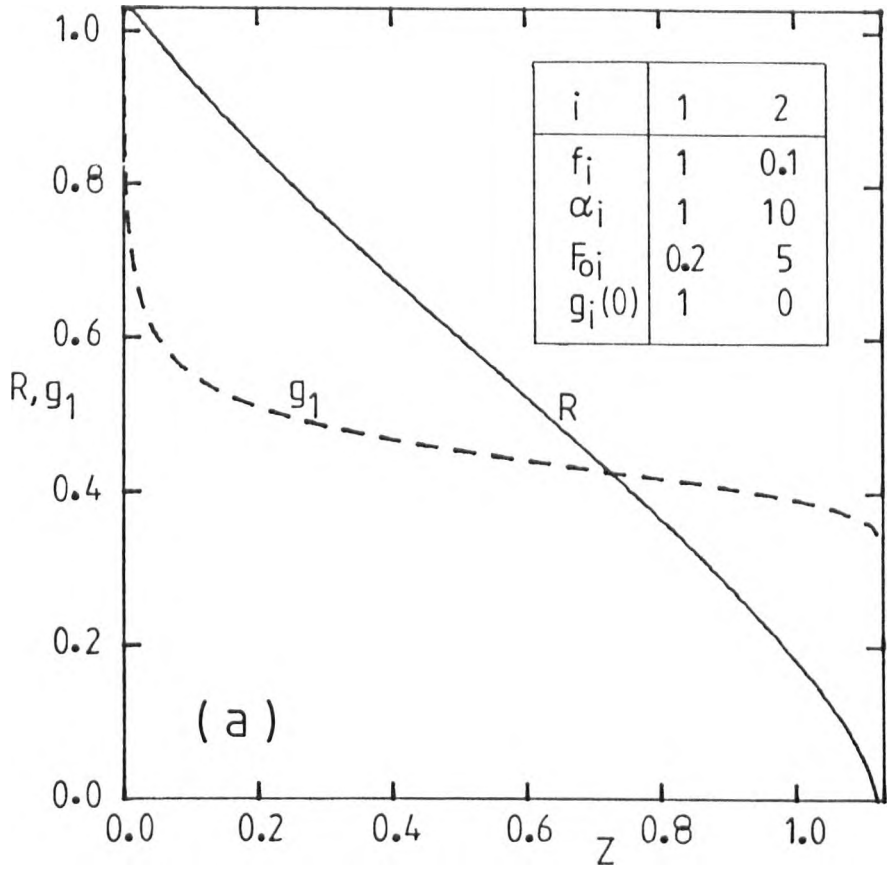

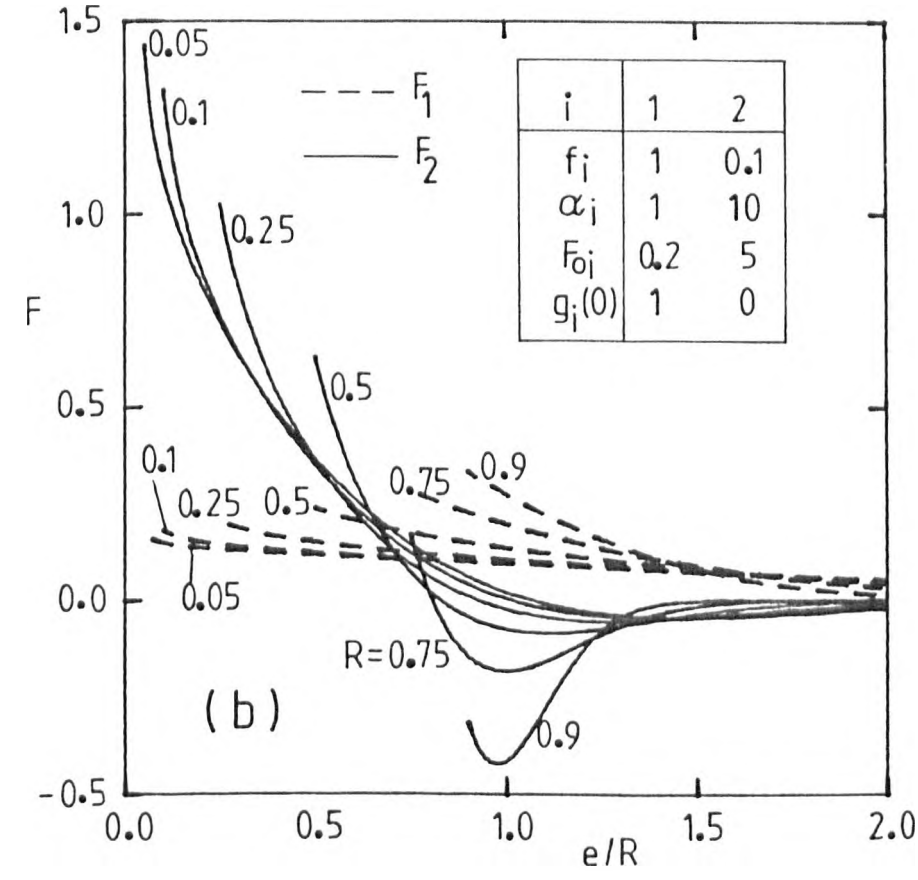

Fig 6.31 : Dissolution of a two-component bubble showing rapid changes of interfacial concentrations and local minima in the concentration-distance curve for species 2 (full lines in figure 6.31b). The numbers show the values of the dimensionless radius R.

Later the local maximum in the curve for F_2 disappears as that species diffuses away in both directions. If R > 10 the concentration profiles of both components have reached asymptotic regimes, which can also be derived from the analytical solutions of growth from zero size (equation (6.7)).

The example illustrated in figure 6.31a also shows unusual evolution of concentration profiles. Again the diffusivity of species 2 is much lower than that of the other species and $F_2(R)$ is very dependent on the gas composition. Initially the flux of the species 2 from the liquid into the bubble exceeds the dissolution rate of gas 1 which causes a rapid drop of g_1 and the initial increase of bubble size.

At $g_2 = 0.5\ F_2(R) = 0$ and one might think that the start of dissolution of species 2 began at this stage. Actually gas 2 started dissolving significantly earlier as shown in figure 6.31b. The concentration profiles shown in figure 6.31b are equivalent to R = 0.9, 0.75, 0.5, 0.25, 0.1 and 0.05. The full lines represent species 2 and the broken lines species 1. Local minima are developed in the curves F_2 against $\underline{e}$. $\left(\frac{\partial F_2}{\partial e}\right)_{e=R}$ becomes negative and therefore species 2 starts dissolving significantly before $F_2(R)$ becomes positive.

These two cases have shown the more important conditions likely to cause maxima or minima in the curves of concentrations versus distance. The interfacial concentration of the species K which shows those unusual features is very sensitive to changes of gas composition and D_K is much lower than the diffusivity of other major constituents of the bubble. Besides during an intermediate stage the changes of gas composition are due to a species other than species K, so that $F_K(R)$ will be forced to change, almost independently of the actual diffusion of species K.

These extreme examples demonstrate how inaccurate quasi steady-state or quasi-stationary multicomponent solutions can be. It was shown in

Chapters IV and V that those approximations have very limited applicability in describing the behaviour of one-component spheres. Their use with multi-component systems is based on assuming that the rate of transport of species i is directly proportional to $F_i(R)$ which may be completely wrong, and adds to the inaccuracy of those approximate one-component solutions. They will often give very inaccurate predictions, except possibly for low absolute numerical values of the "driving-forces" $F_i(R)$; i=1, ..., n.

6.11 Conclusions

Analytical solutions were derived which make it possible to predict the growth of multi-component bubbles from zero size. These solutions are only slightly more complex than equivalent one-component solutions (Scriven, 1959), and can be computed from these previously reported results. The multi-component analytical solutions demonstrate the uniqueness of asymptotic bubble composition and growth rates and growth from finite size converges relatively rapidly to that regime, regardless of the initial bubble composition. Analytical solutions for growth of multi-component bubbles are especially simple in the extreme ranges of very low and very high solubility parameters.

The role of solute concentrations is more important than that of diffusivities, that is, the behaviour of the bubble reacts more rapidly to changes of concentrations in the bulk liquid and solubilities than it reacts to changes of diffusivities. This is true both for growth and for dissolution.

Changes from bubble growth to bubble dissolution or vice versa can be simulated by properly choosing the initial bubble composition, solubilities and concentrations of solutes in the liquid medium. It is also possible to simulate the gradual evolution of bubbles to equilibrium conditions when

the bubble stops growing or dissolving as the gas composition tends to equilibrium and the "driving-forces" vanish. Some of those phenomena have been experimentally observed (Greene and Davies, 1974).

Other occasional characteristics of bubble dissolution occur when the process comes to a halt or the rate of dissolution decreases dramatically (Greene and Kitano, 1959; Nemec, 1969). It has been confirmed that these observations are likely to be due to a relatively inert species which has low solubility or relatively low diffusivity, or both.

That the finite difference method performs very well even with variable interfacial concentrations and simultaneous diffusion of more than one species was demonstrated by comparison with the above-mentioned analytical solutions. For very large increases of bubble size the asymptotic regime after growth from finite radius becomes indistinguishable from the analytically solved growth from zero. The same applies to the equilibrium composition of the bubble. The convergence of the finite difference solutions was demonstrated over a very large range of solubility parameters to prove that the method did not fail even in very extreme conditions.

CHAPTER VII

7.1 Diffusion controlled behaviour of spheres with concentration dependent diffusivity

Crank (1975) discussed some solutions of diffusion controlled processes with variable diffusivity. Philip (1966) developed series solutions for spherically symmetrical diffusion in the liquid medium surrounding a sphere of constant radius. However, these solutions cannot be generalized to growing or dissolving spheres.

The solutions presently derived refer exclusively to one-component spheres. The simultaneous diffusion of two or more species must require complex formulation due to interdependence between the diffusion of the different species. Besides, many systems are controlled by the diffusion of one species so that one-component solutions may frequently provide satisfactory predictions.

Boltzmann transformations have been successfully used to solve diffusion problems, including variable diffusivity treatments (Crank, 1975). This type of solution was also used to solve the growth of spheres from zero size and with constant diffusivity (Chapter IV and VI). In this chapter similar solutions are derived for the diffusion controlled growth of spheres with inclusion of concentration dependent diffusivity.

The finite difference method was also used to compute more general solutions (section 7.6). During growth from finite (non-zero) size the actual solutions converge to an asymptotic regime which is the same as the regime of growth from zero size. Therefore it is possible to test the convergence of the finite difference solutions by comparison with the class of exact solutions described above.

7.2 Material balances for one-component spheres

Equations (2.15) and (2.17) are valid regardless of variable diffusivity but equation (2.5) leads to

$$D(C) \cdot \left[\frac{\partial^2 C}{\partial r^2} + \frac{2}{r} \frac{\partial C}{\partial r} \right] + \left(\frac{dD}{dC} \right) \cdot \left(\frac{\partial C}{\partial r} \right)^2 - \varepsilon \left(\frac{a}{r} \right)^2 \cdot \frac{da}{dt} \frac{\partial C}{\partial r} = \frac{\partial C}{\partial t} \qquad (7.1)$$

where D is a function of the concentration C only. Equation (2.23) is also valid and can be written

$$C_s^\circ \frac{da}{dt} = D_a \left[1 - C_a \cdot v \right]^{-1} \cdot \left(\frac{\partial C}{\partial r} \right)_a \qquad (7.2)$$

where $D(C_a) = D_a$ is a constant because the interfacial solute concentration is assumed to remain constant.

Equations (7.1) and (7.2) can be made dimensionless in order to generalize the solutions and draw the main conclusions about the behaviour of these systems. Thus,

$$\hat{D}(F) \cdot \left[\frac{\partial^2 F}{\partial e^2} + \frac{2}{e} \frac{\partial F}{\partial e} \right] + \frac{d\hat{D}(F)}{dF} \cdot \left(\frac{\partial F}{\partial e} \right)^2 - \varepsilon \left(\frac{R}{e} \right)^2 \cdot \frac{dR}{dZ} \frac{\partial F}{\partial e} = \frac{\partial F}{\partial Z} \qquad (7.3)$$

$$\frac{dR}{dZ} = \left(\frac{\partial F}{\partial e} \right)_R \qquad (7.4)$$

Where e, and R have the usual meaning and

$$\hat{D} = D/D_a$$

$$Z = t \cdot D_a / a_o^2$$

$$F = (C - C_a) \; / \; [(1 - C_a \cdot v) \; C_s^\circ] \qquad (7.5)$$

7.3 Exact solutions for growth from zero size

Boltzmann transformations have frequently been used to solve diffusion controlled problems. Thus on assuming $s = r/(2\sqrt{D_a t})$ and $F(s) = F(r,t)$ also

$$\beta = a/(2\sqrt{D_a t}) = R/(2\sqrt{Z}) \tag{7.6}$$

from which it follows

$$a = 2\beta\sqrt{D_a t}\,; \quad R = 2\beta\sqrt{Z} \quad . \tag{7.7}$$

Therefore, equation (7.3) gives rise to

$$\frac{d^2F}{ds^2} = 2\frac{dF}{ds}\left[\varepsilon\beta^3/(\hat{D}s^2) - s/\hat{D} - 1/s\right] - (\hat{D})^{-1}\frac{d\hat{D}}{dF}\left(\frac{dF}{ds}\right)^2 \quad . \tag{7.8}$$

Also from equations (7.4) and (7.7)

$$\frac{dR}{dZ} = \frac{\beta}{\sqrt{Z}} = \frac{1}{2\sqrt{Z}}\left(\frac{dF}{ds}\right)_{s=\beta} \tag{7.9}$$

or, after rearranging,

$$\left(\frac{dF}{ds}\right)_{\beta} = 2\beta \quad . \tag{7.10}$$

The remaining boundary conditions (equations (2.26)) become

$$F(\infty) = \phi = (C_\infty - C_a)/[(1 - C_a.v)C_s^\circ] \tag{7.11}$$

$$F(\beta) = 0 \quad .$$

The functions $\hat{D}(F)$ and $\frac{d\hat{D}(F)}{DF}$ may assume explicit analytical forms or may be defined by a set of n discrete points $(F_i; \hat{D}_i)$; i=1, ..., n. In any case equation (7.8) must be solved numerically by decomposition into a system of simultaneous ordinary differential equations.

$$\frac{dT}{ds} = 2T\left[\varepsilon\beta^3/(s^2\hat{D}) - s/\hat{D} - 1/s \right] - (\hat{D})^{-1} \frac{d\hat{D}}{dF} T^2 \qquad (7.12)$$

$$\frac{dF}{ds} = T \qquad (7.13)$$

and from equation (7.10)

$$T(\beta) = 2\beta \, . \qquad (7.14)$$

Thus the variable T decreases from 2β to zero at $s=\infty$. This range is very useful in the selection of variable mesh sizes for numerical solution of equations (7.12) and (7.13). Besides the condition $T(\infty) = 0$ can be used to stop the integration at a specified value; that used here was

$$T < 10^{-5}.(2\beta) \, , \qquad (7.15)$$

with negligible errors involved in the final estimate of $\phi = F(\infty)$.

On specifying the solubility parameter ϕ the actual system reduces to a boundary value problem. On the contrary if the growth constant β is specified the problem is of the initial value type, which is much simpler to solve. Fourth-order Runge-Kutta techniques were used to obtain the solutions $\phi(\beta,\varepsilon)$ for the required functions $\hat{D}(F)$ (see appendix 5).

7.4 Quasi steady-state approximations

It was shown in Chapters IV and V that dissolution or growth with low $|\phi|$ always tends to quasi steady-state approximations. If the diffusivity depends on concentration the quasi steady-state simplification of equation (7.3) is

$$\frac{\partial}{\partial e}\left[e^2 . \hat{D}(F) . \frac{\partial F}{\partial e} \right] = 0 \tag{7.16}$$

or

$$e^2 . \hat{D}(F) . \frac{\partial F}{\partial e} = C_1 \cdot \tag{7.17}$$

The constant C_1 must be evaluated by integration of equation (7.17) with boundary conditions

$$F(R) = 0$$

$$F(\infty) = \phi \cdot$$

That is

$$\int_0^{F(e)} \hat{D}(F)\ dF = C_1\left(\frac{1}{R} - \frac{1}{e}\right) \tag{7.18}$$

and

$$\int_0^{\phi} \hat{D}(F)\ dF = \phi\ \hat{D}_{av} = C_1/R \tag{7.19}$$

from which it follows that

$$C_1 = R\ \phi\ \hat{D}_{av} \tag{7.20}$$

$\hat{D}_{av}$ being the average dimensionless diffusivity.

From equations (7.17) and (7.20)

$$\left(\frac{\partial F}{\partial e}\right)_R = \hat{D}_{av}\,\phi/R \tag{7.21}$$

where, by definition, $\hat{D}(O) = 1$ (at the interface). In addition, from equations (7.18) and (7.20)

$$\int_O^{F(e/R)} \hat{D}(F)\,dF = \phi\,\hat{D}_{av}\left(1 - \frac{R}{e}\right) \tag{7.22}$$

and the corresponding constant property solution ($\hat{D} = 1$), is

$$\int_O^{F(e/R)} dF = \phi\left(1 - \frac{R}{e}\right).$$

The rate of the process can be obtained by combining equations (7.4) and (7.21), so that

$$\frac{dR}{dZ} = \hat{D}_{av}\,\phi/R\,, \tag{7.23}$$

and by integration from $Z = O$; $R = 1$

$$R^2 = 1 + 2\,\hat{D}_{av}\,\phi\,Z\,, \tag{7.24}$$

and if $\phi > O$ and $R >> 1$

$$\beta = R/2\sqrt{Z} = [\phi\,\hat{D}_{av}/2]^{\frac{1}{2}}\,. \tag{7.25}$$

7.5 Average diffusivity and its relation to equivalent constant property solutions

Assuming that the actual solutions are accurately predicted by equivalent constant property solutions with equivalent diffusivity D_{eq}

$$Z' = t \cdot D_{eq}/a_o^2 = \hat{D}_{eq} \cdot Z, \tag{7.26}$$

where $\hat{D}_{eq} = D_{eq}/D_a$

so that the time scale is affected by a factor $\hat{D}_{eq}$. Thus the dimensionless time required for complete dissolution is

$$Z_d = Z_o/\hat{D}_{eq} , \tag{7.27}$$

where Z_o is the constant property solution (Chapter V). Also if β_o is the constant property value of the growth constant (Chapter IV) and β the actual solution

$$\beta_o = a/2\sqrt{D_{eq}\, t)} = \frac{a}{2\sqrt{D_a \cdot t}} \cdot \left(\frac{D_a}{D_{eq}}\right)^{\frac{1}{2}} = \beta/(\hat{D}_{eq})^{\frac{1}{2}} . \tag{7.28}$$

From equation (7.24) it is easily recognized that in the case of quasi steady-state approximations the general law which describes growth or dissolution is only affected by a change of time scale, and the equivalent diffusivity is exactly equal to the average diffusivity

$$\hat{D}_{av} = \phi^{-1} \cdot \int_0^{\phi} \hat{D}\, dF . \tag{7.29}$$

7.6 Finite difference method for concentration dependent diffusivity problems

The coefficients $\hat{D}(F)$ and $\frac{d\hat{D}}{dF}$ in equation (7.3) make the finite difference solution somewhat more complex and more likely to become unstable if the diffusivity varies rapidly with concentration. Iterative schemes to correct $\hat{D}(F)$ and $\frac{d\hat{D}}{dF}$ were found to cause instabilities even when implicit finite difference methods were used to calculate the concentration profiles. Usually these instabilities can be avoided if the discrete values $[\hat{D}(F)]_\ell$ and $\left[\frac{d\hat{D}}{dF}\right]_\ell$ at time step ℓ are used to calculate the concentration profile at time step $\ell+1$, without iterative procedure, but these solutions also fail for very large absolute numerical values of the derivative $\left(\frac{d\hat{D}}{dF}\right)$, especially near the interface. For the general case stability is achieved by inclusion of the coefficient $[\hat{D}(F)]_{\ell+1}$ in the implicit scheme used to calculate step $\ell+1$.

It will be shown that the actual class of solutions with concentration dependent diffusivity are similar to the equivalent constant property solutions provided a suitable equivalent diffusivity is taken into account. Therefore the arguments found to justify the transformation $x = e/R$ used in Chapter III are also valid in the present conditions and equation (7.3) becomes

$$\hat{D}(F)\left(\frac{\partial^2 F}{\partial x^2}\right) + \frac{2\hat{D}(F)}{x}\left(\frac{\partial F}{\partial x}\right) + \left(\frac{d\hat{D}}{dF}\right)\left(\frac{\partial F}{\partial x}\right)^2 + R\left(\frac{dR}{dZ}\right)(x - \varepsilon x^{-2})\left(\frac{\partial F}{\partial x}\right) = R^2\left(\frac{\partial F}{\partial Z}\right) . \quad (7.30)$$

This equation is then replaced by the finite difference equation (7.31)

$$\frac{1}{2}\hat{D}_\ell\left[\left(\frac{\partial^2 F}{\partial x^2}\right)_{\ell+1} + \frac{2}{x}\left(\frac{\partial F}{\partial x}\right)_{\ell+1}\right] + \frac{1}{2}\left[\left(\frac{\partial^2 F}{\partial x^2}\right)_\ell + \frac{2}{x}\left(\frac{\partial F}{\partial x}\right)_\ell\right]\hat{D}_{\ell+1} + \left(\frac{d\hat{D}}{dF}\right)_\ell \cdot \left(\frac{\partial F}{\partial x}\right)_\ell \cdot \left(\frac{\partial F}{\partial x}\right)_{\ell+1}$$

$$+ \frac{1}{2} R_{av}\left(\frac{dR}{dZ}\right)_{av} \cdot (x - \varepsilon x^{-2})\left[\left(\frac{\partial F}{\partial x}\right)_\ell + \left(\frac{\partial F}{\partial x}\right)_{\ell+1}\right] = (R^2)_{av} \cdot \left(\frac{\partial F}{\partial Z}\right) \quad (7.31)$$

where the space and time derivatives assume the finite difference forms derived in Chapter III.

As the amplitude of time intervals is controlled (see Chapter III) the changes of concentration at a space mesh point j and per time step are relatively small so that the derivative $\left(\frac{\partial \hat{D}}{\partial F}\right)_{\ell}$ is used as an explicit factor to integrate from time step ℓ to step $\ell+1$, and

$$\hat{D}_{\ell+1} = \hat{D}_{\ell} + \left(\frac{d\hat{D}}{dF}\right)_{\ell} \left(F_{\ell+1} - F_{\ell}\right) . \qquad (7.32)$$

Therefore $\hat{D}_{\ell+1}$ also assumes the form of a linear term which is required for inclusion in the implicit finite difference scheme.

This method resolves the instabilities which might develop when $\hat{D}_{\ell+1}$ is not included as an implicit term and provides a way of using an approximate average between steps ℓ and $\ell+1$. The accuracy of this technique is again confirmed by comparing with the class of exact solutions for growth derived in section 7.3.

If the diffusivity is strongly dependent on the concentration of solute the concentration profiles will be markedly affected and concentration gradients may vary rapidly with distance. This trend occurs if $\left|\frac{d\hat{D}}{dF}\right|$ is very large, especially near the interface. Besides, in the present conditions the concentration gradient at the interface must be estimated from discrete space mesh points close to the interface. Both trends require smaller space mesh sizes than for the constant diffusivity case. However, these effects do not affect most of the results reported in this chapter, and only for $\left|\frac{d\hat{D}}{dF}\right| > 100$ it is necessary to use more than 150 space mesh points. The most severe cases included in this chapter were $|\phi| = 0.001$ and $\hat{D} = (1 + 10 \cdot (F/\phi))$ where $\left|\frac{d\hat{D}}{dF}\right| = 10^4$ and convergence of the finite difference solutions then did require less than 300 space mesh points.

7.7 Growth from zero size

A polynomial $\hat{D}(F)$ function was chosen to illustrate the effect of concentration dependent diffusivity, such that

$$\hat{D}(F) = 1 + d_1 \cdot F + d_2 \cdot F^2 \qquad (7.33)$$

where d_1 and d_2 are constant. All the examples reported in this chapter refer to $\varepsilon = 1$, which is the case with gas bubbles. Values of growth constant β, solubility parameter, ϕ, and constants d_1 and d_2 were used to solve equations (7.12) and (7.13) with the proper initial conditions (7.11) and (7.14).

The characteristic law $R \propto \sqrt{Z}$ which describes the asymptotic regime of growth is valid regardless of the relation between the diffusivity and concentration of solute. Only the growth constant $\beta = R/(2\sqrt{Z})$ is dependent on the actual functional form $\hat{D}(F)$ and it is useful to relate the equivalent dimensionless diffusivity $\hat{D}_{eq}$ (equation (7.28)) to the average diffusivity $\hat{D}_{av}$ (equation (7.29)).

Figures 7.1 and 7.2 show systematic differences between $(\hat{D}_{eq})^{\frac{1}{2}} = \beta/\beta_o$ and $(\hat{D}_{av})^{\frac{1}{2}}$, where β_o represents the constant property solution (for the case $\hat{D} = 1$). The values of β_o obtained by numerical solution of equation (7.8) are the same as Scriven's solutions (1959). The differences between $\hat{D}_{eq}$ and $\hat{D}_{av}$ increase as either d_1 or d_2 (or both) increases.

A summary of results is also shown in table 7.1 where β_1 is the actual growth constant for the case $\phi = 1$, $\varepsilon = 1$, while $\beta_o = 1.320$ is the corresponding constant property solution. The differences between $(\hat{D}_{eq})^{\frac{1}{2}} = \beta_1/\beta_o$ and $(\hat{D}_{av})^{\frac{1}{2}}$ can be as large as 19% of β_1/β_o in case 16, that is when the changes of diffusivity are maximum. The agreement between $\hat{D}_{eq}$ and $\hat{D}_{av}$ is better when $\hat{D}(F)$ is a linear function of F than when $\hat{D}(F) - 1 \propto F^2$. This

conclusion is easily drawn by analysis of growth constants for the set of cases 3, 11, 12 and 13 or the set 5, 14, 15 and 16.

Figure 7.3 illustrates the concentration profiles corresponding to cases 3, 11, 12 and 13 of table 7.1. The dashed line represents the constant property solution, and is clearly distinguished from any of the variable diffusivity cases which tend to show steeper profiles near the interface, but also lower concentration gradients in the tail of the profile where the diffusivity approaches a maximum. At the interface all these variable diffusivity cases have similar concentration gradients, but every functional form $\hat{D}(F)$ gives rise to a different shape of concentration profile. These conclusions are confirmed in figure 7.4 which illustrates the cases 5, 14, 15 and 16 of table 7.1, but the differences between these profiles are greater than in figure 7.3, because the changes of diffusivity throughout the diffusion fields are greater in the cases 5, 14, 15 and 16 than in the other set of cases 3, 11, 12 and 13.

The quasi steady-state approximations have suggested that in the range of very low solubility parameters $\hat{D}_{eq} = \hat{D}_{av}$, and therefore $\beta/\beta_o = (\hat{D}_{av})^{\frac{1}{2}}$. This trend is confirmed in table 7.2 with a reference constant property solution $\phi(\beta;\varepsilon) = \phi(0.01;1) = 1.965 \times 10^{-4}$ and a general relation $\hat{D}(F) = 1 + d \cdot F$. The reference growth constant is $\beta_o = 0.01$ and the remaining values are $\beta = \beta_o \sqrt{\hat{D}'_{av}}$ where $\hat{D}'_{av} = [1 + 1.965 \times 10^{-4}.d/2]$ is the average dimensionless diffusivity in the range $0 \leqslant F \leqslant 1.965 \times 10^{-4}$. If the agreement between the equivalent diffusivity $\hat{D}_{eq}$ and the actual average diffusivity $\hat{D}_{av}$, is exact then $\hat{D}_{av} = \hat{D}_{eq} = (\beta/\beta_o)^2 = \hat{D}'_{av}$ and all the predictions of solubility parameter ϕ must be equal. These conditions are almost fulfilled and the actual solutions of ϕ (equation (7.8)) are close to the quasi steady-state predictions $\phi_{ss} = 2\beta^2/\hat{D}_{av}$ (equation (7.25)).

Table : 7.1

Comparison between exact solutions of growth with variable diffusivity ($\hat{D}=1+a_1F+a_2F^2$), and constant property solutions with average diffusivity (equation (7.29)).

case	a_1	a_2	β_1	β_1/β_o	$(\hat{D}_{av})^{\frac{1}{2}}$
1	0.5	0	1.449	1.098	1.118
2	1	0	1.565	1.185	1.225
3	2	0	1.771	1.341	1.414
4	5	0	2.298	1.741	1.871
5	10	0	2.957	2.240	2.449
6	0	0.5	1.401	1.061	1.080
7	0	1	1.470	1.113	1.155
8	0	2	1.605	1.216	1.291
9	0	5	2.052	1.554	1.633
10	0	10	2.422	1.835	2.082
11	1	1.5	1.749	1.325	1.414
12	0	3	1.723	1.305	1.414
13	-1	4.5	1.699	1.287	1.414
14	5	7.5	2.881	2.182	2.449
15	0	15	2.802	2.122	2.449
16	-5	22.5	2.718	2.059	2.449
17	-0.2	0	1.263	0.958	0.949
18	-0.5	0	1.177	0.892	0.866

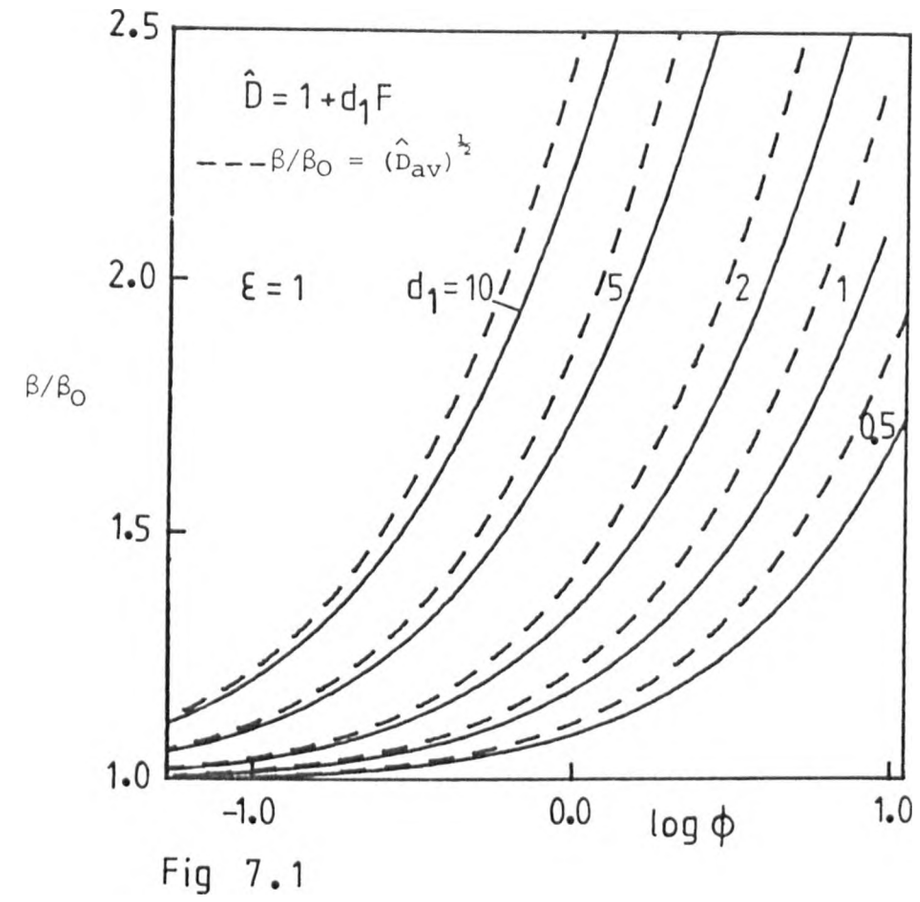

Fig 7.1

Figs 7.1 and 7.2 : Effect of concentration dependent diffusivity on the growth constant β. The dashed lines represent $\beta/\beta_0 = (\hat{D}_{av})^{\frac{1}{2}}$.

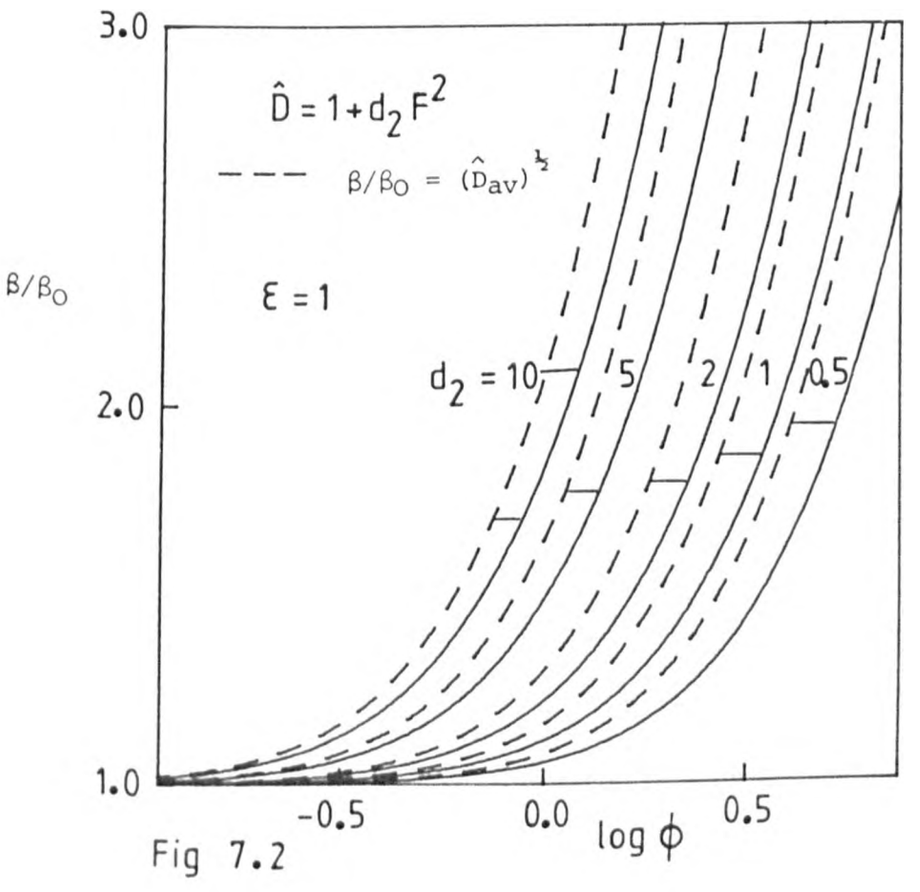

Fig 7.2

Table 7.2

Agreement between the average diffusivity and the equivalent diffusivity for low ϕ.

$10^{-4}.d$	$10^{2}.\beta = (\hat{D}_{eq})^{\frac{1}{2}}$	$10^{4}.\phi$	$(\hat{D}_{eq})^{\frac{1}{2}}$	$10^{4}.\phi_{ss}$
-0.25	0.8686	1.965	0.8686	2.000
0	1	1.965	1	2.000
1	1.4080	1.969	1.409	1.998
2	1.7219	1.969	1.723	1.997
5	2.4316	1.969	2.434	1.996
10	3.2901	1.970	3.294	1.995

7.8 Finite difference solutions for finite initial size

7.8.1 Growth

The modifications of the finite difference method which are required to solve diffusion controlled growth or dissolution of spheres with concentration dependent diffusivity were described in section 7.6. This technique was used to compute (R,Z) data which were inserted into equation (7.7) to confirm the convergence towards the asymptotic regime. For $R \geq 100$ the numerical predictions $\beta_n = R/(2\sqrt{Z})$ remain constant until at least the fourth significant figure and computations were carried out up to $R = 10^5$, that is when the radius had increased by a factor of 10^5. This large increase in size clearly demonstrates that there is no change in the growth law for $R \geq 100$, ($R = 2\,\beta_n\sqrt{Z}$).

The numerical predictions of growth constant β_n were then put into equation (7.12) with the proper function $\hat{D}(F)$ to recover the equivalent "analytical" values of the solubility parameter, ϕ_a. The agreement between the finite difference predictions and the "analytical" solutions is then

Table : 7.3

Comparison between finite difference predictions for $R \gg 100$ and the equivalent exact solutions. ($\hat{D}=1+\dot{d}'(F/\phi)$).

ϕ	0.01		0.1		1		10		100	
$\dot{d}'$	β	ϕ_a	β	ϕ_a	β	ϕ_a	β	ϕ_a	β	ϕ_a
-0.8	0.0593	0.01000	0.2186	0.1002	1.080	1.000	8.50	10.00	82.2	100.1
-0.5	0.0658	0.01002	0.2406	0.1001	1.177	1.001	9.19	10.01	88.7	100.1
-0.25	0.0707	0.01001	0.2577	0.1002	1.253	1.001	9.71	10.00	93.6	100.1
0.5	0.0840	0.01003	0.3031	0.1001	1.448	1.001	11.12	10.02	106.7	100.0
1	0.0918	0.01003	0.3304	0.1002	1.567	1.002	11.93	10.01	114.5	100.1
2	0.1057	0.01002	0.3787	0.1002	1.777	1.002	13.41	10.01	128.8	100.2
5	0.1393	0.01001	0.4965	0.1003	2.294	1.001	17.10	10.01	163.4	100.1
7.5	0.1619	0.01000	0.578	0.1000	2.650	1.001	19.65	10.01	187.4	100.0
10	0.1819	0.01000	0.646	0.1001	2.969	1.001	21.93	10.01	209.1	100.3
0	0.0753	0.01000	0.2734	0.1000	1.320	1.001	10.20	10.01	98.2	100.1

Table : 7.4

Comparison between finite difference predictions for $R \gg 100$ and the equivalent exact solutions, $[\hat{D} = 1 + d''(F/\phi)^2]$.

ϕ	0.01		0.1		1		10		100	
d''	β	ϕ_a	β	ϕ_a	β	ϕ_a	β	ϕ_a	β	ϕ_a
-0.8	0.0655	0.01000	0.2407	0.1001	1.183	1.000	9.27	10.00	89.5	100.0
-0.5	0.0693	0.01000	0.2537	0.1003	1.237	1.001	9.66	10.03	93.2	100.2
-0.25	0.0724	0.01001	0.2638	0.1002	1.281	1.003	9.95	10.03	95.7	100.1
0.5	0.0810	0.01001	0.2927	0.1003	1.400	1.003	10.71	10.01	103.0	100.1
1	0.0864	0.01002	0.3103	0.1002	1.471	1.003	11.21	10.03	107.7	100.3
2	0.0962	0.01002	0.3433	0.1002	1.605	1.002	12.10	10.03	115.9	100.3
5	0.1211	0.01002	0.4276	0.1002	1.951	1.002	14.38	10.03	137.1	100.3
7.5	0.1386	0.01002	0.4871	0.1002	2.198	1.002	16.01	10.03	152.3	100.3
10	0.1543	0.01003	0.540	0.1002	2.417	1.001	17.45	10.01	165.6	100.1
0	0.0753	0.01000	0.2734	0.1000	1.320	1.001	10.20	10.01	98.2	100.1

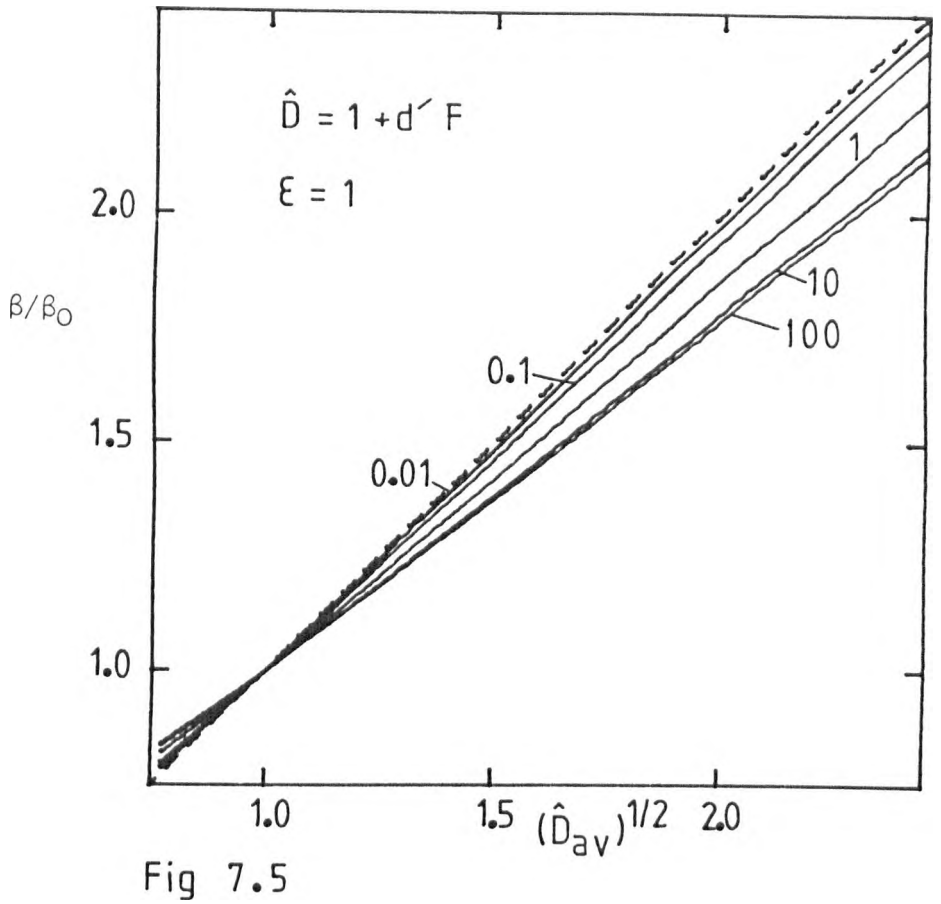

Fig 7.5

Figs 7.5 and 7.6 : Effect of concentration dependent diffusivity on the ratio of the growth constant β for the variable diffusivity problem to the corresponding constant property value β_0. The dashed lines represent the quasi steady-state approximation $\beta/\beta_O = (\hat{D}_{av})^{\frac{1}{2}}$. The numbers show the values of ϕ.

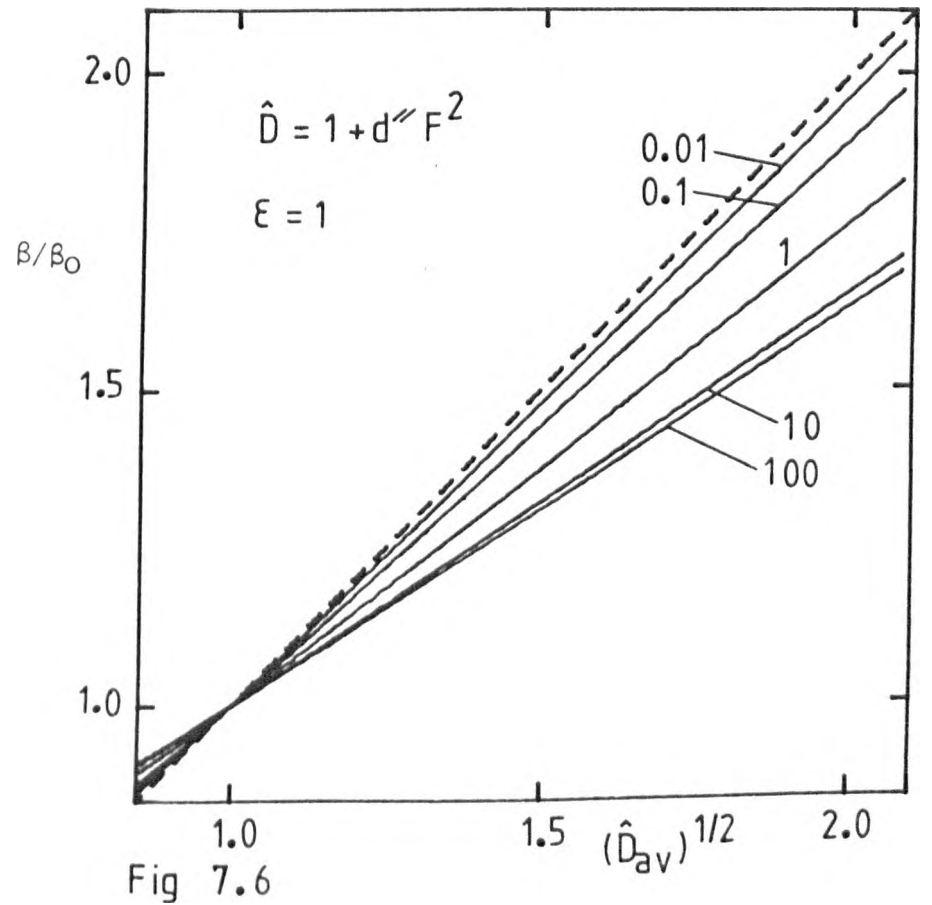

Fig 7.6

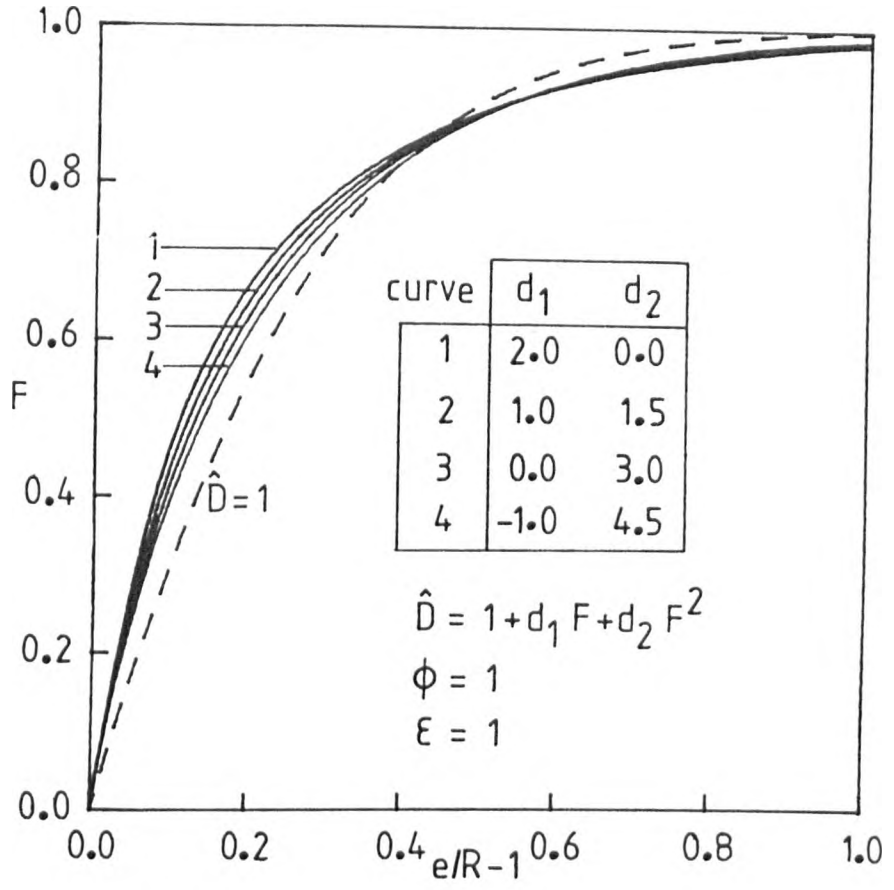

Fig 7.3

Figs 7.3 and 7.4 : Effect of concentration dependent diffusivity on the concentration profiles for growth from zero size.

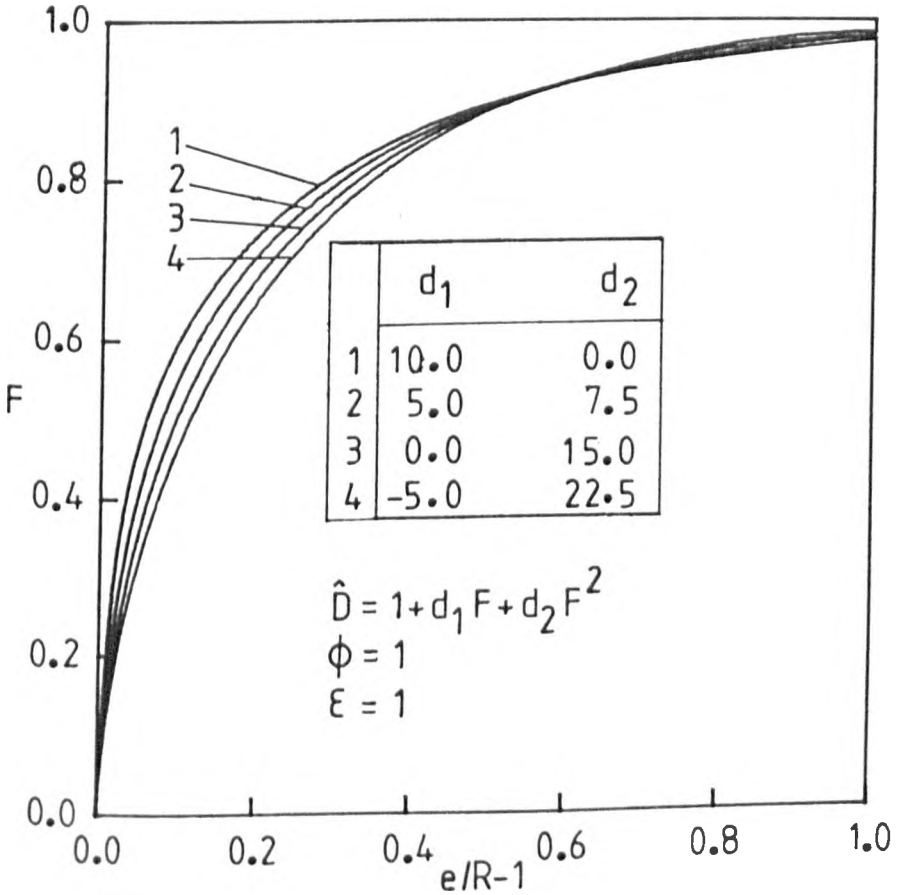

Fig 7.4

easily recognized by comparing the original ϕ values and the derived equivalent values of ϕ_a (see tables 7.3 and 7.4).

The relations between the diffusivity and concentration of solute used in tables 7.3 and 7.4 were

$$\hat{D}(F) = 1 + d' \ (F/\phi) \tag{7.34}$$

and

$$\hat{D}(F) = 1 + d'' \ (F/\phi)^2 \tag{7.35}$$

so that the average dimensionless diffusivity is $\hat{D}_{av} = (1 + d'/2)$ in table 7.3 and $\hat{D}_{av} = (1 + d''/3)$ in table 7.4.

The numerical predictions shown in tables 7.3 and 7.4 were also represented in figures 7.5 and 7.6 to investigate the relation between the equivalent diffusivity, $\hat{D}_{eq} = (\beta/\beta_o)^2$, and the average diffusivity $\hat{D}_{av}$. These results show that $\hat{D}_{eq}$ is close to $\hat{D}_{av}$ for very small values of the solubility parameter ϕ but the differences increase with ϕ and are greater when the diffusivity increases with the square concentration F^2, than when the diffusivity increases with F. In addition the ratios β/β_o between the growth constants for the variable diffusivity case, β, and for the constant property case, β_o, are nearly proportional to the square root of the average dimensionless diffusivity $\hat{D}_{av}$, that is

$$\beta/\beta_o \simeq 1 + S[(\hat{D}_{av})^{\frac{1}{2}} - 1] \ . \tag{7.36}$$

If the diffusivity increases with increasing concentration of solute the minimum value of diffusivity occurs at the interface where the diffusion transport is most important. This might explain why the equivalent diffusivity is lower than the average diffusivity and therefore $\beta/\beta_o = (\hat{D}_{eq})^{\frac{1}{2}} < (\hat{D}_{av})^{\frac{1}{2}}$.

The opposite trend occurs if $\hat{D}(F)$ decreases with increasing F because the diffusivity at the interface is then greater than the average diffusivity. In this case the growth rates for the variable diffusivity problem are always greater than the growth rates for the equivalent constant property problem with the same average diffusivity, that is $\beta/\beta_o > (\hat{D}_{av})^{\frac{1}{2}}$.

7.8.2 Transient regime of growth from finite size

In figures 7.7 and 7.8 the use of the equivalent dimensionless time $Z \cdot \hat{D}_{eq}$ where $\hat{D}_{eq} = (\beta/\beta_o)^2$ (equation (7.28)) makes the representation of the initial stages of growth from finite size almost independent of the actual relation between the diffusivity and concentration of solute. In those figures the full lines represent the solutions for the relation $\hat{D} = [1 + 10 \cdot (F/\phi)]$ and the dashed lines $\hat{D} = [1 - 0.8 \cdot (F/\phi)]$. All the remaining solutions for $\hat{D} = [1 + d' \cdot (F/\phi)]$ with $-0.8 < d' < 10$ lay in between the limiting full and dashed lines shown in figures 7.7 and 7.8, that is, they are nearly indistinguishable. Note that this also includes the constant property case $d' = 0$. Therefore growth is characterized by specifying the equivalent diffusivity and the solubility parameter and the actual solutions for the variable diffusivity cases can be worked out from constant property solutions. From the radius-time relation alone it will be impossible to show whether the diffusivity is nearly constant or varies rapidly with the concentration of solute. These conclusions apply to other functional forms of $\hat{D}(F)$, namely equation (7.35).

Unfortunately the equivalent diffusivity is not the same as the average diffusivity but the relations between $(\hat{D}_{eq})^{\frac{1}{2}}$ and $(\hat{D}_{av})^{\frac{1}{2}}$ are frequently nearly linear over significantly large ranges of values of $\hat{D}_{av}$. Therefore, very few points are needed to obtain accurate relations between $(\hat{D}_{eq})^{\frac{1}{2}}$ and $(\hat{D}_{av})^{\frac{1}{2}}$ from which all the intermediate variable diffusivity solutions may be worked out.

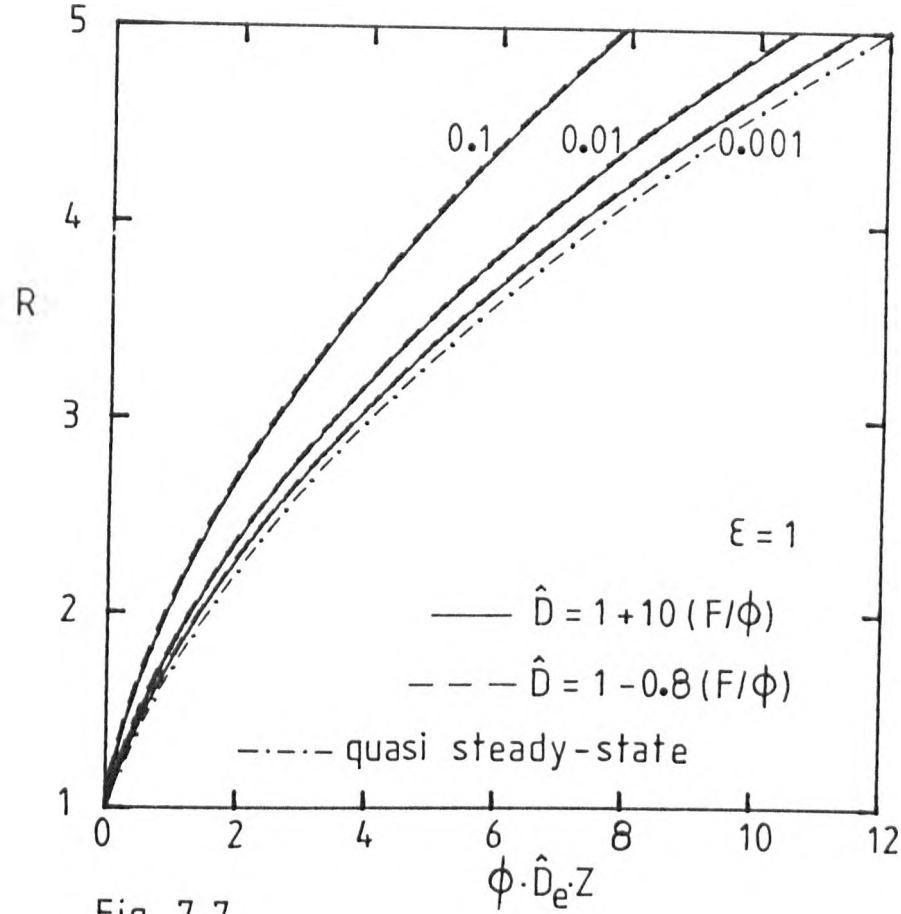

Fig 7.7

Figs 7.7 and 7.8 : Transient stage of growth from finite size with concentration dependent diffusivity. The numbers show the values of ϕ. The dashed-dotted line in fig 7.7 represents the quasi steady-state equation (7.24).

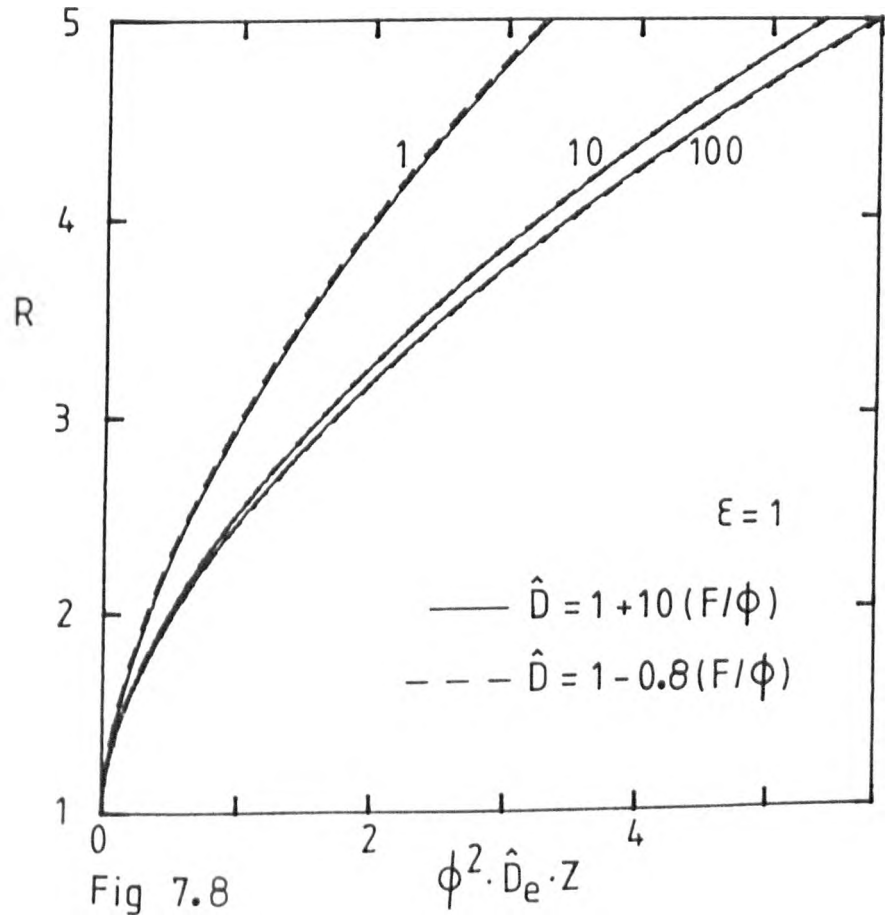

Fig 7.8

Figure 7.7 also confirms that the solutions for variable diffusivity problems with low ϕ converge to the quasi steady-state approximation (equation (7.24)). In the range of very large ϕ the variable diffusivity solutions also converge which has been already found for constant property solutions (figure 4.11).

7.8.3 Dissolution

Figures 7.9 and 7.10 exemplify the diffusion controlled dissolution of bubbles ($\varepsilon = 1$) with variable diffusivity. These results were obtained by finite difference solution of equations (7.3) and (7.4). The modifications required for this type of equation were described in section 7.6. In figure 7.9 the relation between the diffusivity and solute concentration is described by a linear function (equation (7.34)) and in figure 7.10 it is defined by

$$\hat{D} = \exp[d(F/\phi)] \ . \qquad (7.37)$$

In both cases the most important effect of varying the diffusivity is the change of dissolution time. The constant property solutions are represented by the dashed lines.

Figures 7.11 and 7.12 show normalised dissolution curves for the cases of equations (7.34) and (7.37) respectively. The full lines in figure 7.11 represent the solutions for $\hat{D} = [1 + 10 \cdot (F/\phi)]$ and the dashed lines solutions

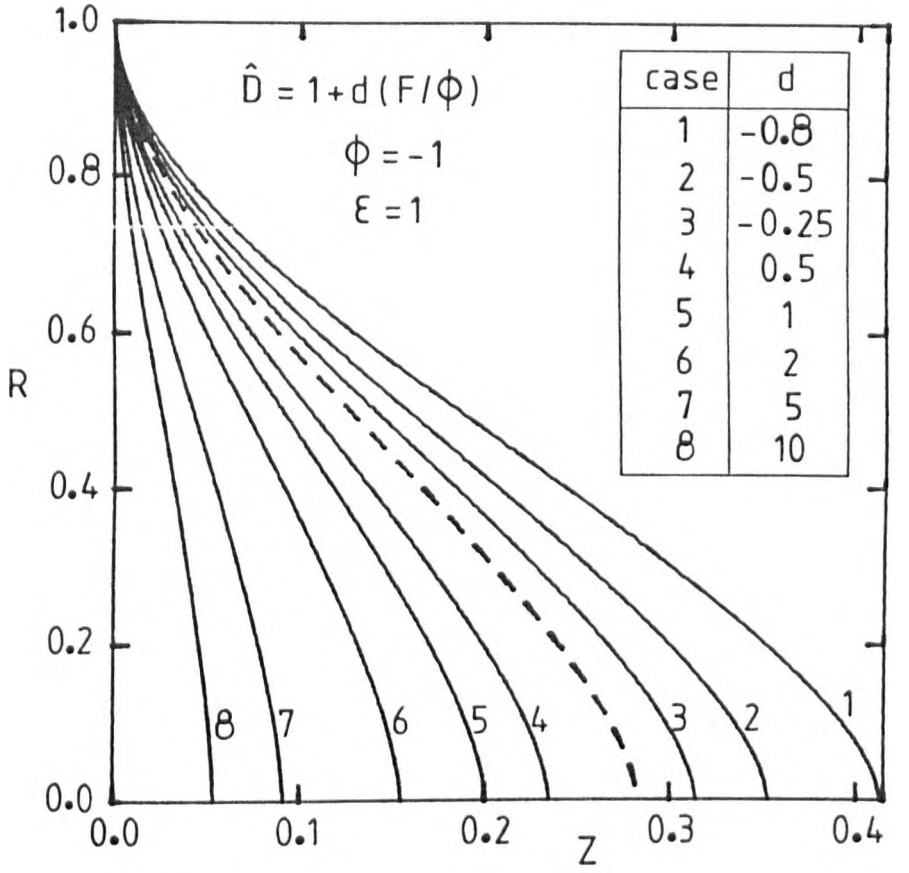

Fig 7.9

Figs 7.9 and 7.10 : Relations between R and Z for dissolution with concentration dependent diffusivity. The dashed lines represent the constant property solutions.

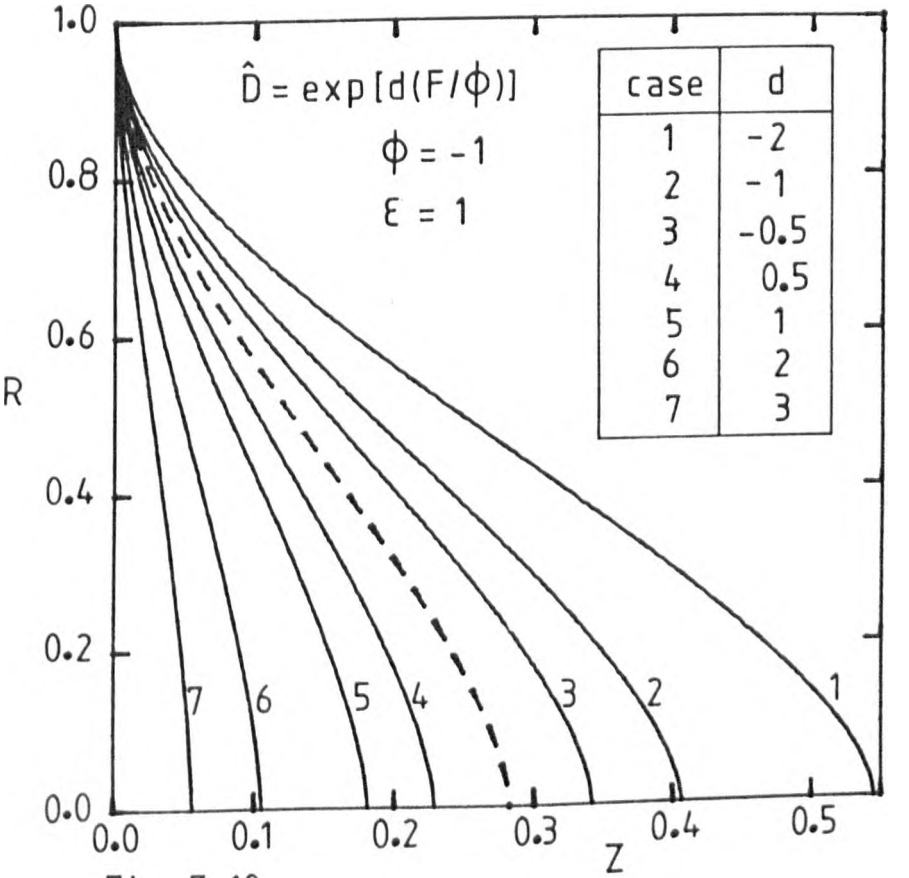

Fig 7.10

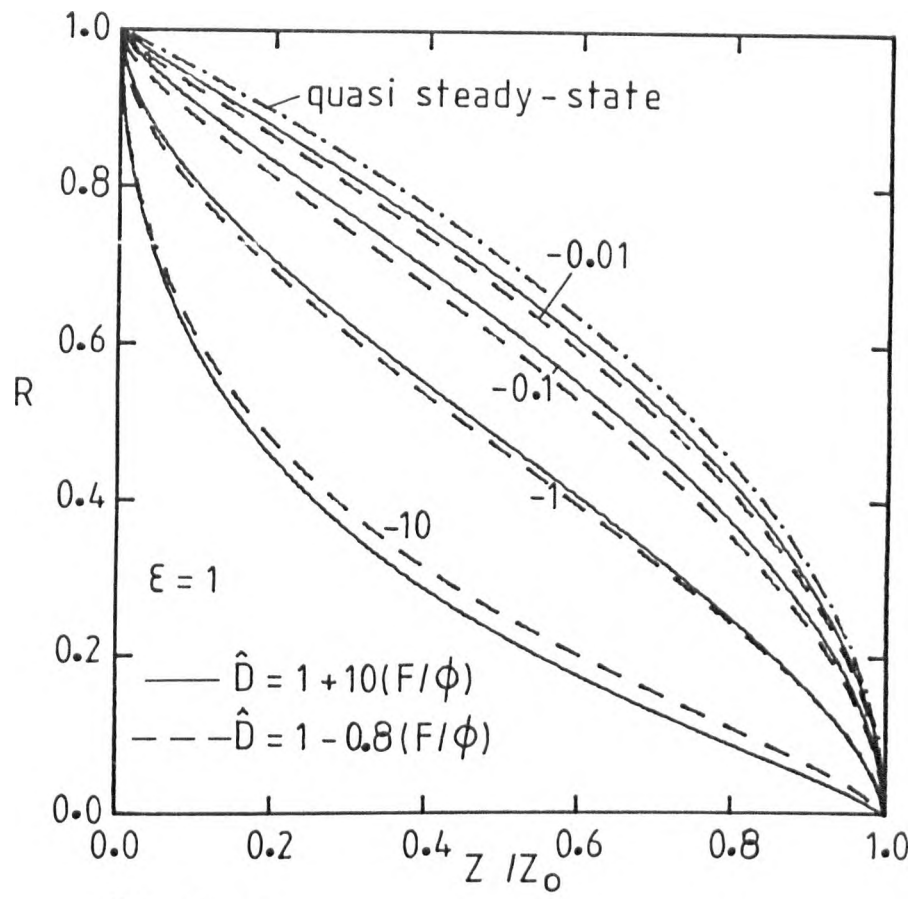

Fig 7.11

Figs 7.11 and 7.12 : Relations between normalized radius and time for dissolution with concentration dependent diffusivity. The numbers show the values of ϕ. The dotted-dashed lines represent the quasi steady-state equation (7.24).

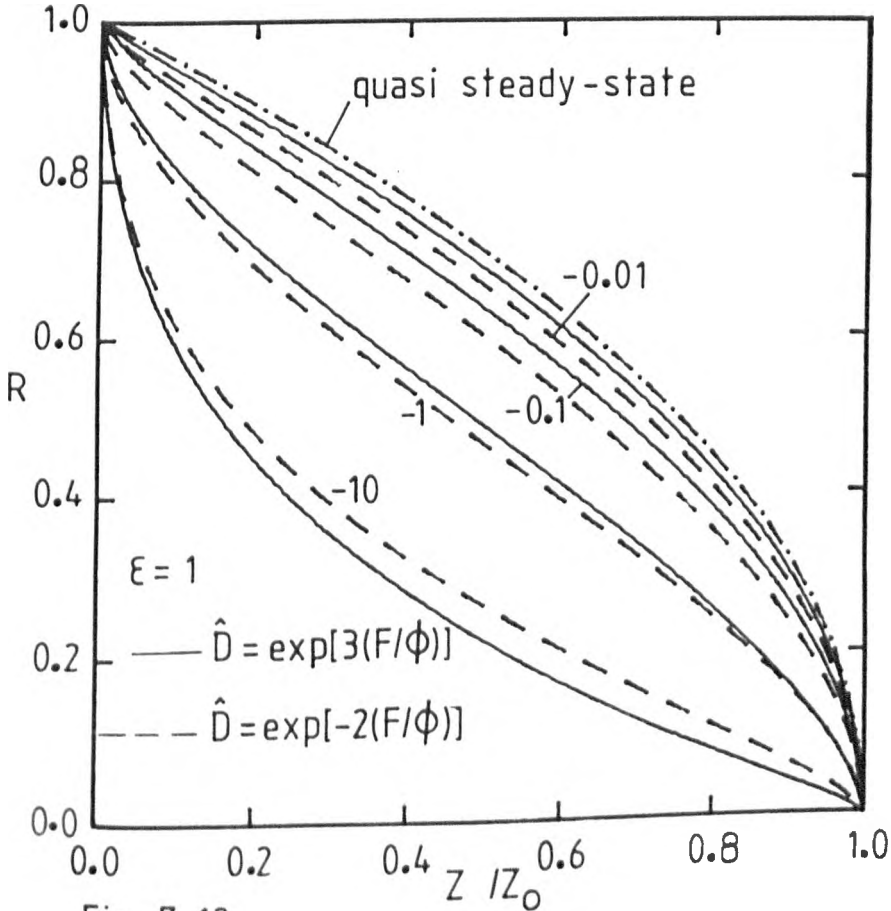

Fig 7.12

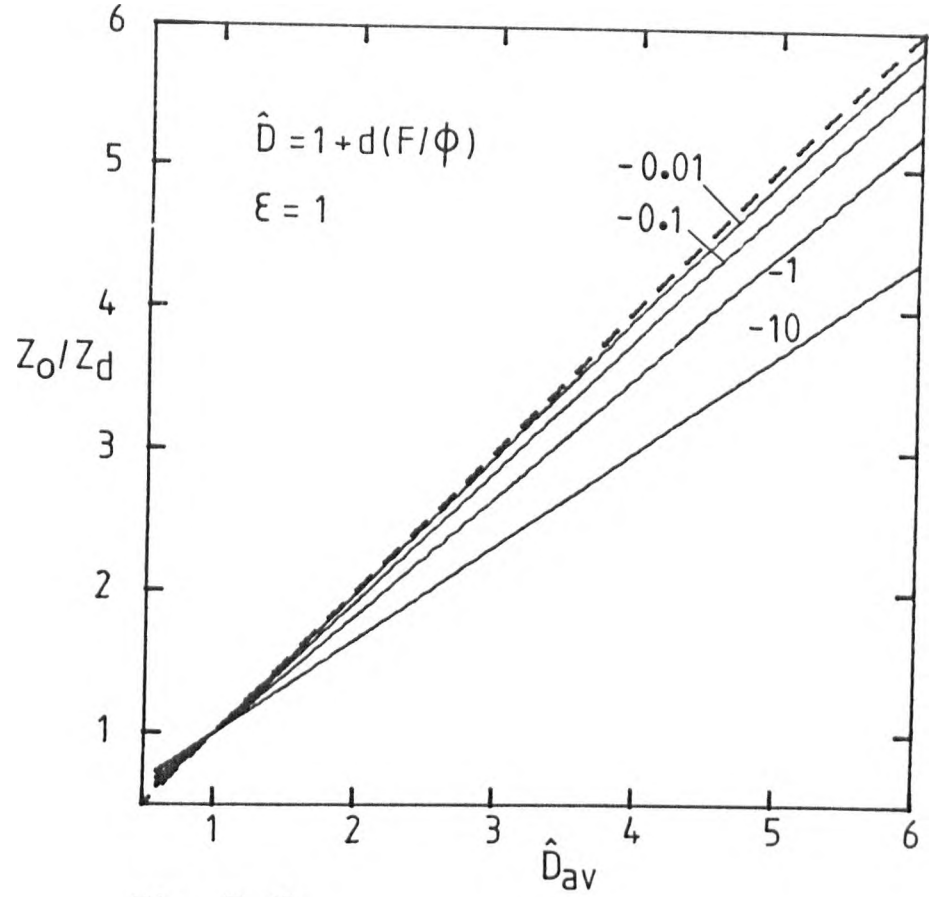

Fig 7.13

Fig 7.13 and 7.14 : Relation between the equivalent dimensionless diffusivity $D_e = Z_o/Z_d$ for dissolution with concentration dependent diffusivity and the average dimensionless diffusivity $\hat{D}_{av}$. The numbers show the values of ϕ.

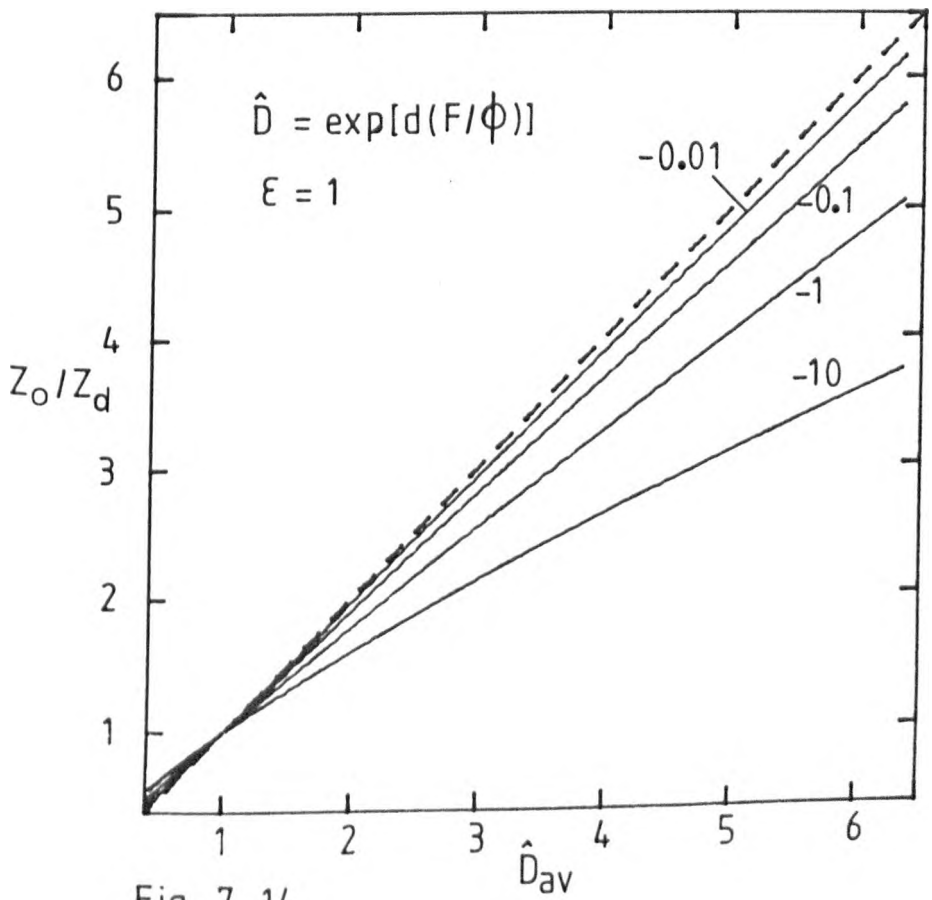

Fig 7.14

Table : 7.5

Effect of concentration dependent diffusivity on the dimensionless time required for complete dissolution Z_d. The symbol * denotes the quasi steady-state equation (7.24).

a) $\hat{D} = 1 + \bar{a}\ (F/\phi)$

ϕ	*	-0.001	-0.01	-0.1	-1	-10
$\bar{a}$				$-\phi\ Z_d$		
10	0.0833	0.0832	0.0791	0.0708	0.0540	0.03682
5	0.1429	0.1411	0.1346	0.1202	0.0914	0.0602
2	0.2500	0.2458	0.2347	0.2076	0.1550	0.0964
1	0.3333	0.3263	0.3116	0.2736	0.2008	0.1204
0.5	0.4000	0.3915	0.3729	0.3251	0.2351	0.1374
-0.25	0.571	0.554	0.525	0.4502	0.3142	0.1743
-0.5	0.667	0.644	0.607	0.515	0.3529	0.1916
-0.8	0.833	0.796	0.743	0.619	0.4134	0.2180
0	0.5000	0.4864	0.4625	0.3994	0.2828	0.1599

b) $\hat{D} = \exp\ (\ \bar{a}\ (F/\phi)\ )$

ϕ	*	-0.001	-0.01	-0.1	-1	-10
$\bar{a}$				$-\phi\ Z_d$		
3	0.0786	0.0779	0.0751	0.0691	0.0560	0.04279
2	0.1565	0.1541	0.1485	0.1344	0.1056	0.0718
1	0.2910	0.2851	0.2732	0.2423	0.1811	0.1112
0.5	0.3854	0.3767	0.3595	0.3147	0.2289	0.1346
-0.5	0.635	0.615	0.582	0.496	0.3422	0.1870
-1	0.791	0.761	0.716	0.602	0.4063	0.2156
-2	1.157	1.100	1.021	0.839	0.545	0.2758

for the cases $\hat{D} = [1 - 0.8 \cdot (F/\phi)]$. Similarly the full lines in figure 7.12 represent $\hat{D} = \exp[3(F/\phi)]$ and the dashed lines $\hat{D} = \exp[-2(F/\phi)]$. The dotted-dashed lines represent the quasi steady-state solutions (equation (7.24)). These figures confirm that concentration dependent diffusivity may be taken into account by changing the time scale, which is the same as using an equivalent diffusivity. All the solutions for $\hat{D} = [1 + d(F/\phi)]$ with $-0.8 < d < 10$ lay in between the extreme cases $d = -0.8$ and $d = 10$, and similarly the solutions for $\hat{D} = \exp[d(F/\phi)]$ with $-2 < d < 3$ lay in between the cases $d = -2$ and $d = 3$. With low $|\phi|$ the actual solutions converge to the quasi steady-state limit.

It has been shown that the time scales, that is, dimensionless dissolution times Z_d, are the most useful data so that the radius-time relations for the concentration dependent diffusivity cases may be obtained from constant property solutions. Dissolution times are shown in table 7.5a for the case of the linear relation $\hat{D} = [1 + d(F/\phi)]$ and in table 7.5b for $\hat{D} = \exp[d(F/\phi)]$. These results are also represented in figures 7.13 and 7.14 in order to relate the equivalent dimensionless diffusivity $\hat{D}_{eq} = Z_o/Z_d$ to the average dimensionless diffusivity $\hat{D}_{av}$; Z_o is the constant property solution.

Figures 7.13 and 7.14 show that there are nearly linear relations between $\hat{D}_{eq}$ and $\hat{D}_{av}$ except possible for $\phi = -10$ in figure 7.14. These relations reduce to

$$\hat{D}_{eq} \simeq 1 + S(\hat{D}_{av} - 1) . \qquad (7.38)$$

One calculation for the middle of the range of $\hat{D}_{av}$ is usually enough to obtain accurate values of S which may be useful for each relation between diffusivity and concentration.

It has been shown that the equivalent diffusivity for growing spheres is lower than the average diffusivity if the diffusivity is a minimum near the

interface and the equivalent diffusivity is higher than the average diffusivity if the diffusivity is a maximum at the interface. The same trends are valid for dissolving spheres as shown in figures 7.13 and 7.14.

The examples shown in figures 7.11 and 7.12 demonstrate that from experimentally measured radius-time curves it is virtually impossible to conclude whether the diffusivity is nearly constant or varies strongly with the concentration of solute. For the cases $\phi = -10$ shown in figure 7.12 the diffusivity in the bulk liquid medium is about 20 times the value at the interface (full line) or about 0.135 times this value (dashed line). Even these extreme cases can only be distinguished if the final stage is accurately measured and this would be very difficult with most experimental techniques. Besides, impurities might easily change the final stage of dissolution (see Chapter VI).

Conclusions

Exact solutions have been derived for diffusion controlled growth of spheres from zero size with concentration dependent diffusivity. These solutions were then used for comparison with finite difference predictions and both methods agree very closely. This demonstrates the accuracy of the finite difference method.

It has been shown that the solutions for growth or dissolution of spheres with concentration dependent diffusivity can be worked out from constant property solutions provided accurate values of the equivalent dimensionless diffusivity $\hat{D}_{eq}$ are known. Unfortunately this equivalent diffusivity is not the same as the average dimensionless diffusivity $\hat{D}_{av}$ except for very low absolute numerical values of the solubility parameter ϕ. However, the relation between $\hat{D}_{eq}$ and $\hat{D}_{av}$ is usually simple and only a few ($\hat{D}_{av}$; $\hat{D}_{eq}$) pairs are needed to obtain all the relevant solutions for a given functional

form D(C) relating the diffusivity and the concentration of solute. This is valid both for growth and dissolution.

The use of the equivalent diffusivity makes all the solutions for growth with large R indistinguishable regardless of the relation between the diffusivity and concentration of solute. During the initial transient stage of growth from finite size the variable diffusivity solutions are also almost indistinguishable from the constant property solution provided the dimensionless time is transformed into $Z \cdot \hat{D}_{eq}$.

During dissolution the evolution of concentration profiles is complex (Chapter V) without evolution to asymptotic regime except for very low ϕ. In spite of that the equivalent diffusivity is still a very useful variable to take into account the relation between diffusivity and concentration of solute. Representation of radius-time relations in terms of $Z \cdot \hat{D}_{eq}$ gives close predictions for very different functional forms $\hat{D}(F)$ so that the variable diffusivity solutions can be worked out from the constant property case with the equivalent diffusivity.

From the shape of radius-time curves it is then practically impossible to conclude whether the diffusivity is strongly dependent on concentration or not.

CHAPTER VIII

Surface Kinetics

8.1 Interfacial conditions

In the previous chapters it has been assumed that the transport of material was controlled by diffusion in the liquid. However, if the diffusion were sufficiently rapid the rate of transfer between the sphere and the liquid medium might be controlled by surface kinetics, or both mechanisms might govern the behaviour of the system. These phenomena are frequent in chemical engineering problems and the rate of transport at the interface, J, (moles per unit area and per unit time) with n-th order kinetics is usually described by (Rosner and Epstein, 1972)

$$J = K'\left[\left(C(a)\right)^n - \left(C^*\right)^n \right] = D\left[1 - C(a)\cdot v\right]^{-1} \cdot \left(\frac{\partial C}{\partial r}\right)_a \qquad (8.1)$$

where $C(a)$ is the actual concentration at the interface, C^* the equilibrium concentration and K' the kinetic constant. The present treatment is restricted to one-component bubbles, so that $C(a)\cdot v \simeq 0$ and the index i previously used to denote the species i can be omitted. The one-component case is sufficient to illustrate the possible behaviour.

In these conditions equation (8.1) can be made dimensionless

$$K\left[\left(F(R) + F_\infty\right)^n - F_s^{\,n}\right] = \left(\frac{\partial F}{\partial e}\right)_R \qquad (8.2)$$

where e, R and Z are defined as usual (Chapter II) and

$$\begin{aligned} F_s &= C^*/C_s^\circ \quad ; \quad F(R) = \left[C(a) - C_\infty\right]/C_s^\circ \\ F_\infty &= C_\infty/C_s^\circ \quad ; \quad F = (C - C_\infty)/C_s^\circ \\ K &= K'.a_o.C_s^{\circ\,-1+n}.D^{-1} \end{aligned} \qquad (8.3)$$

The gas concentration C_s° and the diffusivity D of solute are considered constant. C_∞ denotes the initial bulk concentration of solute so that the additional boundary condition and initial condition are written as usually

$$C(\infty) = C_\infty \quad ; \quad t > 0$$
$$C(r) = C_\infty \quad ; \quad r > a \quad ; \quad t = 0 \, . \tag{8.4}$$

It was shown in chapter II that for gas bubbles $\varepsilon = 1$, so that the material balances (equation (2.28)) can be written

$$\frac{\partial^2 F}{\partial e^2} + \left[\frac{2}{e} - \left(\frac{R}{e}\right)^2 \frac{dR}{dZ} \right] \frac{\partial F}{\partial e} = \frac{\partial F}{\partial Z} \tag{8.5}$$

and

$$\frac{dR}{dZ} = \left(\frac{\partial F}{\partial e}\right)_R \, , \tag{8.6}$$

with boundary condition

$$F(\infty) = 0 \, , \tag{8.7}$$

and initial condition

$$F(e) = 0 \quad ; \quad e > R \quad ; \quad Z = 0 \, . \tag{8.8}$$

Equations (8.2), (8.5) and (8.6) cannot be solved analytically. Numerical solutions were reported by Szekely and co-authors (1971, 1973), but the stability of their method required very small time increments so that such solutions are not efficient to analyse growth or dissolution with low or moderate solubility parameters $|\phi|$.

It has also been emphasized that the assumption of arbitrary functional forms of concentration profiles used by Rosner and Epstein (1972) to derive

their diffusion controlled approximations fails in the ranges of moderate and low solubility parameters. Including surface kinetics in similar ranges of concentration is unlikely to lead to generally acceptable solutions by those methods.

8.2 Quasi steady-state approximations

By integration of the quasi steady-state simplification of the material balance (equation (2.67)) one obtains

$$\left(\frac{\partial F}{\partial e}\right)_R = - F(R)/R \qquad (8.9)$$

and

$$F(e) = F(R) . \left(\frac{R}{e}\right) . \qquad (8.10)$$

By combination of equations (8.2), (8.6) and (8.9) for first order surface kinetics (n=1) one obtains

$$\frac{dR}{dZ} = \frac{K \phi}{1 + K R} , \qquad (8.11)$$

from which it follows that

$$\frac{1}{K} (R - 1) + \frac{1}{2} (R^2 - 1) = \phi Z , \qquad (8.12)$$

with $R = 1$ when $Z = 0$, and $\phi = (C_\infty - C^*)/C_s^\circ$. Equation (8.12) assumes a very simple form and if the kinetic constant is sufficiently small (see figures 8.4 and 8.8)

$$R \simeq 1 + K \phi Z . \qquad (8.13)$$

It will later be shown that equation (8.13) represents the general

solutions of growth or dissolution controlled by first order surface kinetics, regardless of the actual value of the solubility parameter ϕ.

The equilibrium water content in glass melts is known to follow the Sievert's law, that is $C^* \propto P^{\frac{1}{2}}$, where P is the water vapour partial pressure. Other gas-liquid systems may follow Sievert's law and for these cases second order surface kinetics is expected (n=2) (Fast, 1965).

From equations (8.2), (8.6) and (8.9) with second-order surface kinetics one obtains

$$\frac{dR}{dZ} = \frac{F_\infty}{R} + \frac{1}{2KR^2} - \frac{1}{R} \cdot \sqrt{F_s^2 + \left(F_\infty + \frac{1}{2KR}\right)^2 - F_\infty^2} \quad , \tag{8.14}$$

with initial condition $Z = O \;\; ; \;\; R = 1$.

If K is sufficiently low

$$\left| \left(F_\infty^2 - F_s^2\right) \Big/ \left[F_\infty + \frac{1}{2KR} \right]^2 \right| << 1 \tag{8.15}$$

so that

$$\sqrt{F_s^2 - F_\infty^2 + \left(F_\infty + \frac{1}{2KR}\right)^2} \simeq \left(F_\infty + \frac{1}{2KR}\right) \left[1 + \frac{F_s^2 - F_\infty^2}{2\left(F_\infty + \frac{1}{2KR}\right)^2} \right] \tag{8.16}$$

and equation (8.14) therefore tends to

$$\frac{dR}{dZ} \simeq \frac{1}{R} \left(F_\infty + \frac{2}{2KR}\right) \left[1 - 1 + \frac{F_\infty^2 - F_s^2}{2\left(F_\infty + \frac{1}{2KR}\right)^2} \right] \simeq \frac{F_\infty^2 - F_s^2}{2F_\infty R + \frac{1}{K}} \tag{8.17}$$

and on integrating

$$F_\infty(R^2 - 1) + \frac{R - 1}{K} = (F_\infty^2 - F_s^2)Z \quad . \tag{8.18}$$

Again, if K is sufficiently small equation (8.18) tends to the following linear relation

$$R = 1 + K(F_\infty^2 - F_s^2)Z \ . \qquad (8.19)$$

Numerical solutions of equation (8.14) were also computed by using a fourth-order Runge-Kutta technique. These results confirmed the gradual convergence of solutions to equation (8.19) regardless of the values of F_∞ and F_s (see figures 8.10 and 8.12).

8.3 Growth or dissolution controlled by surface kinetics

If the kinetic constant K is sufficiently low, $C(a) \simeq C_\infty$, equations (8.2) and (8.6) reduce to

$$\frac{dR}{dZ} = K[F_\infty^n - F_s^n]$$

or on integrating

$$R = 1 + K[F_\infty^n - F_s^n]Z = 1 + K\,\phi^n\,[(1 + f)^n - f^n] \ , \qquad (8.20)$$

where

$$\begin{aligned} \phi &= F_\infty - F_s \\ f &= F_s/\phi \ . \end{aligned} \qquad (8.21)$$

Equations (8.13) and (8.19) are the first-order case and the second-order case of equation (8.20). Thus, the quasi steady-state approximations converge to the exact limiting surface kinetics mechanism.

8.4 Numerical solutions

As the interfacial concentration varies with the concentration gradient at the interface, F(R) must be solved as one of the discrete values of concentrations calculated by the non-pivoting elimination method described in Chapter III. Otherwise the oscillatory errors grow rapidly and the solution fails. This type of problem was considered by Crank and Nicholson (1947) by assuming a fictitious point where the concentration was expressed as a linear function of the concentrations at the first two mesh points by combination of the diffusion and first order surface kinetics equations.

After the usual transformation of space variable equations (8.5) and (8.6) become

$$R^{-2}\frac{\partial^2 F}{\partial x^2} + \left[\frac{2}{xR^2} + \frac{1}{R}\frac{dR}{dZ}(x - x^{-2})\right]\frac{\partial F}{\partial x} = \frac{\partial F}{\partial Z} \quad , \tag{8.22}$$

and

$$\frac{dR}{dZ} = \frac{1}{R}\left(\frac{\partial F}{\partial x}\right)_{x=1} \tag{8.23}$$

where $x = r/a = e/R$.

At the interface (x=1) equation (8.22) reduces to

$$\frac{\partial^2 F}{\partial x^2} + 2\frac{\partial F}{\partial x} = R^2\frac{\partial F}{\partial Z} \quad ; \quad x = 1 \tag{8.24}$$

and in the case of first order kinetics equation (8.2) becomes

$$\left(\frac{\partial F}{\partial x}\right)_{x=1} = KRF(R) + KR\phi \ . \tag{8.25}$$

In the case of general n-order surface kinetics and, in order to advance from time step ℓ to the next step ℓ+1, one may write

$$(F(R)_{\ell+1} + F_\infty) = (F(R)_\ell + F_\infty).(1 + \delta) \tag{8.26}$$

where δ is expected to remain much smaller than unity, so that

$$\begin{aligned}(F(R)_{\ell+1} + F_\infty)^n &\simeq (F(R)_\ell + F_\infty)^n.(1 + n\delta) \\ &\simeq (F(R)_\ell + F_\infty)^{n-1}\left[nF(R)_{\ell+1} + F_\infty + (1 - n)\cdot F(R)_\ell \right]\end{aligned} \tag{8.27}$$

and from equation (8.2)

$$\left(\frac{\partial F}{\partial x}\right)_{\substack{x=1 \\ \ell+1}} = d_0 + d_1 \cdot F(R)_{\ell+1} \tag{8.28}$$

where

$$d_0 = RK\left\{\left[F(R)_\ell + F_\infty\right]^{n-1}.\left[F_\infty + (1 - n)\cdot F(R)_\ell \right] - F_s^{\,n}\right\}$$

$$d_1 = nRK\left[F(R)_\ell + F_\infty\right]^{n-1} .$$

On assuming a fictitious point at $x_0 = x_1 - \delta x$ where $x_1 = 1$ and $\delta x = x_2 - x_1$ the space derivatives (equations (3.9)) and (3.10) reduce to

$$\left(\frac{\partial F}{\partial x}\right) = \frac{F_2 - F_0}{2\delta x} , \tag{8.29}$$

$$\left(\frac{\partial^2 F}{\partial x^2}\right) = \frac{F_2 - 2F_1 + F_0}{(\delta x)^2} , \tag{8.30}$$

and the time derivative is replaced by

$$\left(\frac{\partial F}{\partial Z}\right)_{x=1} = (F_{1,\ell+1} - F_{1,\ell}) \;/\; \delta Z , \tag{8.31}$$

where ℓ denotes the time step, $\delta Z = Z_{\ell+1} - Z_\ell$, and

$$F_{1,\ell} = F(R)_{\ell} \quad .$$

By combination of equations (8.24), (8.28), (8.29), (8.30), and (8.31) one obtains

$$F_{2,\ell+1} - [1 + \alpha + d_1 \cdot \delta x(1 - \delta x)]F_{1,\ell+1}$$

$$= 2\delta x(1 - \delta x) \cdot d_0 + [1 + d_1 \cdot \delta x(1 - \delta x) - \alpha]F_{1,\ell} - F_{2,\ell} \quad , \qquad (8.32)$$

where

$$\alpha = (R^2)_{av} \cdot (\delta x)^2/\delta Z$$

$$(R^2)_{av} = (R^2_{\ell+1} + R^2_{\ell} + R_{\ell} \cdot R_{\ell+1})/3 \quad .$$

Equation (8.32) assumes the form of the boundary equation (3.23) required for the application of the finite difference implicit method described in Chapter III. The present treatment is based on assuming the fictitious point (Crank and Nicolson, 1947) but extends the solutions to n-order surface kinetics.

In order to obtain the quasi-stationary approximation of the initial profile the interfacial concentration $F(R)_0$ at time step 0 can be obtained by combining equations (8.2) and (8.6) with the transformed quasi-stationary equation (2.60) so that

$$K[(F(R)_0 + F_{\infty})^n - F_s^n] = - \frac{F(R)_0}{R_0} \left[1 + \frac{1}{\sqrt{\pi Z_0}}\right] \quad . \qquad (8.33)$$

In the case of first-order kinetics (n=1) equation (8.33) leads to

$$F(R)_0 = \frac{-\phi}{1 + \lambda/(KR_0)} \qquad (8.34)$$

where $\lambda = 1 + 1/\sqrt{\pi Z_0}$

and in the case of second-order kinetics (n=2)

$$F(R)_O = \left[\frac{F_\infty \cdot \lambda}{KR_O} + \left(\frac{\lambda}{2KR_O} \right)^2 + F_s^2 \right]^{\frac{1}{2}} - F_\infty - \frac{\lambda}{2KR_O} \quad . \tag{8.35}$$

Therefore the finite difference scheme described in Chapter III can be used to solve problems which involve the contributions of diffusion and surface kinetics. In the ranges of K values where surface kinetics controls growth or dissolution our finite difference predictions agree very well with the predictions of equation (8.20). This demonstrates the accuracy of that technique.

8.5 First-order surface kinetics

8.5.1 Growth

Figures 8.1, 8.2 and 8.3 illustrate the progressive transition from diffusion controlled growth to growth controlled by first-order surface kinetics. If K is sufficiently low the initial stage is controlled by surface kinetics, but at sufficiently large times the solutions always converge to the diffusion controlled regime (dashed-lines). This evolution can be observed for the largest values of the kinetic constant in figures 8.1, 8.2 and 8.3 and is characterized by a change of slopes from 1 towards 1/2 in those figures. The transition for small values of K occurs at considerably longer times.

In the case $\phi = 0.001$; $K = 0.1$ the initial stage is controlled by surface kinetics up to about $R = 2$ (dashed-dotted lines). However, if $K > 1$ the surface kinetics mechanism fails to describe even the initial stage of growth, and if $K > 10$ the surface kinetics can be neglected.

With $\phi = 1$ the surface kinetics causes significant deviations from the

diffusion-controlled regime even in the case K = 10. Again if K < 0.1 there is an initial stage which is controlled by surface kinetics.

In the case ϕ = 1000 the initial stage is controlled by surface kinetics if K < 100, and even if K = 1000 the surface kinetics causes important deviations from the diffusion-controlled case at least up to R = 10.

Taking into account the linear relationship between radius and time in the case of growth controlled by surface kinetics a single point (R;Z) is sufficient to characterize that regime. The dimensionless time, Z_g, required to double the size of the bubble was used for that purpose. The transformed time ϕZ was used in table 8.1 and figure 8.4 for clearer illustration of the unique surface kinetics controlled regime. These results show that the actual solutions are always between the quasi steady-state limit (for low ϕ), and equation (8.13) (growth controlled by surface kinetics). It was shown earlier that the quasi steady-state converges to equation (8.13) in the range of low kinetic constants (K < 0.01). The quasi steady-state approximations are reasonable solutions in the range of very low ϕ, ($\phi \leq$ 0.001), regardless of the value of the kinetic constant.

8.5.2 Dissolution

Figures 8.5, 8.6 and 8.6 illustrate the transition from diffusion-controlled dissolution towards dissolution controlled by surface-kinetics (dashed-dotted lines) which is given by equation (8.13). The actual solutions are close to this regime (equation (8.13)) if K = 0.1, especially for very large $|\phi|$. With K < 0.01 the actual solutions become almost indistinguishable from the limiting predictions by equation (8.13). The quasi steady-state approximations are indistinguishable from the actual finite difference solutions if $-\phi$ < 0.01 and K < 0.1. Quasi steady-state predictions are also reasonably close to the actual solutions if K < 0.1 with moderate or large values of $|\phi|$. All the actual solutions lay in between the predictions of equation (8.12),

Table : 8.1

*Effect of first order surface kinetics on the time required to double the size of bubbles. * represents the quasi steady-state equation (8.12) and ** represents the growth controlled by surface kinetics (equation (8.13)).*

ϕ	*	0.001	0.01	0.1	1	10	100	1000	**
K	$\phi.Z_g$								
0.001	1001.5	1001.	1001.	1001.	1001.	1001.	1001.	1000.	1000
0.01	101.5	101.4	101.4	101.4	101.2	100.9	100.5	100.2	100
0.1	11.5	11.48	11.43	11.25	10.91	10.49	10.21	10.09	10
0.2	6.5	6.48	6.40	6.18	5.80	5.38	5.15	5.06	5
0.5	3.5	3.46	3.357	3.091	2.646	2.267	2.094	2.033	2
1	2.5	2.446	2.330	2.029	1.551	1.203	1.067	1.023	1
2	2	1.942	1.811	1.481	0.975	0.655	0.548	0.516	0.5
5	1.7	1.636	1.496	1.141	0.605	0.3111	0.2316	0.2099	0.2
10	1.6	1.534	1.389	1.024	0.479	0.1886	0.1232	0.1090	0.1
100	1.51	1.441	1.293	0.917	0.3447	0.0653	0.01947	0.01235	0.01
1000	1.501	1.432	1.284	0.907	0.3313	0.0506	0.00684	0.001954	0.001
∞	1.5	1.425	1.281	0.905	0.3294	0.04888	0.00516	0.000519	0

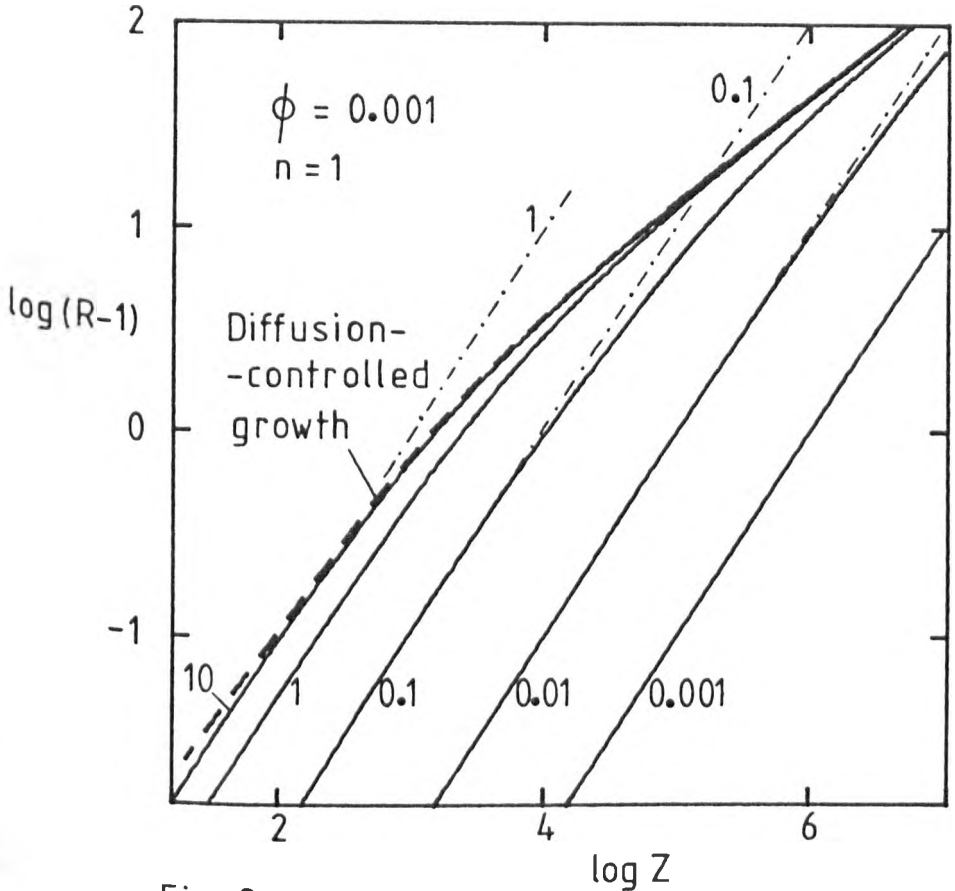

Fig 8.1

Figs 8.1, 8.2 and 8.3 : Effect of first order surface kinetics on growth of bubbles. The numbers show the kinetic constant K. The dashed line represents the diffusion controlled growth. The dashed-dotted lines represent growth controlled by surface kinetics (equation (8.13)). The solubility parameter is shown in the figures.

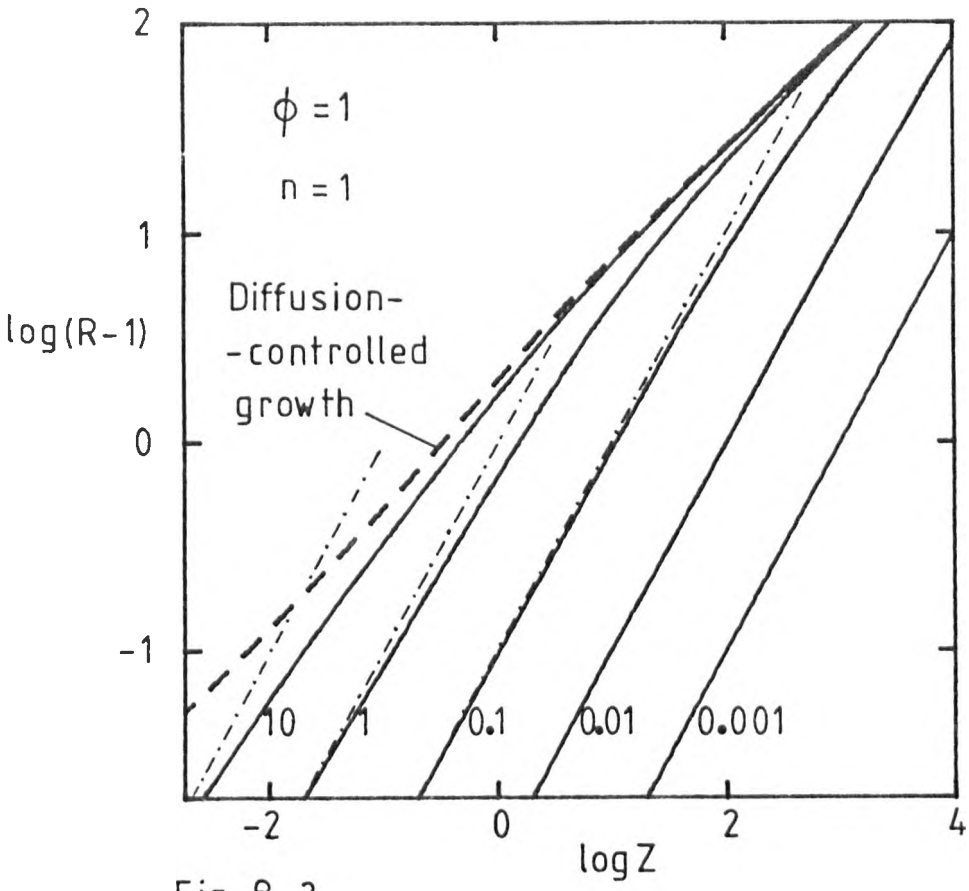
2
1
0
-1
log(R-1)
ϕ = 1
n = 1
Diffusion-
-controlled
growth
10
1
0.1
0.01
0.001
-2
0
2
4
log Z

Fig 8.2

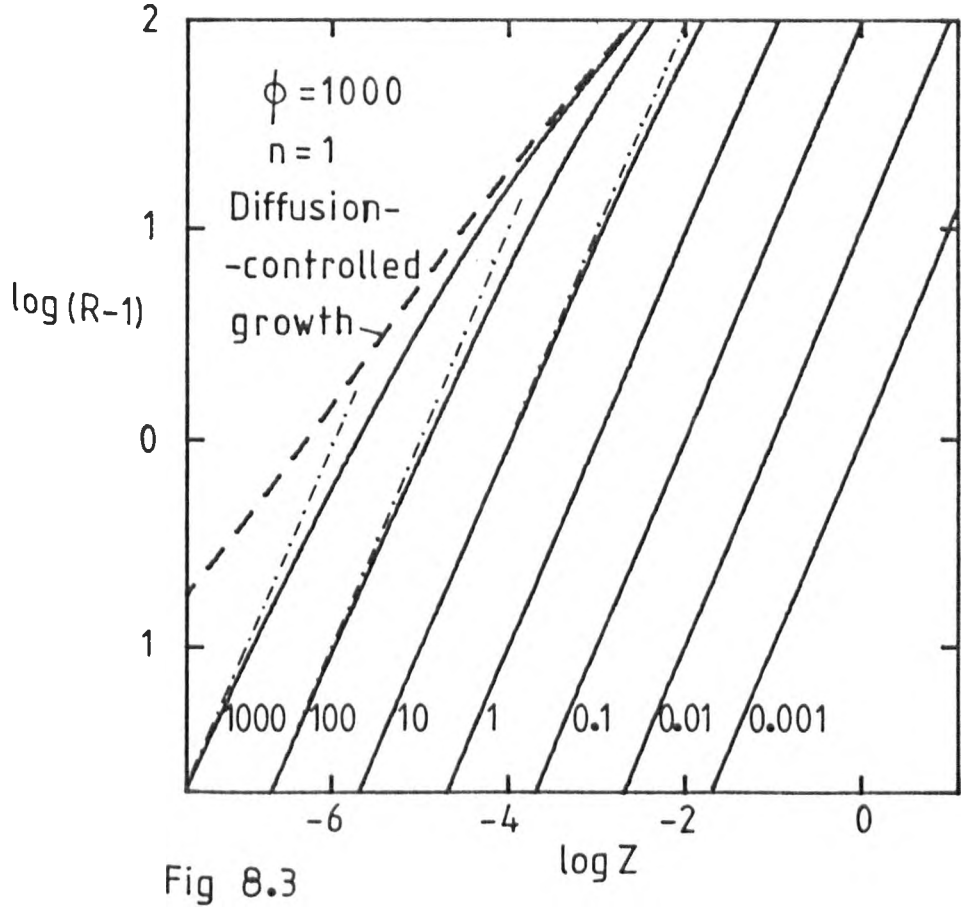
2
1
0
1
log(R-1)
ϕ = 1000
n = 1
Diffusion-
-controlled
growth
1000
100
10
1
0.1
0.01
0.001
-6
-4
-2
0
log Z

Fig 8.3

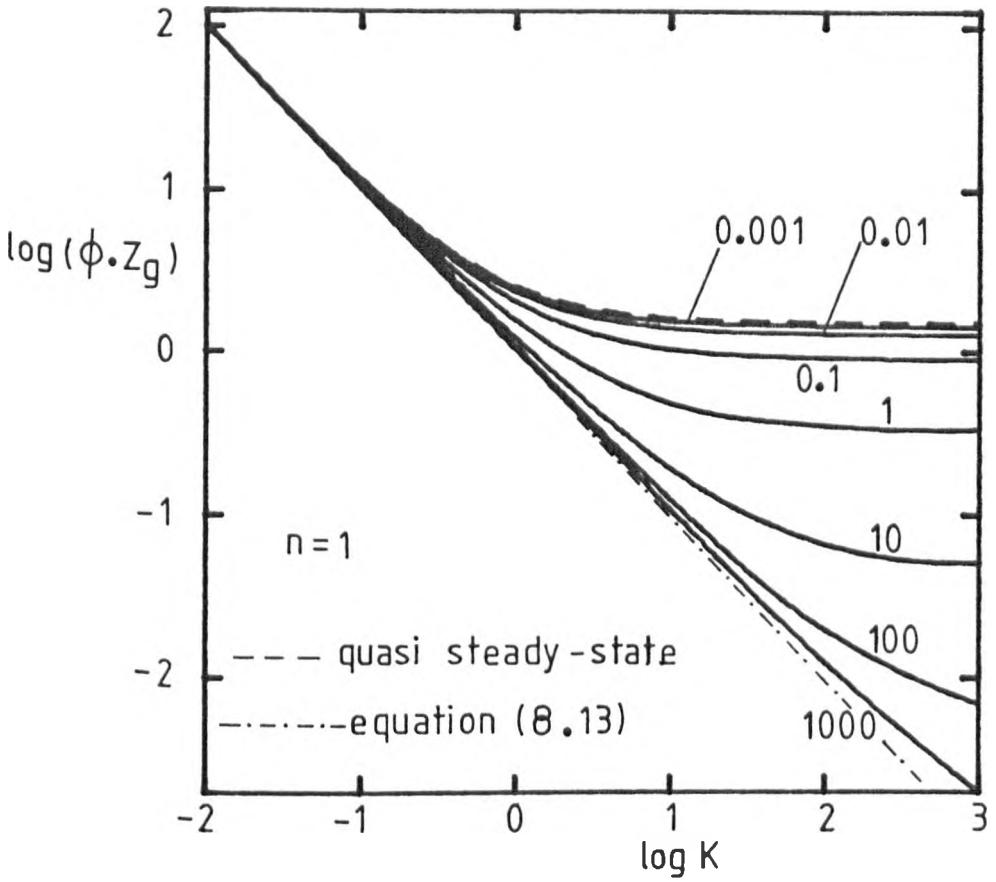

Fig 8.4 : Effect of first-order surface kinetics on the dimensionless time required to double the size of a bubble. The figures show the solubility parameter ϕ. The dashed line represents the quasi steady-state equation (8.12) and the dotted-dashed line represents the cases when growth is controlled by surface kinetics, (equation (8.13)).

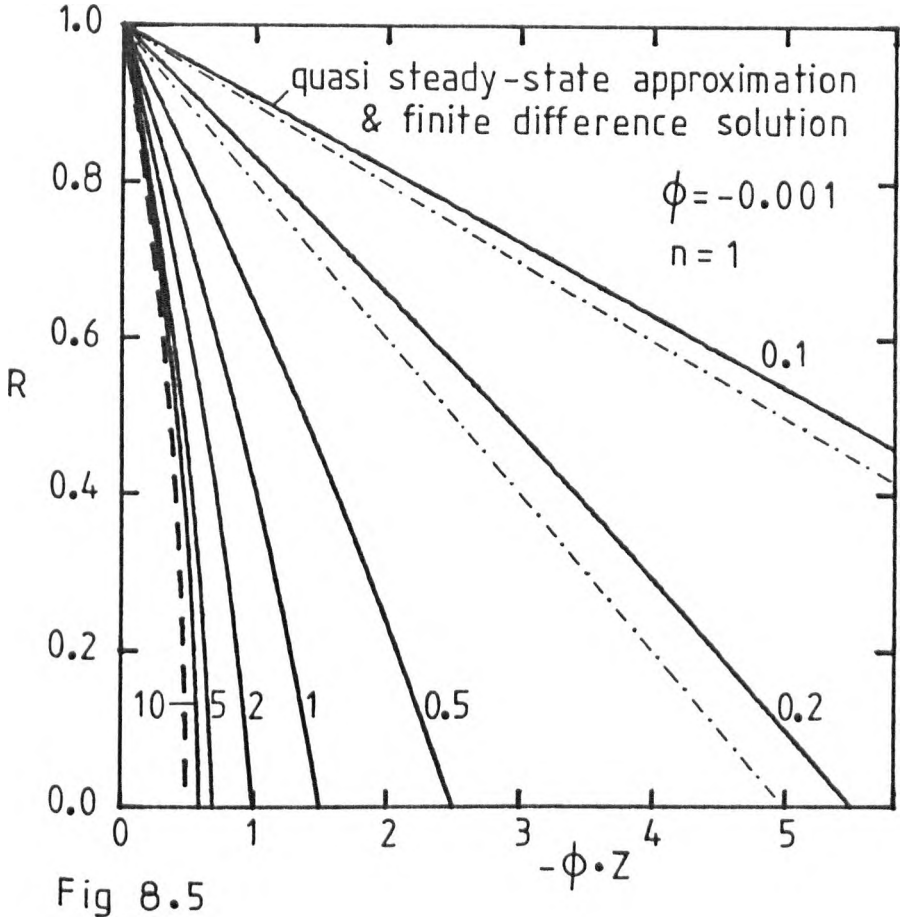

Fig 8.5

Figs 8.5, 8.6 and 8.7 : Effect of first order surface kinetics on dissolution of bubbles. The numbers show the kinetic constant K. The dashed lines represent diffusion controlled dissolution (left) or the quasi steady-state equation (8.12) (upper curve). The dashed-dotted lines represent equation (8.13). The solubility parameters are also shown in the figures.

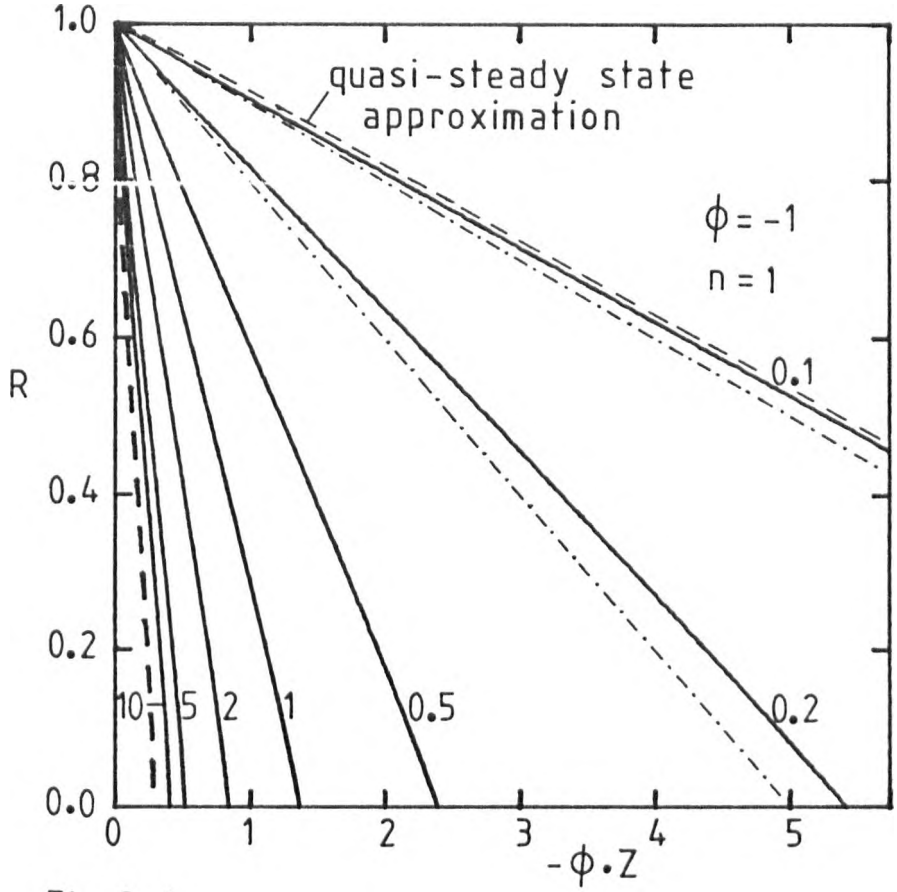
1.0
0.8
0.6
0.4
0.2
0.0
R
quasi-steady state
approximation
ϕ = -1
n = 1
0.1
0.2
0.5
1
2
5
10
0
1
2
3
4
5
-ϕ.Z

Fig 8.6

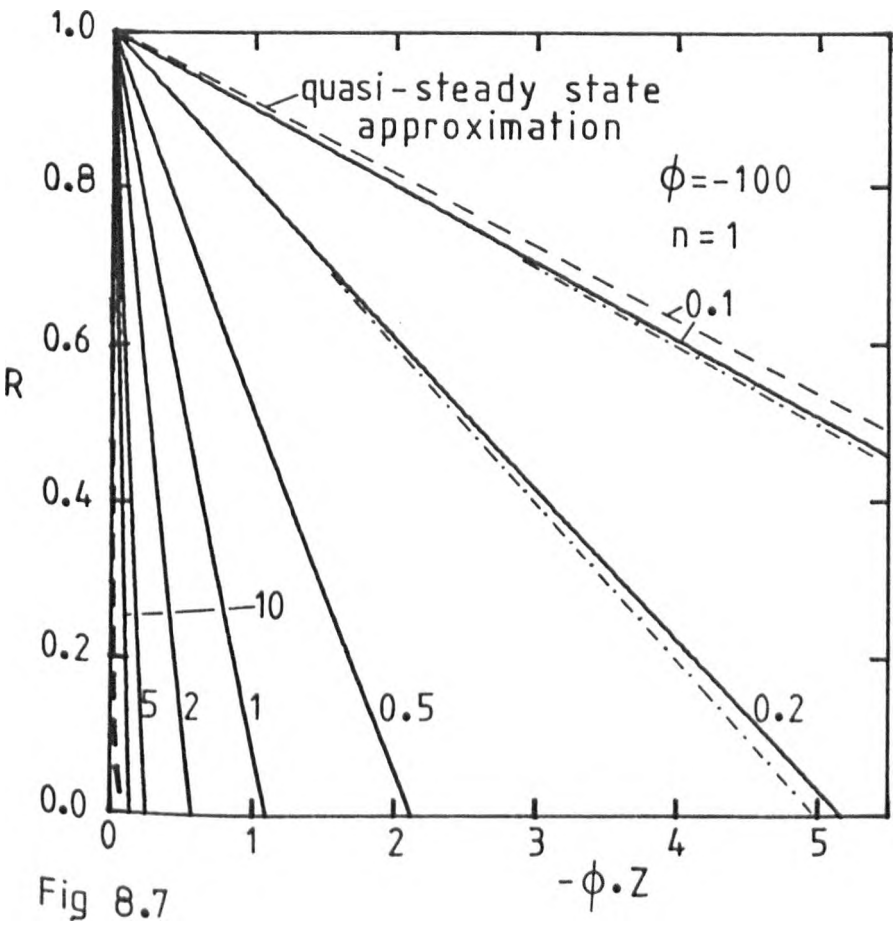
1.0
0.8
0.6
0.4
0.2
0.0
R
quasi-steady state
approximation
ϕ=-100
n = 1
0.1
0.2
0.5
1
2
5
10
0
1
2
3
4
5
-ϕ.Z

Fig 8.7

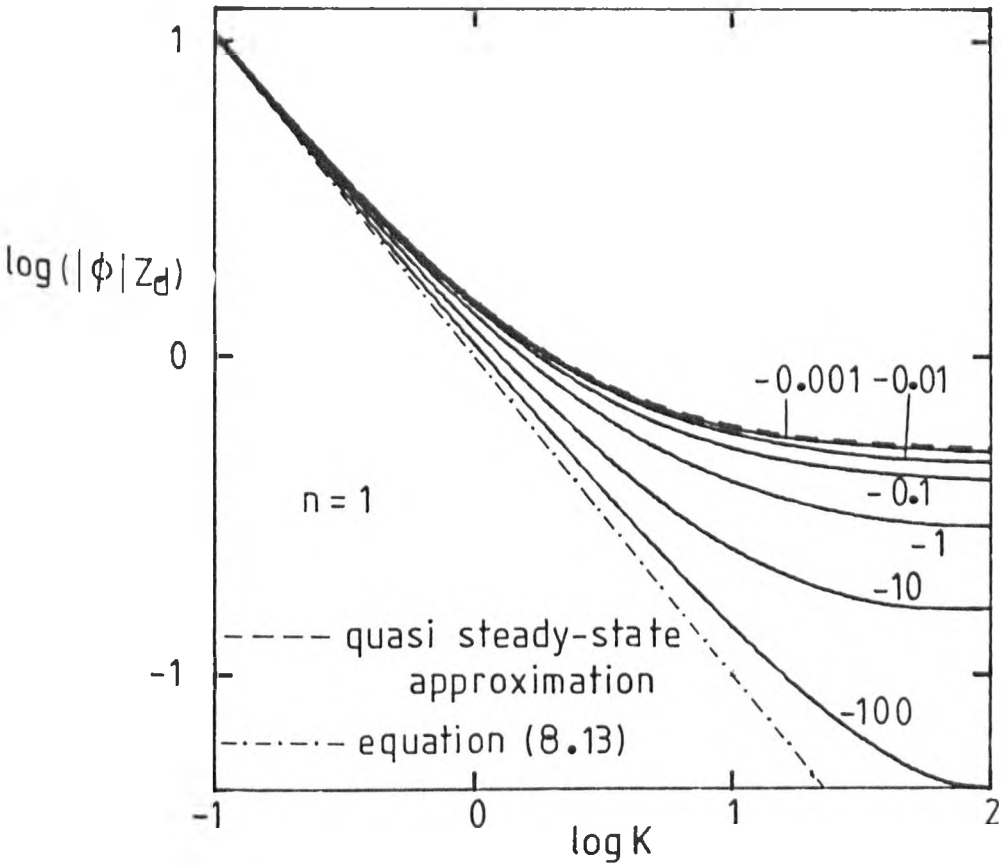

Fig 8.8 : Effect of first-order surface kinetics on the dimensionless time required for complete dissolution of a bubble. The figures show the solubility parameter ϕ. The dashed line represents the quasi steady-state equation (8.12) and the dotted-dashed line represents equation (8.13).

Table : 8.2

Effect of first order surface kinetics on the time required for complete dissolution. * *represents the quasi steady-state equation (8.12) and* ** *represents the dissolution controlled by surface kinetics (equation (8.13)).*

$-\phi$	*	0.001	0.01	0.1	1	10	1000	**
K	$\lvert\phi\rvert . Z_d$							
0.001	1000.5	1000.	1000.	1000.	1000.	1000.	1000.	1000
0.01	100.5	100.4	100.4	100.5	100.5	100.4	100.3	100
0.1	10.5	10.50	10.49	10.47	10.43	10.35	10.21	10
0.2	5.5	5.50	5.49	5.46	5.42	5.32	5.17	5
0.5	2.5	2.495	2.487	2.457	2.391	2.267	2.125	2
1	1.5	1.495	1.483	1.445	1.365	1.224	1.095	1
2	1	0.994	0.978	0.934	0.840	0.692	0.574	0.5
5	0.7	0.692	0.673	0.622	0.515	0.3603	0.2521	0.2
10	0.6	0.591	0.569	0.513	0.4084	0.2475	0.1411	0.1
100	0.525	0.500	0.4640	0.4090	0.2937	0.1618	0.04364	0.01
∞	0.5	0.4864	0.4625	0.3994	0.2828	0.1599	0.0814	0

(quasi steady-state), and equation (8.13), (controlled by surface kinetics), regardless of the values of ϕ and K.

The transformed time $Z_d \cdot |\phi|$, where Z_d is the dimensionless time required for complete dissolution, is also a generic characterization of the transition between the extreme mechanisms (table 8.2 and figure 8.8). Again the solutions always lay in between the quasi steady-state and the surface kinetics mechanism. If $-\phi < 0.01$ the quasi steady-state is reasonable when the dissolution is diffusion-controlled and becomes excellent if the dissolution is controlled by surface kinetics.

8.6 Second-order surface kinetics

8.6.1 Growth

Figure 8.9 illustrates the transition between extreme mechanisms, that is from diffusion controlled growth to growth controlled by second-order surface kinetics. Again the linear relation between R and Z characterizes the growth controlled by surface kinetics (dashed-dotted lines), and the actual solutions lay in between the growth controlled by surface kinetics (equation (8.19)) and the quasi steady-state approximations (equation (8.14)) which are represented by dashed-lines. Equations (8.14) and (8.19) converge as the kinetic constant K decreases.

Other values of solubility parameter ϕ and $f = F_s/\phi$ have confirmed those characteristics of second-order surface kinetics. At large times the growth evolves from the surface kinetics controlled stage towards the limiting diffusion controlled regime, regardless of the values of f and ϕ. That transition is shifted to progressively larger times as the kinetic constant K decreases.

Figure 8.10 also illustrates the fact that the actual solutions lay in between the quasi steady-state predictions (equation (8.14)) and growth

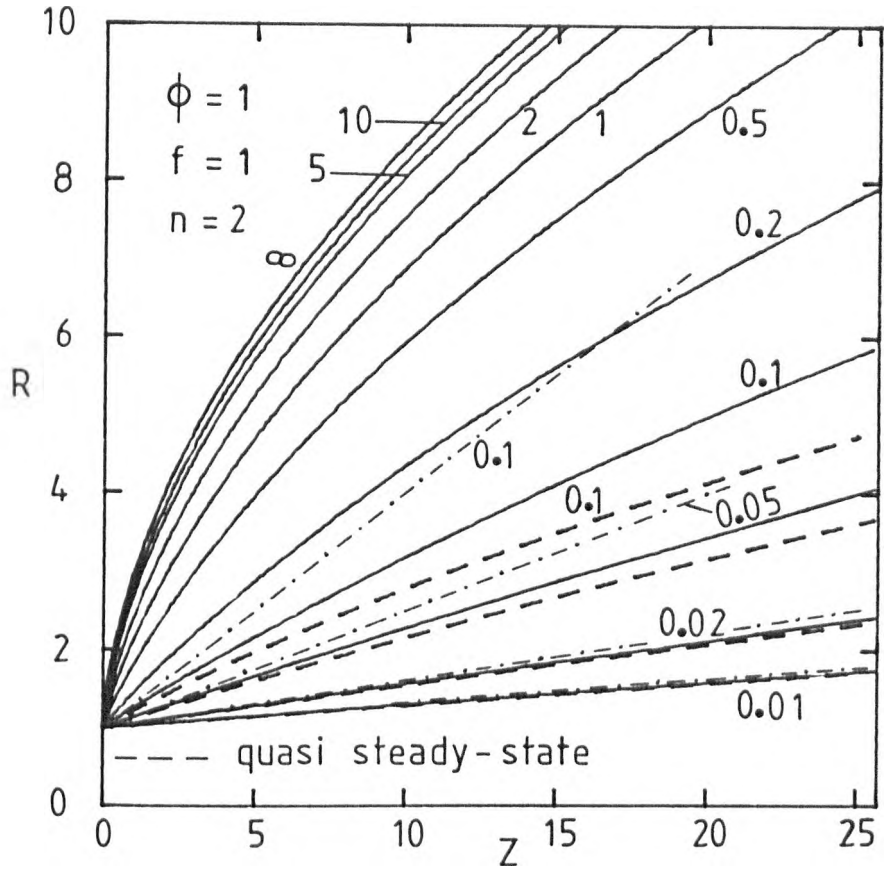

Fig 8.9 : Effect of second-order surface kinetics on growth for the case $\phi = 1$, $f = 1$. The figures show the kinetic constant K. The dashed lines represent the quasi steady-state equation (8.14) and the dotted-dashed lines represent equation (8.19). The symbol (∞) denotes diffusion controlled growth.

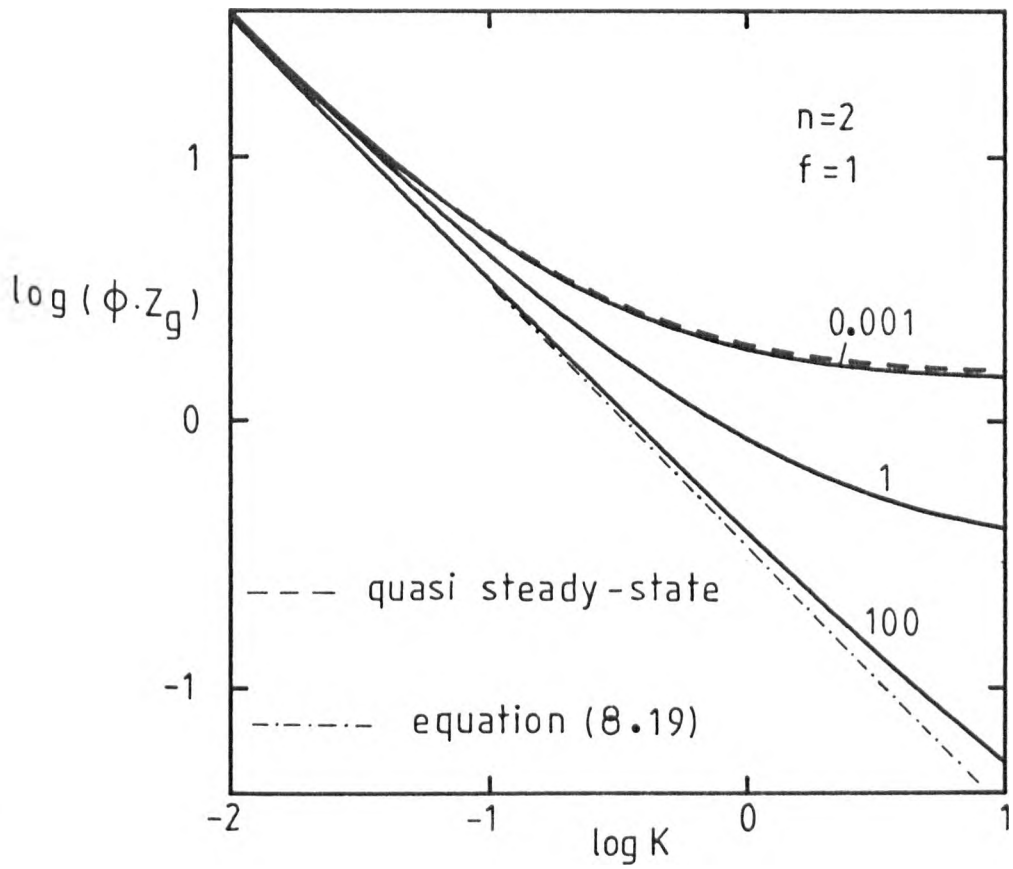

Fig 8.10 : Effect of second-order surface kinetics on the dimensionless time required to double the size of a bubble. The figures show the solubility parameter ϕ. The dashed line represents the quasi steady-state equation (8.14) and the dotted-dashed line represents equation (8.19).

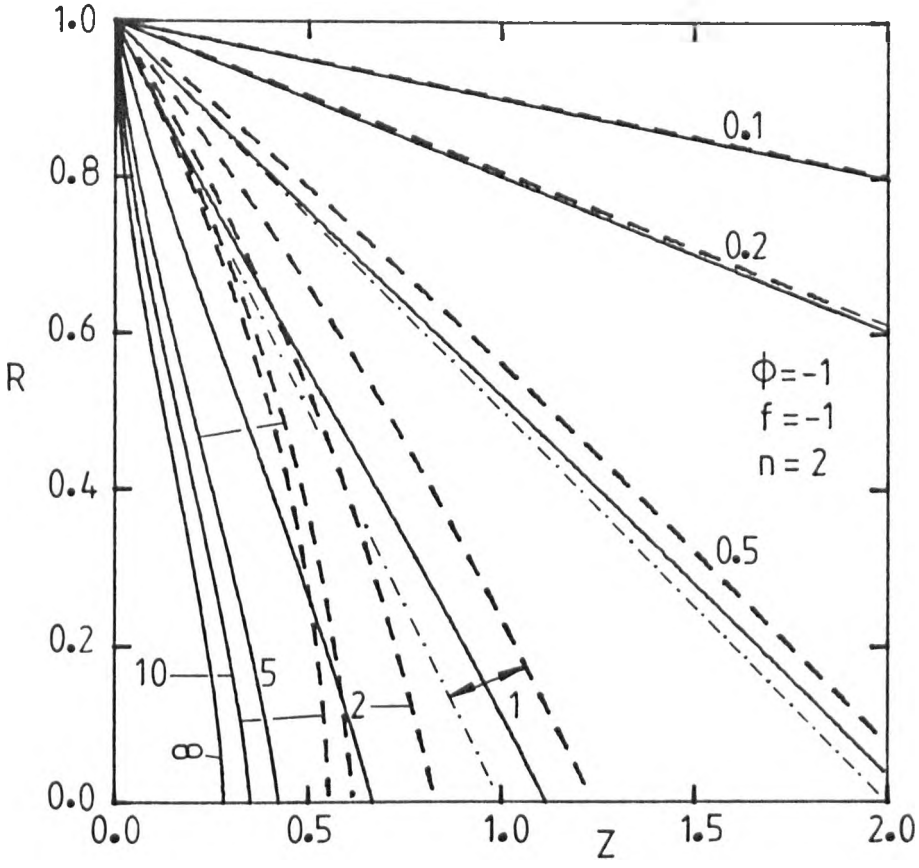

Fig 8.11 : Effect of second-order surface kinetics on dissolution for ϕ = -1, f = - 1. The figures show the kinetic constant K. The dashed lines represent the quasi steady-state equation (8.14) and the dotted-dashed lines represent equation (8.19). The symbol (∞) denotes diffusion controlled dissolution.

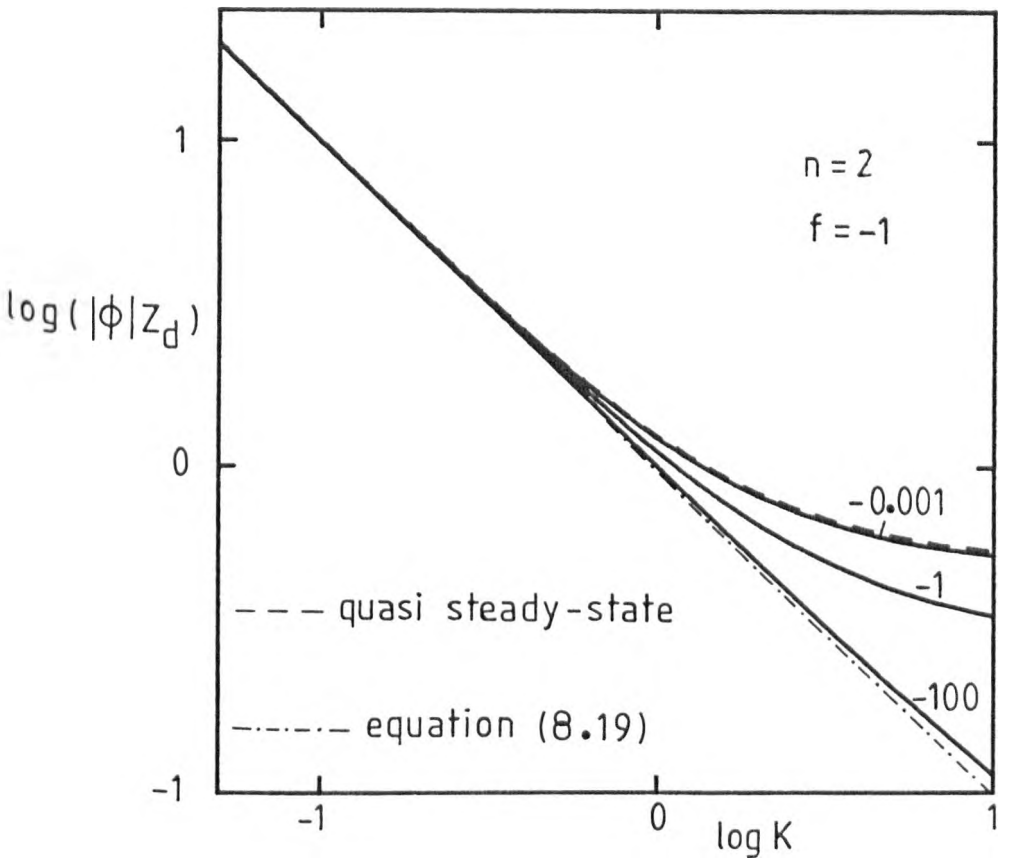

Fig 8.12 : Effect of second-order surface kinetics on the dimensionless time required for complete dissolution. The figures show the values of the solubility parameter ϕ. The dashed line represents the quasi steady-state equation (8.14) and the dotted-dashed line represents equation (8.19).

Table : 8.3

Effect of second order surface kinetics on the time Z_d required for complete dissolution, and on the time Z_g required to double the size of a bubble.

f	1	1	1	-1	-1	-1
ϕ	0.001	1	100	-0.001	-1	-100
K	$\phi.Z_g$			$\|\phi\|.Z_d$		
0.01	35.25	34.79	33.74	100.0	100.0	100.0
0.05	8.48	7.74	6.87	20.02	20.01	20.00
0.1	5.14	4.271	3.485	10.03	10.02	10.01
0.2	3.394	2.458	1.777	5.06	5.04	5.01
0.5	2.289	1.294	0.739	2.144	2.079	2.009
1	1.885	0.866	0.4119	1.233	1.124	1.020
2	1.673	0.628	0.2050	0.823	0.675	0.511
5	1.534	0.4658	0.0922	0.609	0.4317	0.2129
10	1.486	0.4041	0.0524	0.546	0.3582	0.1142
100	1.427	0.3385	0.01168	0.490	0.2904	0.0492

controlled by surface kinetics (equation (8.19)) which represents the limits in the ranges of very low and very large ϕ respectively.

8.6.2 Dissolution

Figure 8.11 shows the progressive enhancement of surface kinetics during dissolution as K decreases. The limiting second-order surface kinetics regime (dashed-dotted lines) is indistinguishable from the actual solutions if $K < 0.2$ and the quasi steady-state approximations (dahsed-lines) are also good in the same range. Dissolution is described by $1-R \propto Z$ if second-order surface kinetics controls the transfer of material.

These conclusions are valid for any value of $\phi < 0$ and the relations between the dimensionless time Z_d required for complete dissolution and K are exemplified in table 8.3 and figure 8.12. Again, the actual solutions lay in between the limiting equations (8.14) and (8.19).

8.7 Conclusions

Reactions with first-order and second-order kinetics at the interface were investigated. If the growth or dissolution are controlled by surface kinetics the radius of the sphere is proportional to time. This process may cover the whole dissolution process but is typically transient during growth in which case the actual solutions converge to the diffusion controlled regime at large times. As the kinetic constant decreases the initial stage of growth controlled by surface kinetics becomes progressively longer. These conclusions are verified independently of the order of surface kinetics.

Quasi steady-state approximations also converge to the surface kinetics controlled regime and become accurate for any value of solubility parameter ϕ, provided K is sufficiently low.

The performance of the finite difference method was again demonstrated by reproducing the exact limiting solutions of the surface kinetics controlled regime. Very wide ranges of solubility parameters $0.001 \ll \phi \ll 1000$; or $-100 \ll \phi \ll -0.001$ were covered to ensure that there is no failure of the method.

CHAPTER IX

Effects of surface tension, viscosity and inertia

9.1 Equation of motion

The changes in volume and mass due to gases dissolved in the liquid can usually be ignored so that changes of gas concentration do not affect the density of the liquid. The liquid is thus considered to have constant and uniform density ρ, be incompressible and of constant viscosity, μ. The hypothesis of constant viscosity may not be strictly true in glass melts, but that assumption is not expected to invalidate significantly the analysis of the present problem.

In these conditions the equation of motion can be written (Bird et al., 1960),

$$\rho \frac{Du}{Dt} = - \text{grad } P + \mu \nabla^2 u + \rho g \tag{9.1}$$

where P is the pressure and g the gravitational acceleration. This equation is known as the Navier-Stokes equation and in conditions of spherical symmetry reduces to

$$\frac{\partial u}{\partial t} + u \frac{\partial u}{\partial r} = - \frac{1}{\rho} \frac{\partial P}{\partial r} - \frac{2\mu}{\rho} \frac{\partial^2 u}{\partial r^2} \tag{9.2}$$

where from equation (2.15), $u = (r/a)^{-2} \frac{da}{dt}$, when $\varepsilon = 1$, (negligible volume contribution of solute). Thus, equation (9.2) can be integrated from the interface $r = a$ to infinity giving rise to

$$P(a) - P_\infty = a\rho \frac{d^2 a}{dt^2} + \frac{3}{2} \rho \left(\frac{da}{dt}\right)^2 + \frac{4\mu}{a} \frac{da}{dt} \tag{9.3}$$

where $P(\infty) = P_\infty$ is considered constant.

In dimensionless terms equation (9.3) can be rewritten so that

$$P(a)/P_\infty = 1 + h\left[R\,\frac{d^2R}{dZ^2} + \frac{3}{2}\left(\frac{dR}{dZ}\right)^2 \right] + \frac{4\eta}{R}\,\frac{dR}{dZ} \qquad (9.4)$$

where $h = \rho.D^2/(a_o^2.P_\infty)$ = inertia parameter

$\eta = \mu.D/(a_o^2.P_\infty)$ = viscosity parameter

and R and Z are defined as usually.

The total gas pressure P_g in the bubble must be obtained by adding the surface tension term to the pressure P(a) in the liquid at the interface so that

$$P_g = P(a) + 2\sigma/a$$

or in dimensionless variables

$$P_g/P_\infty = 1 + 2S/R + h\left[\frac{d^2R}{dZ^2} + \frac{3}{2}\left(\frac{dR}{dZ}\right)^2 \right] + \frac{4\eta}{R}\,\frac{dR}{dZ} \qquad (9.5)$$

where σ denotes the surface tension and the surface tension parameter is

$$S = \sigma/(a_o.P_\infty) \quad .$$

9.2 Rates of growth or dissolution

One-component gas bubbles

If a bubble contains a single ideal gas $C_s \propto P_g$, so that

$$P^* = C_s/C_s^\circ = P_g/P_\infty$$

$$= 1 + 2S/R + h\left[R\,\frac{d^2R}{dZ^2} + \frac{3}{2}\left(\frac{dR}{dZ}\right)^2 \right] + \frac{4\eta}{R}\,\frac{dR}{dZ} \qquad (9.6)$$

where C_s and C_s° are the gas molar concentrations at pressures P_g and P_∞ respectively. Thus, in the absence of effects by surface tension, viscosity or inertia $C_s = C_s^\circ$ and $P^* = 1$.

On assuming Henry's law the concentration of solute at the interface will be

$$C(R) = H\,P_g = H\,P_\infty\,P^* = C^*\,P^*$$
$$= C^*\left[\,1 + 2S/R + h\left(R\,\frac{d^2R}{dZ^2} + \frac{3}{2}\left(\frac{dR}{dZ}\right)^2\right) + \frac{4\eta}{R}\,\frac{dR}{dZ}\,\right] \qquad (9.7)$$

where C^* denotes the solute concentration in equilibrium with gas at pressure P_∞.

In dimensionless form equation (9.7) becomes

$$F(R) = (C(R) - C_\infty)/C_s^\circ = (C^*/C_s^\circ)P^* - C_\infty/C_s^\circ$$
$$= -\phi\left\{1 - q\left[\,2S/R + h\left(R\,\frac{d^2R}{dZ^2} + \frac{3}{2}\left(\frac{dR}{dZ}\right)^2\right) + \frac{4\eta}{R}\,\frac{dR}{dZ}\,\right]\right\} \qquad (9.8a)$$

where

$\phi = (C_\infty - C^*)/C_s^\circ$ = solubility parameter

$q = C^*/(C_\infty - C^*)$ = saturation parameter

$F = (C - C_\infty)/C_s^\circ$.

Occasionally a law of the form $C(R) \propto P_g^{\,x}$ is needed to describe the system which is being considered (in the case of Sievert's law $x = 1/2$). Thus

$$C(R) = C^*(P^*)^x$$

and from equation (9.6)

$$F(R) = -\phi\left(1 + q - q\left[1 + 2S/R + h\left(R\frac{d^2R}{dZ^2} + \frac{3}{2}\left(\frac{dR}{dZ}\right)^2\right) + \frac{4\eta}{R}\right]^x\right)$$

$$= (C^*/C_s^\circ)\,(P^*)^x - \frac{C_\infty}{C_s^\circ} \quad . \tag{9.8b}$$

The ratio $-F(R)/\phi$ is a suitable measure of the relative effects of those non-equilibrium effects on the "driving-force" of the diffusion controlled processes and P* is the corresponding measure of the effects on gas concentration. The actual solutions are here expressed in terms of the dimensionless parameters S, h, η, ϕ, and q.

The number of moles of ideal gas in a bubble can be expressed by

$$N = \frac{4\pi}{3}\,a^3 \cdot C_s = 4\pi a^3 \cdot C_s^\circ \cdot P^*$$

or, in dimensionless terms

$$G = \frac{N}{a_o^3 \cdot C_s^\circ} = \frac{4\pi}{3}\left(R^3 + 2SR^2 + h\left[R^4 \cdot \frac{d^2R}{dZ^2} + \frac{3}{2}R^3\left(\frac{dR}{dZ}\right)^2\right] + 4\eta \cdot R^2 \cdot \frac{dR}{dZ}\right) = \frac{4\pi}{3}R^3 \cdot P^* \quad . \tag{9.9}$$

Also from equation (2.48)

$$\frac{dG}{dZ} = 4\pi R^2\left(\frac{\partial F}{\partial e}\right)_R = 4\pi R\left(\frac{\partial F}{\partial x}\right)_{x=1} \tag{9.10}$$

where $x = e/R$. Thus, from equations (9.9) and (9.10)

$$\frac{dR}{dZ}\left(R + \frac{4}{3}S\right) + \frac{4\eta}{3}\left[2\left(\frac{dR}{dZ}\right)^2 + R\frac{d^2R}{dZ^2}\right] + h\left[\frac{3}{2}R\left(\frac{dR}{dZ}\right)^3 + \frac{7}{3}R^2 \cdot \frac{dR}{dZ}\frac{d^2R}{dZ^2} + \frac{R^3}{3}\frac{d^3R}{dZ^3}\right]$$

$$= \left(\frac{\partial F}{\partial x}\right)_{x=1} \quad . \tag{9.11}$$

The non-equilibrium effects of viscosity and inertia become effective only as material starts to be transferred between the bubble and the liquid medium. Therefore

$$P^*(O) = 1 + 2S \quad . \tag{9.12}$$

when $Z = O$; and $R = 1$. Thus, if $\eta \neq O$

$$\left(\frac{dR}{dZ}\right) = O \quad ; \quad Z = O \tag{9.13}$$

and if $h \neq O$

$$\left(\frac{dR}{dZ}\right) = O \ , \qquad \frac{d^2R}{dZ^2} = O \quad ; \quad Z = O \ . \tag{9.14}$$

For one-component bubbles $\varepsilon = 1$, and the general material balance (equation (2.28)) reduces to

$$\frac{\partial^2 F}{\partial e^2} + \left[\frac{2}{e} - \left(\frac{dR}{dZ}\right)\left(\frac{R}{e}\right)^2 \right] \frac{\partial F}{\partial e} = \frac{\partial F}{\partial Z} \quad . \tag{9.15}$$

9.3 Solution of material balances

Surface tension has been the most commonly studied among these factors. Quasi stationary approximations were proposed by Epstein and Plesset (1950) and Cable (1961a) among other authors. Some approximate solutions of bubble growth were derived on assuming thin boundary layers (Plesset and Zwick, 1954; Barlow and Langlois, 1962), or on assuming arbitrary functional forms of concentration profiles while satisfying the overall material conservation (Rosner and Epstein, 1972). This second class of solutions was derived for the general case, while only the surface tension was included in the quasi-stationary approximations.

Numerical techniques were also used to solve the material balances with inclusion of surface tension alone (Weinberg, 1980) or simultaneous inclusion

of surface tension, viscosity and inertia terms (Szekely and co-authors, 1971 and 1973). However the technique proposed by Szekely and co-authors may require undue numbers of time steps to solve processes with low or moderate rates of growth or dissolution (as discussed in Chapter III). Weinberg's method reduces basically to the finite difference method of Duda and Vrentas (1969) which was not conceived to optimize the mesh sizes. Very few examples were shown in Weinberg's work so that the efficiency of that method was not demonstrated especially in extreme conditions.

Minor modifications were added to the finite difference method described in Chapter III to extend its use to the actual class of problems (see appendix 6).

Quasi-steady state approximations were also derived in this work and their range of applicability was established.

9.4 Quasi steady state approximations

Effect of surface tension in the case of Henry's law

If both viscous and inertia effects are ignored equations (9.6), (9.8a) and (9.11) reduce to

$$p^* = 1 + 2S/R\,, \tag{9.16}$$

$$F(R) = -\phi\,(1 - 2Sq/R)\,, \tag{9.17}$$

$$\left(\frac{\partial F}{\partial e}\right)_{e=R} = \left(1 + \frac{4}{3}\frac{S}{R}\right)\frac{dR}{dZ}\,. \tag{9.18}$$

By integration of the quasi steady-state simplification (equation (2.67)) with boundary conditions, $F(\infty) = 0$, one obtains

$$\left(\frac{\partial F}{\partial e}\right)_R = -F(R)/R\,, \tag{9.19}$$

and upon combination of equations (9.17), (9.18) and (9.19)

$$\frac{[R + (4/3)S]R}{R - 2Sq}\frac{dR}{dZ} = \phi \tag{9.20}$$

which can be solved analytically on making the transformation $W = R - 2Sq$.

$$\frac{1}{2}\left[(R - 2Sq)^2 - (1 - 2Sq)^2\right] + 4(R-1)S(q + \frac{1}{3})$$

$$+ 2S^2 \cdot q(2q + \frac{4}{3})\ln\left(\frac{R - 2Sq}{1 - 2Sq}\right) = \phi Z \tag{9.21}$$

This quasi steady state simplification suggests a unique dependence on the transformed time (ϕZ). It will be shown that such quasi steady-state approximations are the limit of actual solutions for growth or dissolution for very low solubility parameters $|\phi|$.

9.5 Physical properties of glass melts and common values of the dimensionless parameters S, h, η

Typical values of density and surface tension of glass melts are often of the order of magnitude of $\rho = 2.3 \times 10^3$ Kg m^{-3} and $\sigma = 300$ dyne $cm^{-1} = 0.3$ N m^{-1}. The viscosity of the melt and the diffusivity of gases in glass melts are very dependent on the temperature and also significantly dependent on the composition of the melt, with common values in the ranges 10-1000 Kg m^{-1} s^{-1} for viscosity and $10^{-11} - 10^{-9}$ m^2 s^{-1} for diffusivity. These values were used to construct table 9.1 with ambient pressure 10^5 N m^{-2}.

Table 9.1

Common values of dimensionless parameters S, η and h in glass melts.

a_o (m)	$10^{10} . D_1$ ($m^2\ s^{-1}$)	μ (Kg $m^{-1}\ s^{-1}$)	S	$10^6 . \eta$	$10^{15} . h$
10^{-5}	1	10	0.3	100	2300
10^{-4}	1	10	0.03	1	23
10^{-3}	1	10	0.003	0.01	0.23
10^{-3}	0.1	10	0.003	0.001	0.0023
10^{-3}	10	10	0.003	0.1	23
10^{-4}	10	10	0.03	10	2300
10^{-3}	1	1	0.003	0.001	0.23
10^{-3}	1	100	0.003	0.1	0.23
10^{-3}	1	1000	0.003	1	0.23
10^{-4}	10	1000	0.03	1000	2300

It will be shown that with h in the range of table 9.1 inertia can always be ignored, even in the range of very large solubility parameters (including solutions up to $|\phi| = 100$). The effects of viscosity are also very dependent on the value of ϕ but can also be ignored except with very large $|\phi|$.

The effects of surface tension are enhanced as the dissolution of bubbles proceeds but decrease in the case of growing bubbles. This is a consequence of the effect of surface tension being dependent on the bubble size but not on the rate of the process. The relative effects of surface tension on the rates of the processes are also much less dependent on the solubility parameter than the relative effects of viscosity or inertia. This finding is easily understood taking into account that ϕ is a convenient representation of the range of rates of growth or dissolution, which affect the role of viscosity and inertia but not the role of surface tension.

9.6 Effects of surface tension on growth or dissolution of bubbles

In this section the viscous and inertial effects are ignored ($\eta = 0$; $h = 0$) to investigate the role of surface tension on the growth or dissolution of bubbles. Henry's law is generally assumed so that the interfacial concentration is given by equation (9.17).

9.6.1 Case A) $\phi < 0$

If $\phi < 0$, $C_\infty < C^*$ and $q = C^*/(C_\infty - C^*) \leq -1$, and from equation (9.8a) $F(R) > |\phi|$, that is the "driving force" is always enhanced from the beginning and relative to the case when the role of surface tension is negligible. Simultaneously the initial gas pressure increases by a factor $P^* = 1 + 2S$ (equation (9.16)) due to surface tension. If Henry's law is valid the effect of surface tension on the interfacial concentration (equation (9.17)) always exceeds the effect on the initial gas pressure in what concerns the rate of bubble contraction. On the contrary, this situation may not occur if Sievert's law applies (equation (9.8b) and this is due to the fact that the interfacial concentration increases less rapidly with decreasing radius when $C(R) \propto p_g^{1/2}$.

There is a dual effect of surface tension on the rate of contraction $\left(\frac{dR}{dz}\right)$ of dissolving bubbles, the first due to a progressive increase of interfacial concentration (and consequently the increase of "driving force") and the second due to the increase of gas pressure as the bubble size decreases. The effect on the interfacial concentration modifies the concentration profiles, especially near the interface, and opposes the effect of solute accumulation which was found to be severe during the last stage of dissolution with large $|\phi|$ and negligible surface tension (Chapter V). Accumulation was then responsible for a relatively slow final stage which accounted for most of the total dissolution time. Increasing the interfacial

concentration as the radius decreases (due to surface tension) keeps the concentration profile steep near the interface and enhances the dissolution rate at the stage when the dissolution rate was lower in the case of negligible surface tension. The effect of surface tension on pressure in bubble increases $\left(\frac{dR}{dZ}\right)$ as R tends to zero. Taken together both factors may cause the total dissolution time to be significantly reduced due to effects of moderate values of surface tension ($S < 0.1$).

In the range of very low $|\phi|$ the dissolution tends to quasi steady-state and the dissolution rate increases continuously after a very short initial stage (Chapter V). Thus the effect of surface tension is enhanced during the most rapid stage and the total time Z_d, required for complete dissolution, decreases by a much smaller fraction than in the case of high $|\phi|$.

These trends are clearly shown in figures 9.1 and 9.2 where Z_o denotes the time required for complete dissolution with negligible surface tension ($S = 0$). As $|\phi|$ decreases the actual finite difference predictions (full lines) approach the quasi steady-state predictions (equation (9.21)) represented by the dashed lines.

If $S < 0.1$, increasing the surface tension parameter with constant saturation parameter, $q = -1$, has important effects on the dissolution time. Further increases of surface tension, (especially if $S > 0.2$) cause much smaller decreases of dissolution time probably because the gas pressure and molar content of a bubble with reference radius a_o increases and compensates more efficiently for the increase of interfacial concentration with increasing S.

On the contrary, increasing $|q|$ with $S = 0.1$ enhances the "driving-force", but the initial content of the bubble with radius a_o remains the same in all cases. Therefore the dissolution time always decreases significantly as the absolute numerical value of the saturation parameter $|q|$ increases.

Table : 9.2

Effect of surface tension on the time required for complete dissolution of bubbles, for low and moderate $|\phi|$. Viscous and inertial effects are ignored ($\eta = 0$, $h = 0$). The symbol * denotes quasi steady-state approximations, (equation (9.21)).

S	$-\phi$	*	0.001	0.01	0.1	1
	-q	$\|\phi\|$ Z_d				
0	1	0.500	0.486	0.462	0.3994	0.2828
0.001	1	0.4993	0.485	0.461	0.3975	0.2799
0.01	1	0.4939	0.480	0.455	0.3900	0.2628
0.05	1	0.4747	0.4610	0.4335	0.3620	0.2240
0.1	1	0.4572	0.4423	0.4139	0.3392	0.1995
0.2	1	0.4335	0.4181	0.3885	0.3116	0.1715
0.3	1	0.4177	0.4022	0.3720	0.2943	0.1558
0.5	1	0.3977	0.3820	0.3514	0.2733	0.1383
0.7	1	0.3855	0.3697	0.3389	0.2610	0.1287
1	1	0.3740	0.3582	0.3273	0.2496	0.1203
0.1	1.25	0.4300	0.4155	0.3871	0.3144	0.1776
0.1	1.5	0.4067	0.3921	0.3640	0.2912	0.1591
0.1	2	0.3670	0.3527	0.3252	0.2549	0.1313
0.1	2.5	0.3347	0.3208	0.2939	0.2261	0.1108
0.1	3	0.3080	0.2945	0.2682	0.2028	0.0951
0.1	4	0.2658	0.2530	0.2280	0.1673	0.0725
0.1	5	0.2341	0.2218	0.1980	0.1414	0.0573

Table : 9.3

Effect of surface tension on the time required for complete dissolution of bubbles with moderate and large $|\phi|$. Viscous and inertial effects are ignored ($\eta = 0$; $h = 0$).

	$-\phi$	1	10	100
S	-q		$\phi^2 z_d$	
0.0	1	0.2828	1.599	8.14
0.001	1	0.2799	1.466	4.70
0.01	1	0.2628	1.125	2.197
0.05	1	0.2240	0.736	1.063
0.1	1	0.1995	0.570	0.750
0.2	1	0.1715	0.4301	0.531
0.3	1	0.1558	0.3651	0.439
0.5	1	0.1383	0.3025	0.3545
0.7	1	0.1287	0.2716	0.3143
1.0	1	0.1203	0.2462	0.2820
0.1	1.25	0.1776	0.4718	0.598
0.1	1.5	0.1591	0.3994	0.493
0.1	2	0.1313	0.2997	0.3557
0.1	2.5	0.1108	0.2346	0.2716
0.1	3	0.0951	0.1896	0.2152
0.1	4	0.0725	0.1320	0.1460
0.1	5	0.0573	0.0974	0.1062

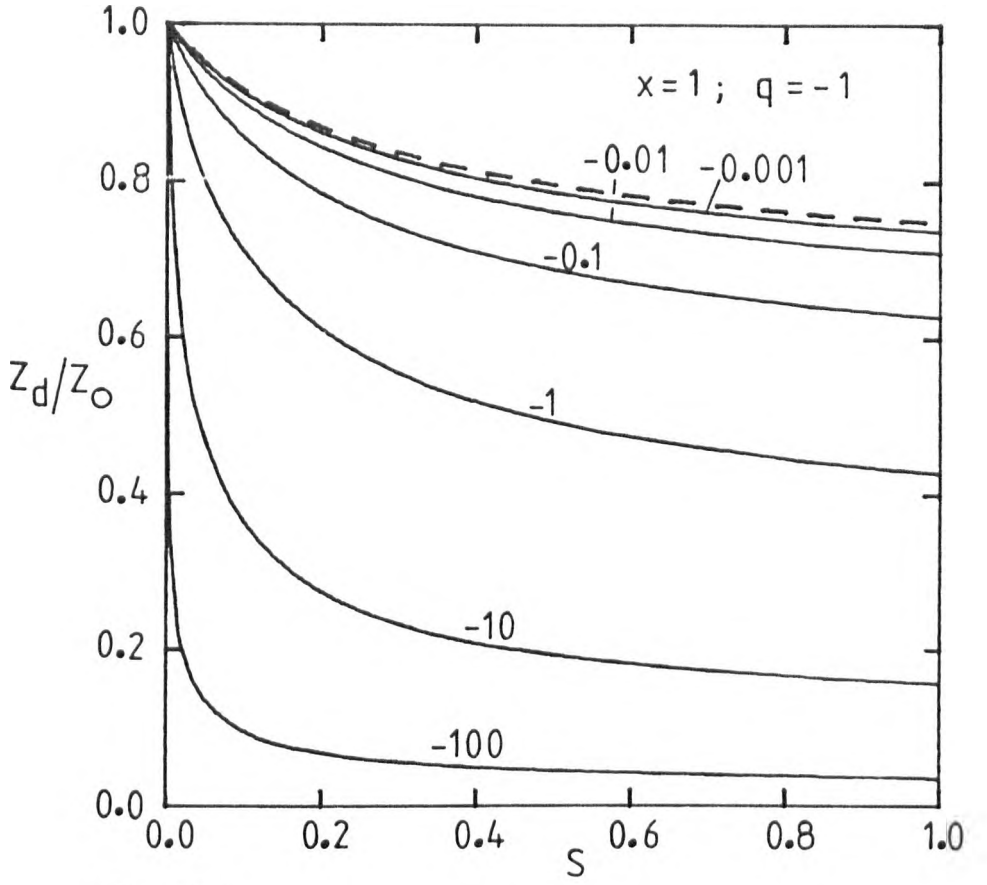

Fig 9.1

Figs 9.1 and 9.2 : Effect of surface tension on the dimensionless time required for complete dissolution of bubbles. The numbers show the values of ϕ.

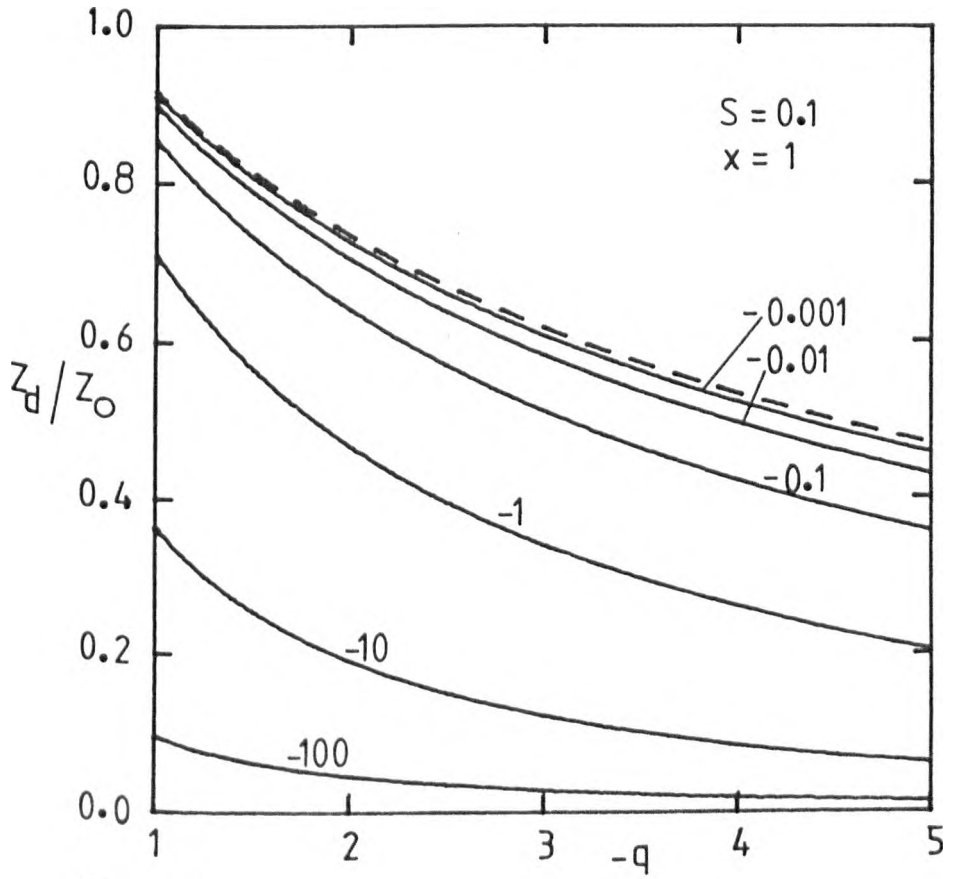

Fig 9.2

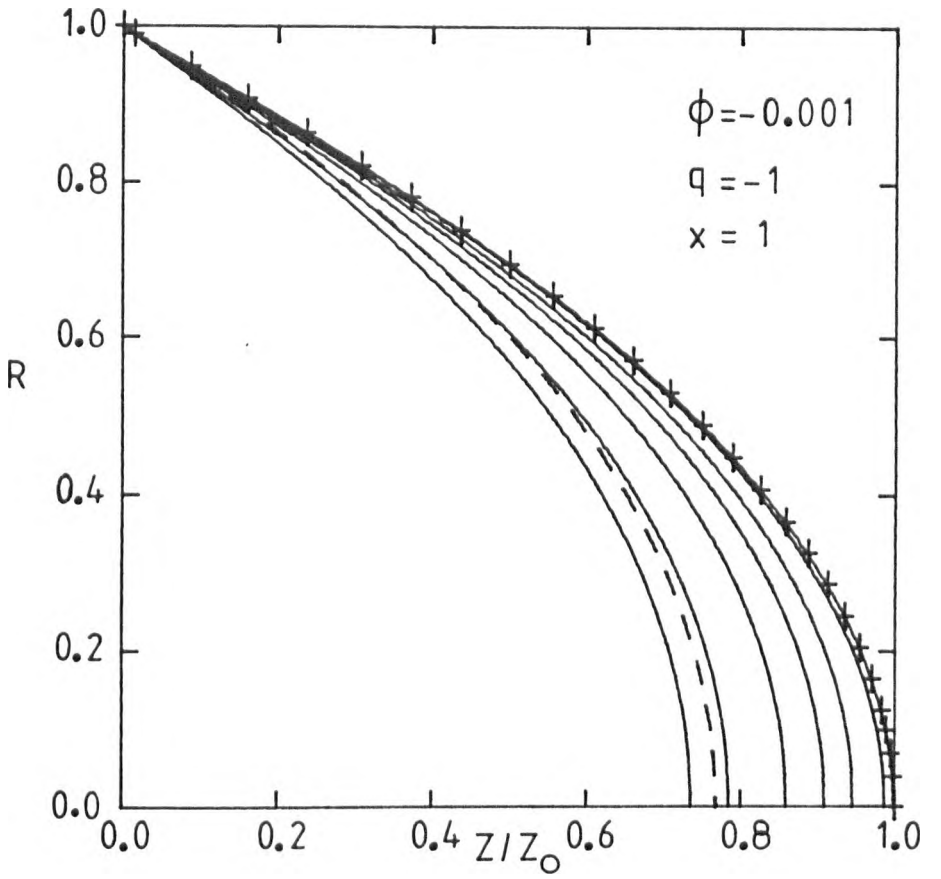

Fig. 9.3 : Effect of surface tension during dissolution of a bubble with very low $|\phi|$. The dashed line represents the quasi steady-state solution of equation (9.21) for the case S=1; q = -1. The full lines represent from right to left S = 0.001, 0.01, 0.05, 0.1, 0.2, 0.5 and 1.

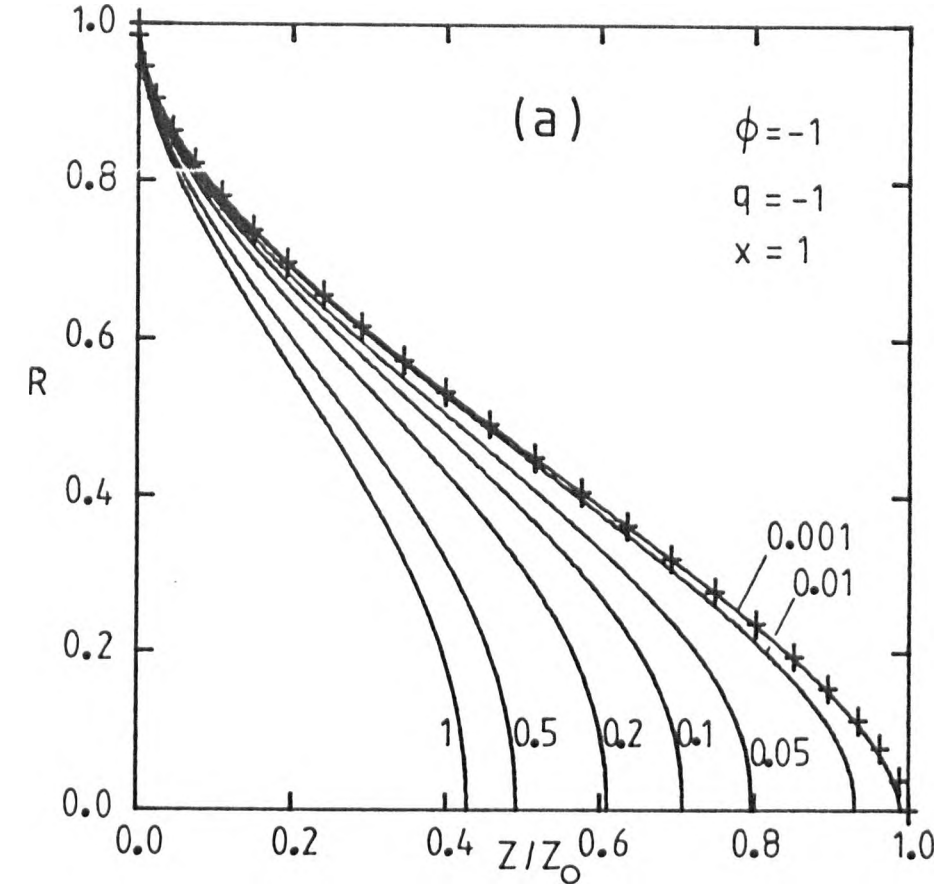

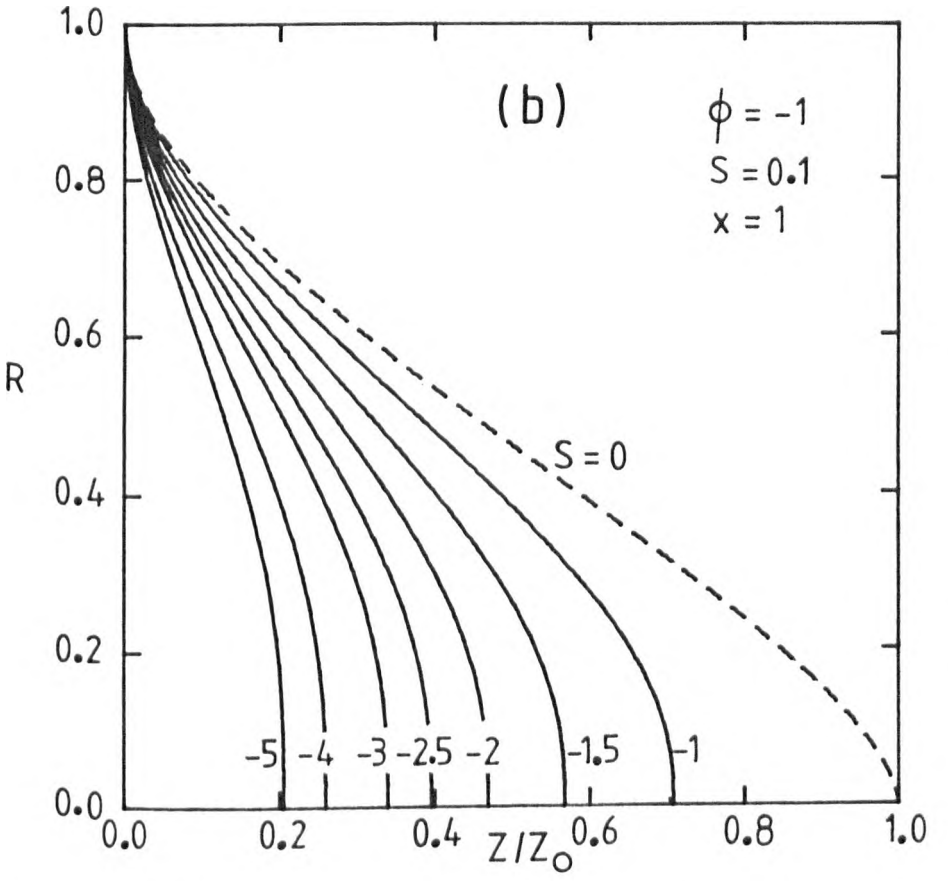

Figs 9.4 : Effects of surface tension during dissolution of a bubble with a moderate value of $|\phi|$. The symbols + and the dashed line represent the case S=0. The numbers show the values of S in figure 9.4a and q in figure 9.4b.

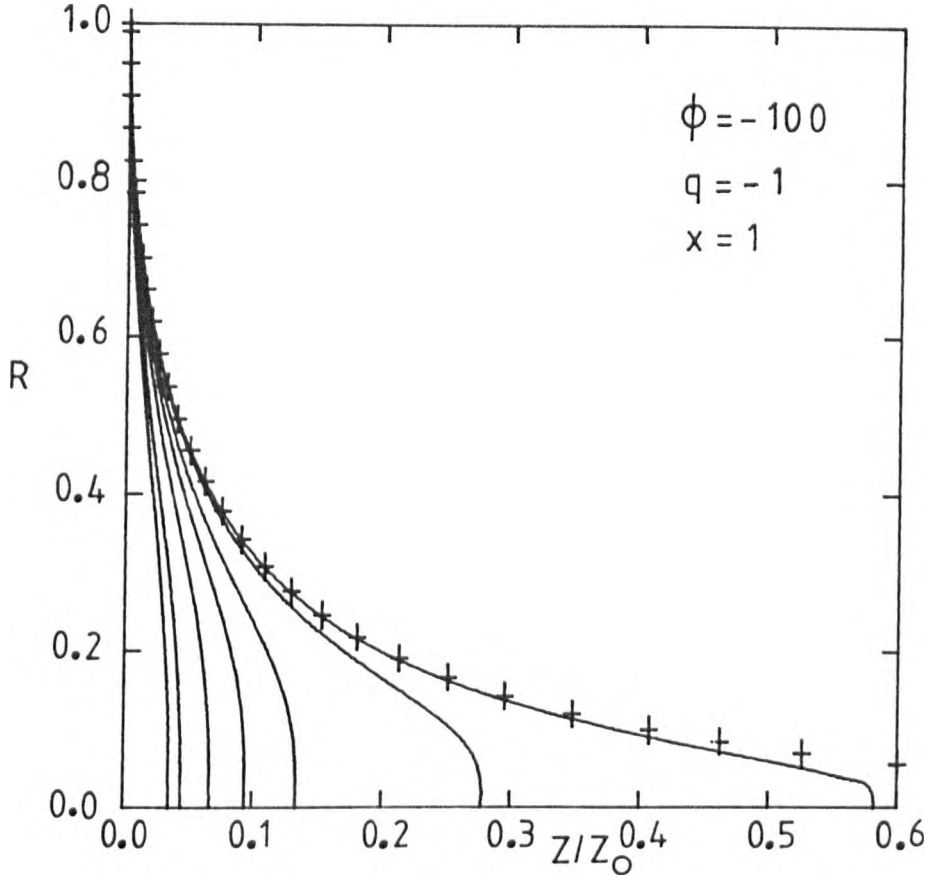

Fig. 9.5 : Effect of surface tension during dissolution of a bubble with very large $|\phi|$. The symbols represent the case S=0. The curves represent from right to left S = 0.001, 0.01, 0.05, 0.1, 0.2, 0.5 and 1.

The quasi steady-state solutions (equation (9.21)) suggest a unique solution in terms of the transformed time $|\phi|z$, and this was used to organize the results for dissolution times shown in table 9.2 (in the range of very low to moderate solubility parameters $|\phi|$). That representation is reasonable with $|\phi| < 0.01$ and low or moderate S, but becomes progressively poorer as both $|\phi|$ and S increase.

The enhanced effect of surface tension with increasing value of S is illustrated in figures 9.3, 9.4a and 9.5. In figure 9.3 the dashed line represents the quasi steady-state solutions of the case $S = 1$; $q = -1$ and is slightly poorer approximation to the real solutions than in the case of negligible surface tension. If $q = -1$ and $S < 0.01$ the effects of surface tension on bubble dissolution can be ignored with $|\phi| < 0.1$ but are significant for moderate and large $|\phi|$, $(-\phi > 1)$.

With $\phi = -100$ values of surface tension parameter as low as $S = 0.001$ are only effective during the final stage but are responsible for a reduction of about 42% of the original dissolution time (figure 9.5). These results are a good illustration that for large values of $|\phi|$ the role of surface tension is enhanced, speeding up the final stage.

Figure 9.4b shows that for a constant value of S the rate of dissolution is greatly enhanced as the absolute numerical value of the saturation parameter $|q|$ increases. Therefore relatively small values of surface tension parameter should not be ignored if $|q|$ is large.

9.6.2 Effect of surface tension on the concentration profiles during dissolution

The solution of the quasi steady state approximation (equation (2.67)) with interfacial concentration given by equation (9.17) leads to

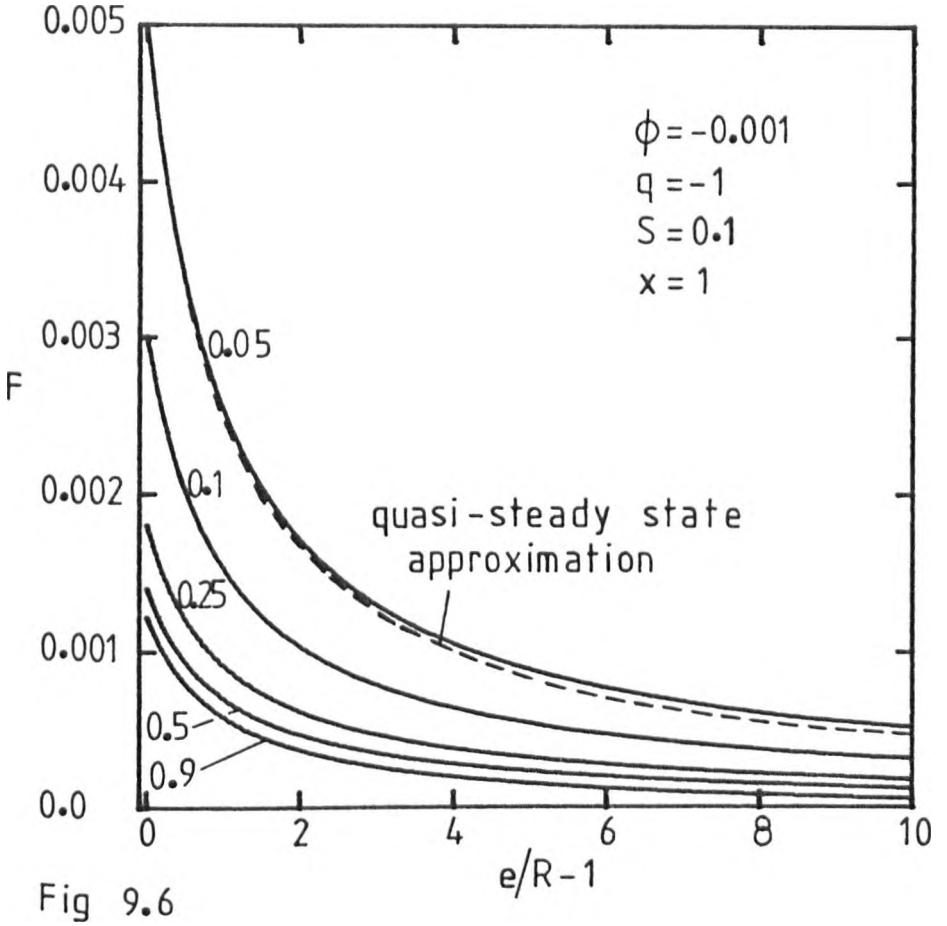

Fig 9.6

Figs 9.6, 9.7 and 9.8 : Concentration profiles in the liquid medium surrounding dissolving bubbles. The numbers show the values of R. The dashed line in figure 9.6 represents the quasi steady-state approximation, (equation (9.22)), for the case R = 0.05.

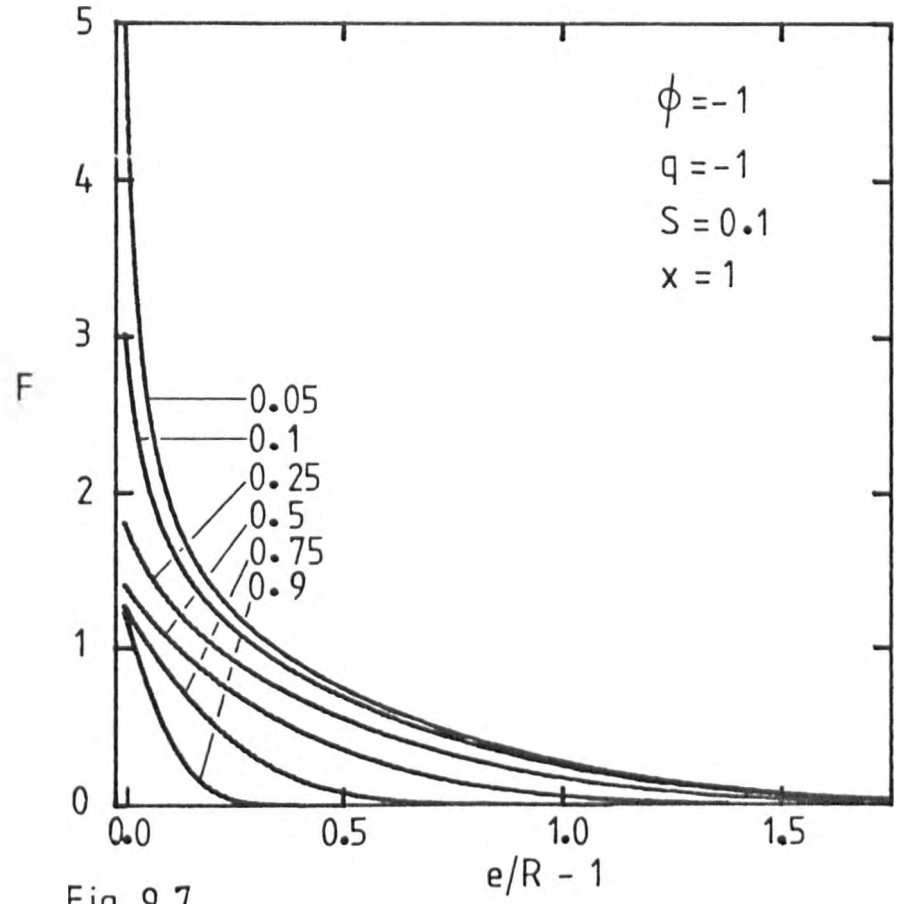
5
4
3
2
1
0
F
$\phi = -1$
q = -1
S = 0.1
x = 1
0.05
0.1
0.25
0.5
0.75
0.9
0.0
0.5
1.0
1.5
e/R - 1

Fig 9.7

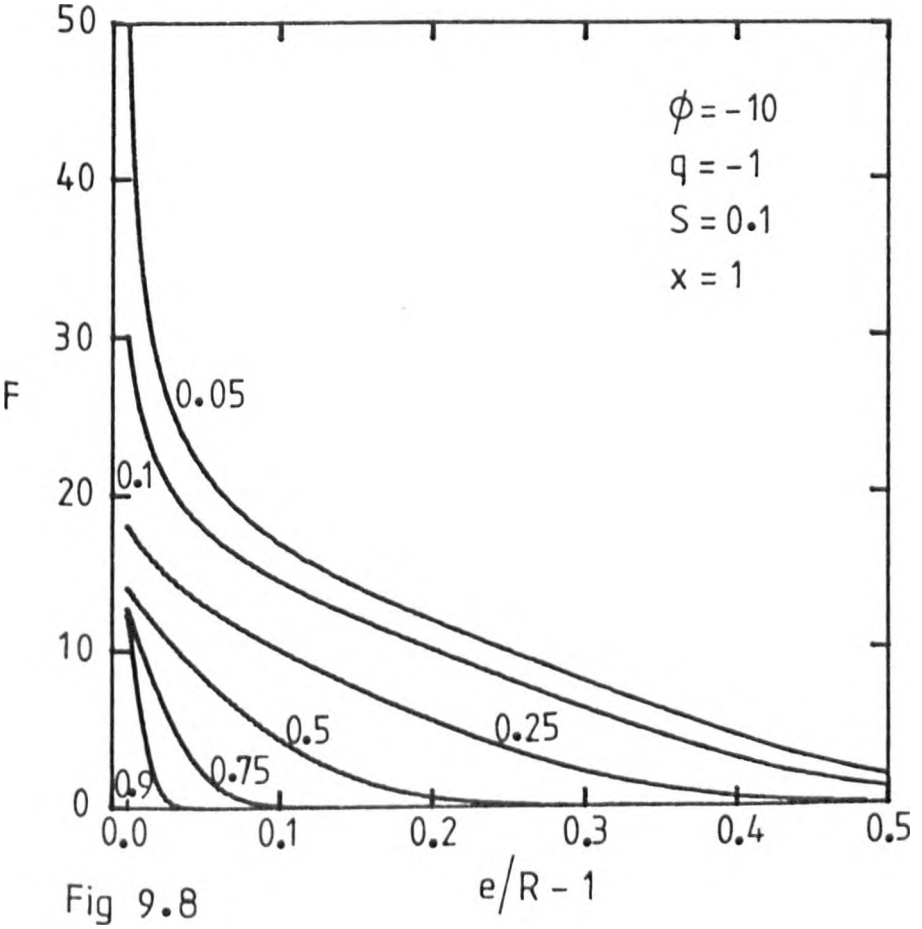
50
40
30
20
10
0
F
$\phi = -10$
q = -1
S = 0.1
x = 1
0.05
0.1
0.25
0.5
0.75
0.9
0.0
0.1
0.2
0.3
0.4
0.5
e/R - 1

Fig 9.8

$$F(e/R) = - \phi \ (1-2q\ S/R) \ (R/e) \ . \qquad (9.22)$$

Figure 9.6 illustrates concentration profiles for the case $\phi = -0.001$, $S = 0.1$, and $q = -1$, at different stages of dissolution. The dashed line represents the quasi steady-state prediction for the case $R = 0.05$ and is close to the actual finite difference prediction for the same radius. Thus, once more the quasi steady-state solutions provide a reasonable quantification of profiles for very low $|\phi|$.

Figures 9.7 and 9.8 illustrate the effects of surface tension on the dissolution with moderate and large $|\phi|$. During the initial and intermediate stages the interfacial concentration increases relatively slowly, so that the shape of the concentration profile is being adjusted by diffusion. However, during the final stage F(R) increases very rapidly and this change cannot be compensated by diffusion throughout the intermediate region of the concentration profile. Therefore the concentration profile becomes steep near the interface which explains the enhancement of dissolution during the final stage.

9.6.3 Case B) $\phi > 0$

For growth to occur $C(R) < C_\infty$ or $F(R) < 0$. Thus, if viscous and inertial effects are ignored,

$$F(R) = - \phi \ (1 - 2Sq/R) < 0 \ ,$$

with $\phi > 0$; and $q > 0$, so that the bubble starts growing ($R > 1$) if

$$S.q < 1/2 \ ,$$

and growth will continue because the effects of surface tension decrease progressively as the size of the bubble increases. On the contrary, dissolution occurs if

$$S\,q > 1/2 \ ,$$

and in these conditions dissolution will proceed with increasing "driving-force" F(R), (due to decreasing radius), until complete dissolution. If $S.q = 1/2$ the bubble is in equilibrium and will not change radius because the interfacial concentration equals the bulk solute concentration. However, a minor deviation from the equilibrium condition $S.q = 1/2$, (due to a small increase or decrease of bubble radius), leads to permanent growth or permanent dissolution.

These characteristics of bubble behaviour are illustrated in figures 9.9 and 9.10. In figure 9.9 the effect of increasing the surface tension parameter S, with constant saturation parameter $q = 1$, can be achieved by changing the initial radius of the bubble. This is an important illustration of the different rates of growth or dissolution in a dispersion of bubbles with a distribution of sizes. Bubbles of radius $a_o < a_{min} = 2\sigma q/P_\infty = 2\sigma/[P_\infty(C_\infty/C^* - 1)]$ will dissolve and the rate of dissolution will increase with decreasing initial radius a_o. On the contrary if $a_o > a_{min}$ the bubbles will grow at a rate which increases with a_o.

Near the point $S\,q = 1/2$ both growth and dissolution are very slow, but the rates are progressively enhanced as the bubble radius increases or decreases. In both cases $|F(R)|$ increases as the radius of the bubble departs from a_{min}.

Figure 9.10 demonstrates that convenient changes of saturation parameter q lead to bubble behaviour which is qualitatively similar to that of a dispersion of bubbles whose radii are distributed about the equilibrium size $a = 2\sigma/\left[P_\infty\left(\frac{C_\infty}{C^*} - 1\right) \right]$. However, the examples illustrated in figure 9.10 represent bubbles in media of different concentrations, or bubbles in different subregions of a larger inhomogeneous medium.

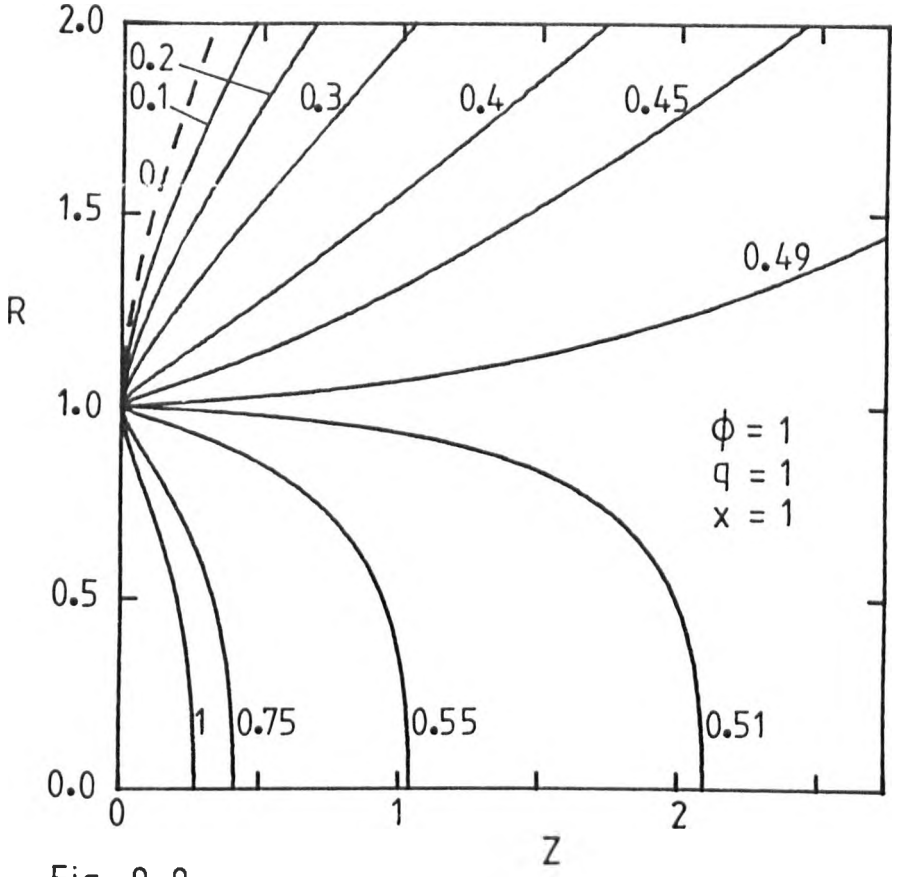

Fig 9.9

Figs 9.9 and 9.10 : Effect of surface tension for $\phi > 0$. The dashed lines represent the case S=0. The numbers show the values of

a) S in figure 9.9

b) q in figure 9.10.

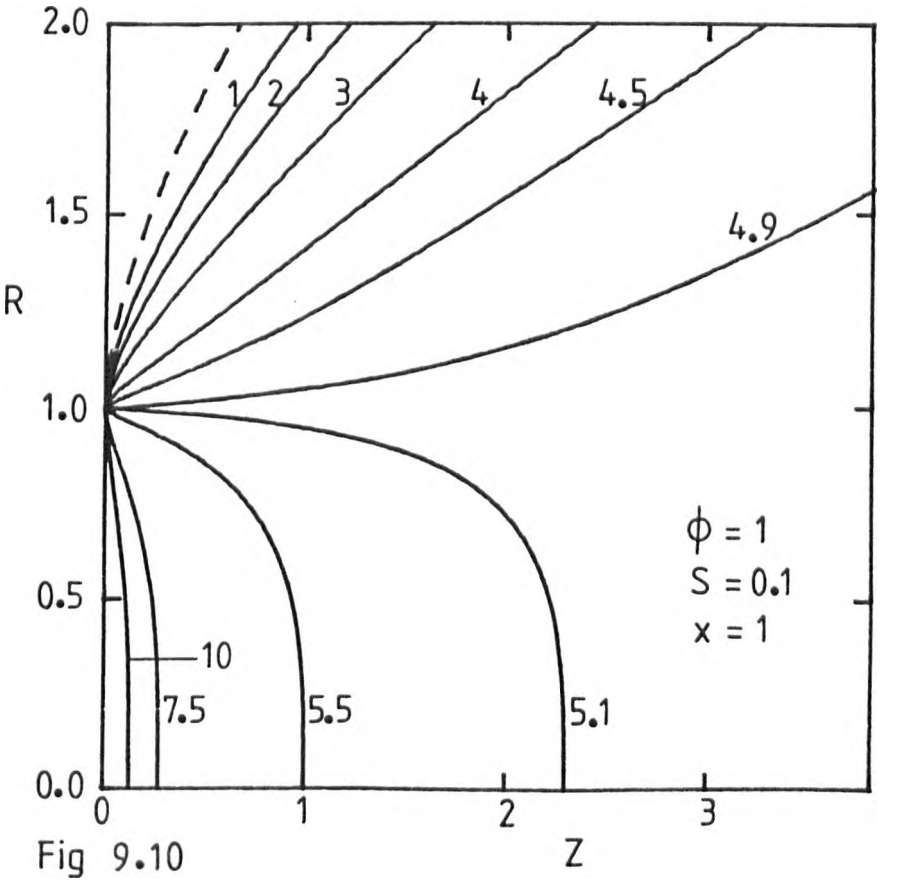

Fig 9.10

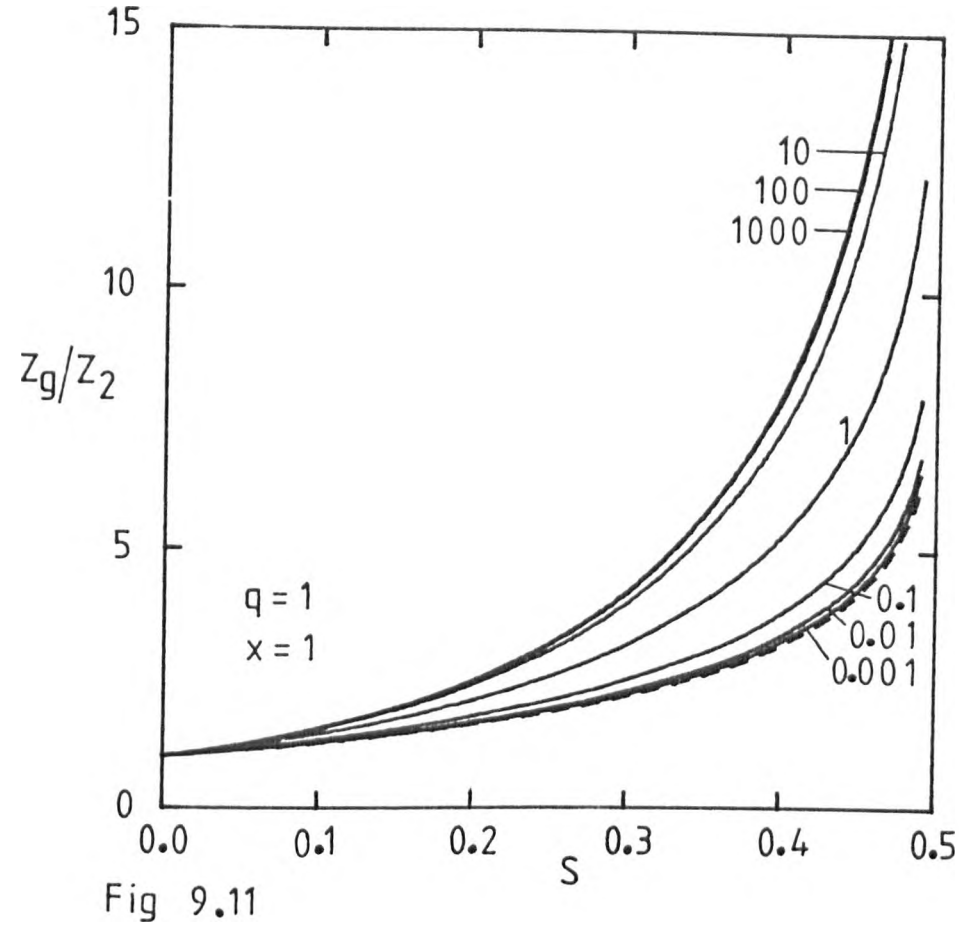

Fig 9.11

Figs 9.11 and 9.12 : Effect of surface tension on the dimensionless time required to double the size of bubbles. The numbers show the values of ϕ.

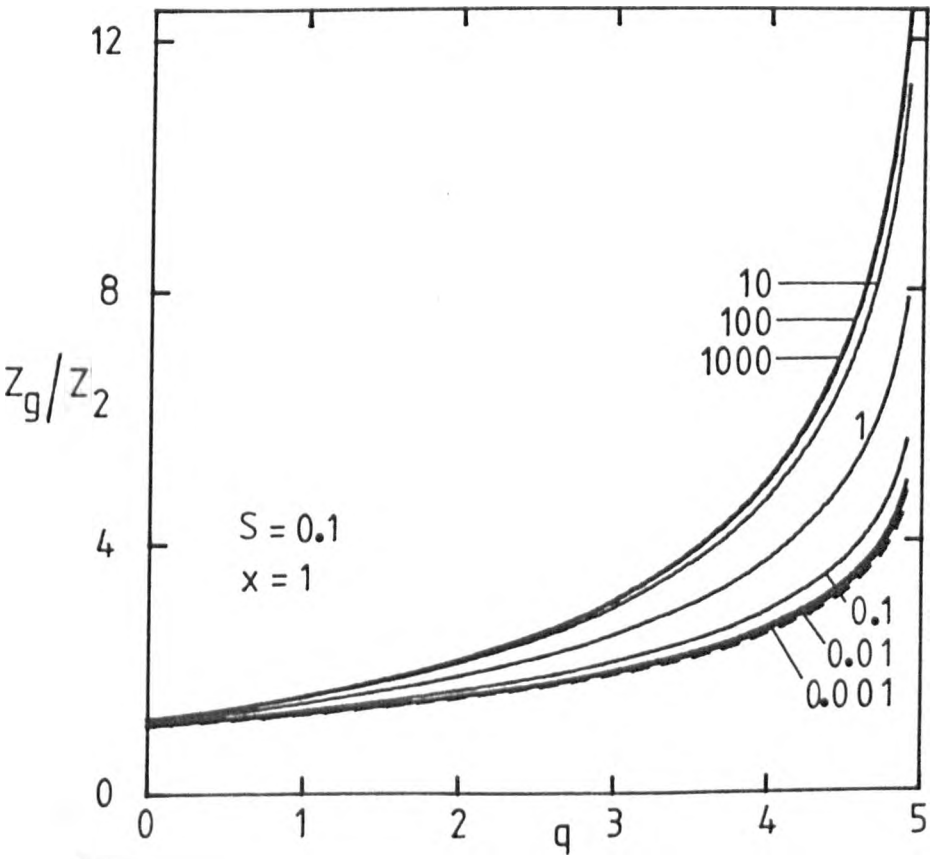

Fig 9.12

Table : 9.4

Effects of surface tension on the dimensionless time Z_g required to double the size of bubbles for low and moderate solubility parameter ϕ . The quasi steady-state (equation (9.21)) is denoted by the symbol * .

	ϕ	*	0.001	0.01	0.1	1
S	q	ϕZ_g				
0.0	1	1.500	1.425	1.281	0.905	0.3294
0.1	1	1.887	1.802	1.634	1.194	0.4714
0.2	1	2.428	2.331	2.133	1.606	0.687
0.3	1	3.252	3.137	2.897	2.245	1.041
0.4	1	4.745	4.604	4.288	3.420	1.727
0.45	1	6.24	6.08	5.69	4.607	2.439
0.475	1	7.66	7.53	7.07	5.78	3.150
0.49	1	9.43	9.42	8.87	7.32	4.07
0.1	0	1.633	1.556	1.403	1.010	0.3807
0.1	2	2.243	2.148	1.958	1.457	0.604
0.1	3	2.785	2.676	2.453	1.861	0.816
0.1	4	3.771	3.639	3.359	2.604	1.217
0.1	4.5	4.763	4.613	4.275	3.357	1.632
0.1	4.75	5.72	5.59	5.19	4.112	2.048
0.1	4.9	6.90	6.88	6.41	5.13	2.626

Table : 9.5

Effects of surface tension on the dimensionless time required to double the size of bubbles in the ranges of moderate to very large ϕ.

	ϕ	1	10	100	1000
S	q	$\phi^2 Z_g$			
0.0	1	0.3294	0.4888	0.5161	0.5186
0.1	1	0.4714	0.745	0.796	0.801
0.2	1	0.687	1.168	1.266	1.277
0.3	1	1.041	1.930	2.136	2.160
0.4	1	1.727	3.568	4.071	4.131
0.45	1	2.439	5.41	6.32	6.43
0.475	1	3.150	7.31	8.69	8.86
0.49	1	4.07	9.87	11.90	12.20
0.1	0	0.3807	0.580	0.615	0.619
0.1	2	0.604	0.998	1.075	1.084
0.1	3	0.814	1.424	1.553	1.568
0.1	4	1.217	2.290	2.545	2.574
0.1	4.5	1.632	3.232	3.647	3.695
0.1	4.75	2.048	4.205	4.80	4.87
0.1	4.9	2.626	5.58	6.44	6.54

A number of authors (Greenwood, 1956; Wagner, 1961; Lifshitz and Slyozov, 1961; Thomas et al., 1979) have suggested mathematical and computational methods to interpret the tendency for relatively large particles to grow in a saturated solution whilst the smaller particles dissolve. Those authors used approximate relations to describe the rate of growth or dissolution. Accurate predictions require the computation of data of the kind of results illustrated in figure 9.9 and involve the numerical solution of the partial differential equations which describe the diffusion in the liquid medium surrounding the sphere. However, in the case of solid particles Henry's law ($C(a) \propto (2\sigma/a + 1)$) is usually replaced by the Thomson-Freundlich equation ($C(a) \propto \exp(2\sigma/a)$) and the material balances have to be reformulated to take into account that the concentration of solute and its volume fraction in the liquid at the interface vary in time. This invalidates the material balances derived in Chapter II (equation (2.28)). The study of this problem is an interesting one and modifications of the relevant partial differential equations should involve no major difficulties in applying the finite difference method. Therefore, it may be suggested as a very useful extension of the present work.

During growth the effects of surface tension on the concentration of gas and on the interfacial concentrations of solute decrease with increasing radius. These effects are negligible by the time the radius of the bubble has increased by a factor of 100 even if the initial conditions were only slightly above the equilibrium condition $Sq = 1/2$. The surface tension can therefore be considered a transient factor and, if Z_g represents the dimensionless time required to double the size of the bubble and Z_2 its value in the case when the surface tension is ignored, Z_g/Z_2 represents a measure of the relative effects of surface tension (figures 9.11 and 9.12). The effects of varying S or q on Z_g are also shown in tables 9.4 and 9.5.

Figures 9.11 and 9.12 show that the quasi steady-state, (equation (9.21)), is the lower limit of actual solutions for very low solubility parameter ϕ. With very large ϕ the actual solutions also converge to a unique regime;(the cases ϕ = 100 and ϕ = 1000 are indistinguishable). The transition between those two limits occurs in the range $0.1 < \phi < 10$. From figures 9.11 and 9.12 it may also be concluded that surface tension effects are more important for large ϕ than for low ϕ.

The time required to double the size of bubbles increases rapidly as the product Sq approaches the value 1/2. It was earlier shown that this is due to a drop of "driving-force" $|F(R)|$ to zero at Sq = 1/2.

The unique representation in terms of ϕZ is characteristic of quasi steady state predictions (equation (9.21)) and was used to allow the rationalization of the actual solutions for low values of ϕ (table 9.4). On the contrary it is possible to identify the upper limit for very large ϕ by use of $\phi^2 Z$ (table 9.5). As shown in Chapter IV ϕZ and $\phi^2 Z$ are also the convenient transformations of time to interpret limiting regimes in the ranges of very low and very high ϕ respectively. Therefore, the convergence of solutions in tables 9.4 and 9.5 constitutes no surprise.

The characteristic growth constant β for the asymptotic growth from zero size (without surface tension) tends to the limits $(\phi/2)^{\frac{1}{2}}$ for very low and $\phi(3/\pi)^{\frac{1}{2}}$ for very high ϕ. Therefore the rate of the process is expected to be more sensitive to a relative decrease of "driving-force" $|F(R)/\phi|$, (equation (9.17)), with large ϕ than in the range of low ϕ. This explains the relative positions of the different curves in figures 9.11 and 9.12.

Figures 9.13 and 9.14 show illustrations of the convergence of the most important part of the transient regimes of growth from finite size with important contributions from surface tension. It is clear that the convergence of solutions for $\phi < 0.001$ and $\phi > 100$ extends over the whole range of times.

The dashed line in figure 9.14 represents a solution of equation (9.23) which was derived and integrated from the general approximate equation proposed by Rosner and Epstein (1972).

$$(R^2 - 1)/4 + S\left(q + \frac{5}{3}\right)(R - 1) + \left(2q^2 + \frac{10}{3} + \frac{4}{3}\right) S^2 . \ln\left(\frac{R - 2Sq}{1 - 2Sq}\right)$$

$$+ \frac{(1 + 2S)}{12Sq^2}(3q + 2) \ln\left(\frac{1 - 2Sq}{1 - 2Sq/R}\right) + \frac{1 + 2S}{3q}(1 - 1/R) = \phi^2 Z \quad . \qquad (9.23)$$

It is clear that that approximation is poor in quantifying the transient regime.

Figures 9.15 and 9.16 illustrate the effects of increasing either S or q. During the initial stage growth becomes very slow as S.q approaches 1/2 but the growth rate increases with increasing radius. For moderate S values the effects of surface tension may be neglected from R = 10, (that is when the bubble radius reaches ten times the initial size). In the case q = 1; S = 0.45 the time required to reach R = 10 and R = 100 is about 65% and 5% in excess relatively to the case of negligible surface tension (S = 0). Therefore, only when very close to the initial equilibrium condition (Sq = 1/2) will surface tension affect growth after an increase of size by a factor of 100.

Other examples have been computed for different values of ϕ. They all show similar curves log R versus log Z, except for the actual range of the time scales.

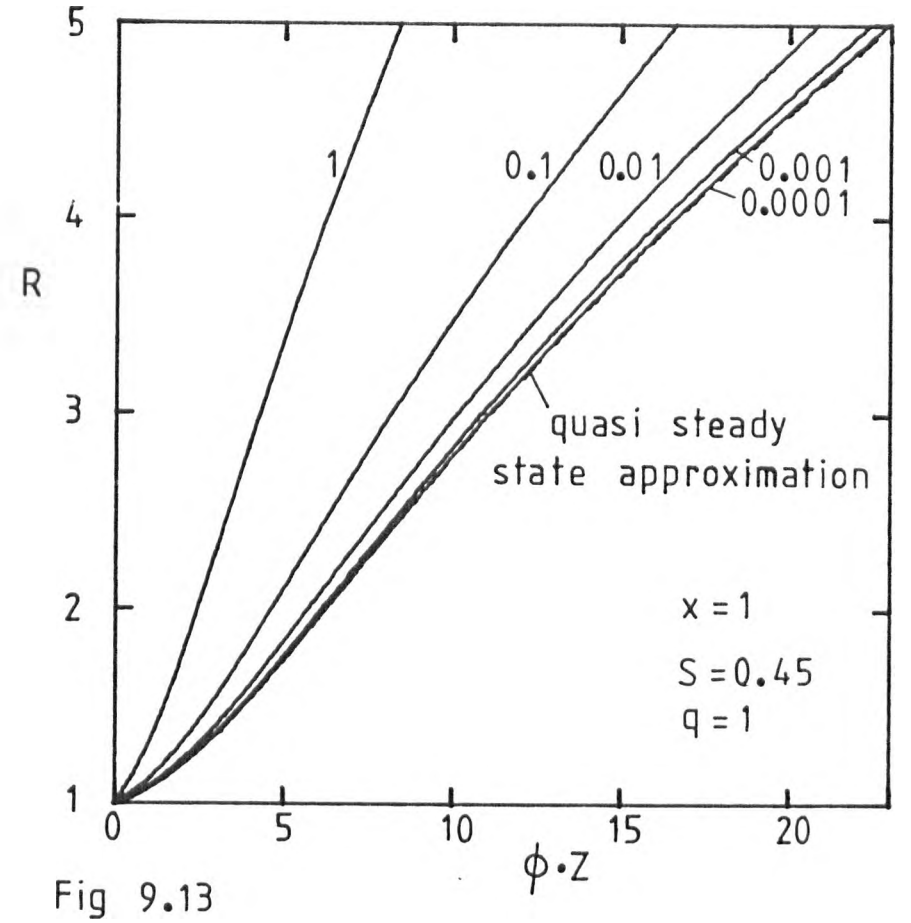

Fig 9.13

Figs 9.13 and 9.14 : Convergence of solutions for growth from finite size for low or high values of ϕ including surface tension. The numbers show the values of ϕ. The dashed line in fig. 9.14 represents equation (9.23).

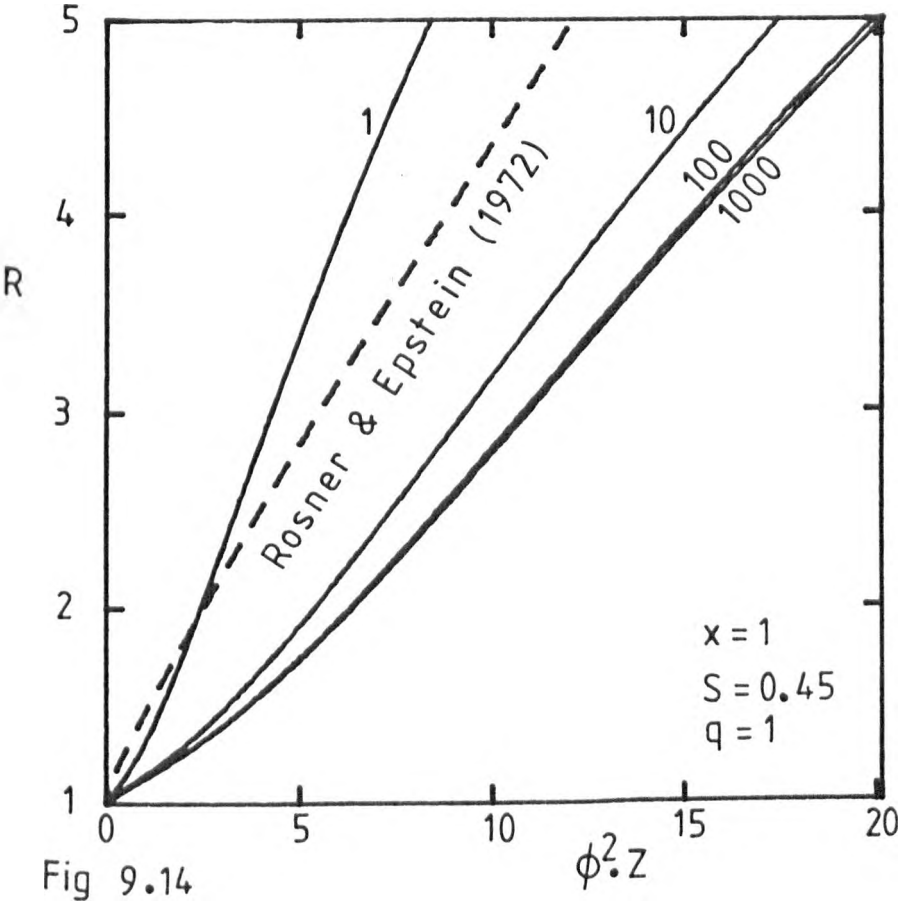

Fig 9.14

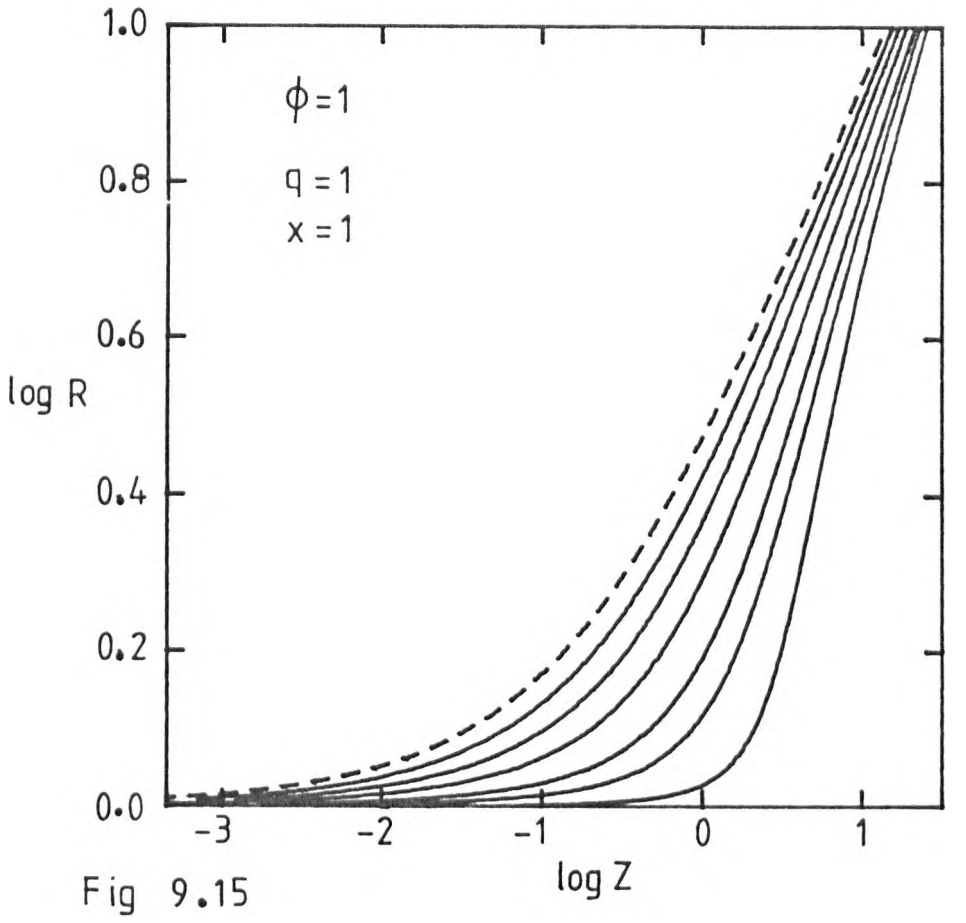

Fig 9.15

Figs 9.15 and 9.16 : Effect of surface tension on growth from finite size. The dashed lines represent the case S=0. The full lines represent S = 0.1, 0.2, 0.3, 0.4, 0.45 and 0.49 in figures 9.15, and q = 0,1, 2, 3, 4, 4.5 and 4.9 in figure 9.16 from left to right.

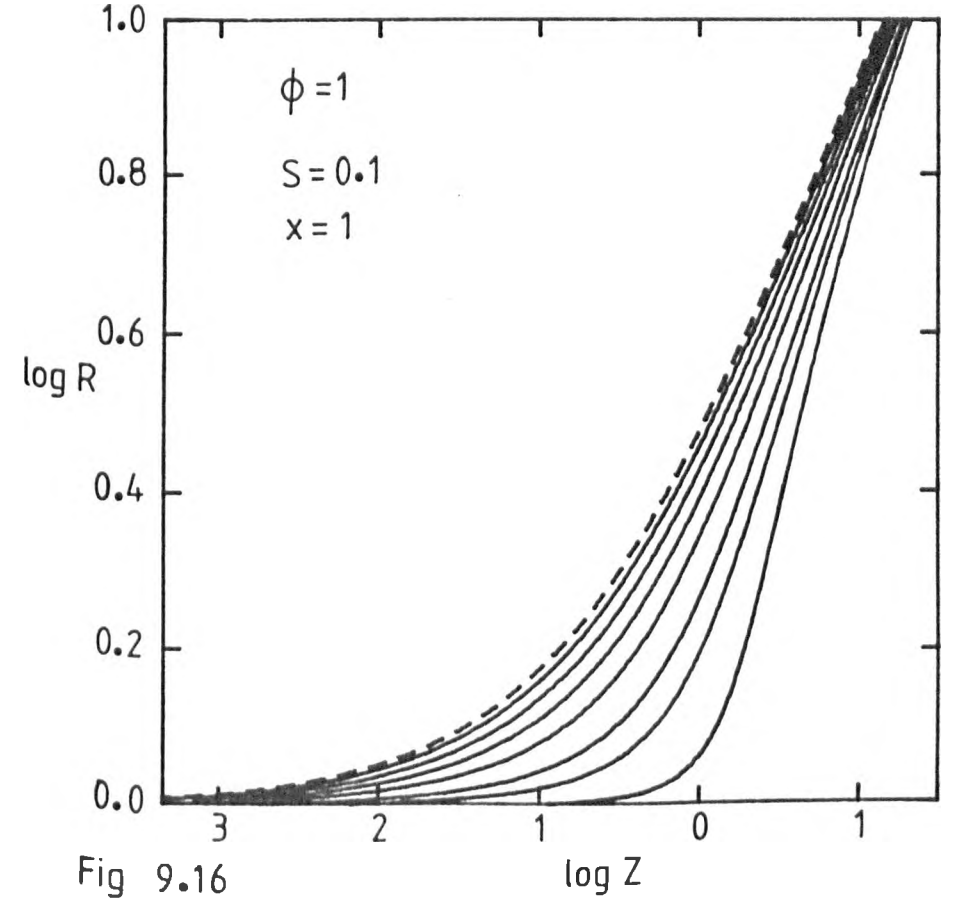

Fig 9.16

9.6.4 Sievert's law

9.6.4.1 $\phi > 0$

If Sievert's law is valid, ($C(a) \propto P_g^x$), and viscous and inertial effects are ignored equation (9.8b) reduces to

$$F(R) = -\phi\,(1 + q) + \phi\, q\,(1 + 2S/R)^{\frac{1}{2}} \qquad (9.24)$$

whilst the gas pressure will be given by equation (9.16) as in the case of Henry's law.

From equation (9.24) the conditions required for growth to occur can be written $\phi > 0$; $q > 0$; and $F(R) < 0$ and therefore

$$q\,(1 + 2S/R)^{\frac{1}{2}} - q < 1 \qquad (9.25)$$

or, as $R > 1$, if $q = 1$ from condition (9.25) $S < 1.5$, and if $S = 0.1$ $q < 10.477$.

Illustration of these conditions is shown in figure 9.17. These examples are qualitatively similar to the equivalent treatment of the Henry's law (figure 9.9) but near the equilibrium conditions the increase of rates of growth or dissolution (with increasing or decreasing radius respectively) is less rapid in the case of Sievert's law. This is due to the linear relation between the interfacial concentration and surface tension, $F(R) = -\phi + 2qS\phi/R$, in the case of Henry's law whilst in the case of Sievert's law the interfacial concentration is given by equation (9.24). Equation (9.16) describes the effect of surface tension on the gas pressure and is valid for both laws.

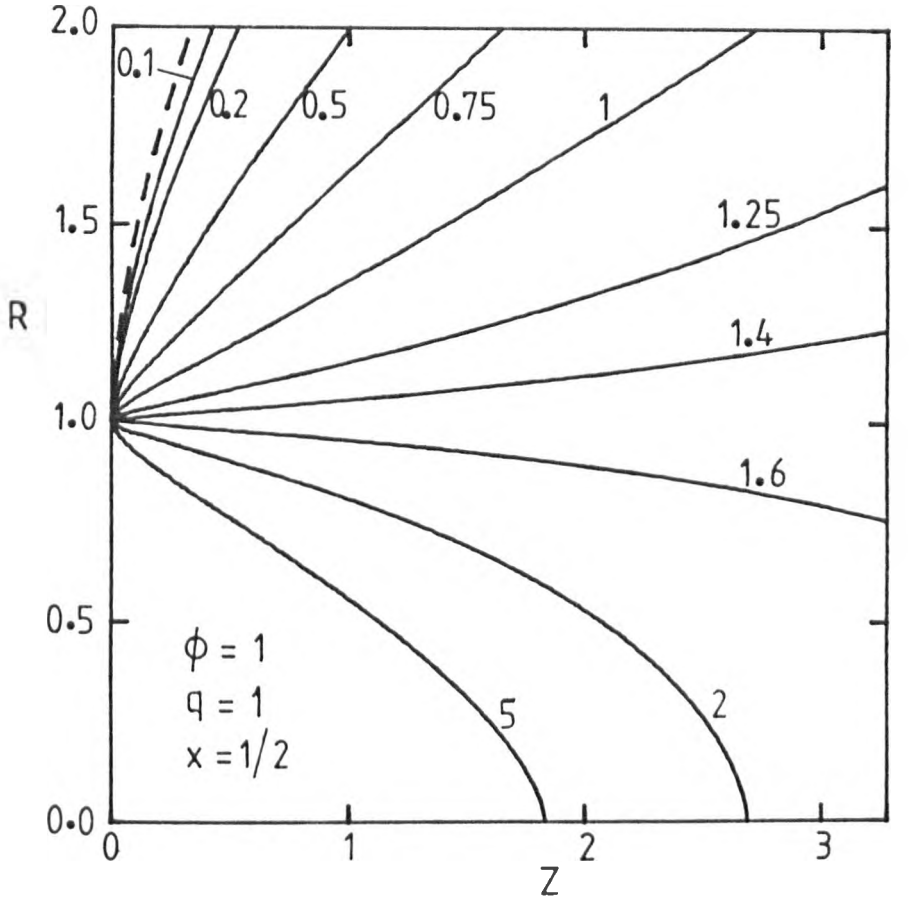

Fig. 9.17 : Effect of surface tension for $\phi > 0$ and interfacial concentration of solute given by Sievert's law. The dashed line represents the case S=0. The figures show the values of S.

9.6.4.2 $\phi < 0$

The effects of surface tension on the dissolution of bubbles in the cases of Sievert's law (full lines) and Henry's law (dashed lines) are compared in figure 9.18. The dissolution is always quicker in the case of Henry's law because the interfacial concentration is then more sensitive to changes of surface tension while the dependence of gas pressure on the surface tension is the same in both cases.

The examples illustrated in figure 9.18 may seem unexpected because with moderate and large S the dissolution rate $\left|\left(\frac{dR}{dZ}\right)\right|$ decreases as S increases. In order to explain that trend it is necessary to take into account that the initial content of the bubbles increases more rapidly with S than the simultaneous increase of the initial "driving-force" F(R) at R = 1.

In the case of the Henry's law with negligible viscous and inertial effects equation (9.9) reduces to

$$G(R) = \frac{4}{3}\pi R^3.(1 + 2S/R) \tag{9.26}$$

and the same relation applies in the case of the Sievert's law.

In the quasi steady-state limit the dissolution rate for Henry's law is given by equation (9.20) and if q = - 1,

$$-\frac{dR}{dZ} = -\frac{\phi}{R}.\frac{(1 + 2S/R)}{\left[1 + \frac{4}{3}S/R\right]} > -\phi/R\,, \tag{9.27}$$

where $\frac{dR}{dZ} = \phi/R$ if surface tension is ignored. Similarly if $x = 1/2$, (Sievert's law), combination of equations (9.18), (9.19) and (9.24) with q = - 1 leads to

$$-\frac{dR}{dZ} = -\frac{\phi}{R}\left[\frac{1 + 2S/R}{1 + \frac{8}{3}S/R + \frac{16}{9}S^2/R^2}\right]^{\frac{1}{2}} < -\phi/R\,. \tag{9.28}$$

Relation (9.28) shows that in the quasi steady-state limit for the Sievert's law case with $q = -1$ the dissolution rate $\left|\frac{dR}{dZ}\right|$ decreases with increasing surface tension, whilst it always increases in the case of Henry's law. These trends are confirmed in figure 9.20 where the dimensionless dissolution time Z_d increases with increasing surface tension (or decreasing initial radius) for $\phi = -0.001$.

For moderate or large $|\phi|$ (with $\phi < 0$) the relation between Z_d and S shows a minimum. In these cases if S is low Z_d may decrease with increasing S because of the increase of "driving-force" F(R) during the last stage of dissolution. This may occur in spite of the fact that at time $Z = 0$, $(R = 1)$, the "driving-force" increases less rapidly with increasing S than the initial content of the bubble $G(1) = \frac{4\pi}{3}(1 + 2S)$. The factor $(1 + 2S)$ represents the relative increase of initial bubble content due to surface tension and, from equation (9.24), the relative increase of "driving-force" $|F(R)/\phi|$, exceeds $(1 + 2S)$ for $R < q/(2S/q - 2)$, where $q \ll -1$. This effect for small S may also be related to the fact that surface tension opposes severe accumulation. It was shown in Chapter V that accumulation might be responsible for a relatively slow final stage.

As S further increases the condition $|F(R)/\phi| > 1 + 2S$ might occur too late (for small R) to avoid an increase in dissolution time and this always occurs if S is sufficiently large.

Figure 9.19 shows that increasing the absolute numerical value of the saturation parameter promotes increasingly rapid dissolution in both cases of Henry's law (dashed lines) and Sievert's law (full lines). For a given value of q dissolution is always quicker in the case of Henry's law than in the case of Sievert's law. These trends occur because of the increase in "driving-forces" F(R), whilst the initial content of the bubble G(1) is unaffected. The symbols (+) denote dissolution in the case of negligible surface tension.

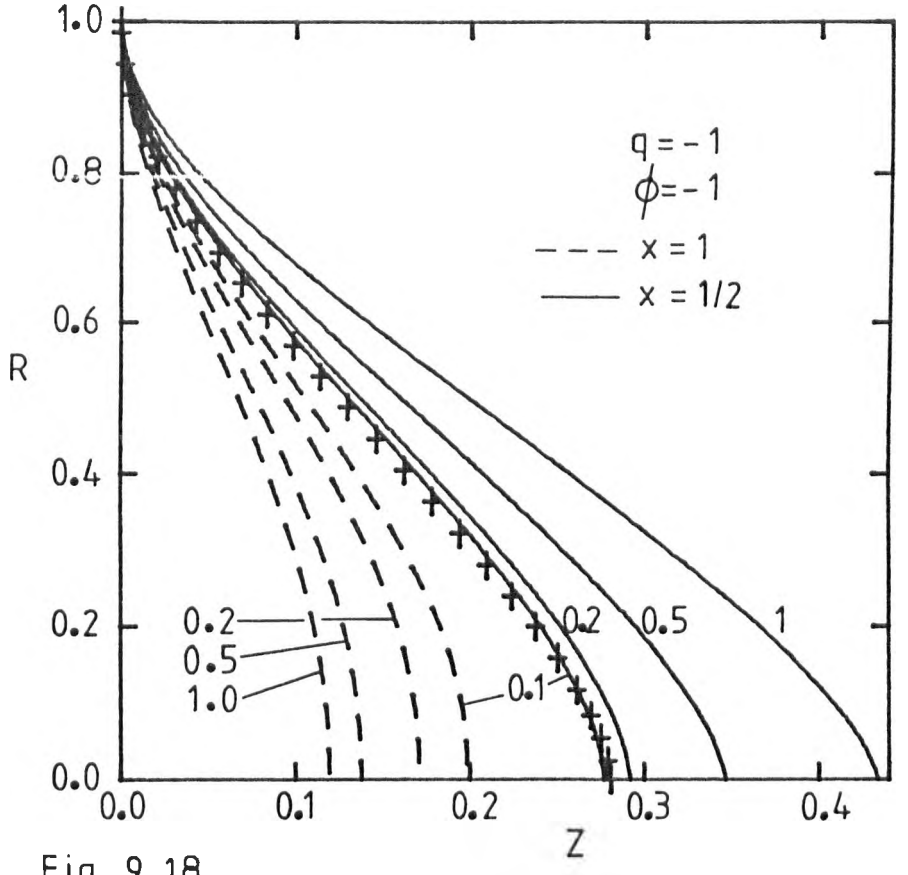

Fig 9.18

Figs. 9.18 and 9.19 : Effect of surface tension for $\phi < 0$. The symbols + represent the case S=0. The full lines represent Sievert's law and the dashed lines Henry's law. The numbers show the values of S in figure 9.18 and the values of q in figure 9.19.

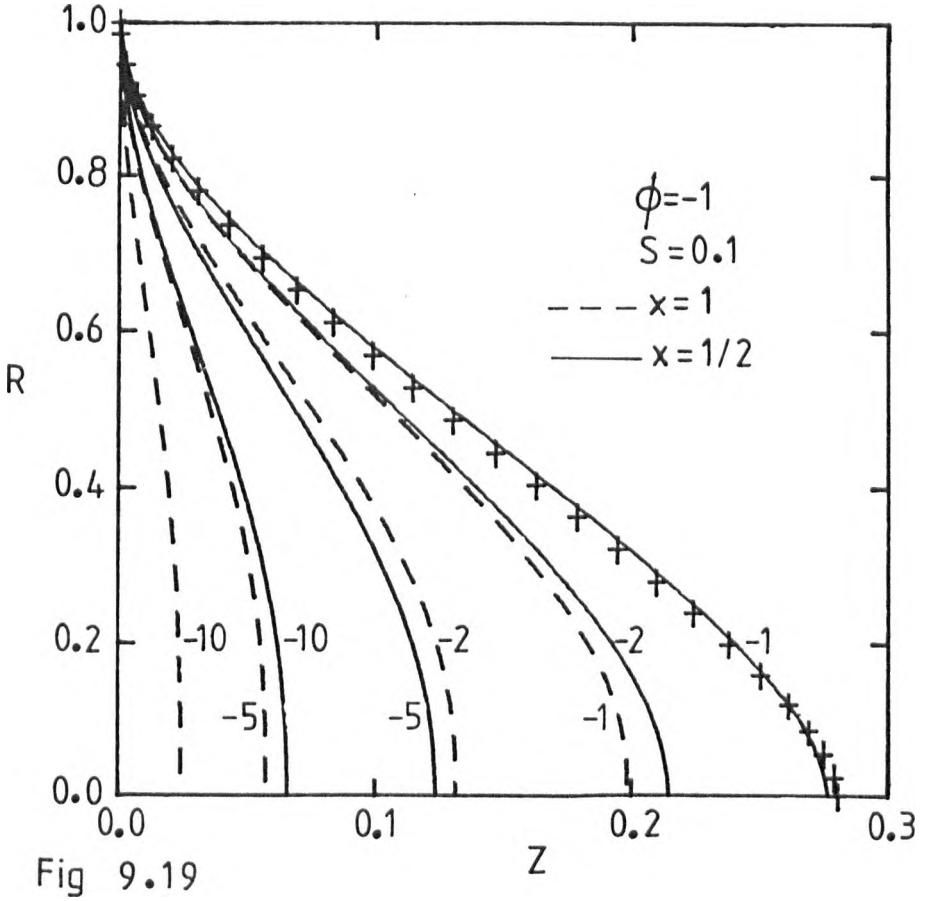

Fig 9.19

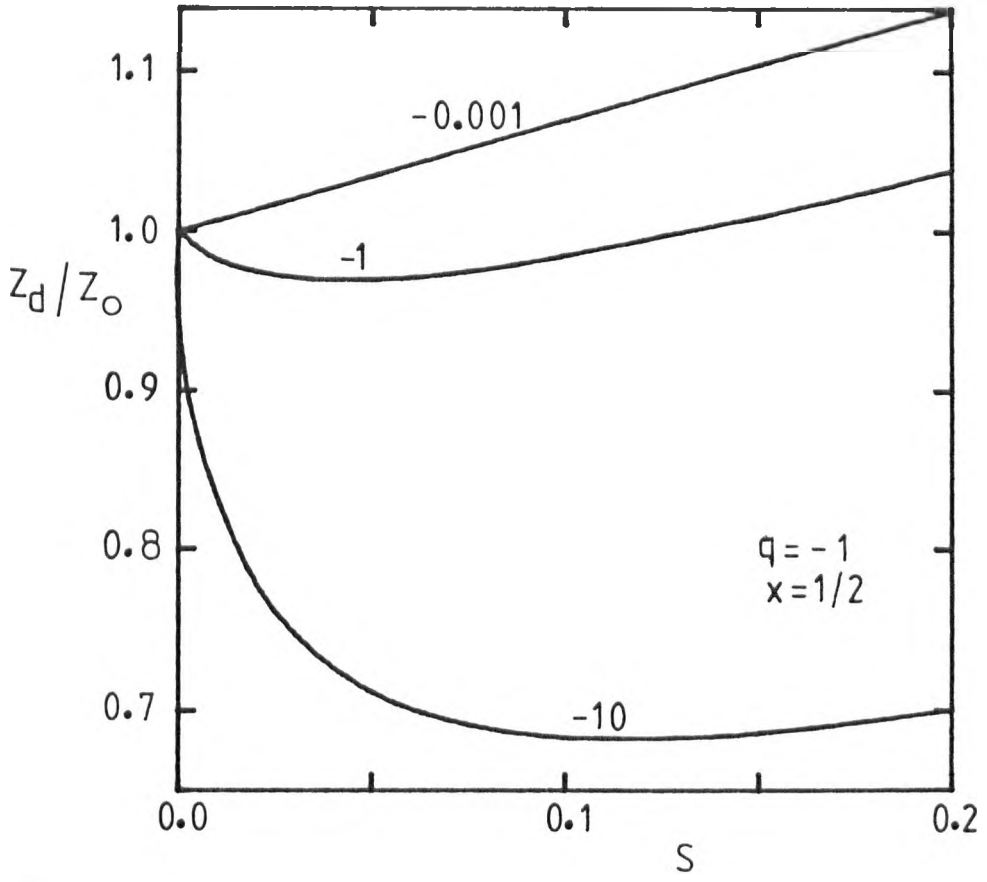

Fig. 9.20 : Effect of surface tension on the time required for complete dissolution for the case of Sievert's law. The figures show the values of ϕ.

9.7 Effects of viscosity on growth or dissolution

Unless specified, the effects of surface tension and inertia are ignored in this section in order to investigate the contributions of viscous forces during growth or dissolution of gas bubbles in a liquid. Figures 9.21 and 9.23 exemplify the effects of viscosity on the behaviour of gas bubbles and show that the greatest contributions occur during the final stage of dissolution and during the initial stage of growth. The effect of viscosity on the initial stage of dissolution may also be significant because of the decrease in gas pressure as the dissolution rate increases.

In figure 9.21a the relative gas pressure P^* (equation (9.6)) is represented by the dashed line for the case $\eta = 0.02$ and by the dotted-dashed line for $\eta = 0.05$. Initially P^* decreases rapidly in both cases as the dissolution rate increases from zero. During the intermediate stage $-\frac{dR}{dZ}$ decreases whilst (1/R) increases and the gas pressure may increase when $\left(-\frac{1}{R}\frac{dR}{dZ}\right)$ decreases with increasing time. This occurs for moderate values of the viscosity parameter, ($\eta < 0.02$), but P^* always decreases for $\eta > 0.05$. During the final stage the radius decreases more rapidly than its derivative so that $\left(-\frac{1}{R}\frac{dR}{dZ}\right)$ decreases and the gas pressure drops approaching zero as R tends to zero. This also causes a decrease in "driving-force", F(R), (equation (9.8a), and consequently $\frac{dR}{dZ}$ tends to zero. The mathematical solution predicts that the time required for complete dissolution will be infinite if viscosity is considered, but surface tension increases the gas pressure and opposes the effect of viscosity as seen in figure 9.22. For this reason the solutions in figures 9.21 were stopped for $R < 0.01$ that is for the last 1% decrease in size.

As $\left|\frac{dR}{dZ}\right|$ increases with $|\phi|$ it should be possible to define a range of values of $|\phi|\eta$ for which the effect of viscosity may be ignored. Figure 9.21a

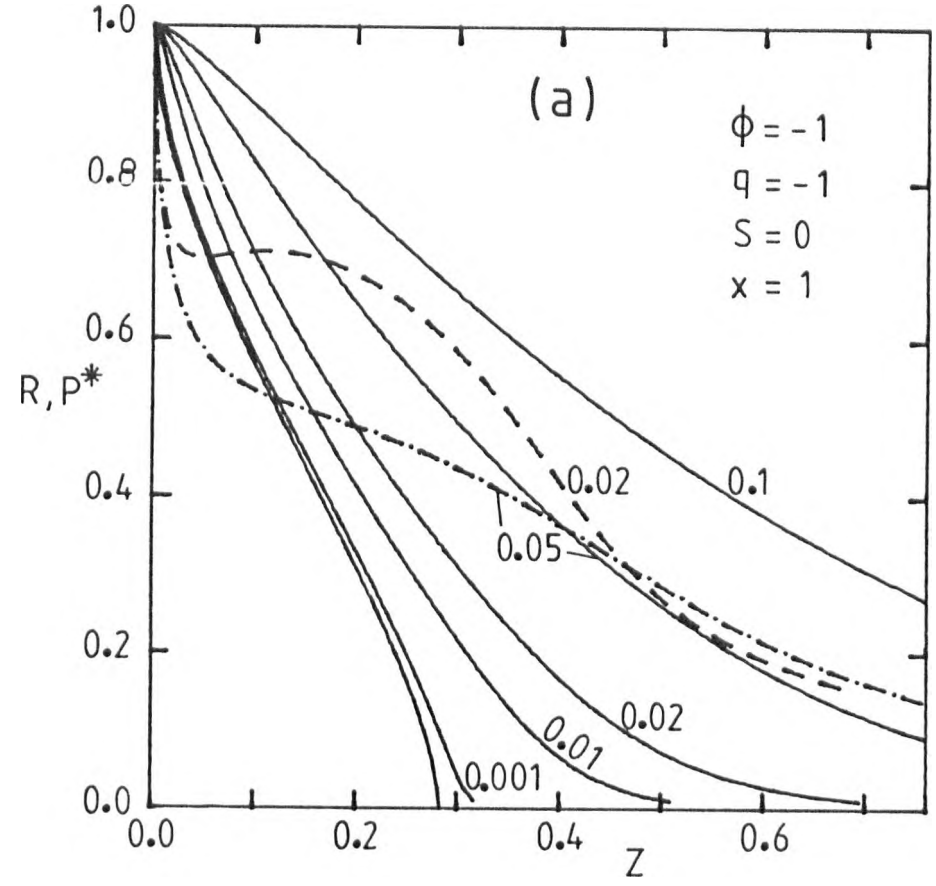

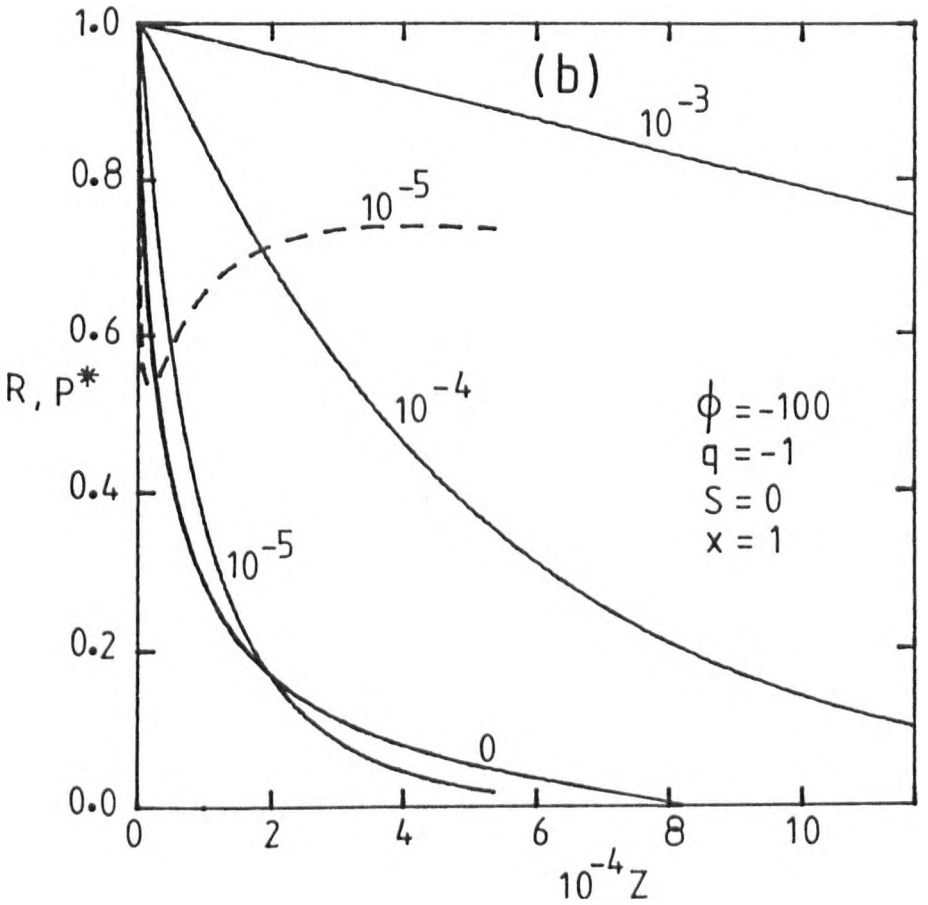

Figs 9.21 : Effect of viscosity on the dissolution of bubbles. The dashed-dotted and dashed lines represent P* and the full lines R. The numbers show the values of η.

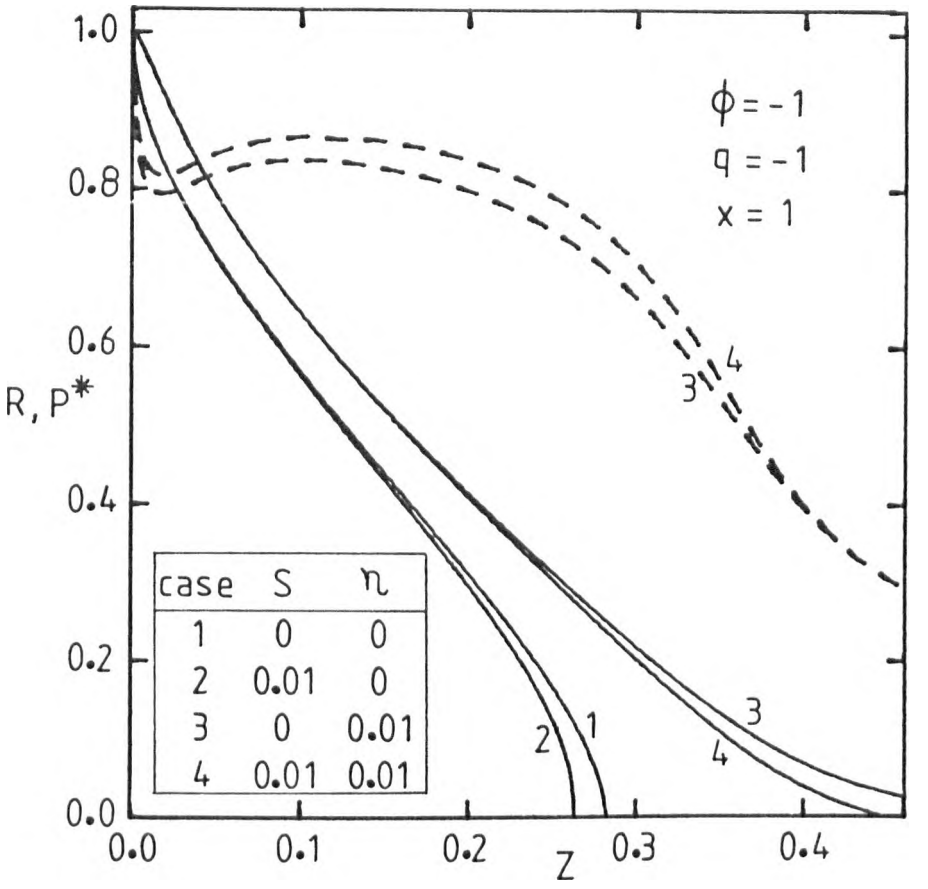

Fig. 9.22 : Effects of surface tension and viscosity on dissolution of a bubble. The dashed lines represent P*.

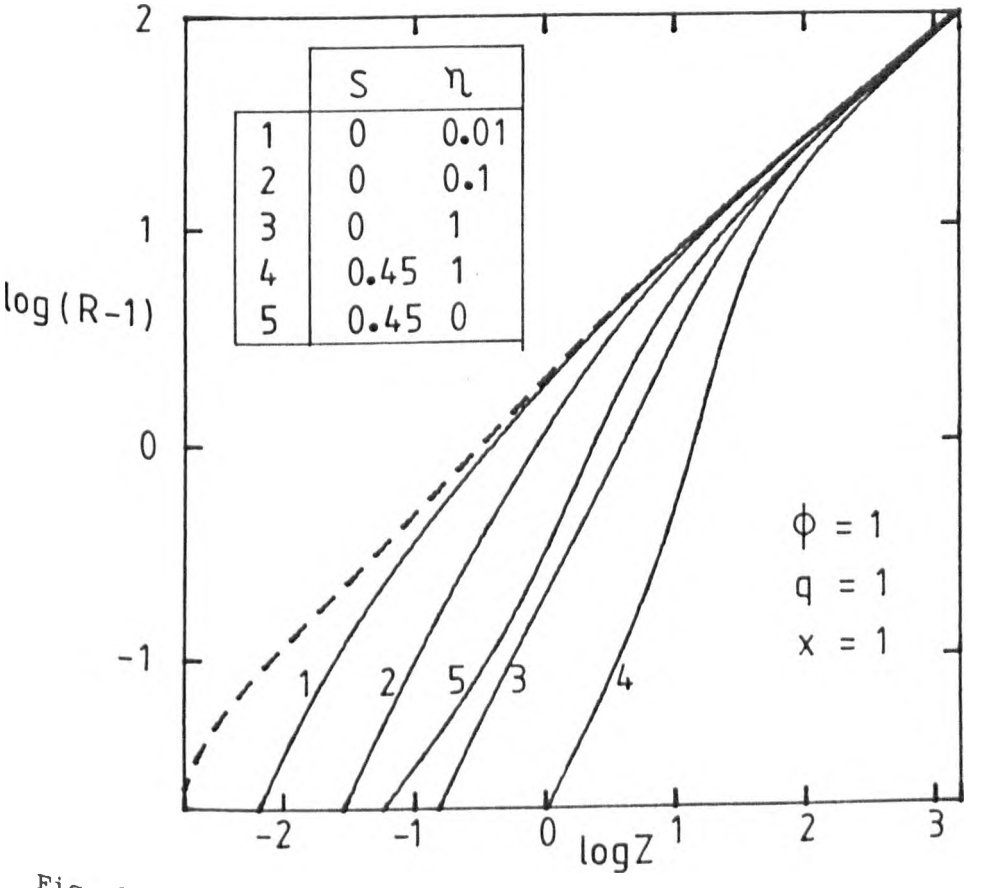

Fig. 9.23 : Effects of viscosity and surface tension on growth of a bubble. The dashed line represents the case S=0; η=0.

Table : 9.6

Effect of viscosity on the dimensionless time required to decrease to 10% of the initial size $Z_{0.1}$, or to double the size of bubbles Z_2 for $|q| = 1$.

$\|\phi\|\eta$	0	0.0001	0.001	0.01	0.1
ϕ			$-\phi\, Z_{0.1}$		
-0.01	0.456	0.462	0.468	0.538	0.954
-0.1	0.3911	0.3961	0.4044	0.484	1.096
-1	0.2680	0.2724	0.2826	0.3720	1.161
-10	0.1280	0.1307	0.1382	0.2094	1.037
-100	0.03319	0.03161	0.02758	0.1167	0.694
			$\phi\, .\, Z_2$		
0.01	1.281	1.284	1.288	1.335	1.768
0.1	0.905	0.910	0.916	0.970	1.434
1	0.3294	0.3337	0.3409	0.4067	0.893
10	0.0489	0.0505	0.0583	0.1183	0.507
100	0.00516	0.00513	0.01233	0.0529	0.3542

suggests that viscosity may be ignored for $|\phi|\eta < 0.001$, which is also confirmed in table 9.6 except for very large values of solubility parameters $|\phi| > 10$. If $|\phi| > 10$ viscosity should be included in the full solutions when $|\phi|.\eta > 0.0001$, which with $|\phi| = 100$ correspond to a relatively low value of the viscosity parameter $\eta = 10^{-6}$ (see table 9.1). In the most common range of solubility parameters, $|\phi| < 10$, viscosity may be ignored except for small bubbles ($a_o < 0.1$ mm) and highly viscous melts ($\mu > 10^3$ Kg m^{-1} s^{-1} = 10^4 poise). For $|\phi| = 0.1$, 1 and 10 viscosity may be ignored if $\eta < 10^{-2}$, $\eta < 10^{-3}$ and $\eta < 10^{-4}$ respectively.

In figure 9.21b the radius-time curve for the case $\eta = 10^{-5}$ follows the expected trends during the initial and intermediate stages, but for relatively small radii ($R < 0.175$) dissolution may become faster than in case $\eta = 0$. This trend would be reversed for very small R as $\left|\frac{dR}{dZ}\right|$ decreases and may approach zero but by this time surface tension may not be ignored, so that it makes no sense to extend the curve $\eta = 10^5$ for $R < 0.01$.

Understanding of that trend is clearer by taking into consideration that:

- the overall rate of transfer increases if relatively large interfacial areas are maintained for much of the process, and this can be achieved by preventing a very rapid initial decrease in radius without stopping transport of material,
- a decrease in the rate of transport makes it possible that a larger proportion of dissolved material might diffuse to somewhat larger distances from the centre which opposes severe accumulation near the interface
- there is an intermediate stage during which the gas pressure and "driving-force" F(R) increase which also contributes to oppose the accumulation near the interface. Note that for relatively large viscosity the initial drop of "driving-force" is not reversed and dissolution remains slower than in the case $\eta = 0$.

Figure 9.22 exemplifies the simultaneous effects of surface tension and viscosity on bubble dissolution. The dashed lines represent P* for the cases 3 and 4 and the full lines represent R. Surface tension alone enhances dissolution relative to the case $S = 0$; $\eta = 0$ when both surface tension and viscosity are ignored. If the viscosity is too high to be ignored the gas pressure drops significantly before decrease in radius becomes noticeable. This is due to transfer of material out of the bubble. During this stage surface tension may be ignored except for unusually large values of S. The role of surface tension becomes important during the final stage when viscosity tends to cause a progressive decrease of gas pressure and a decrease in $\left|\frac{dR}{dZ}\right|$ which tends to zero in the case $S = 0$. At this stage even a small value of surface tension parameter (see table 9.1) plays a significant role due to a contribution $2S/R$ to the relative gas pressure P* and a contribution $-2Sq\phi/R$, $(q < -1)$, to the "driving-force" F(R), and makes it possible for a bubble to dissolve completely.

The conditions $\phi\eta < 0.001$ for $0 < \phi < 10$ and $\phi\eta < 0.0001$ for $\phi > 10$ may also be used as a criterion to decide in which conditions the role of viscosity may be ignored during bubble growth. Figure 9.23 shows that growth may be affected by viscosity during the initial stage of growth but this effect always vanishes for sufficiently large sizes of bubbles. Notice that after that initial stage the growth rate $\frac{dR}{dZ}$ and R^{-1} decrease with time so that the effect of viscosity on the gas pressure (equation (9.6)) vanishes more rapidly than the effect of surface tension which decreases only with R^{-1}.

Both surface tension and viscosity cause slower growth and therefore their effects are additive (equation (9.6)). Also both effects increase with increasing saturation parameter ($q > 0$). However, the effects of surface tension cause dissolution when $\phi > 0$ and $S.q > 1/2$ in the case of Henry's law ($\alpha = 1$), whilst growth always occurs if $\phi > 0$, $q > 0$; $S = 0$ and $\eta > 0$.

During the initial stage the curves 1, 2 and 3 in figure 9.23 have slopes greater than 1, so that the radius of the bubble increases more rapidly than the predictions by a linear relation between radius and time. After the initial transient stage the solutions converge to the diffusion controlled regime which corresponds to a low $R \propto \sqrt{Z}$. Barlow and Langlois (1962) predicted that viscous relaxation was responsible for a linear relation between radius and time, but their analysis was based on assuming thin boundary layers which is not valid except for very large solubility parameters ϕ.

9.8 Effects of inertia on growth or dissolution of bubbles

It has been shown in Chapters IV and V that during the initial stage of growth or dissolution the actual predictions for large $|\phi|$ are close to predictions of the flat slab model. This approximate model becomes $R = 1 + 2\phi\sqrt{Z/\pi}$ and therefore

$$\frac{dR}{dZ} = \frac{\phi}{\sqrt{\pi Z}} = \frac{2\phi^2}{\pi\ (R - 1)} \tag{9.29}$$

and

$$R\ \frac{d^2R}{dZ^2} = -\ R\ \frac{\phi}{2\sqrt{\pi}}\ Z^{-3/2} = -\ \frac{4}{\pi^2}\ \frac{\phi^4}{(R - 1)^2}\left(\frac{1}{R-1} + 1\right) . \tag{9.30}$$

For $|R-1| > 0.05$, that is excluding the initial 5% change in radius, equations (9.29) and (9.30) lead to

$$\left(\frac{dR}{dZ}\right)^2 < 162\ \phi^2$$

and

$$R\left|\frac{d^2R}{dZ^2}\right| < 3.4 \times 10^3\ \phi^4 .$$

Therefore, for $|\phi| = 100$, $\left(\frac{dR}{dZ}\right)^2 < 1.62 \times 10^6$ and $R\left(\frac{d^2R}{dZ^2}\right) < 3.4 \times 10^{11}$ so that only for $h > 10^{-14}$ might inertia become significant (equation (9.6)). This range is unlikely to be found in practice as is $|\phi| > 100$. Even $|\phi| > 10$ must be rare and inertia might then be ignored for $h < 10^{-10}$ which is unrealistically high as shown in table 9.1.

9.9 Conclusions

Surface tension is responsible for an increase of gas pressure inside bubbles and consequently the solute concentration in the liquid at the interface is also enhanced. Henry's law is commonly assumed and predicts linear relations between equilibrium solute concentration and gas pressure. Positive or negative deviations from Henry's law are occasionally found, including linear relations between the equilibrium solute concentration and the square root of the gas pressure (Sievert's law).

The effects of surface tension are dependent on the physical property σ and on the size of the sphere. Other non-equilibrium effects are also dependent on the size of the bubble but only act in dynamic conditions, that is due to motion of the interface. These differences are important especially during dissolution when surface tension is responsible for the enhancement of rates of material transfer whilst the effects of viscosity and inertia hinder dissolution.

Viscosity may usually be ignored but whenever dissolution or growth rates are sufficiently large for viscosity to have an effect it causes a decrease in pressure and rates of transfer during dissolution or an increase in pressure and decrease in rates of transfer during growth. Inertia is very unlikely to play a significant role during either dissolution and growth.

During growth the combined effects of surface tension and viscosity

decrease as the radius of the bubble increases. Therefore those effects may be considered transient and the actual solutions converge to the diffusion controlled regime for large radii. As the surface tension acts independently of motion, a bubble may dissolve in a saturated solution provided its radius is smaller than a critical value. This critical radius is not only dependent on the value of the surface tension but also on the degree of oversaturation.

Surface tension is the most important among the present factors which cause deviations from a simple diffusion controlled behaviour. Its effects may be important over the entire range of solubility parameters (ϕ) likely to be found in practice. Viscosity and inertia may be neglected because they become effective only for very large rates of growth or dissolution, that is for very large $|\phi|$. The present study includes a large number of simulations of bubble behaviour over a very large range of ϕ values which may include all the cases of practical interest. Large values of surface tension parameter were also included to investigate even the most extreme conditions and draw attention to the more important trends of bubble growth or dissolution.

CHAPTER X

Discussion of behaviour of bubbles in glass melts and suggestions for further work

10.1 Introduction

Several authors have studied growth or dissolution of individual bubbles in the hope that the results would help to understand refining. This type of experiment suggests that bubble behaviour is diffusion controlled but precise analysis of those experiments has been poor especially because of inadequate theoretical models and poor knowledge of solubilities and diffusivities. Unfortunately these data are scarce and not completely reliable. As the temperatures used for such determinations were often significantly lower than typical melting temperatures those experiments might be of little use even when they are accurately designed and interpreted. In fact solubilities and diffusivities of gases in glass melts usually vary rapidly with temperature. This property might promote dissolution of some bubbles as the glass melt is cooled to working temperatures and the solubility of some gases (especially CO_2 and O_2) increases. Not all gases necessarily have negative temperature coefficients of solubility.

The most commonly used methods of studying refining have been the measurements of number N of bubbles per unit volume, bubble size distribution and composition of individual bubbles after different founding times. These studies might be useful to follow the process but do not provide information about the behaviour of individual bubbles when several mechanisms and several gases may be involved. Efficient control of refining requires precise understanding and description of individual bubbles. The assumption that individual bubbles can be treated as isolated ones in uniform surroundings may not be justified. Slow degasification might occur during refining which

makes the interpretation of changes in number, size distribution and composition of bubbles more difficult.

A sensible way of studying refining would include direct observation of individual bubbles in glass melts. Unfortunately this method involves serious experimental difficulties and has rarely been used. Besides it only provides information about velocity and change in size of bubbles but not about bubble composition. Bubble nucleation might also be observed.

It has been pointed out that the mathematical solution of the behaviour of moving bubbles is complex due to difficulties in equating accurate material balances and solving the relevant partial differential equations. These difficulties exist even in the axially symmetric case (free rise exclusively due to buoyancy).

There is experimental evidence that the rate of transport around a rising bubble is greater than around a stationary bubble (Greene and Lee, 1965); thus diffusion seems to be the most likely controlling mechanism in both cases. Therefore solubilities, bulk concentrations and diffusivities must be the essential parameters in both cases and bubble motion is dependent on the viscosity of the melt and size of the bubble. The main difference between behaviour of rising and stationary bubbles must be a significant change in time scale. Solutions for multi-component stationary bubbles are used in this chapter to discuss some possible interpretations of phenomena which involve bubbles in motion. Such solutions must not be taken as quantitative predictions of the behaviour of bubbles in those cases.

10.2 Studies of bubbles in glass melts

Greene and co-authors (1959, 1965, 1969, 1974), measured radius-time curves for bubbles held almost stationary by rotating the sample. Most of their experiments used one-component bubbles but the glass samples may have contained several dissolved gases. Nevertheless they used a one-component theoretical model. Doremus (1960) used a transformed quasi stationary one-component model (equation (2.61)) to analyse some of those results and obtain estimates of the diffusivity D and solubility parameter F_a. Brown and Doremus (1976) used the same model to analyse the behaviour of bubbles containing oxygen, nitrogen or air. However, oxygen may diffuse into a nitrogen bubble or vice-versa, and air bubbles need a model for two-component bubbles. Therefore, Brown and Doremus's analysis might not be justified.

There are also several reasons to question the method used by Brown and Doremus to obtain estimates of D and F_a:

- often the initial size may not be measured accurately,
- the initial stage often deviates from the expected shape of diffusion controlled dissolution (Greene and co-authors, 1959),
- the final stage is usually slower than expected which might be caused by impurities present in the initial gas bubbles or diffusing from the melt into the bubble (see Chapter VI),
- the transformed quasi-stationary model gives inaccurate predictions of both dissolution time and shape of radius-time curve except for very low values of $|\phi|$. Inaccurate prediction of radius-time curves is serious if both the diffusivity and solubility parameter are to be estimated from the experimental dissolution curve. Therefore the estimates of diffusivity and solubility parameters obtained by Doremus (1960) for oxygen bubbles in glass melts might involve significant errors.

It has been said that change in diffusivity causes a change in time scale only. Besides, if $F_a < 0.1$ the shape of normalized radius-time curves varies little on changing F_a after taking into account the change in time scale. In this range of low F_a the time scale is nearly proportional to D^{-1} and F_a^{-1} so that quite different combinations of diffusivity and solubility parameter may fit the experimental results equally well. This trend is obviously more serious when the initial radius is not accurately measured and the resolution of the initial and final stages is poor. In this case it is difficult to obtain accurate estimates of both D and F_a even in the ranges of moderate and large solubility parameters ($F_a > 0.1$). Unfortunately those limitations are common in the case of bubbles in glass melts.

Somewhat better predictions are expected if the solubility parameter is known and the problem reduces to finding the value of the diffusivity, (Frischat and Oel, 1965 and 1967b; Nemec, 1969). In this case the most serious errors result from the use of poor mathematical analysis (Nemec, 1969). However, this case requires accurate measurements of concentrations and solubilities which are available for water and possibly inert gases but are scarce or non-existent for the most important components of gas bubbles during refining (carbon dioxide, oxygen and physically dissolved nitrogen).

10.3 Changes of gas composition in bubbles during refining

There is some direct experimental evidence that individual bubbles can change composition in glass melts (Cable and Haroon, 1970; Mulfinger, 1972). However, these observations were made in melts at temperatures significantly lower than typical melting and refining conditions and assuming similar changes at these higher temperatures might not be justified. A change in temperature could reverse the flux of a gas into or out of a bubble simply because of the change in solubility with temperature. Analysis of gas bubbles

in glass samples after different founding times also show changes of gas composition (Slavyanski, 1957; Cable et al., 1969; Cable and Naqvi, 1975; Mulfinger, 1976), but there is no direct evidence that all the observed changes represent what typically happens in one particular bubble. Growth and rise to the surface as well as nucleation of new bubbles might cause change in bubble population present in the melts especially if the founding time is sufficiently long. The typical sequence of changes is from CO_2 to O_2 and then to N_2.

The change from CO_2 to O_2 occurs relatively early whilst the change from O_2 to N_2 seems generally to occur only in the last stages of refining and is usually observed after long founding times. After the change $CO_2 \rightarrow O_2$ the bubble density (N) decreases markedly and there often is a linear relation between log N and t. At low N this law changes and further decrease in N is much slower which suggests change in controlling mechanisms. It is not understood whether growth of the bubbles present at the time when the melt becomes batch-free and elimination by rise to the surface might explain the linear relation between log N and t, or if other mechanisms play an important role. The velocity of rising bubbles is usually proportional to the square of the radius (a^2) (Solinov and Pankova, 1965), so that the time required for a bubble to rise from a depth $\underline{h}$ to the surface of the melt increases rapidly with decreasing radius. Growth (or dissolution) and nucleation of new bubbles also affect the rate of disappearance of bubbles. The rate of nucleation seems to decrease rapidly when the melt becomes batch-free (Solinov and Pankova, 1965) and bubbles often grow during refining of glass. Therefore, many bubbles are likely to be eliminated by growth and rise to the surface. In such cases the rate of disappearance must decrease as the average size decreases and understanding the relation between N and t requires information about the size distribution at batch-free time, growth

rates and their changes with bubbles size (especially for small bubble sizes) and time. The velocity of rise u due to buoyancy can be worked out from the size of the bubble ($u \propto a^2$). The role of bubble rise in the elimination of bubbles is also demonstrated by some experimental evidence which shows that bubble count in quenched samples can decrease more rapidly in the bottom layers than in those near the free surface of the melt (Von Reth and Van Velzen, 1973).

Melts without any refining agent tend only to contain CO_2 bubbles. The change $CO_2 \rightarrow O_2$ might not be complete at batch-free time but the proportion of O_2 is then often considerably above 50% unless insufficient additive (arsenic or antimony) is used. In small crucible melts the change $O_2 \rightarrow N_2$ may not be observed because most of the bubbles may disappear before this can happen.

Assuming that both changes $CO_2 \rightarrow O_2$ and $O_2 \rightarrow N_2$ occur in the same bubbles there should be three different stages controlled by each of the components of the bubbles in turn CO_2, O_2 and N_2. The evidence is insufficient to know whether these bubbles are growing or dissolving. Both possibilities need to be examined. The initial component (CO_2) is replaced relatively rapidly by O_2. During the intermediate stage the proportion of O_2 is high ($\%O_2 > 80\%$) and might even reach close to 100%. This stage is often long and the $\%O_2$ tends to remain at a nearly constant value for relatively long times before starting to decrease slowly being replaced by nitrogen. Meanwhile N decreases markedly.

Figure 6.25 showed one example of a three-component stationary dissolving bubble with three distinct stages. Replacement of the first component by the second component requires very different diffusivities or solubilities. Besides, nearly complete dissolution of the first and second components requires that the ratios F_{O_1}/α_1 and F_{O_2}/α_2 should be very small, that is the

solute concentrations in the bulk liquid must be negligible. However, relatively rapid dissolution of the first component of bubbles in glass melts (CO_2) opposes what is usually assumed. Also the ratios F_{O_1}/α_1 for CO_2 and F_{O_2}/α_2 for oxygen are likely to be greater than unity and these species are likely to diffuse into the bubbles. In fact, some of the few observations of bubbles during refining showed that bubbles usually grow as their composition changes from CO_2 to O_2 (Nemec, 1974). Some of these observations were for additions of refining agent (arsenic) much larger than usually found effective.

It has been demonstrated that the case shown in figure 6.25 is very different from the conditions which are likely to occur during refining. Figure 10.1 and 10.2 also show the type of conditions required for a bubble to have three clearly distinguished stages. These show that the bubble starts to grow as the second change in composition occurs. This would be equivalent to a bubble which shrinks as CO_2 dissolves but then starts growing as oxygen is replaced by nitrogen. It seems impossible for a bubble to show an increase in the mole fraction of the second component g_2 followed by a decrease in g_2 without initial decrease in size.

The relative duration of each of the three stages shows some differences between the behaviour shown in figures 6.25, 10.1 and 10.2 and the expected changes in bubbles in glass melts. During refining the second stage (bubbles with large proportions of oxygen) is usually well defined and relatively long compared with the time for the $CO_2 \rightarrow O_2$ change, but this is not general (Apak, 1975). Besides the changes in composition in bubbles during refining can conveniently be represented against the real time whilst in the simulated examples a square root time scale is usually needed to distinguish the second stage and the proportion of the second component does not remain at its maximum for a significant time.

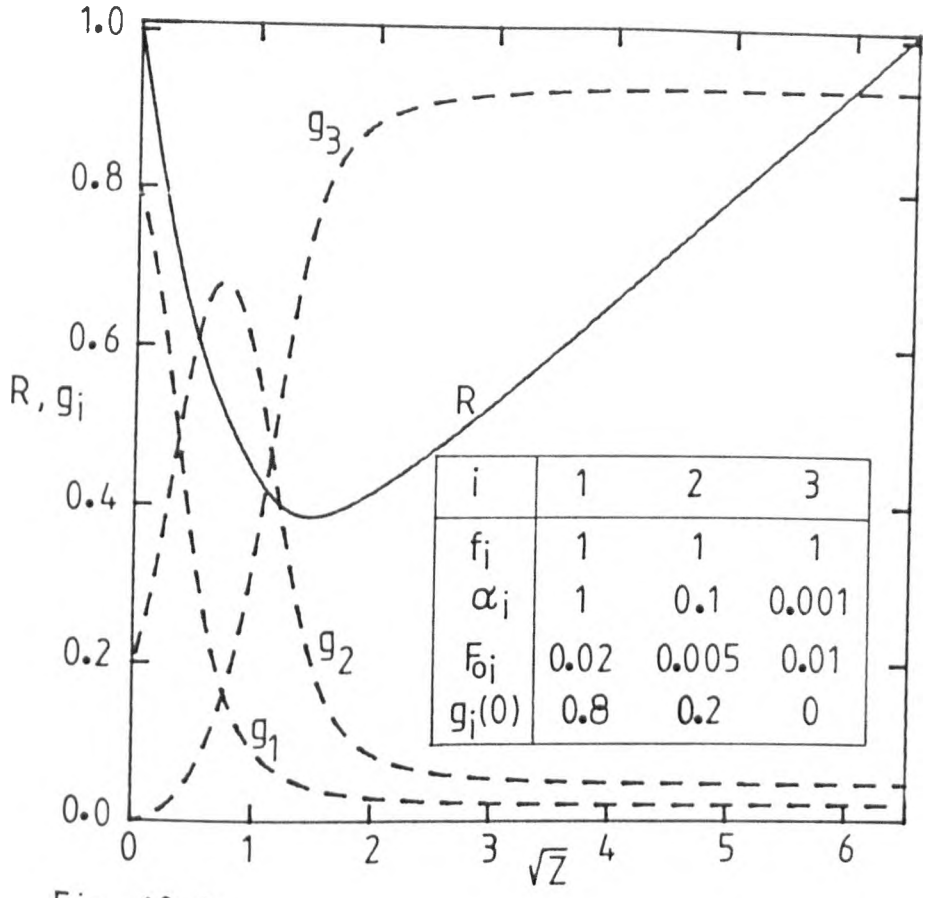

Fig 10.1

Figs 10.1 and 10.2 : Illustrations of behaviour of three-component stationary bubbles with three distinct stages and growth after the transient stage.

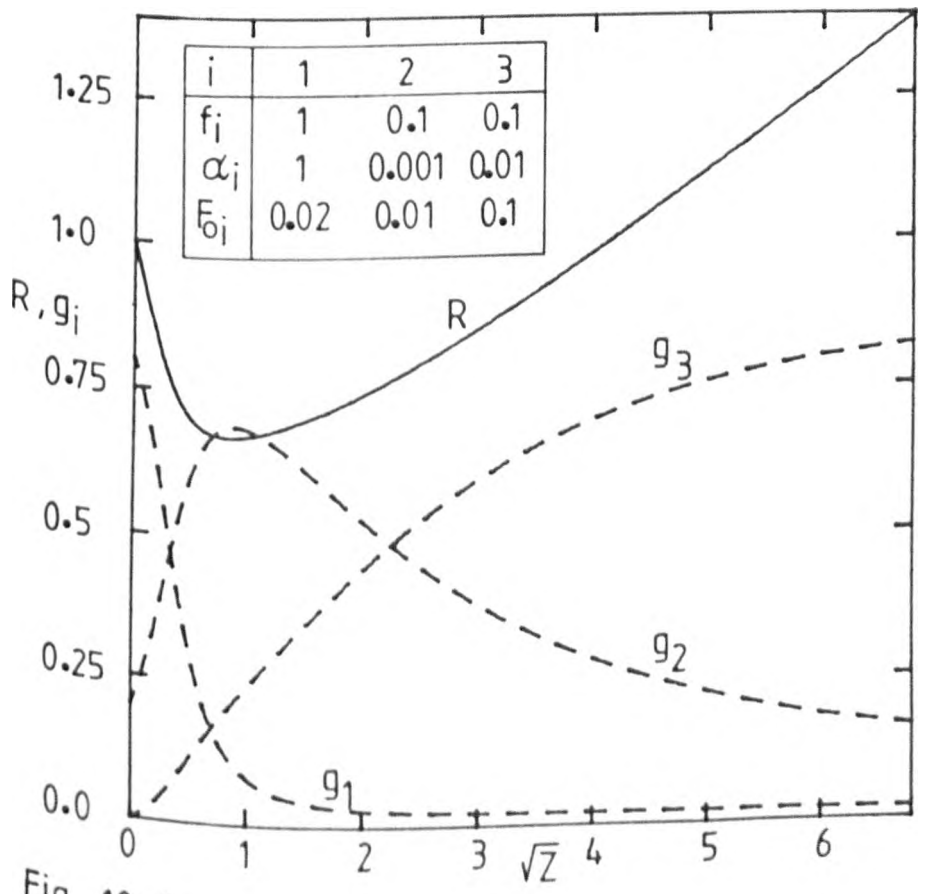

Fig 10.2

Carbonates decompose rapidly by reacting with silica and giving rise to large volumes of CO_2 and relatively basic melts. These reactions are very rapid even at temperatures significantly lower than typical melting temperatures and large proportions of CO_2 available from batch must be lost relatively early. Meanwhile the initial basic melts are in good contact with those large volumes of CO_2 being released and the concentration of CO_2 in those phases might be close to saturation. Further dissolution of silica increases the acidity and decreases the solubility of CO_2 in the melt which might cause oversaturation and diffusion of CO_2 into bubbles present in the melt or nucleation of new bubbles. Investigation of these hypotheses might be useful.

It is well known that the change in gas composition from CO_2 to O_2 is promoted by adding arsenic or antimony to the batch. This does not occur at about 1200°C or less (Nemec, 1974) and there is evidence that arsenic and antimony are converted to the pentavalent state as the temperature of the batch increases. Cable (1961b) found that if a mixture of arsenic and Na_2CO_3 is heated above 360°C the proportion of arsenate will be high. Oxygen might be dissolved during the change from trivalent to pentavalent state as the temperature of the batch increases and it has been suggested that nitrate acts as a oxigizing agent. The proportion in the pentavalent state which was found in glass was often slightly increased by adding nitrate to the batch (Cable et al., 1969; Cable and Naqvi, 1975) but these differences might also be related to the tendency to change in valency at higher temperatures from pentavalent to trivalent arsenic or antimony (Kuhl et al., 1938; Baak, 1959; Baak and Hornyak, 1966). This change supports the view that oxygen also diffuses into bubbles when refining is improved by arsenic or antimony, but there is no direct evidence that the partial pressure of oxygen at which the melt is equilibrated exceeds 1 atm.

An example of the behaviour of a two-component stationary bubble is shown in figure 10.3 where species 1 corresponds to oxygen and species 2 corresponds to CO_2. The constant α_2 was chosen from the typical range of Ostwald solubility coefficients for CO_2 in soda-lime-silica melts above 1300°C (Kroger and Goldmann, 1962). The concentration of CO_2 in the bulk melt is assumed to be 2, 10 and 100 times greater than the solubility (in cases 1, 3 and 4 respectively). The solubility of oxygen was also chosen from values corresponding to about 0.5 wt.% arsenic (equation (1.4)), and the bulk concentration of oxygen is assumed to be twice its solubility ($F_{O_1} = 2\alpha_1 = 8$). Figure 10.3 shows that in those conditions the change in gas composition is relatively quick and close to completion during the time required to double the size of the bubbles. This occurs even if the diffusivity of CO_2 is 100 times greater than that of oxygen (case 2) or if the relative oversaturation with CO_2 is high (case 4).

Diffusion of both oxygen and carbon dioxide into growing bubbles, and rise to the surface would lead to progressive degasification. Investigating how far this process could proceed during refining might provide useful information, but involves difficult measurements of the "effective" concentrations of CO_2 and O_2 dissolved in glass. Measurements of proportions of trivalent and pentavalent arsenic (or antimony) at different founding times might give useful information but the investigation should be extended for times considerably longer than usually used in laboratory melting (Cable et al., 1969).

Excessive arsenic or antimony makes refining worse, especially if nitrate is not added to the batch (Cable et al., 1969; Cable and Naqvi, 1975). This suggests some relation between good refining and efficient degasification. In fact a large proportion of arsenic and antimony converts to the pentavalent state as the batch is heated and the amount of oxygen which must be given off

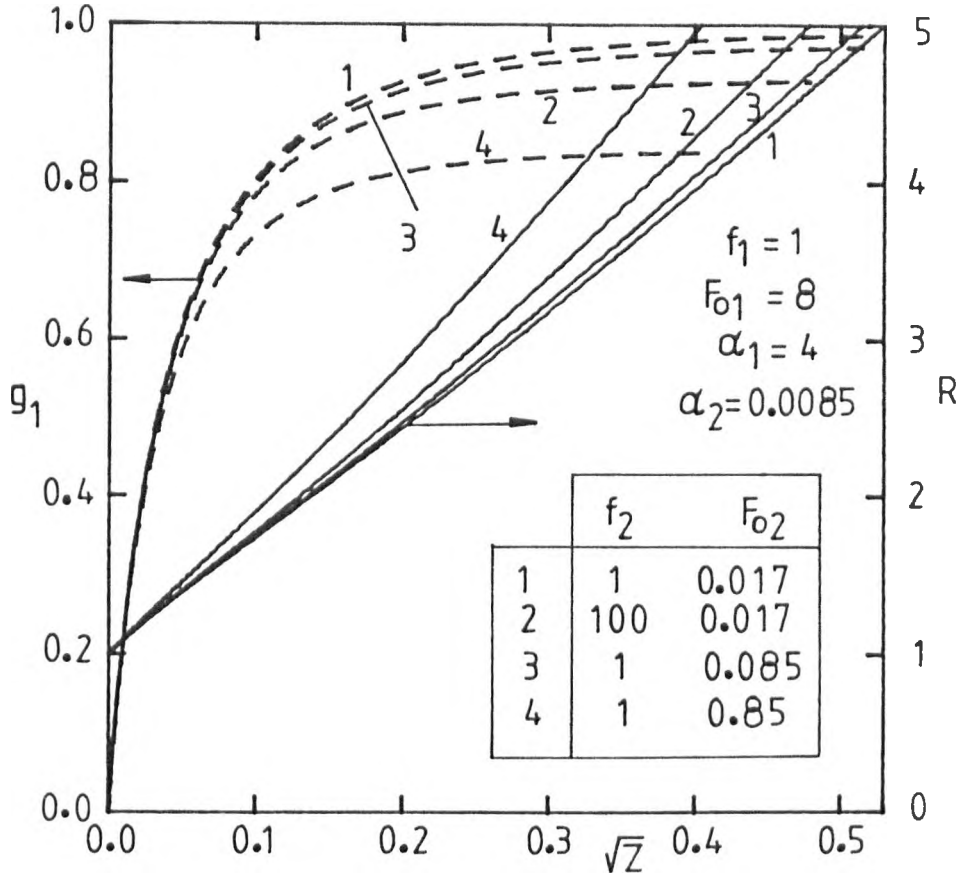

Fig 10.3 : Changes in composition of bubbles containing gases which diffuse into the bubbles at very different rates.

by the melt for the degasification to be efficient may increase with increasing additions of arsenic or antimony. Nemec (1974) also found that during refining the rates of bubble growth increased with increasing arsenic additions up to 2% As_2O_3. However, this value is a large excess relative to the values which are usually considered optimum in refining (Cable et al., 1969), and excessive arsenic (or antimony) also involves less rapid replacement of CO_2 by O_2 in the bubbles during the earliest stages of refining (Cable et al., 1969; Cable and Naqvi, 1975). Decrease in rate of diffusion of oxygen into growing bubbles whilst keeping to the flux of CO_2 constant would cause an increase in the proportion of CO_2 but also decrease rates of bubble growth. On the contrary, increase in both the proportion of CO_2 and in rates of bubble growth might be due to increase in the rate of diffusion of CO_2 especially during the earliest stages of refining. This also suggests that arsenic (or antimony) might be responsible for increasing the concentration of CO_2 which was dissolved in the initial basic liquid phases formed by reaction of carbonates with silica. Studying the effect of reducing conditions on the solubility of CO_2 or CO in glass melts might clarify whether or not that process is related to the changes in valency of arsenic or antimony.

Degasification of the melt might occur by diffusion from the surface of the melt to the atmosphere and by nucleation, growth and rise of large numbers of bubbles. Diffusion from the surface is unlikely to play a significant role when the melt becomes almost quiescent, that is when convection does not promote replacement of the top layers of the melt. Nucleation of new bubbles, followed by their growth and rise to the surface might be assisted by the presence of undissolved solid particles (Solinov and Pancova, 1965). Therefore, a rapid dissolution of the most refractory components of the batch might be a disadvantage. Some facts agree with this hypothesis, namely the evidence that too fine sand dissolves quickly and

causes decrease in batch-free time but makes refining worse (Cable, 1958), and the role of nitrate which assists refining but also causes an increase in batch-free time (Cable et al., 1969). In this second case residual sand grains might provide sites for heterogeneous nucleation whilst in the first case the rate of homogeneous bubble nucleation might be too low even with high oversaturations preventing efficient degasification. Finally, assuming that the bulk solute concentration is constant might be a poor approximation.

Understanding why nitrogen replaces oxygen in bubbles is also difficult. The change occurs only after long melting times especially in glass melted in industrial pot or tank furnace (Slavyanski, 1957; Mulfinger, 1976) and is unlikely to occur in glasses melted in a small crucible. Long founding times might allow nitrogen to diffuse from the atmosphere and diffuse later into bubbles when bubbles were dissolving (Mulfinger, 1972). However, increase in the proportion of nitrogen in growing bubbles is very unlikely except after very efficient degasification (especially losses of oxygen). In addition a dramatic change in solubility of oxygen might cause dissolution of oxygen, decrease in size of the bubble, and increase in proportion of nitrogen in the residual bubble.

In fact, Slavyanski (1957) reported some results which show that nitrogen rich bubbles are more likely to occur in glass samples collected from the furnace during the cooling to working temperatures, especially below 1250°C. However, such changes also occurred in melts held at constant temperature (about 1400°C) throughout refining. During that decrease in temperature the equilibrium for arsenic is shifted towards large proportions in the pentavalent state (Baak, 1959), which might cause a significant increase in solubility of oxygen. Nemec (1974) also showed that bubbles in a melt containing 2% As_2O_3 and 1% Na_2O supplied as nitrate in the batch decreased in size as the temperature dropped from 1400 to 1150°C, whilst a

similar drop in temperature caused little or no decrease in size of bubbles in a melt without refining agents.

The differences in solubility of oxygen and nitrogen in glass melts at temperatures below about 1300°C might explain why bubbles with small proportions of nitrogen become rich in this species. Figures 10.4 and 10.5 illustrate that type of behaviour. The solubilities were chosen in the ranges suggested in Chapters I and II. The bulk concentration of nitrogen (species 2) is assumed to be 80% of its solubility ($F_{O_2} = 0.8\ \alpha_2$). The composition of the bubbles is very dependent on the bulk concentration of oxygen (F_{O_1} is the dimensionless equivalent variable). This suggests a strong relation to degasification. Increase in the proportions of species 2 is enhanced if the equilibrium for species 1 is given by Sievert's law, instead of Henry's law. In the case of Sievert's law the interfacial concentration is expressed by

$$F_1(R) = \alpha_1\sqrt{g_1} - F_{O_1}$$

as shown in appendix 7 . Note that Sievert's law is suggested by equation (1.4) but this equation is wrong in what concerns the effect of the basicity of the melt. Sievert's law does hold for dissolution of water.

Mulfinger (1976) found bubbles rich in nitrogen and CO_2 in glass samples collected from the hottest zone of a tank furnace, which is in apparent contradiction to the previously formulated hypothesis. In this case dissolution of oxygen should be rapid during the time required to collect the samples and cool them to room temperatures. This is not unrealistic if efficient decrease in concentration of oxygen is achieved at those high melting temperatures (close to 1600°C). In case (e) shown in figure 10.5 the mole fraction of the most soluble gas decreases to 0.5 at Z = 0.029, so

Table 10.1 : Relevant parameters for the examples shown in figs. 10.4 amd 10.5.

a)

i	1	2
f_i	1	1
α_i	8	0.001
F_{oi}	*	0.0008
g (0)	0.99	0.01

b)

*	F_{o1}
a	7.5
b	7
c	6
d	4
e	2

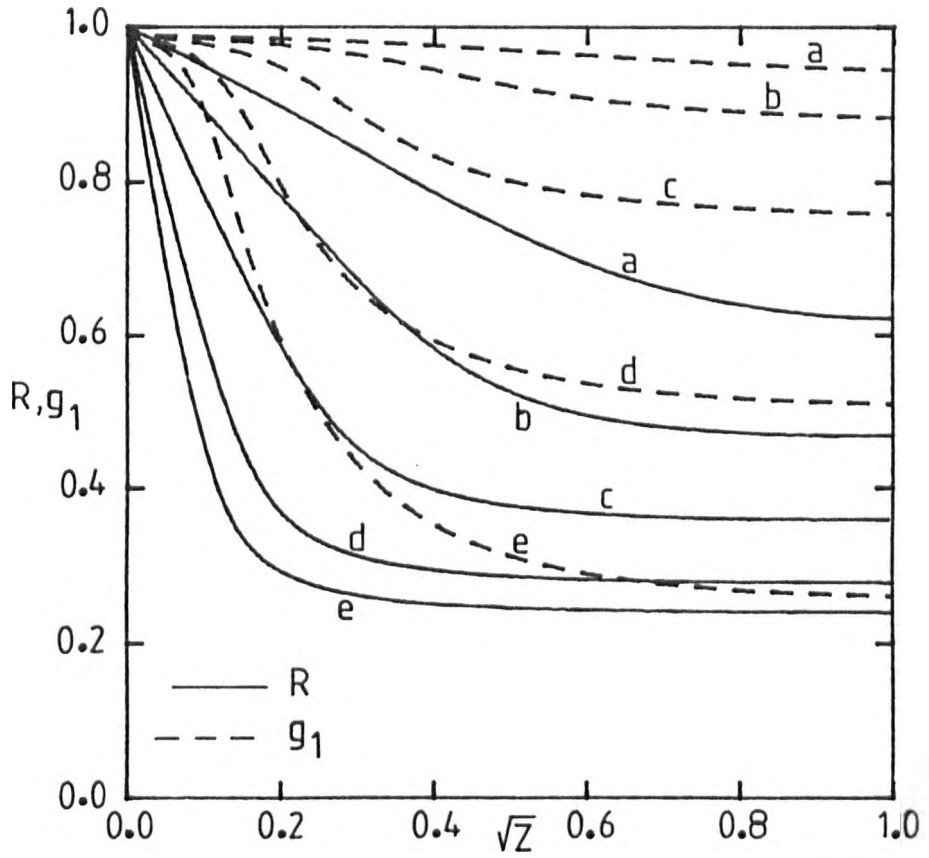

Fig. 10.4 : Dissolution of stationary bubbles containing two gases of very different solubilities. The relevant dimensionless parameters are given in table 10.1. Henry's law is assumed for both species.

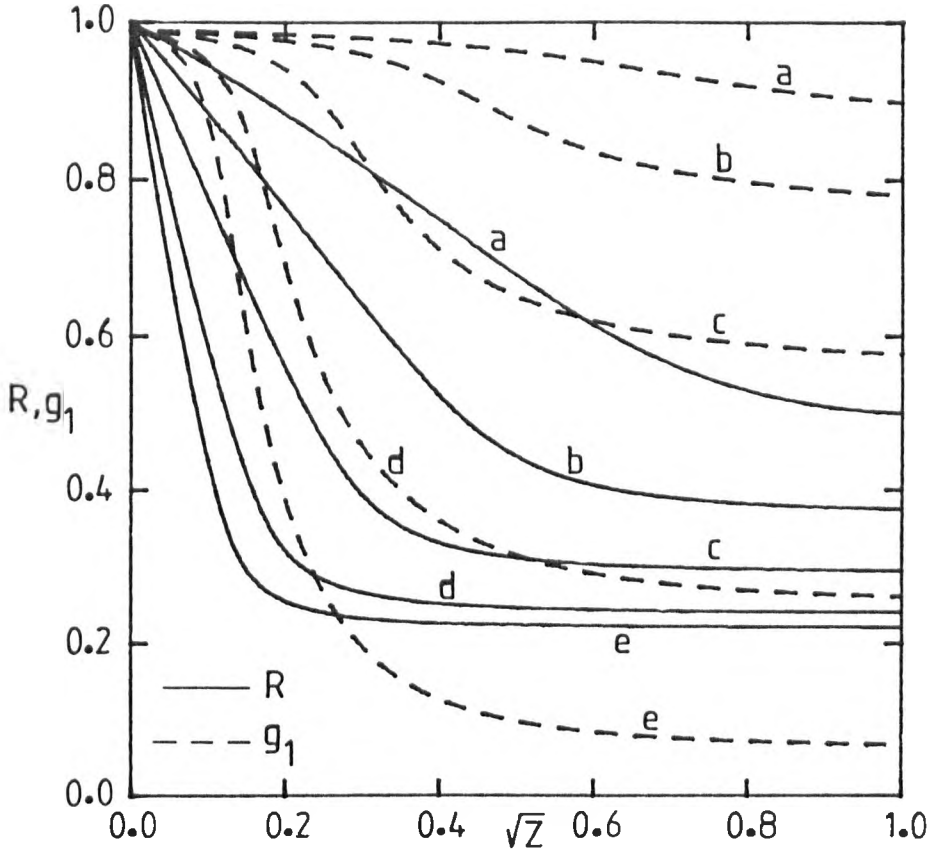

Fig. 10.5 : Dissolution of stationary bubbles containing two gases of very different solubilities. The relevant parameters are given in table 10.1. The Henry's law is assumed for species 2 ($F_2(R) = \alpha_2 g_2 - Fo_2$) but Sievert's law is assumed to describe the equilibrium at the interface for species 1 ($F_1(R) = \alpha_1 \sqrt{g_1} - Fo_1$). The full lines represent the radius of the bubble and the dashed lines the mole fraction of species 1.

that if the initial bubble size is a_o = 1 mm and the diffusivity D_1 = 10^{-6} cm^2/sec, the time equivalent to Z = 0.029 is 290 sec. In the case of a rising bubble the time scale may be much shorter than in the case of a stationary bubble (Greene and Zee, 1965) and 1 min could be enough to promote that decrease in proportion of O_2 in the bubble.

The study carried out by Mulfinger (1976) also suggests that the average size of bubble decreases when oxygen had been replaced by nitrogen or carbon dioxide. However, increase in temperature causes decrease in viscosity and increase of the velocity of bubbles, which might have also contributed to decrease in average size of bubbles collected from the hottest zone of the furnace.

Much shorter melting times are used in small scale experiments and drop from melting temperatures to annealing temperatures is usually rapid, which might explain why nitrogen is rare and its proportions are small in bubbles analysed in glass samples obtained in this way.

Assuming that nitrogen diffuses from the atmosphere before diffusing into bubbles suggests that the proportion of nitrogen in residual bubbles might be greater in glass samples collected from near the surface of the melt than in samples collected from the bulk melt.

The thermodynamics of arsenic differs somewhat from that of antimony. In both cases lowering the temperature of the melt favours formation of the pentavalent form and thus an increase in O_2 solubility. However, at the same temperature arsenic is usually more oxidized than antimony. Therefore, in the case of antimony the degasification might be more efficient and the increase in solubility of oxygen is expected to occur at lower melting temperatures than for glasses containing arsenic. During cooling to working temperatures the dissolution of oxygen might start later when its diffusivity has also decreased further and the proportion of oxygen in bubbles in glasses

containing antimony might remain higher than in glass with arsenic. However, this interpretation must take into account the effective bulk concentration of oxygen which depends on how efficient the degasification is. Figures 10.4 and 10.5 have clearly shown that the mole fractions of oxygen in bubbles decrease with decreasing bulk concentration of that species.

Experimental study of the effects of a drop in temperature on the composition of bubbles might be a convenient test for the hypotheses formulated here.

10.4 Suggestions for further work

The state of understanding of refining shows that measurements of solubilities, diffusivities and bulk concentrations of gases dissolved in glass melts are essential. Understanding of these processes might be improved by studying the changes of bulk concentrations of gases dissolved in the melts. Description of the phenomena requires measurement of solubilities and diffusivities and their changes with temperature; CO_2, O_2, N_2 and SO_2 must be the most important gases. Nitrogen might be less important in spite of its frequent occurrence in bubbles in finished glass samples because it has low solubility and low diffusivity.

Different techniques are likely to be needed for efficient analysis of different gases. Vacuum extraction has often been used in the past but it involves serious difficulties especially due to condensation of alkali compounds in the coldest parts of the apparatus. An alternative technique involves decomposition of powdered glass with HF and analysis of gases thereby released (Simhan, 1973). So far results obtained by this technique are inconclusive and further investigation should be carried out.

Accurate mathematical analysis of the behaviour of freely-rising bubbles

is also required, involving multicomponent systems (simultaneous diffusion of more than one gas). The effect of varying the concentration of gases dissolved in the bulk melt must be investigated.

Observations of bubbles in glass melts make it possible to measure sizes, rates of growth and velocity of bubbles in glass melts. These observations should be extended for longer times, especially at low concentrations of bubbles (N). Measurements have usually shown highly scattered growth rates (Nemec, 1974) which shows that the assumption of uniform bulk concentrations might not be completely justified. Analysis of bubble composition also show significant scattering but this seems to decrease with increasing time (Cable et al., 1969). Scatter of growth rates is also expected to decrease as the homogeneity of the melt improves. Scattering might be due to the presence of bubbles of different ages formed in rather different conditions.

Finally, adding fine sand during refining to previously batch-free melts might give some insight into the role of bubble nucleation in the evolution of refining and possibly on the role of degasification. It would be interesting to solve the question of how far solid particles can promote the heterogeneous nucleation of bubbles in melts which had been freed from bubbles.

Much work, both experimental and theoretical remains to be done before the refining of glass melts will be properly understood.

APPENDIX 1

Multistep formulas

Multistep integration is frequently used to integrate ordinary differential equations and is discussed in textbooks (Burden et al., 1981). Variable mesh methods are discussed by Van Wyk (1968). If $f(Z,y) = \frac{dy}{dZ}$, the dependent variable y is solved on integrating the following interpolation polynomial, P(Z).

$$y_\ell = y_{\ell-1} + \int_{Z_{\ell-1}}^{Z_\ell} P(Z)\, dZ \qquad (1A)$$

where P(Z) is the Lagrange interpolation polynomial,

$$P(Z) = p_n \cdot f_{\ell-n} + p_{n-1} \cdot f_{\ell-n+1} + \ldots + p_1 \cdot f_{\ell-1} + p_0 \cdot f_\ell \qquad (2A)$$

with

$$p_i = \prod_{\substack{K=\ell-n \\ K\neq\ell-i}}^{\ell} \left[\frac{(Z - Z_K)}{(Z_{\ell-i} - Z_K)}\right] \qquad i=0,1,2,3,4,\ldots,n$$

The Z_K ; (K = ℓ-n, ℓ-n+1, ..., ℓ) points must be distinct and the derivatives $f_K = f(Z_K, y_K)$ must be known, so that there is a unique polynomial, P(Z).

In order to derive a four-step formula (n=4) the p_i terms must be included in equation (1A) and the handling of that polynomial is simplified after the following transformation of independent variable

$$\zeta = (Z_{\ell-1} - Z)/\delta Z$$

where $\delta Z = Z_\ell - Z_{\ell-1}$.

Also discrete ζ_i; (i=0,1,2,3,4) are defined as follows

$$\zeta_i = (Z_{\ell-1} - Z_{\ell-i})/\delta Z$$

where $\zeta_1 = 0$, and $\zeta_0 = -1$.

After expanding $P(\zeta)$, rearranging, and integrating it one obtains the implicit formula

$$y_\ell = y_{\ell-1} + \delta Z[P_0 \cdot f_\ell + P_1 \cdot f_{\ell-1} + P_2 \cdot f_{\ell-2} + P_3 \cdot f_{\ell-3} + P_4 \cdot f_{\ell-4}] \quad . \qquad (3A)$$

If the step size is constant $\zeta_2 = 1$, $\zeta_3 = 2$, and $\zeta_4 = 3$, the coefficients P_i are easily obtained and equation (3A) reduces to

$$y_\ell = y_{\ell-1} + \frac{\delta Z}{720}[351 f_\ell + 646 f_{\ell-1} - 264 f_{\ell-2} + 106 f_{\ell-3} - 19 f_{\ell-4}] \qquad (4A)$$

which is the Adams-Moulton four-step formula.

Otherwise

$$P_4 = -\frac{[1/20 + (\zeta_2 + \zeta_3)/12 + \zeta_2 \zeta_3/6]}{\zeta_4(\zeta_4 - \zeta_3)(\zeta_4 - \zeta_2)(\zeta_4 + 1)}$$

$$P_3 = \frac{[1/20 + (\zeta_2 + \zeta_4)/12 + \zeta_2 \zeta_4/6]}{\zeta_3(\zeta_3 - \zeta_2)(\zeta_4 - \zeta_3)(\zeta_3 + 1)}$$

$$P_2 = -\frac{[1/20 + (\zeta_3 + \zeta_4)/12 + \zeta_3 \zeta_4/6]}{\zeta_2(\zeta_3 - \zeta_2)(\zeta_4 - \zeta_2)(\zeta_2 + 1)}$$

$$P_1 = \frac{1}{2} + \frac{1/20 + (\zeta_2 + \zeta_3 + \zeta_4)/12}{\zeta_2 \zeta_3 \zeta_4} + \frac{1}{6}\left[\frac{1}{\zeta_2} + \frac{1}{\zeta_3} + \frac{1}{\zeta_4}\right]$$

$$P_0 = 1 - P_1 - P_2 - P_3 - P_4 \quad .$$

If f_ℓ is not known then the interpolation polynomial must become

$$P(Z) = p_n \cdot f_{\ell-n} + p_{n-1} \cdot f_{\ell-n+1} + \ldots + p_2 \cdot f_{\ell-2} + p_1 \cdot f_{\ell-1} \qquad (5A)$$

where

$$p_i = \prod_{\substack{K = \ell-n \\ K \neq \ell-i}}^{\ell-1} \left[\frac{Z - Z_K}{Z_{\ell-i} - Z_K} \right] \quad ; \quad i = 1,2,3,4 \quad .$$

In these conditions the solution of equation (1A) leads to

$$y_\ell = y_{\ell-1} + \delta Z[P_1' \cdot f_{\ell-1} + P_2' \cdot f_{\ell-2} + P_3' \cdot f_{\ell-3} + P_4' \cdot f_{\ell-4}] \qquad (6A)$$

$$P_4' = \frac{2(2 + 3\zeta_2)(\zeta_3 + \zeta_2) + 3(1 - 2\zeta_2^2)}{12\zeta_4(\zeta_4 - \zeta_2)(\zeta_3 - \zeta_4)}$$

$$P_3' = \frac{2 + 3\zeta_2 - 6\zeta_4(\zeta_4 - \zeta_2)P_4'}{6\zeta_3(\zeta_3 - \zeta_2)}$$

$$P_2' = -\frac{1}{\zeta_2}\left[\frac{1}{2} + \zeta_4 \cdot P_4' + \zeta_3 \cdot P_3' \right]$$

$$P_1' = 1 - P_2' - P_3' - P_4' \quad .$$

If the step size is constant $\zeta_2 = 1$, $\zeta_3 = 2$ and $\zeta_4 = 3$ and equation (6A) reduces to the Adams-Bashforth four-step formula

$$Y_\ell = y_{\ell-1} + \frac{\delta Z}{24}[55f_{\ell-1} - 59f_{\ell-2} + 37f_{\ell-3} - 9f_{\ell-4}] \quad .$$

If $\ell < 4$ these four-point formulas may not be used so that in these initial cases

$$P_4' = P_3' = P_2' = 0$$

$$P_1' = 1$$

and

$$P_4 = P_3 = P_2 = 0$$

$$P_1 = P_0 = 0.5 \quad .$$

Appendix 2

Runge-Kutta-Fehlberg method

Error estimates are sometimes used to control the step size of Runge-Kutta techniques. A popular fourth-order Runge-Kutta-Fehlberg solution (Burden et al., 1981) uses a Runge-Kutta method with truncation errors of order five

$$y'_{\ell+1} = y_\ell + \frac{16}{135} K_1 + \frac{6656}{12825} K_3 + \frac{28561}{56430} K_4 - \frac{9}{50} K_5 + \frac{2}{55} K_6 \qquad (1B)$$

to estimate the most significant part of the truncation error of a Runge-Kutta method of order four,

$$y_{\ell+1} = y_\ell + \frac{25}{216} K_1 + \frac{1408}{2565} K_3 + \frac{2197}{4104} K_4 - \frac{1}{5} K_5 \qquad (2B)$$

where $f = \frac{dy}{dx}$, Z is the independent variable and

$$\delta Z = Z_{\ell+1} - Z_\ell$$

$$K_1 = \delta Z.f(Z_\ell, y_\ell)$$

$$K_2 = \delta Z.f(Z_\ell + \delta Z/4,\ y_\ell + K_1/4)$$

$$K_3 = \delta Z.f\left(Z_\ell + \frac{3}{8}\delta Z,\ y_\ell + \frac{3}{32} K_1 + \frac{9}{32} K_2\right)$$

$$K_4 = \delta Z.f\left(Z_\ell + \frac{12}{13}\delta Z, y_\ell + \frac{1932}{2197} K_1 - \frac{7200}{2197} K_2 + \frac{7296}{2197} K_3\right)$$

$$K_5 = \delta Z.f\left(Z_\ell + \delta Z,\ y_\ell + \frac{439}{216} K_1 - 8K_2 + \frac{3680}{513} K_3 - \frac{845}{4104} K_4\right)$$

$$K_6 = \delta Z.f\left(Z_\ell + \delta Z/2,\ y_\ell - \frac{8}{27} K_1 + 2K_2 - \frac{3544}{2565} K_3 + \frac{1859}{4104} K_4 - \frac{11}{40} K_5\right) .$$

The most important part of the local truncation error of $y_{\ell+1}$ is then

$$e_{\ell+1} = \left[y'_{\ell+1} - y_{\ell} \right] / \delta Z$$

and as $e_{\ell+1}$ is of order $O(\delta Z^4)$, a constant K exists such that

$$e_{\ell+1} (\delta Z) \approx (\delta Z)^4 K .$$

Let us replace the step size δZ by $q\delta Z$ where $q > 0$ and q is bounded above zero, so that

$$\begin{aligned} e_{\ell+1} (q.\delta Z) &= K \cdot (q.\delta Z)^4 = q^4 . K (\delta Z)^4 \\ &= q^4 (y'_{\ell+1} - y_{\ell}) / \delta Z \end{aligned}$$

and if the local errors are bounded by e_{max}

$$\left| e_{\ell+1} (q.\delta Z) \right| \leq e_{max}$$

or

$$q < \left(\frac{\delta Z . e_{max}}{\left| y'_{\ell+1} - y_{\ell} \right|} \right)^{\frac{1}{4}} .$$

A common choice is to use a safety factor of about 2 so that

$$q = \left(\frac{\delta Z . e_{max}}{2 \left| y'_{\ell+1} - y_{\ell} \right|} \right)^{\frac{1}{4}}$$

and the next step size will be $Z_{\ell+2} - Z_{\ell+1} = q . \delta Z$.

This method has clear advantages over a common Runge-Kutta technique when the domain of the function is large and variable step size is needed. It also represents economy of computing relatively to the use of arbitrary methods of

order four and five used together to obtain the difference, $y'_{\ell+1} - y_\ell$, which require ten evaluations of the derivative f per step.

Appendix 3

The solution of the double integral in equation (4.7) can be divided into two steps; namely the solution of the integral

$$g(w) = \int_0^w \exp\left[\beta^2[1 + 2\varepsilon x - (1 - x)^{-2}]\right] dx \qquad (1C)$$

and then the solution of

$$I_1(w) = \int_0^w f(w)\,dw \ , \qquad (2C)$$

where $0 < w < 1$, and

$$f(w) = (1 - w)^{-4}\,[g(1) - g(w)] \ , \qquad (2C)$$

so that

$$I = 6\,\beta^2 \left(\frac{1 - C_a v}{1 - C_\infty v}\right) I_1(1) \ . \qquad (3C)$$

Equation (1C) was solved by using the fourth-order Runge-Kutta-Fehlberg technique outlined in appendix 2 and the integration carried out until $w = 1$, with storage of the n discrete pairs w_ℓ; $f(w_\ell)$; $(\ell=1; \ldots, n)$. This set of values was then used to integration equation (2C).

Appendix 4

Estimating analytical solutions of growth of n-component bubbles from one-component solutions

Given the dimensionless data α_i, F_{O_i} and f_i; i=1, ..., n, and a set of m pairs β_j'; $\phi(\beta_j')$ with $\varepsilon = 1$ (Scriven, 1959) the multi-component solution is obtained by minimizing the error

$$\varepsilon_s(\beta) = \left[\sum_{i=1}^{n} (\phi_i/\phi(\beta_i)) - 1 \right]^2 \tag{1D}$$

where

$$\beta_i = \beta/f_i^{\frac{1}{2}}$$

$$\phi_i = F_{O_i} - \alpha_i \, g_{i,eq} \tag{2D}$$

$$g_{i,eq} = \phi_i/\phi(\beta_i) \quad ; \quad i=1, \ldots, n$$

From equations (1D) and (2D)

$$g_{i,eq} = F_{O_i} / [\alpha_i - \phi(\beta_i)] \tag{3D}$$

and

$$\phi_i = F_{O_i} \left[1 - \frac{\alpha_i}{\alpha_i + \phi(\beta_i)} \right] \tag{4D}$$

so that equation (1D) becomes

$$\varepsilon_s(\beta) = \left[\sum_{i=1}^{n} \frac{F_{O_i}}{\phi(\beta_i)} \left(1 - \frac{\alpha_i}{\alpha_i + \phi(\beta_i)} \right) - 1 \right]^2 \tag{5D}$$

The function $\phi(\beta)$ (with $\varepsilon = 1$) was solved by Scriven (1959) for a large set of discrete values of β. Four-point polynomial interpolations were used to obtain the required $\phi(\beta_i)$ predictions from a set of m discrete

pairs β_j; $\phi(\beta_j)$; (j=1, ... m). All the values of $\beta_i = \beta/f_i^{\frac{1}{2}}$ are obtained from the independent variable β and the objective function $\varepsilon_s(\beta)$ was optimized by using sequential selection of β values according to the modified Fibonacci method (Beveridge and Schechter, 1970). The lower and upper limits of β were chosen as described in Chapter VI.

Appendix 5

Variable mesh size Runge-Kutta technique to solve growth from zero size with concentration dependent diffusivity (Chapter 7, Section 7.3)

Equations (7.12) and (7.13) with initial conditions $F(\beta) = 0$ and $T(\beta) = 2\beta$ must be solved for $s \geq \beta$, after inclusion of the functional form of $\hat{D}(F)$.

A standard Runge-Kutta technique with constant mesh size is not suitable for a large range of values of s. Concentration profiles are usually steep near the interface ($s = \beta$) but concentration varies slowly with distance for large s. The derivative $\frac{dT}{ds}$ is a function of T and $\hat{D}(F)$ so that truncation errors may be kept small by adding restrictions to the changes in T and $\hat{D}(F)$ per computing step. It was shown that T drops from 2β at $s = \beta$ to 0 at infinity. Therefore the increment δs required to advance from step ℓ to step $\ell+1$ is controlled by

$$\delta s < 2\,\beta \,/\, \left| \, n.\left(\frac{dT}{ds}\right)_{\ell} \, \right|$$

and

$$\delta s < D(F)_{\ell} \,/\, \left| \, n.T_{\ell} \,.\left(\frac{dD}{dF}\right)_{\ell} \, \right|$$

where n is an estimate of the number of steps.

For small T the previous restrictions do not prevent large $(\delta s)/s$ values so that an additional restriction is used

$$\delta s < s/n \ .$$

All three of these criteria are used to optimize the solutions.

Appendix 6

Inclusion of viscous effects in finite difference predictions of growth or dissolution (Chapter IX)

The effect of surface tension is dependent on the radius of the bubble but is independent of time derivatives of the radius. Therefore the finite difference solutions do not involve additional difficulties if $\eta = 0$ and $h = 0$, that is, if viscous and inertial effects are negligible. However, if $\eta \neq 0$ the solution of equations (9.8) and (9.11) requires estimates of both $\frac{dR}{dZ}$ and $\frac{d^2R}{dZ^2}$. Alternatively the method can be based on using an explicit-implicit multistep scheme to calculate the dimensionless content of the bubble G amd advance from time step ℓ to step $\ell+1$.

Let $R'_{\ell+1}$ be the estimate of R obtained by an explicit multistep formula (appendix 1). From the implicit multistep formula the following relation can also be derived.

$$\left(\frac{dR}{dZ}\right)_{\ell+1} = d_0 + d_1 \cdot R_{\ell+1} \qquad (1F)$$

where $R_{\ell+1}$ is the correct value of R at the new step $\ell+1$ and

$$d_1 = 1/(P_0 \cdot \delta Z)$$

$$d_0 = - R_\ell \cdot d_1 - \left[P_1\left(\frac{dR}{dZ}\right)_\ell + P_2\left(\frac{dR}{dZ}\right)_{\ell-1} + P_3\left(\frac{dR}{dZ}\right)_{\ell-2} + P_4\left(\frac{dR}{dZ}\right)_{\ell-3} \right] / P_0$$

$$\delta Z = Z_{\ell+1} - Z_\ell$$

Combination of equations (9.9) and (1F) with $h = 0$ leads to

$$G_{\ell+1} = \frac{4\pi}{3}\left[R^3_{\ell+1} + 2s \cdot R^2_{\ell+1} + 4\eta \cdot d_0 \cdot R^2_{\ell+1} + 4\eta \cdot d_1 \cdot R^3_{\ell+1} \right] \qquad (2F)$$

In addition, the relative changes in radius per time step are kept small and also

$$R_{\ell+1} = R'_{\ell+1} \cdot (1 + \delta)$$

where $\delta << 1$. Therefore

$$R^3_{\ell+1} \simeq 3\left(R'_{\ell+1}\right)^2 \cdot R_{\ell+1} - 2\left(R'_{\ell+1}\right)^3 \qquad (3F)$$

$$R^2_{\ell+1} \simeq 2R'_{\ell+1} \cdot R_{\ell+1} - \left(R'_{\ell+1}\right)^2 \qquad (4F)$$

and from equations (2F), (3F), and (4F) $R_{\ell+1}$ can be estimated.

The overall scheme can be summarized as follows:

1) Calculate $G_{\ell+1}$ by explicit multistep formula,
2) use the time derivatives at previous time steps to obtain equations (1F) and (2F),
3) combine equations (2F), (3F), and (4F) to obtain $R_{\ell+1}$,
4) establish a relation between the concentration gradient at the interface and the interface solute concentration to include the local balance in the implicit finite difference scheme described in Chapter III,
5) calculate the concentration profile at step $\ell+1$,
6) recalculate the concentration gradient at the interface and obtain the corrected value of $G_{\ell+1}$ by implicit multistep formula,
7) recalculate $R_{\ell+1}$ by combining equations (2F), (3F), and (4F),
8) calculate $\left(\frac{dR}{dZ}\right)_{\ell+1}$ from equation (1F),
9) start a new time step or stop.

The relation between interface concentration and concentration gradient (step 4) is required to avoid instabilities which would result from the inclusion of $\left(\frac{dR}{dZ}\right)$ in the calculations of F(R), (equation (9.8a)). From equation (9.8a) and taking into account the definitions of q and ϕ

$$F(R)_{\ell+1} = q\ \phi\ P^* - (1 + q)\ \phi \qquad (5F)$$

and from equation (9.9)

$$G_{\ell+1} = \frac{4\pi}{3} R^3_{\ell+1}\ P^* \ . \qquad (6F)$$

Also from equation (9.10)

$$\frac{4\pi}{3} R^3_{\ell+1}\ P^* = G_{\ell+1} = G_\ell + (\delta Z) \cdot R_{\ell+1} \cdot \left[\frac{\partial F}{\partial x}\right]_{\substack{x=1 \\ \ell+1}} \ . \qquad (7F)$$

Finally, combination of equations (5F), (6F) and (7F) leads to

$$\left[\frac{\partial F}{\partial x}\right]_{\substack{x=1 \\ \ell+1}} = c_o + c_1 \Big[\ F(R)\ \Big]_{\ell+1} \qquad (8F)$$

where c_o and c_1 are obtained from the values of q, ϕ, G, R, and $\frac{dG}{dZ}$.

In order to obtain equation (3.23) (at the interface), the concentration gradient can be approximated by

$$\left[\frac{\partial F}{\partial x}\right]_{x=1} = (F_2 - F_1) \ / \ \delta x \qquad (9F)$$

where F_1 and F_2 are the dimensionless concentrations at the two first radial mesh positions and δx is the mesh size. As $F_1 = F(R)$, from equations (8F) and (9F)

$$- F_{1,\ell+1}[1 + c_1(\delta x)] + F_{2,\ell+1} = c_o(\delta x) \ , \qquad (10F)$$

which is equivalent to equation (3.23). Alternatively a fictitious point may be used (Crank and Nicolson, 1947) to solve the diffusion equation at the interface. This method has been described in Chapter VIII involving a linear relation similar to equation (8F). A fully implicit formula was also

used to avoid instabilities. The space derivatives (equations (8.29) and (8.30)) are replaced by their values at step $\ell+1$ only, instead of the average used in Chapter VIII (section 8.4). Therefore, from equations (8.24), (8.29), (8.30), (8.31) and (8F) one obtains

$$F_{2,\ell+1} - [1 + \alpha + C_1 \cdot (\delta x) \cdot (1 - (\delta x)] \cdot F_{1,\ell+1} = (\delta x) \cdot (1 - \delta x) \cdot C_O - \alpha \cdot F_{1,\ell} \tag{11F}$$

where

$$\alpha = \frac{1}{2} (R^2)_{av} (\delta x)^2 / (\delta Z) \ .$$

Note that inclusion of either equation (10F) or equation (11F) in the finite difference scheme described in Chapter III leads to indistinguishable results. This can only be achieved if proper redistribution of space mesh points is used. Otherwise the first space interval might become excessively large causing equation (10F) to be less accurate.

Appendix 7

Interfacial concentrations for multicomponent bubbles

Equation (3.50) describes the boundary conditions for multicomponent bubbles when Henry's law is assumed. In more general conditions the interfacial concentration $C_i(a)$ is given by

$$C_i(a) = H_i \, p_i^{x_i} \quad ; \quad i=1,\ldots, n, \tag{1G}$$

which includes both positive and negative deviations from Henry's law. H_i is a characteristic constant and p_i is the partial pressure of gas i in the bubble. In dimensionless terms equation (1G) becomes

$$F_i(R) = \alpha_i \cdot g_i^{x_i} - F_{O_i} \tag{2G}$$

where

$$F_{O_i} = C_{\infty_i}/C_s^{\circ}$$

$$\alpha_i = H_i \cdot P^{x_i}/C_s^{\circ}$$

P is the total gas pressure and C_s° the concentration of gas in the bubble.

As the numerical solution advances from time step ℓ to step $\ell+1$ $F_i(R)$ might change by a relatively small fraction so that one might write

$$\left[F_i(R) \right]_{\ell+1} + F_{O_i} = \left[(F_i(R))_{\ell} + F_{O_i} \right] (1 + \delta) \tag{3G}$$

and from equation (2G)

$$\begin{aligned} g_{i,\ell+1} &= \left[\left(F_i(R)_{\ell+1} + F_{O_i} \right) / \alpha_i \right]^{1/x_i} \\ &\simeq \left[\left(F_i(R)_{\ell} + F_{O_i} \right) / \alpha_i \right]^{1/x_i} \cdot (1 + \delta/x_i) \\ &\simeq b_0 + b_1 \left[F_i(R) \right]_{\ell+1} \end{aligned} \tag{4G}$$

where

$$b_1 = \frac{1}{\alpha_i x_i} \left[\left(F_i(R)_{\ell} + F_{O_i} \right) / \alpha_i \right]^{(1/x_i - 1)}$$

$$b_O = \left[\left(F_i R_{\ell} + F_{O_i} \right) / \alpha_i \right]^{1/x_i} - b_1 \left[F_i(R) \right]_{\ell}$$

Equation (4G) assumes the form of a linear relation between $\left[F_i(R) \right]_{\ell+1}$ and $g_{i,\ell+1}$ which is required to include the boundary conditions in the implicit finite difference scheme described in Chapter III.

Appendix 8

Operators used in Chapter II

Given a vector $\vec{u}$ the operator $\nabla.\vec{u}$ in rectangular coordinates is given by

$$\nabla.\vec{u} = \frac{\partial u_x}{\partial x} + \frac{\partial u_y}{\partial y} + \frac{\partial u_z}{\partial z}$$

and in spherical coordinates (Bird et al., 1960)

$$\nabla.\vec{u} = \frac{1}{r^2}\frac{\partial}{\partial r}(r^2 u_r) + \frac{1}{r\sin\theta}\frac{\partial}{\partial\theta}(\sin\theta\, u_\theta) + \frac{1}{r\sin\theta}\frac{\partial u_\phi}{\partial\phi} \quad .$$

If the system is spherically symmetrical

$$\nabla.\vec{u} = \frac{1}{r^2}\frac{\partial}{\partial r}(r^2 u_r) \quad .$$

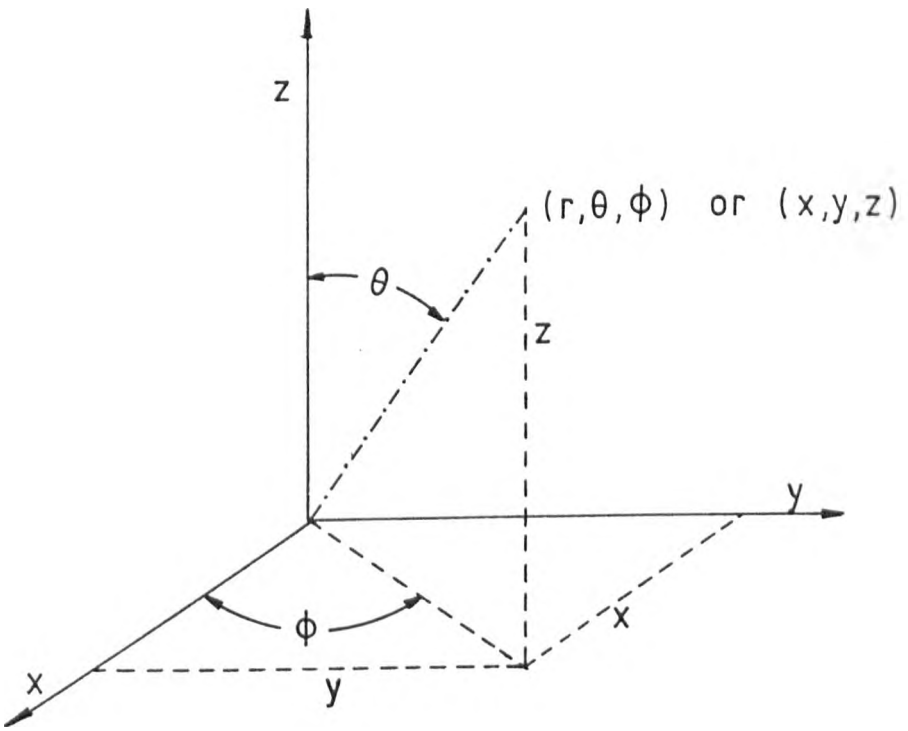

Fig. F1 Spherical coordinates. The ranges of the variables are $0 < r < \infty$, $0 < \theta < \pi$; $0 < \phi < 2\pi$.

In isotropic media the diffusion flux j_D is usually written

$$j_D = D \text{ grad } C$$

where

$$\text{grad } C = \frac{\partial C}{\partial x}i + \frac{\partial C}{\partial y}j + \frac{\partial C}{\partial z}k$$

and therefore

$$\nabla . j_D = \frac{\partial}{\partial x}\left(D \frac{\partial C}{\partial x}\right) + \frac{\partial}{\partial y}\left(D \frac{\partial C}{\partial y}\right) + \frac{\partial}{\partial z}\left(D \frac{\partial C}{\partial z}\right)$$

or in spherical coordinates

$$\nabla . j_D = \frac{1}{r^2}\left[\frac{\partial}{\partial r}\left(r^2 D \frac{\partial C}{\partial r}\right) + \frac{1}{\sin\theta}\frac{\partial}{\partial \theta}(DC \sin\theta)\right.$$

$$\left. + \frac{D}{\sin^2\theta}\frac{\partial^2 C}{\partial \phi^2}\right] .$$

If the system is spherically symmetrical

$$\nabla . j_D = \frac{1}{r^2}\frac{\partial}{\partial r}\left(r^2 D \frac{\partial C}{\partial r}\right) .$$

References

E. T. Allen & E. G. Zies,(1918)
J. Amer. Ceram. Soc., 1,739-786

C. Apax,(1975)
PhD Thesis, University of Sheffield

C. Apax & M. Cable,(1977)
Proc. XI Int. Cong. Glass, Prague, Vol. 4,167-176

A. Appen & L. Polyakova,(1938)
Stek. Prom., 7,18-21

T. Baak,(1959)
J. Amer. Ceram. Soc., 42,27-29

T. Baak & J. Hornyak,(1966)
Glass Ind., 47,374-377,418-420,455-458

D. F. Barlow,(1965)
Proc. VII Int. Cong. Glass, Brussels, Paper 19

E. J. Barlow & W. E. Langlois,(1962)
IBM Journal, 329-337

R. E. Bastick,(1955)
Symp. sur l'Affinage du Verre, Charleroi, USCV, 127-138

G. Beveridge & R. Schechter,(1970)
"Optimization, Theory and Practice", Mc. Graw-Hill

M. M. Bhuiyan & M. Cable,(1965)
Glass Tech., 6,206-212

R. B. Bird, W. E. Stewart, and E. N. Lightfoot,(1960)
"Transport Phenomena", John Wiley & Sons, New York

R. B. Brow & R. H. Doremus,(1976)
J. Amer. Ceram. Soc., 59,510-514

R. Bruckner,(1961)
Glastech. Ber., 34,438-456,515-528

R. Bruckner,(1962)
Glastech. Ber., 35,93-105

R. L. Burden & alia,(1981)
"Numerical Analysis", Second Edition

M. Cable,(1958)a
J. Soc. Glass Tech., 42,20T-31T

M. Cable,(1958)b
Symp. sur la Fusion du Verre, Charleroi, USCV, 253-267

M. Cable,(1960)a
Glass Tech., 1,139-143

M. Cable,(1960)b
Glass Tech., 1,144-154

M. Cable,(1961)a
Glass Tech., 2,60-70

M. Cable,(1961)b
Glass Tech., 2,151-158

M. Cable & alia,(1968)
Glass Tech., 9,101-104

M. Cable & alia,(1969)
Glass Tech., 10,15-21

M. Cable & D. J. Evans,(1967)
J. Appl. Phys., 38,2899-2906

M. Cable & M. A. Haroon,(1970)
Glass Tech., 11,48-53

M. Cable & A. Naqvi,(1975)
Glass Tech., 16,2-11

R. J. Callow,(1949)
J. Soc. Glass Tech., 33,255T-266T

R. J. Callow & G. Lawson,(1952)
J. Soc. Glass Tech., 36,266T-274T

R. A. Cameron,(1965)
"Kinetics of Arsenic-Antimony Fining",
Symposium on Gases in Glass, Philadelphia
67th Annual Meeting of the American Ceramic Society,

H. S. Carslaw & J. C. Jaeger,(1959)
"Conduction of Heat in Solids", Clarendon press, Oxford

D. R. Cockram & alia,(1969)
Phys. Chem. Glasses, 10,18-22

A. R. Conroy & alia,(1963)
Glass Ind., 44,139-143,175-177

A. R. Conroy & alia,(1966)
Glass Ind., 47,84-89,110,133-139

J. Crank,(1975)
"The Mathematics of Diffusion", Clarendon Press, Oxford

J. Crank & P. Nicolson,(1947)
Proc. Camb. Phil. Soc., 43, 50-67

R. H. Dalton,(1933)
J. Amer. Ceram. Soc., 16,425-432

R. H. Dalton,(1935)
J. Amer. Ceram. Soc., 17,2150-2153

D. R. Doremus,(1960)
J. Amer. Ceram. Soc., 43,655-661

R. W. Douglas & alia,(1965)
Phys. Chem. Glasses, 6,197-223

L. Dubrul,(1955)
Symp. sur l'Affinage du Verre, Paris, USCV, 445-451

J. L. Duda & J. S. Vrentas,(1969)
A. I. Ch. E. J., 15,351-356

J. L. Duda & J. S. Vrentas,(1971)
I. J. Heat Mass Transfer, 14,395

W. Eitel & W Weyl,(1932)
J. Amer. Ceram. Soc., 15,159-166

P. S. Epstein & M. S. Plesset,(1950)
J. Chem. Phys., 18,1505-1509

K. Van Erk & alia,(1977)
Proc. XI Int. Cong. Glass, Prague, Vol. 4,137-146

S. P. Faile & D. M. Roy,(1966)
J. Amer. Ceram. Soc., 49,638-642

J. D. Fast,(1965)
"Interactions of Metals and Gases", Vol. I,
Thermodynamics and Phase relations,
Academic Press, New York

E. Fehlberg,(1970)
Computing, 6,61-71

V. A. Ferrandis & alia,(1972)
Glastech. Ber., 45,397-406

C. J. B. Fincham & F. D. Richardson,(1962)
Proc. Roy. Soc. London, A223,40-62

R. W. Fisher,(1976)
MSc. Thesis, University of Sheffield

E. C. du Fort & S. P. Frankel,(1953)
Natl. Res. Council Math. Tabl., 7,135

F. C. Frank,(1950)
Proc. Roy. Soc., A201,586-599

H. Franz,(1965)
Glastech. Ber., 38,54-59

H. Franz,(1966)
J. Amer. Ceram. Soc., 49,473-477

H. Franz & H. Scholze,(1963)
Glastech. Ber., 36,347-356

G. H. Frischat & alia,(1978)
Glastech. Ber., 51,321-327

G. H. Frischat & H. J. Oel,(1965)
Glastech. Ber., 38, 156-166

G. H. Frischat & H. J. Oel,(1967)a
Glastech. Ber., 40,311

G. H. Frischat & H. J. Oel,(1967)b
Phys. Chem. Glasses, 8,92-95

S. Garbe,(1961)
Glastech. Ber., 34,413-417

G. Gehlhoff & alia,(1930)
Glastech. Ber., 8,1-30

V. Gottardi & alia,(1973)
Symp. sur l'Elaboration du Verre, Madrid, USCV, 229-255

J. Gotz,(1974)
Proc. X Int. Cong. Glass, Tokyo, Part I,2,132-140

C. H. Greene & D. H. Davis,(1974)
Proc. X Int. Cong. Glass, Tokyo, Part I,3,59

C. H. Greene & R. F. Gaffney,(1959)
J. Amer. Ceram. Soc., 42,271-275

C. H. Greene & J. Kitano,(1959)
Glastech. Ber., 32K,V44
Proc. V Int. Cong. Glass

C. H. Greene & H. A. Lee,(1965)
J. Amer. Ceram. Soc., 48,528-533

C. H. Greene & D. R. Platts,(1969)
J. Amer. Ceram. Soc., 52,106-109

G. W. Greenwood,(1956)
Acta Metallurgica, 4,243-248

C. Griffin,(1971)
PhD. Thesis, University of Sheffield

R. Guy,(1961)
Bull. Cent. Glass Ceram. Res. Inst., 8,79-80

M. A. Haroon,(1967)
PhD. Thesis, University of Sheffield

G. A. Higham & M. Cable,(1965)
Symp. sur l'Elaboration du Verre, Madrid, USCV, 205

C. Hirayama & F. E. Camp,(1969)
Glass Tech., 10,123-127

S. Holmquist,(1966)
J. Amer. Ceram. Soc., 49,467-473

E. Kordes & alia,(1951)
Z. Anorg. Allg. Chem.,264,255-271,272-284

F. Kramer,(1979)
Glastech. Ber., 52,43-50

I. M. Krieger & alia,(1967)
J. Phys. Chem., 71,1123-1129

C. Kroger & N. Goldmann,(1962)
Glastech. Ber., 35,459-466

C. Kroger & D. Lummerzheim,(1965)
Glastech. Ber., 38,229-232

C. Kühl & alia,(1938)
Glastech. Ber., 16,37-51

C. R. Kurkjian & L. E. Russelt,(1958)
J. Soc. Glass Tech., 42,130T-144T

V. G. Levich,(1962)
"Physicochemical Hydrodynamics", Prentice Hall

L. Liebermann,(1957)
J. Appl. Phys., 28,205-211

I. M. Lifshitz & V. S. Slyozov,(1961)
J. Phys. Chem. Solids, 19, 35

A. K. Lyle,(1945)
J. Amer. Ceram. Soc., 28,282-287

A. K. Lyle,(1956)
Proc. IV Int. Cong. Glass, Paris, Paper II-4,93-102

F. Mahieux,(1956)
Verres et Refractaires, 10,277-298,342-356

F. Mahieux,(1957)
Verres et Refractaires, 11,9-17

D. M. J. P. Manley,(1960)
B. J. Appl. Phys., 11,38-42

W. H. Manring & alia,(1967)
Glass Ind., 48,374-380

W. H. Manring & D. W. Hopkins,(1958)
Glass Ind., 39,139-142

G. P. Martins,(1969)
PhD. Thesis, University of New York at Buffalo

H. Meyer & alia,(1977)
Proc. XI Int. Cong. Glass, Prague, Vol. 2,317-326

H. O. Mulfinger,(1962)
Glastech. Ber., 35,466-478

H. O. Mulfinger,(1966)a
J. Amer. Ceram. Soc., 49,462-467

H. O. Mulfinger,(1966)b
Symp. on Defects in Glass, Tokyo, 82

H. O. Mulfinger,(1972)
Glastech. Ber., 45,238-243

H. O. Mulfinger,(1976)
Glastech. Ber., 49,232-245

H. O. Mulfinger & alia,(1972)
Glastech. Ber., 45,389-396

H. O. Mulfinger & H. Franz,(1965)
Glastech. Ber., 38,235-242

H. O. Mulfinger & G. Meyer,(1963)
Glastech. Ber., 36,481-483

H. O. Mulfinger & H. Scholze,(1962)a
Glastech. Ber., 35,466-478

H. O. Mulfinger & H. Scholze,(1962)b
Glastech. Ber., 35,495-500

L. Nemec,(1969)
Glass tech., 10,176-181

L. Nemec,(1974)
Glass Tech., 15,153-156

L. Nemec,(1977)a
J. Amer. Ceram. Soc., 60,436-440

L. Nemec,(1977)b
Proc. XI Int. Cong. Glass, Prague, Vol. 4,155-165

P. Onorato & alia,(1981)
J. Amer. Ceram. Soc., 64,676-682

K. Papadopoulos,(1973)
Phys. Chem. Glasses, 14,60-65

M. Parkin & alia,(1937)
J. Soc. Glass Tech., 40,153T-166T

A. Paul & D. Lahiri,(1963)
Trans. Indian Ceram. Soc., 22,146-150

M. L. Pearce,(1964)
J. Amer. Ceram. Soc., 47,342-347

M. L. Pearce,(1965)
J. Amer. Ceram. Soc., 48,175-178

J. R. Philip,(1966)
Proc. Unesco Netherlands Symp. Water Undersaturated Zone, Wageningen

M. S. Plesset & S. A. Zwick,(1954)
J. Appl. Phys., 25,493-500

J. C. Potts,(1941)
J. Amer. Ceram. Soc., 24,43-50

D. W. Readey & A. R. Cooper jr.,(1966)
Chem. Eng. Sci., 21,917-922

P. H. V. Reth & H. V. V. Velzen,(1973)
Symp. sur l'Elaboation du Verre, Madrid, 31-42

D. Rosner & M. Epstein,(1972)
Chem. Eng. Sci., 27,69-88

E. Ruckenstein,(1964)
Chem. Eng. Sci., 19,131-146

E. Ruckenstein & E. J. Davis,(1970)
J. Colloid Int. Sci., 34,142-158

L. E. Russelt,(1957)
J. Soc. Glass Tech., 41,307T-317T

L. E. Russelt & C. R. Kurkjian,(1958)
J. Soc. Glass Tech., 42,130T-144T

H. Scholze,(1959)
Glastech. Ber., 32,81-88,142-152,278-281,314-320

H. Scholze,(1960)
Naturwissenchaften, 47,226

H. Scholze,(1962)
Advances in Glass Technology,
Proc. VI Int. Cong. Glass, 230-248

H. Scholze,(1968)
Proc. VIII Int. Cong. Glass, 69-83

H. Scholze & H. O. Mulfinger,(1959)
Glastech. Ber., 32,381-386

L. E. Scriven,(1959)
Chem. Eng. Sci., 10,1-13

F. Shaw & S. Jones,(1966)
Bull. Amer. Ceram. Soc., 45,1004

R. Simham,(1973)
PhD. Thesis, University of Sheffield

V. T. Slavyanski,(1957)
"Gases in Glass",(in Russian), Oborongiz, Moscow

G. D. Smith,(1965)
"Numerical Solution of Partial Differential Equations",
Oxford University Press

F. G. Solinov & N. A. Pankova,(1965)
Proc. VII Int. Cong. Glass, Brussels, Vol. 2, Paper 341

Z. Strnad,(1971)
Phys. Chem. Glasses, 12,152-155

R. S. Subramanian & Chi,(1980)
Chem. Eng. Sci., 35,2185

R. S. Subramanian & M. C. Weinberg,(1980)
A. I. Ch. E. J., 27,739-748

J. Szekely & S. D. Fang,(1973)
Chem. Eng. Sci., 28,2127-2140

J. Szekely & G. P. Martins,(1971)
Chem. Eng. Sci., 26,147

R. Terai & Y. Oishi,(1977)
Glastech. Ber., 50,68-73

S. W. Thomas & alia,(1979)
Metal Science, 13,651-659

J. W. Tomlinson,(1956)
J. Soc. Glass Tech., 40,25T-31T

H. Uhlig,(1937)
J. Phys. Chem., 41,1215

J. S. Vrentas & D. Shin,(1980)
Chem. Eng. Sci., 35,1687-1705

C. Wagner,(1961)
Z. Electrochem., 65,581-591

M. C. Weinberg,(1980)
Chem. Eng. Sci., 36,137

M. C. Weinberg & alia,(1980)
J. Amer. Ceram. Soc., 63,435-438

M. C. Weinberg & R. S. Subramanian,(1980)
J. Amer. Ceram. Soc., 63,527-531

W. Weyl,(1931)
Glastech. Ber., 9,641-660

R. Van Wyk,(1968)
NASA Report,CR-1247

E. Zschimmer & alia,(1926)
Sprechsaal, 56,331-333,353-357,393-395,411-413,422-425

E. Zschimmer & L. Erneyi,(1932)
Sprechsaal, 65,177-197